

KINETICS AND MECHANISMS OF HYDRATED ELECTRON REACTIONS DURING
ADVANCED REDUCTION PROCESSES

by

Camille K. Amador

A thesis submitted to the Faculty and the Board of Trustees of the Colorado School of Mines in partial fulfillment of the requirements for the degree of Doctor of Philosophy (Materials Science).

Golden, Colorado

Date _____

Signed: _____

Camille K. Amador

Signed: _____

Dr. Timothy J. Strathmann

Thesis Advisor

Signed: _____

Dr. Shubham Vyas

Thesis Advisor

Golden, Colorado

Date _____

Signed: _____

Dr. Eric Toberer

Professor and Director of Materials Science

Department of Physics

ABSTRACT

Advanced reduction processes (ARPs) are a class of water treatment technologies that have great potential in remediating recalcitrant contaminants that are resistant towards traditional oxidation methods such as chlorinated solvents, toxic oxyanions, and more recently, per- and polyfluoroalkyl substances (PFASs). Although ARPs have been shown to completely mineralize persistent organic pollutants, their operation efficiency is highly dependent on sourcewater composition since the reactive species, hydrated electron (e_{aq}^-), can be rapidly quenched by non-target constituents present in natural water. Current means of optimizing ARP reaction conditions involve UV photolysis experiments that require performing multiple batch experiments which can be time and resource intensive. Moreover, means of measuring fundamental kinetics values of e_{aq}^- reactions (i.e., k_2 ; $M^{-1} s^{-1}$) such as laser flash photolysis (LFP) and pulse radiolysis contradict results in photolysis experiments and values vary widely in the literature.

Kinetic models are an alternative approach for gaining quantitative information regarding the photochemistry dictating ARP treatment results. This work investigates the kinetics and mechanisms of e_{aq}^- reactions during ARPs for the development of a photochemical model to quantitatively predict PFAS degradation in diverse environments. The first objective of this thesis focused on measuring kinetics and elucidating mechanisms of PFAS degradation by e_{aq}^- using laser flash photolysis (LFP) and density functional theory (DFT). Reactivity of the compounds in the dataset varied widely despite their structural similarities and it was proposed that polyfluorinated carboxylates can undergo non-degradative reaction pathways posing additional challenges for treating diverse PFAS mixtures. The second objective involved quantitatively describing the effect of solution pH and acid-base speciation of common water constituents on e_{aq}^- availability during ARPs. Carbonate species, ubiquitous in natural waters, were found to significantly inhibit PFAS degradation, and species-specific k_2 values were determined using LFP and nonlinear regression analysis. The third and final objective was to develop a photochemical model for predicting PFAS degradation during UV-sulfite treatment using the kinetics values and mechanistic insights obtained in the first two objectives. This model facilitates the (1) quantitative interpretation of the effect of system and solution parameters on treatment efficacy, (2) reconciliation of UV photolysis and LFP/pulse radiolysis methodologies, and (3) prediction of PFAS degradation during UV-sulfite treatment in different environments based on geochemical solution conditions and UV light source.

TABLE OF CONTENTS

ABSTRACT.....	iii
TABLE OF CONTENTS.....	iv
LIST OF FIGURES	vi
LIST OF TABLES.....	x
ACKNOWLEDGEMENTS.....	xi
CHAPTER 1 INTRODUCTION	1
1.1 Motivation.....	1
1.2 PFAS Background	2
1.3 UV-ARP Background.....	4
1.4 System and Solution Effects on UV-ARPs.....	5
1.5 Research Goals.....	9
CHAPTER 2 KINETICS AND MECHANISMS OF HYDRATED ELECTRON REACTIONS WITH ULTRA-SHORT CHAIN FLUOROCARBOXYLATES	12
2.1 Abstract.....	12
2.2 Introduction.....	13
2.3 Materials and Methods.....	14
2.4 Results and Discussion	16
2.5 Conclusions.....	29
CHAPTER 3 INFLUENCE OF CARBONATE SPECIATION ON HYDRATED ELECTRON TREATMENT PROCESSES.....	31
3.1 Abstract.....	31
3.2 Introduction.....	32
3.3 Materials and Methods.....	34
3.4 Results and Discussion	35
CHAPTER 4 KINETIC MODEL FOR PREDICTING PFAS DEGRADATION DURING UV- SULFITE TREATMENT.....	46
4.1 Abstract.....	46
4.2 Introduction.....	47
4.3 Materials and Methods.....	49
4.4 Results and Discussion	50
4.5 Practical Implications.....	65
CHAPTER 5 CONCLUSIONS AND FUTURE WORK	66
5.1 Chapter Summaries.....	66

5.2	Future Work.....	67
REFERENCES	72
APPENDIX A	SUPPLEMENTARY INFORMATION FOR CHAPTER 2.....	86
A.1	Methods.....	86
A.2	Chemical Interpretations of Select DFT Parameters.....	91
A.3	Additional data.....	92
APPENDIX B	SUPPLEMENTARY INFORMATION FOR CHAPTER 3.....	105
B.1	Methods.....	105
B.2	Additional Data.....	108
B.3	LFP Transient Traces and Stern-Volmer Plots.....	110
APPENDIX C	SUPPLEMENTARY INFORMATION FOR CHAPTER 4.....	114
C.1	Methods.....	114
C.2	Additional Data.....	118
APPENDIX D	COPYRIGHT PERMISSIONS.....	127

LIST OF FIGURES

Figure 2.1	<p>(A) Kinetic transient absorption traces for e_{aq}^- decay (measured at 690 nm) at pH 9.2 (40 mM borate buffer) in solutions containing 0 – 50 mM PFBA. Solution conditions: 40 μM $K_4Fe(CN)_6$, 10 μM $K_3Fe(CN)_6$, ionic strength = 630 mM (balanced using NaCl). (B) Resulting Stern-Volmer plot generated from model fits of the traces to determine e_{aq}^- lifetimes (τ; μs) in each solution. Individual kinetic traces in panel (A) represent one of the triplicate measurements, and error bars in panel (B) represent one standard deviation based upon triplicate measurements. Traces and Stern-Volmer plots for all other compounds available in Appendix A.....</p>	18
Figure 2.2	<p>(A) Stern-Volmer plots for mono-, di-, and trifluoroacetate. Solution conditions are the same as Figure 1. Units for the k_2 values shown are $M^{-1}s^{-1}$. (B) Influence of solution ionic strength (μ) on k_2 for e_{aq}^- reaction with TFA, including data from the present study (\bullet) and from Huang et al. (\blacksquare)⁵⁰ Dashed line shows linear extrapolation between the data sets.....</p>	23
Figure 2.3	<p>Scatter correlation plots between measured $\log k_2$ values and DFT-calculated molecular descriptors for (A) all compounds, (B) perfluorinated carboxylates only (\bullet), (C) perfluorinated and C2 carboxylates (\blacktriangle), and (D) polyfluorinated carboxylates only (\blacksquare).....</p>	26
Scheme 2.1	<p>Proposed mechanism for the initial reduction events involving (A) stepwise C-F bond cleavage for PFBA, (B) stepwise C-F bond cleavage for TriFBA, and (C) associative deactivation of e_{aq}^- for TriFBA. BDEs of bonds of interest are provided in blue in units of kcal/mol.....</p>	28
Figure 3.1	<p>Effect of dissolved carbonate on the observed rate constant for PFOS degradation during UV-sulfite treatment. Reaction conditions: $[PFOS]_{initial} = 70 \mu g/L$, 3 mM Na_2SO_3, irradiation with LP-Hg light source, pH 10.0 (5 mM borate buffer), 20 °C. Error bars represent duplicate measurement-derived standard deviations.....</p>	36
Figure 3.2	<p>(A) Kinetic transient absorption traces for e_{aq}^- decay (measured at 690 nm) at pH 9.3 in solutions amended with varying concentrations of dissolved carbonate prepared from $NaHCO_3$. Solution conditions: 40 μM $K_4Fe(CN)_6$, 10 μM $K_3Fe(CN)_6$, ionic strength = 0.47 M (balanced using NaCl). (B) Stern-Volmer plots for selected pH conditions generated from model fits of the traces to determine e_{aq}^- lifetimes in each solution (results for all pH conditions provided in SI). (C) Stern-Volmer plot for acidic solutions (pH 5.0 – 5.5) prepared by equilibrating $CO_{2(g)}$ with aqueous solutions then adding $K_4Fe(CN)_6$, $K_3Fe(CN)_6$ and NaCl. Individual kinetic traces in panel (A) represent the average of the triplicate measurements, and error bars in panels (B) and (C) represent one standard deviation based upon triplicate measurements. Apparent rate constants derived from Stern-Volmer analyses provided in Table 3.1.....</p>	38
Figure 3.3	<p>Effect of pH on measured and model-predicted apparent rate constants for e_{aq}^- reaction with dissolved carbonate species. Simulated contributions of $H_2CO_3^*$ (beveled orange line), HCO_3^- (beveled blue line), and CO_3^{2-} (beveled green line) to the overall quenching (solid black line) are also shown. Dashed black line shows model predictions using rate constants previously reported in literature.^{47,129,130}.....</p>	41

Figure 3.4	Simulation of the rates e_{aq}^- scavenging by dissolved carbonate species in comparison with other common scavengers expected during groundwater treatment with UV-sulfite. (A) influence of pH, and (B) influence of variable carbonate concentration at pH 7.0.....	45
Figure 4.1	Effect of (A) dissolved carbonate and (B) pH on the observed rate constant of PFBA degradation during UV-sulfite treatment. Reaction conditions for $[PFBA]_{initial} = 100 \mu\text{g/L}$, 10 mM Na_2SO_3 , irradiation with LP-Hg light source, 20°C. For (A) pH was adjusted to 9.5 ^a for each condition, and for (B) 5 mM carbonate buffer was used. Error bars represent duplicate measurement-derived standard deviations. ^a The 0 mM $\text{C}_{\text{T,CO}_3}$ experiment was buffered at pH 9.5 using 5 mM borate buffer, known to be unreactive towards e_{aq}^- . ¹⁴	51
Figure 4.2	Degradation profiles of PFBA during UV-sulfite photolysis at (A) various $\text{C}_{\text{T,CO}_3}$ conditions and (B) pH conditions. Symbols represent experimental data while solid lines represent model predictions. Reaction conditions are described in Figure 4.1.....	55
Figure 4.3	(A) Kinetic transient absorption traces for e_{aq}^- decay (measured at 690 nm) at pH 9.5 in solutions amended with varying concentrations of PFHxA and (B) its corresponding Stern-Volmer plot. Solution conditions 40 μM $\text{K}_4\text{Fe}(\text{FN})_6$, 10 μM $\text{K}_3\text{Fe}(\text{FN})_6$, ionic strength = 0.137 M (balanced using NaCl), T = 20 °C, and 40 mM borate buffer. (C) Degradation profile of PFHxA at pH 9.5 and 12 along with model predictions shown as solid lines. Reaction conditions: 10 mM sulfite, 5 mM carbonate, T = 20 °C.....	58
Figure 4.4	Degradation profile for (A) PFOA, (B) PFOS, (C) PFHxS, and (D) PFBS during UV-sulfite photolysis. Reaction conditions: 10 mM sulfite, 5 mM carbonate, T = 20 °C. Experimental data are shown as circles while model simulations using k_{est} values are shown as solid lines.....	59
Figure 4.5	Influence of chain length on rate constant for PFCAs vs. PFSAs.....	62
Figure A.1	Lifetime of e_{aq}^- in the absence of added fluorocarboxylate quencher (i.e, the 0 mM control samples) using excitation wavelengths: (A) 254 nm and (B) 266 nm.....	88
Figure A.2	TFA Stern-Volmer plots determined following $\text{Fe}(\text{CN})_6^{4-}$ photolysis by 254 nm (left) and 266 nm (right) light. Detailed solution conditions can be found in Figure 2.1.....	89
Figure A.3	Example calculation of BDE and E_s° of PFBA determined using the $\omega\text{B97-XD/ aug-cc-pVDZ}$ basis set and level of theory. The SMD implicit solvent model to mimic an aqueous solution environment and all PFCAs were taken to be in the anionic state. “H” denotes enthalpy, while G, n, F, and SHE represent Gibbs free energy, number of electrons transferred, Faraday’s constant, and the standard hydrogen electrode, respectively.....	90
Figure A.4	Effects of (A) pH and (B) ionic strength on lifetimes of e_{aq}^- in the absence of fluorocarboxylate quenchers, along with comparison of the kinetics of e_{aq}^- reaction with PFBA measured at (C) pH 9.2 and pH 12, and (D) $\mu = 0.2$ and 0.63. Solution conditions are the same as those in Figure 1. Ionic strength in (A) kept constant at 0.63 using NaCl. Solution pH in (B) titrated to pH 12 using 1 M NaOH (no buffer). Ionic strength in (C) is 0.63. Solution pH in (D) is 9.2.....	92

Figure A.5	Plots showing influence of ionic strength on measured $\log k_2$ values for PFBA and TFA, including data from the present study (blue symbols) and data previously reported by Huang et al. ⁵⁰ (black symbols). Dashed blue lines show extrapolation of the trend reported by Huang and co-workers to conditions used in the present study.....	92
Figure A.6	e_{aq}^- lifetime measurements in the absence and presence of various fluorocarboxylates added at a concentration of 0.1 mM. Other solution conditions: 40 μ M $K_4Fe(CN)_6$, 10 μ M $K_3Fe(CN)_6$, 40 mM borate buffer, pH 9.2, ionic strength kept constant at 630 mM using NaCl.....	93
Figure A.7	Stern-Volmer plots for mono-, di-, and trichloroacetate reduction by e_{aq}^- produced at similar conditions as those described in Figure 2.1.....	94
Figure A.8	Bond dissociation energies for each unique C-C and C-F bond in the fluorocarboxylate structures. Values provided in kcal/mol and are separated by two carbon (left), three carbon (middle), and four carbon (right) compounds. Bonds highlighted in red depict strong bonds that are relatively hard to break (≥ 100 kcal/mol), while yellow and green depict moderate (90–100 kcal/mol) and weak (< 90 kcal/mol) bonds, respectively. Red atoms = oxygen; blue = fluorine; grey = hydrogen.....	95
Figure A.9	Reduction potentials in volts for each unique C-F bond. As before, these are separated by four, three, and two carbon compounds. Values in red represent bonds that are relatively hard to reduce (≥ 2 V), while yellow and green depict moderately (1.7–1.9 V) and easily (< 1.7 V) reducible bonds, respectively.....	96
Figure A.10	(Left) Transient absorbance traces depicting the decay of the characteristic 690 nm e_{aq}^- peak after photolyzing $K_4Fe(CN)_6$ with 254 or 266 nm light (specified in Table 2.1). (Right) Corresponding Stern-Volmer plots. Error bars represent one standard deviation, and uncertainties of the k_2 values represent standard errors of the regression-derived slope values using the <i>linest</i> function in Excel. Solution conditions the same as Figure 2.1.....	97
Figure B.1	Hydrated electron lifetimes measured at various pH conditions in the absence of added carbonate. Reaction conditions are listed in Table 3.1.....	108
Figure B.2	Speciation diagram of dissolved carbonate at I.S. = 0.5 M and 20 °C calculated using Visual MINTEQ.....	108
Figure B.3	Stern-Volmer plot for all LFP measurements at pH conditions < 9 where e_{aq}^- lifetimes are plotted as a function of $H_2CO_3^*$. Species concentrations were calculated using Visual MINTEQ.....	109
Figure B.4	Bronsted law for the conversion of e_{aq}^- to H^\bullet by HCO_3^- (from this study), as well as values for other protonated acids. Solid black line represents the line of best fit determined from linear regression used to predict $k_{H_2CO_3}$ ($pK_a = 3.5$, red symbol). Refs. ^{68,134,162,163}	109
Figure B.5	(Left) Transient absorbance traces depicting the decay of the characteristic 690 nm e_{aq}^- peak after photolyzing $K_4Fe(CN)_6$ with 266 nm light. (Right) Corresponding Stern-Volmer plots. Error bars represent one standard deviation. Uncertainties of the k_{app} values represent standard errors of the regression-derived slope values using the <i>linest</i> function in Excel. Solution conditions are outlined in Table 3.1.....	110
Figure C.1	k_2 dependence on μ for TFA and PFBA obtained from Huang et al. (solid markers) and this study (hollow markers) used for ionic strength corrections.....	117

Figure C.2	Effect of dissolved carbonate on observed rate constants of (left) PFPrA and (right) TFA. Reaction conditions are described in Figure 4.1.....	119
Figure C.3	Effect of pH on observed rate constants of (left) PFPrA and (right) TFA. Reaction conditions are described in Figure 4.1.....	119
Figure C.4	Degradation profiles of (top) PFPrA and (bottom) TFA during UV-sulfite photolysis at various C_{T,CO_3} conditions. Symbols represent experimental data while solid lines represent model predictions. Reaction conditions are described in Figure 4.1.....	120
Figure C.5	Degradation profiles of (top) PFPrA and (bottom) TFA during UV-sulfite photolysis at various pH conditions. Symbols represent experimental data while solid lines represent model predictions. Reaction conditions are described in Figure 4.1.....	121
Figure C.6	Degradation profiles of (top) TriFBA and (bottom) TFMS during UV-sulfite photolysis at pH 9.5 and 12. Experimental data is represented by symbols while model simulations are shown as solid lines. Bimolecular rate constant for TriFBA modeling was measured in our previous work, while that for TFMS was estimated using a method described in Chapter 4.....	122
Figure C.7	(Top) Kinetic transient absorption traces for e_{aq}^- decay (measured at 690 nm) at pH 9.5 in solutions amended with varying concentrations of PFOA and (bottom) its corresponding Stern-Volmer plot. Solution conditions are described in Figure 4.3.....	123
Figure C.8	(Top) Kinetic transient absorption traces for e_{aq}^- decay (measured at 690 nm) at pH 9.5 in solutions amended with varying concentrations of PFBS and (bottom) its corresponding Stern-Volmer plot. Solution conditions are described in Figure 4.3.....	124
Figure C.9	(Top) Kinetic transient absorption traces for e_{aq}^- decay (measured at 690 nm) at pH 9.5 in solutions amended with varying concentrations of PFHxS and (bottom) its corresponding Stern-Volmer plot. Solution conditions are described in the main text in Figure 4.3.....	125
Figure C.10	Degradation profile for (A) TFA and (B) PFOA during UV-sulfite photolysis. Reaction conditions: 10 mM sulfite, 5 mM carbonate, T = 20 °C. Experimental data are shown as circles while model simulations are shown as lines. Rate constants are from Amador et al., ¹²¹ Huang et al., ⁵⁰ and Maza et al. ⁸⁷	126
Figure C.11	Observed rate constants of (A) PFCAs vs. (B) PFSA. Reaction conditions are described in Figure 4.4.....	126

LIST OF TABLES

Table 2.1	Summary of abbreviations, structures, solutions conditions, and k_2 values of ultra-short chain fluorocarboxylates determined in the current work along with previously reported values. Solution preparation details and kinetics data values can be found Appendix A.....	19
Table 3.1	Summary of k_{app} values determined at various pH conditions using LFP along with corresponding α values at each condition determined using Visual MINTEQ at ionic strength (μ) of 0.5 M and temperature fixed at 20 °C.....	39
Table 4.1	Summary of rate constants of per- and polyfluoroalkyl substances. Reaction conditions: 10 mM sodium sulfite, 5 mM sodium bicarbonate. ^a Unless otherwise noted, rate constants are from Amador et al. ¹²¹ ^b Estimated bimolecular rate constants. ^c Rate constant determined using LFP in this study. ^d Tenorio et al. ⁸⁵ Reaction conditions: 10 mM sodium sulfite, 5 mM sodium bicarbonate, pH 9.5, T = 20 °C.....	63
Table A.1	Chemical concentrations of stock solutions used in experiments. ^a Fluorocarboxylate stock solutions were prepared in deoxygenated water from chemicals containing no organic cosolvent to avoid artifacts such as e_{aq}^- reacting with non-target constituents...	87
Table A.2	Equations used to calculate global properties of fluorocarboxylates using DFT-calculated properties.....	90
Table A.3	Global molecular properties of fluorocarboxylates in the anionic singlet state calculated by density functional theory.....	94
Table A.4	Optimized ω B97-XD/aug-cc-pVDZ geometries in SMD.....	101
Table B.1	Chemical concentrations of stock solutions used in constant irradiation (C.I.) and laser flash photolysis (LFP) experiments.....	107
Table B.2	Gradient pump method used for PFOS analysis on LC-QqQ-MS.....	107
Table C.1	Chemical concentrations of stock solutions used in constant irradiation (C.I.) and laser flash photolysis (LFP) experiments.....	116
Table C.2	Gradient pump method used for PFOS analysis on LC-QqQ-MS.....	116
Table C.3	Comparison of measured, estimated, and corrected rate constants for reactions of e_{aq}^- with target contaminants and other quenchers at specified ionic strengths.....	117
Table C.4	Values to determined rate of hydrated electron production , background scavenging capacity, and hydrated electron availability at pH 9.5 and 12.....	118

ACKNOWLEDGEMENTS

I would like to express my deepest gratitude to my mother and father who have no idea what a dissertation is but have emphasized the importance of education my entire life. You inspired me and my brother to pursue PhDs without us (or you) even knowing.

Of course this work would not have been possible without my advisors. My greatest respects go to Prof. Timothy Strathmann, whose mentorship and expertise were indispensable throughout this process. I thank you for setting high standards, allowing me to explore my own ideas, and providing the guidance I needed to bring those ideas to fruition. Learning from you during my time at Mines has allowed me to grow into a more efficient, confident, and thorough researcher. I am also very grateful to Prof. Shubham Vyas, who welcomed me into his research group with energy, enthusiasm, and about a thousand research questions. Thank you for always getting me excited about science.

Thank you to my thesis committee, Prof. Christopher Higgins, Prof. Bettina Voelker, and Prof. Cristian Ciobanu for their valuable feedback and thought-provoking questions which helped guide this research. Special thanks to Prof. Chris Higgins for fostering community amongst research groups and taking an active interest in the success of his students and those around him.

I would also like to thank members of the Strathmann and Vyas research groups who made this journey far more tolerable. Dr. Shilai Hao, you are a remarkably impressive scientist and an equally impressive snowboarder. Thank you for introducing me to authentic Chinese food, teaching me the funniest card games, and being the best snowboarding student. Dr. Asa Carre-Burritt, thank you for always going out of your way to help others, being an integral part of the Vyas group (especially with that laser!), and setting high standards with your writing. Dr. Raul Tenorio and Dr. Jiaoqin Liu, thank you both for training me and sharing laughs while doing it. Dr. Charlie Liu and Dr. Daniel Van Hoomissen, thank you for setting an example of quality research and allowing me to learn from you both. All other members, both current and previous, as well as my friends in CEE, materials science, and chemistry departments, I'll never forget the camping, backpacking, and ski trips, GCB outings, 14ers, potlucks, and game nights that we've shared. I have countless cherished memories from graduate school thanks to each of you. And finally, I would like to thank my partner, Nicholas Gonda, for the endless love, support, and patience that he gave me during these stressful years. Our sunset hikes up to high peaks, long conversations on the roof, snowboard lines down steep gullies, and our chill days doing nothing when we needed to relax are what got me through grad school.

Iniaalay ko ito kay nanay at tatay

CHAPTER 1 INTRODUCTION

1.1 Motivation

In the 1962 environmental science book “Silent Spring,” author Rachel Carson warns of how unchecked production of pesticides, pharmaceuticals, and other industrial chemicals have polluted all environmental systems and caused severe medical issues for animals and humans alike.¹ At that time, there were 200 pesticides on the US market whose production was over 600 million pounds.² Carlson’s publication has been credited with catalyzing the modern environmental movement and launching the field of ecotoxicology. Despite increased interest in environmental conservation over the past few decades, production of synthetic chemicals continues to grow at an alarming rate. In fact, the production capacity of the global chemical industry has almost doubled from 1.2 billion tons in 2000 to 2.3 billion tons in 2017.³ In 2020, Wang and co-workers created the first global inventory listing the number of chemicals on the market, reporting that more than 350,000 chemicals and mixtures of chemicals are registered for commercial production, a number 3x more than what was previously estimated.⁴ Of this alarming amount of chemicals produced globally, roughly 120,000 substances could not be conclusively identified. Mass production of synthetic compounds causes their inevitable release into the environment, polluting the air, water, soil, and sediments. Unfortunately, technologies and practices for detecting, removing, and destroying these chemicals cannot keep up with their staggering production amounts and chemical diversity.

Water contamination is especially important because it is both scarce and crucial for essentially every aspect of life. Less than 1% of the total water supply on earth is available for human use with the rest being held up in saline bodies of water such as seas, oceans, and bays or locked in glaciers, icecaps, and permanent snowfields. Water reserves are even further diminished because of the chemical pollution released by manufacturing, industry, and agriculture, as was warned by Carson decades ago. Waterborne diseases (e.g., diarrhea, endocrine disruption, cancer, etc.) are strongly associated with water contamination and have caused an estimated 1.7 billion illnesses and 1.4 million premature deaths worldwide in 2015, representing one of the most important issues facing us today.^{5,6}

Urbanization and industrialization will continue to contaminate our water reserves, highlighting the need for highly effective and sustainable water purification methods (i.e., disinfection, decontamination, remediation, etc.) to sustain life on Earth. What’s more is that these synthetic chemicals are often engineered to possess high stability which renders them remarkably resistant towards natural attenuation processes and leads them to accumulate in high concentrations in the environment.^{7,8} Conventional and advanced techniques including adsorption, membranes, biological methods, oxidation

using chlorine and ozone, among others, have been greatly successful in purifying water, however the rate at which new chemicals are synthesized is astounding, making it difficult for these treatment techniques to keep up.²

1.2 PFAS Background

One such class of environmental contaminants that are unabated by conventional water treatment methods are known as per- and polyfluoroalkyl substances (PFASs). These are anthropogenic organic chemicals that contain at least one carbon-fluorine bond; however typically PFASs are highly fluorinated.⁹ The properties that these chemicals possess make them remarkably unique and incredibly useful in everyday applications as well as industrial use. The C-F bond is the strongest single bond known in organic chemistry (105.4 kcal/mol).¹⁰ Fluorine, being the most electronegative element, pulls electron density away from carbon and towards itself, causing a large degree of polarization between carbon and fluorine with partial positive and negative charges on each atom, respectively. The C-F bond is covalent in nature; however, this polarization imparts additional stabilization through strong electrostatic interactions. This bond strength yields PFAS thermally stable up to 1,000 °C for certain compounds.^{11,12}

The electronegativity of fluorine also confers resistance towards chemical reduction because of the poor polarizability of the C-F bond making fluoride a poor leaving group when compared to chlorinated analogues.^{13,14} Further adding to their inertness, fluorinated compounds are also resistant towards oxidation. Fluorine is about 25% larger than hydrogen (1.47 Å and 1.2 Å, respectively),^{10,14} making fluoroalkyl moieties sterically bulkier than the corresponding hydrocarbons. This steric hindrance contributes to the helical nature of perfluorinated compounds which effectively shields the carbon backbone from oxidative attack.^{13,15} In addition to remarkable chemical and thermal stability, the physical properties PFAS possess render them uniquely useful among a variety of applications. Their low coefficient of friction allows them to repel both aqueous and organic media, a characteristic which gave them much use in nonstick cookware, stain resistance, and water proofing.¹⁶ Meanwhile, a large subset of PFAS exists as perfluoroalkyl acids (PFAAs) which are distinguished by the presence of both hydrophobic and hydrophilic moieties giving them use as surfactants and emulsifiers.

While these properties make PFAS incredibly useful in various products and processes, their stability poses significant remediation challenges because conventional water treatment methods are insufficient at destroying PFAS, and they are not known to readily degrade in the environment.¹⁷ This recalcitrance, along with their mobility in water, allow them to undergo long range transport, and as a result, they have been detected in high concentrations in remote locations around the globe such as the Arctic.^{18,19} Along their journey across the globe, PFASs have made their way into 97% of Americans and have been detected at alarmingly high concentrations in fish as well as other biota.²⁰ The widespread use

and occurrence of PFASs are especially concerning because of the potential health risks that these compounds have been associated with such as impacts on developmental, liver, immune and thyroid systems, as well as cancer.²¹⁻²³ The discussion above collectively highlight why PFAS are of such importance in environmental science and engineering today: they are toxic,²⁴⁻²⁶ bio-accumulative,^{27,28} recalcitrant,²⁹ and widespread.^{30,31}

Remediation of PFAS-impacted water is typically achieved through adsorption using activated carbon and ion exchange; however, this is less effective for short-chain PFAS.³² Membrane technologies such as reverse osmosis and nanofiltration have shown promise for removing most PFAS, including short chains, and can meet the low levels required of treated water. These methods, however, are purely separative and create a PFAS-concentrated byproduct stream (e.g., saturated adsorbents and membrane reject) that must be further dealt with prior to disposal. Destroying PFAS is extremely challenging due to their unique characteristics discussed above. Many researchers are investigating potential technologies for PFAS destruction, including thermal-, oxidation-, and reduction-based technologies. However, success of these technologies has been limited.³³ Electrochemical oxidation (EO) operates by exerting high electrical current densities through a conductive solution between an anode and a cathode. This results in PFAS degradation via two mechanisms: direct oxidation involving electron transfer from PFAS to the anode, and indirect oxidation involving electron transfer from PFAS to powerful oxidants generated throughout the solution. Treatment of PFAS-contaminated water has demonstrated impressive removal efficiencies (> 99% for long-chain PFAS); however treatment of PFAS precursors by EO has led to an increase in concentration of stable, chain-shortened PFAS products.³⁴⁻³⁶ Another method involving sonochemistry employs the use of acoustic energy to generate and implode vapor bubbles which results in the breakdown a molecule through combustion, pyrolysis, and radical reaction mechanisms which occur at a bubble-water interface.³⁷ Sonolytic treatment has proven to be extremely efficient, achieving near-complete mineralization of PFOA and PFOS to CO, CO₂, F⁻, and SO₄²⁻.³⁸ However, success of this method relies on localized incineration which is only active for short periods of time (ns) and thus requires partitioning to the bubble-water interface. This renders it less effective for short-chain structures which are not likely to partition to these reactive localities. In addition, sonolysis has been shown to form nitrite and nitrate ions which could be problematic at scale.³⁹ The most widely used destruction method for PFAS is that of thermal degradation or incineration which can be applied to various contaminated media. Incineration facilities are common in the industry and therefore cost of implementing this technique is expected to be comparatively lower than other treatment methods.⁴⁰ The major downfall of incineration involves the generation of waste byproducts including bottom ash, particulate matter, volatile products, and importantly, products of incomplete combustion (PICs) such as smaller PFAS.

1.3 UV-ARP Background

Advanced reduction processes (ARPs) have emerged as a promising means of PFAS treatment due to their wide applicability, ability to achieve complete mineralization of organic pollutants, and efficiency.⁴¹ ARPs are a class of water treatment technologies that generate reductive radicals which are highly reactive towards various classes of recalcitrant contaminants. ARPs operate similarly to the better-known advanced oxidation processes (AOPs) except that reducing free radicals such as e_{aq}^- and $H\cdot$ are produced rather than oxidizing free radicals such as $OH\cdot$. The development of ARP treatment technologies is motivated from the fact that many pollutants ubiquitously found in the waters, particularly highly oxidized contaminants, are not easily abated by traditional AOP methods. Among the many substrates, in addition to PFAS, which have been found to readily transform during ARP treatment are oxyanions, highly oxidized metals, and chlorinated solvents.⁴²⁻⁴⁴

ARPs are generally based on the photochemical production of e_{aq}^- by UV light. The hydrated electron possesses a low and negative reduction potential of -2.9 V, making it a potent reducing species with strong nucleophilic character.^{45,46} In addition, e_{aq}^- preferentially attacks electron withdrawing groups on organic compounds which could promote halogen release during the remediation of persistent organic pollutants over chain-shortening, a mechanism which occurs in the oxidative degradation of PFAS and yields stable perfluorinated transformation products.

Investigations into e_{aq}^- processes for contaminant degradation are most commonly performed in constant UV irradiation, or bulk photolysis, systems which are representative of UV treatment in practice. Bulk photolysis methods generate a steady-state concentration of e_{aq}^- throughout the duration of the reaction (typically minutes to hours), and samples are periodically collected to measure the disappearance of the target contaminant of interest. While these studies provide valuable information regarding the implementation of e_{aq}^- processes for remediation under specific conditions, these systems are limited to measuring apparent rates of degradation for target contaminants since identities and concentrations of transient reactive species (including e_{aq}^-) are typically not monitored with these methodologies. This makes comparison across different systems and environments difficult due to the overall lack of knowledge of the complex roles that various system and solution parameters have on treatment results.

Pulse radiolysis is a method for generating reactive species by causing molecular rupture using ionizing radiation.⁴⁷ Decomposition of water via pulse radiolysis is one of the most important and well-known radiation-based chemical reactions. Hydrated electrons were first discovered in the 1960s using this method, and although this method produces a variety of other reactive species (e.g., $H\cdot$, $OH\cdot$, O_3), it is often considered one of the simpler ways to study the system because e_{aq}^- is generated directly from water.⁴⁸

Laser flash photolysis is another method for studying reactive species. This method involves photoexcitation of a chemical sensitizer rather than molecular rupture. Unlike constant UV irradiation systems, both pulse radiolysis and LFP provide direct kinetic measurements of reactions of short-lived species such as e_{aq}^- . This eliminates other adventitious processes downstream of the initial reduction event that might also affect overall reactions of interest because measurements occur on such short timescales (i.e., ns– μ s). In addition, the large extinction coefficient of e_{aq}^- allows researchers to study e_{aq}^- reactions in complex solutions because the broad features in its transition absorption spectrum ($\lambda_{max} \sim 690$ nm) do not overlap with the spectra of many other chemical species, particularly organic molecules.^{48–50} Therefore, pulse radiolysis and LFP techniques are favorable over bulk photolysis when information regarding the fundamental kinetics of e_{aq}^- reactions are desired.

1.4 System and Solution Effects on UV-ARPs

As previously mentioned, investigations into the use of e_{aq}^- -based UV-ARPs for PFAS remediation have typically been performed using bulk photolysis methods and report the effects of various parameters on treatment efficacy, potential mechanisms, and means of optimization.

Impact of Sensitizers. One such parameter of interest for optimization is choice of photosensitizer. Hydrated electrons can be generated from the photolysis of many organic and inorganic chemicals using appropriate wavelengths of light. Sensitizers capable of ejecting an electron using 254 nm light are of particular interest due to the widespread use of these light sources in established water treatment technologies. Among the various chemicals capable of e_{aq}^- production, various photosensitizers have already been reported to effectively destroy PFAS in water such as sulfite (SO_3^{2-}), iodide (I^-), ferrocyanide ($[\text{Fe}(\text{CN})_6]^{4-}$), nitriloacetic acid (NTA), and indole.⁵¹ The amount of e_{aq}^- produced will vary with identity of the photosensitizer because these differ in molar absorptivity (ϵ), quantum yield (ϕ), and in the formation of other reactive species and byproducts upon photolysis.

Iodide salts have been one of the most commonly studied sensitizers for production of hydrated electrons because iodide ion (I^-) absorbs UV light efficiently ($\epsilon = 172 \text{ M}^{-1} \text{ s}^{-1}$ at 254 nm), and e_{aq}^- release is photolabile via charge transfer to solvent (CTTS) transition with a quantum yield of 0.286 at 248 nm.^{52,53} While UV-iodide has been applied to successfully eliminate several persistent contaminants including PFAS,⁵⁴ performance of this system is significantly hindered by e_{aq}^- scavenging by dissolved oxygen and reactive iodine species (RIS) generated during the UV activation process. Qu et al. studied the effect of iodide dose on decomposition rate and observed a clear maximum at 0.3 mM.⁵⁴ Judicious sensitizer dose is imperative not only to maximize e_{aq}^- production and minimize its quenching by RIS, but also to avoid adding high concentrations of iodide to treated water.

Another aqueous ion ferrocyanide ($[\text{Fe}(\text{CN})_6]^{4-}$), while not relevant for practical applications due to the presence of cyano groups, has an extremely high extinction coefficient and quantum yield of $4273 \text{ M}^{-1} \text{ cm}^{-1}$ and 0.674 at 248 nm, respectively, and is capable of producing abundant e_{aq}^- .⁵⁵ This makes ferrocyanide an attractive sensitizer to use in LFP experiments, a method which, as previously mentioned allows for the direct measurement of e_{aq}^- processes.

Indole derivatives, such as 3-indoleacetic acid, have been investigated for UV-ARP sensitizers, and due to their high extinction coefficient of $3400 \text{ M}^{-1} \text{ cm}^{-1}$ and relatively high QY of 0.14 both at 254 nm, they are expected to yield high rates of e_{aq}^- formation.⁵⁶ However, previous studies of this system observed no difference between the results for direct photolysis and 1 mM 3-indoleacetic acid suggesting that its effect was negligible.⁵⁷ The authors attribute this finding to high rate of e_{aq}^- scavenging by indole photoproducts, and remedied this by incorporating organo-modified montmorillonite clay into the system which provides a negatively charged surface that can stabilize indole radical cations thus hindering their reaction with e_{aq}^- . In the UV-NTA-montmorillonite system, PFOA can be completely removed after about 6 h; however practical implementation is challenged by the cost and resources required to synthesize indole molecules at scale as well as the high organic carbon residual left in the treated water.

Aminopoly(carboxylic acid)s (APCAs) have recently been proposed to enhance e_{aq}^- concentration in bulk solution during water photolysis by quenching the oxidative species produced in the process, namely hydroxyl radicals ($\text{OH}\cdot$). Studies employing nitritotriacetic acid (NTA) for contaminant degradation have shown promise;⁵⁸ however application of UV-NTA in field applications may be complicated by groundwater matrices and the generation of urea byproducts which cause a pungent odor, both of which are not ideal for practical treatment.⁵⁹ In addition, important characteristics of photochemical systems such as molar absorptivity and quantum yield are either not known or not well understood. For example, while molar absorptivity of NTA is known ($\epsilon = 26.3 \text{ M}^{-1} \text{ cm}^{-1}$ at 254 nm), it itself is not producing e_{aq}^- . Rather, photoexcited NTA (NTA*) serves as an $\text{OH}\cdot$ quencher to allow e_{aq}^- generated from water photolysis to escape into the bulk solution.⁵⁸ Therefore, the molar absorptivity of NTA cannot be directly used to estimate e_{aq}^- generation. For similar reasons, the quantum yield of NTA is not known.

Perhaps the most well studied and practically implemented ARP system is UV-sulfite. However, with an extinction coefficient of $18.4 \text{ M}^{-1} \text{ cm}^{-1}$ at 254 (almost 10x lower than iodide) and a quantum yield of 0.116 at 248 nm, the UV-sulfite system is not expected to have a high e_{aq}^- formation rate.^{55,60} Nevertheless, it is preferred to other systems for a few reasons. Sulfite salts are low cost and the main byproduct of sulfite activation, sulfate, is nontoxic and ubiquitous in natural waters. In fact, sulfite has an extensive history of use at wastewater treatment facilities for dechlorination of treated wastewater before

discharging.⁶¹ A very important advantage is sulfite's ability to scavenge dissolved oxygen (DO), an efficient e_{aq}^- quencher ($k_2 = 1.9 \times 10^{10} \text{ M}^{-1} \text{ s}^{-1}$).⁶² UV-ARP operation using other sensitizers require extensive steps to remove DO before treatment; otherwise little to no degradation is observed, whereas the autoxidation of sulfite ions can rapidly deplete DO from the system allowing it to be applied to water sources that are initially oxidic.^{59,63}

Impact of Weak Acids and Other Common Water Constituents. While extinction coefficient and quantum yield are important parameters which affect treatment efficacy through e_{aq}^- generation, it is the steady state e_{aq}^- concentration ($[e_{aq}^-]_{ss}$) during UV-ARPs that is critical to ensuring reaction with the target contaminants. For example, although sulfite does not absorb light very well and electron ejection is not photolabile, sulfite's ability to inhibit the reaction between e_{aq}^- and DO has yielded it the most successful for practical applications because it increases $[e_{aq}^-]_{ss}$ by decreasing e-aq scavenging.

Common water constituents such as carbonate, nitrate, dissolved oxygen, among others are also known to affect e_{aq}^- treatment processes. Their effect can be through many processes such as e_{aq}^- scavenging, UV shielding, further e_{aq}^- production, among others. Dissolved oxygen, nitrate, and carbonate, common in natural waters, are all efficient quenchers of e_{aq}^- , therefore their presence decreases the $[e_{aq}^-]_{ss}$ as well as the overall efficiency of UV-ARPs.^{62,64} Meanwhile, chloride and phosphate, also common in natural waters, have shown negligible effect of UV-ARPs suggesting these are poor e_{aq}^- scavengers.⁶⁴

The effect of dissolved/natural organic matter (DOM/NOM) is more complicated than the effect of the most other common water constituents such as those previously mentioned. Reports investigating the role of humic acid (HA), representative of DOM, have shown both enhancement as well as inhibition on UV-ARP treatment. HA effects are dependent on HA concentration as well as sensitizer system, suggesting that various competitive pathways dictate its influence. In the UV-iodide system, Sun et al. report enhanced and inhibited PFOS degradation in the UV-iodide system in the presence of 1 and 30 mg/L HA, respectively.⁶⁵ Interestingly, both the inhibitory and enhanced impact of HA on PFOS degradation percent seem to only affect the UV-iodide system during the first 4 hours, after which it reached a plateau (~95%). However, defluorination percent (deF%), which is defined as the ratio of the concentration of F⁻ released during a reaction over the total F in the parent compounds initially, was highest in the presence of 30 mg/L HA (near 100% after 8 h).⁶⁵ The effect of HA on PFOS degradation in the UV-sulfite system has been studied in the vacuum UV-sulfite (VUV-sulfite) system up to 5.43 mg/L DOC in which only an inhibitory effect was observed. Ren et al. also showed inhibitory effects of HA on PFOA degradation, although the lowest concentration studied was 10 mg/L.⁶⁴ Among the main inhibitory mechanisms of HA are UV blocking effects, generation of oxidative e_{aq}^- quenchers (e.g., OH[•], ¹O₂,

H₂O₂), and presence of electron withdrawing moieties within the HA structure which are also capable of reacting with e_{aq}^- .⁵¹

Impact of pH. Solution pH also plays a complex role in efficacy of UV-ARPs. Literature results indicate that higher pH facilitates the reductive destruction of PFAS. The increased efficacy of e_{aq}^- processes at highly alkaline pH conditions (~12.0) has principally been attributed to less e_{aq}^- scavenging by H⁺ ($k_2 = 2.3 \times 10^{10} \text{ M}^{-1} \text{ s}^{-1}$),⁶² and thus a higher amount of e_{aq}^- available for PFAS destruction. However, at the alkaline pH conditions frequently used in UV-ARPs, H⁺ scavenging is mostly negligible in common sensitizer systems.⁶⁶

The effect of solution pH on ARP efficiency truly comes into play when considering speciation of common water constituents as well as the sensitizer. For example, the UV-NTA system operates by eliminating OH[•] generated from water photolysis. This allows e_{aq}^- to escape reactive spurs and diffuse into the bulk solution.⁵⁸ The reactivity of NTA with OH[•] is dependent on its level of deprotonation, with the fully deprotonated species being the most reactive (pK_as = 0.8, 1.9, 2.48, and 9.65). As such, UV-NTA operates most efficiently at alkaline pH conditions.⁶⁵

The UV-sulfite system also performs best at highly alkaline pH conditions. As previously mentioned, multiple studies attribute this to less quenching of e_{aq}^- by H⁺; however, speciation of the sulfite sensitizer is more likely the reason for the enhanced degradation. The pK_a of bisulfite (HSO₃⁻, conjugate acid of the sulfite sensitizer) is 7.2 meaning that in a system containing 0.01 M total dissolved sulfite (C_{T,S03}) at 20 °C and 0.05 M ionic strength (μ; M), there will be $2.65 \times 10^{-5} \text{ M}$ and $8.40 \times 10^{-8} \text{ M}$ bisulfite present at pH 9.5 and 12, respectively, a difference of more than three orders of magnitude. Speciation of sulfite as bisulfite is important because photolysis of HSO₃⁻ has a low quantum yield of e_{aq}^- ($\phi_{e_{aq}^-}$)⁶⁷ which in turn generates less e-aq. More importantly, bisulfite itself is a e_{aq}^- scavenger ($1.2 \times 10^8 \text{ M}^{-1} \text{ s}^{-1}$).⁶⁸ Therefore, pH affects both the generation and scavenging aspects of the UV-sulfite system; however, the latter plays a far greater role in overall ARP treatment efficiency (discussed *vide infra*).

In contrast, UV-ARPs employing iodide and indole derivatives have not shown the same pH sensitivity. For example, Tian et al. investigate the UV-indole-montmorillonite UV-ARP system from pH 3.0 – 11.0 and report no significant difference between the conditions for PFOA degradation throughout the entire reaction.⁵⁷ The authors postulate that this pH independence is due to microenvironments within the organo-modified clay where small cations are substantially replaced by large modification organic cations which effectively inhibits quenching of photo-generated e_{aq}^- by H⁺. Similarly, Park et al. report pH independence of apparent rate constant (k_{app}) in the UV-iodide system from pH 2.0–12.0 because photoproduction of e_{aq}^- from I⁻ is unaffected by pH above a value of 3.⁶⁹ Hydrated electron quenching by H⁺ in acidic conditions, however, will be orders of magnitude greater than in circumneutral conditions,

and so the pH invariance between pH 2.0 and 12.0 is surprising. It is likely that at the high $[I^-]$ dose used by Park et al. (10 mM) yields elevated concentrations of RIS making them the most prevalent e_{aq}^- quencher rather than H^+ .

1.5 Research Goals

Many solution conditions can affect UV-ARP treatment efficacy. To ascertain individual solution impacts, multiple batch experiments must be run varying one parameter systematically while keeping all other conditions constant. This method is inefficient since it is time and resource intensive. What's more is that comparison across studies in the literature is often complicated because of the multifaceted effects many parameters impart on treatment results. This highlights the need for more systematic approaches to optimize solution conditions more efficiently and quantitatively interpret the individual effects of various water quality parameters.

The overall objective of this thesis is the development of a comprehensive UV-sulfite photochemical model for the prediction of treatment efficacy in new environments which can facilitate treatment optimization as well as the quantitative elucidation of how individual system and solution parameters effect treatment results. Specifically, this thesis will investigate the kinetics and mechanisms of e_{aq}^- reactions with PFAS and common water constituents, then use these fundamental insights to adapt a kinetic model to simulate parent compound degradation in different geochemical conditions.

The first and second objectives of this thesis were to investigate the kinetics and mechanisms of the reactions between e_{aq}^- and ultra-short chain PFCAs and ubiquitous carbonate species, respectively, while the third objective was to incorporate insights from the previous two objectives with kinetics equations to adapt a model for predicting PFAS degradation during UV-sulfite treatment. This thesis provides the tools needed to optimize UV-sulfite ARPs more efficiently and serves as a framework for kinetics models in different UV-ARP systems (e.g., iodide, indole, NTA, etc.).

Chapter 2: Kinetics and Mechanisms of Hydrated Electron Reactions with Ultra-Short Chain Fluorocarboxylates

Traditional laboratory techniques are unable to measure the fundamental kinetics of e_{aq}^- reactions since these occur on nanosecond timescales. Information regarding e_{aq}^- reactions with target contaminants are largely drawn from experiments performed in constant UV irradiation systems in which only apparent rates of degradation can be inferred since the identity and concentrations of transient reactive species, including e_{aq}^- , are unknown. Therefore, the first objective was to accurately measure bimolecular rate constants (k_2 ; $M^{-1} s^{-1}$) of e_{aq}^- reactions with PFASs and elucidate the initial mechanisms by which these

reactions occur. To this end, LFP was employed to directly measure e_{aq}^- processes with PFAS targets, and density functional theory (DFT) was used to calculate molecular properties and provide mechanistic information into how these reactions take place. A suite of ultra-short chain fluorocarboxylates were investigated because these structures are soluble into the millimolar range without micellar aggregation being prevalent. In addition, ultra-short chain PFAS are often overlooked in literature studies despite their ubiquity in the environment, and so focusing on this subclass will provide much needed insights into their behavior and properties.

Chapter 3: Influence of Carbonate Speciation on Hydrated Electron Treatment Processes

UV-ARPs based on the photochemical generation of e_{aq}^- have been reported to achieve complete defluorination of PFAS at highly alkaline pH conditions yet perform poorly at moderately alkaline and lower pH conditions. The inadequacy of e_{aq}^- processes at lower pH conditions has most often been attributed to scavenging by H^+ . However, recent studies suggest that changing speciation of e_{aq}^- quenchers in the solution could instead be the reason.^{66,68} Therefore, the second objective of this thesis was to reinvestigate the reasons for poor performance of e_{aq}^- processes at lower pH conditions. To achieve this, e_{aq}^- scavenging by ubiquitous carbonate species was evaluated and compared with sulfite and H^+ across a broad pH range. In addition, the impact of total dissolved carbonate and sulfite were compared with scavenging by NO_3^- and DO, two other established e_{aq}^- quenchers that are ubiquitous in natural aquatic systems. To accurately describe scavenging by carbonate, determination of biomolecular rate constants for each species ($H_2CO_3^*$, HCO_3^- , CO_3^{2-}) are needed. To this end, LFP was used with nonlinear regression analysis to determine species-specific rate constant values of carbonate with e_{aq}^- . The resulting values were then used together with reported rate constants for other e_{aq}^- quenchers in model simulations spanning a wide range of conditions that might be expected when treating PFAS-contaminated groundwater with UV-sulfite ARP.

Chapter 4: Kinetic Model for Predicting PFAS Degradation During UV-Sulfite Treatment

Development of a photochemical model to predict target contaminant degradation across diverse environments is an alternative approach to optimizing e_{aq}^- processes and minimize the need to run multiple batch experiments to ascertain the effect of a single parameter. These models require accurate k_2 values of e_{aq}^- with target contaminants and important scavengers as well as information regarding the irradiation source and geochemical conditions. Therefore, the third objective of this thesis will incorporate the kinetics values measured in the previous two objectives into a comprehensive photochemical model to simulate UV-sulfite treatment results for different water matrices, UV irradiation,

and sensitizer conditions. This objective provides a framework for future UV-ARP models and importantly links two different methods (LFP and constant UV irradiation) of investigating e_{aq}^- processes whose results have been in misalignment (*vide infra*). A model was adapted to include important kinetics values as well as parameters relating to the system, light source, and geochemical solution conditions. The impact of pH and alkalinity on PFCA degradation were systematically investigated, then the model was tested using a suite of PFCAs and PFSAs in different environments.

CHAPTER 2
KINETICS AND MECHANISMS OF HYDRATED ELECTRON REACTIONS
WITH ULTRA-SHORT CHAIN FLUOROCARBOXYLATES

Based on a paper published in *Chemosphere*.*

Camille K. Amador^{1,2}, Daniel J. Van Hoomissen¹, Jiaqin Liu^{1,2}, Timothy J. Strathmann², Shubham Vyas¹

2.1 Abstract

Recent reports demonstrate that technologies generating hydrated electrons (e_{aq}^- ; e.g., UV-sulfite) are a promising strategy for destruction of per- and polyfluoroalkyl substances, but fundamental rate constants are lacking. This work examines the kinetics and mechanisms of e_{aq}^- reactions with ultra-short chain (C2-C4) fluorocarboxylates using experimental and theoretical approaches. Laser flash photolysis (LFP) was used to measure bimolecular rate constants (k_2 ; $M^{-1} s^{-1}$) for e_{aq}^- reactions with thirteen per-, and for the first time, polyfluorinated carboxylate structures. The measured k_2 values varied widely from 5.26×10^6 to $1.30 \times 10^8 M^{-1} s^{-1}$, a large range considering the minor structural changes among the target compounds. Molecular descriptors calculated using density functional theory did not reveal correlation between k_2 values and individual descriptors when considering the whole dataset, however, semiquantitative correlation manifests when grouping by similar possible initial reduction event such as electron attachment at the α -carbon versus β - or γ - carbons along the backbone. From this, it is postulated that fluorocarboxylate reduction by e_{aq}^- occurs via divergent mechanisms with the possibility of non-degradative pathways being prominent. These mechanistic insights provide rationale for contradictory trends between LFP-derived k_2 values and apparent degradation rates recently reported in UV-sulfite constant irradiation treatment experiments.

*See Appendix D for permissions

¹Department of Chemistry, Colorado School of Mines

²Department of Civil and Environmental Engineering, Colorado School of Mines

2.2 Introduction

Per- and polyfluoroalkyl substances (PFASs) have been used unregulated in many applications for decades,⁷⁰ but have recently been recognized to be toxic,^{21–23} bioaccumulative,^{27,28} and recalcitrant.²⁹ Unfortunately, environmental release was already widespread by the time their hazards became well known.^{30,31} Treatment of PFAS-contaminated water typically involves physical separation,^{71–75} but these processes ultimately produce a PFAS-enriched byproduct stream that requires further treatment if destruction is the final objective. As a result, there are growing efforts to study the effectiveness of a range of potential destructive treatment technologies, including electrochemical, plasma, photochemical, and thermochemical processes.^{76–80} One group of technologies of interest are advanced reduction processes (ARPs) based on the photochemical generation of hydrated electrons (e_{aq}^-), a transient species with low reduction potential (-2.9 V) and strong nucleophilic character.^{45,46} Recently, many reports have focused on treatment of PFASs and other persistent organic pollutants with e_{aq}^- generated by photo-detachment from sulfite (SO_3^{2-}) upon excitation with common UV light sources, although other sensitizers have been investigated as well.^{41,81–83} From a practical standpoint, e_{aq}^- based technologies are promising because, unlike oxidative hydroxyl radicals, the reactive species is not inhibited by the presence of many ubiquitous constituents in natural water sources such as chloride, phosphate, and hydroxide.⁶⁴ In addition, the autoxidation of sulfite ions in solution acts to scavenge dissolved oxygen, an efficient e_{aq}^- quencher ($1.9 \times 10^{10} \text{ M}^{-1}\text{s}^{-1}$),⁶² facilitative for application to water sources that are initially oxic.^{63,84} In fact, Liu et al. demonstrated >90% PFAS destruction in a pilot treatment study where no efforts were made to remove dissolved oxygen from the groundwater prior to UV-sulfite treatment.⁵⁹

While reports of UV-sulfite and other UV-based technologies for e_{aq}^- generation have shown promise for treatment of PFAS-contaminated water, these studies have largely been limited to measuring apparent rates of degradation for target PFASs under constant UV irradiation conditions where the identity and concentrations of transient reactive species, including e_{aq}^- , are unknown.⁸⁵ While these studies provide valuable information needed for further technology development, comparison among different experimental systems and prediction of treatment efficacy in new environments remains challenging due to a lack of absolute rate constants and a comprehensive photochemical model for generation and reaction of e_{aq}^- .

Laser flash photolysis (LFP) is a method for studying the reactions of short-lived reactive species (i.e., ns – μs lifetimes), such as e_{aq}^- , providing direct kinetic measurements of reactions with target analytes like PFASs while eliminating other adventitious reactions downstream of the initial reduction event. To our knowledge, there are only three previous reports of k_2 measurements for e_{aq}^- reactions with

PFASs and these are limited to fully fluorinated perfluoroalkyl acid structures.^{50,86,87} There are no reports for reactions with partially fluorinated structures despite the growing recognition of their abundance in many sources of PFAS contamination such as aqueous film forming foams (AFFF)⁸⁸ and the environment.⁸⁹ Moreover, there are major discrepancies among these earlier reports. For example, while earlier reports by Huang et al. and Anbar et al. measured k_2 values ranging from $2.3 - 3.4 \times 10^6 \text{ M}^{-1} \text{ s}^{-1}$ for trifluoroacetate (TFA) and $1.3 \times 10^7 \text{ M}^{-1} \text{ s}^{-1}$ for perfluorobutanoate (PFBA), a more recent study by Maza and coworkers reported k_2 values for TFA ($5.0 \times 10^8 \text{ M}^{-1} \text{ s}^{-1}$) and PFBA ($5.4 \times 10^8 \text{ M}^{-1} \text{ s}^{-1}$) that are orders of magnitude greater.^{50,86,87} This large discrepancy highlights the need for additional studies to confirm k_2 values for these structures and to extend the approach to a broader range of both per- and polyfluorinated structures.

Parent compound decay profiles, which are often used to assess the efficacy of ARPs, are highly sensitive to rate constant, and so accurate k_2 values will be key in modeling these processes in different environments. Here, we report on the application of LFP to directly measure k_2 values for e_{aq}^- reacting with thirteen ultra-short chain (C2-C4) fluorocarboxylate structures including fully and partially fluorinated structures, the latter of which has never been measured before. To date, most studies have focused on e_{aq}^- based treatment of longer-chain perfluoroalkyl acids and much less has been reported on ultra-short chain structures despite recent trends wherein manufacturers are substituting shorter chain analogues for legacy PFASs such as perfluorooctanoic acid (PFOA) and perfluorooctane sulfonic acid (PFOS).^{90,91} Since LFP measurements occur on an extremely short timescale, results can be taken as a “snapshot” of the initial reduction events absent of nontarget pathways that might contribute to variable results observed during long-term (e.g., hours or days) UV irradiation experiments. Kinetic parameters and reactivity trends are compared with previous reports from LFP and constant irradiation methods highlighting both similarities and discrepancies among available reports. Variation in k_2 values among the fluorocarboxylates measured here are also analyzed in relation to molecular property descriptors calculated with density functional theory (DFT). The experimental data presented herein alongside computations of molecular property descriptors warrants an extensive computational study on the impact that structural changes of PFAS have on reductive degradation mechanisms. Analysis of the resulting trends are suggestive of divergent rate-determining pathways for e_{aq}^- consumption which has consequence in the design and implementation of ARPs for PFAS treatment.

2.3 Materials and Methods

Reagents and Solutions. A full list of chemical reagents is provided in Appendix A. All stock solutions and reaction samples for LFP experiments were prepared inside an anaerobic chamber (Coy Lab Products; 97% N₂, 3% H₂) using deoxygenated water prepared as described in Appendix A. Samples

prepared in quartz cuvette cells (1 × 1 cm) were capped and sealed with parafilm before removing from the anaerobic chamber to prevent oxygen exposure during LFP measurements.

Laser Flash Photolysis Setup and Procedure. A Nd:YAG laser (Surelite EX, Continuum) operating at 1064 nm with a 10 Hz repetition rate and 4 ns time resolution was used with a 4th harmonic generator to produce 266 nm light. Transient absorbance spectra were collected using LP980 spectrophotometer (Edinburgh Instruments) equipped with ICCD camera and photomultiplier tube. The transient species, e_{aq}^- , was produced by irradiating a mixture of 40 μM $\text{K}_4\text{Fe}(\text{CN})_6$ and 10 μM $\text{K}_3\text{Fe}(\text{CN})_6$ with an 8-10 mJ laser pulse. Decay of e_{aq}^- was monitored by tracking the change in absorbance of its characteristic peak ($\epsilon = 20560 \text{ M}^{-1} \text{ cm}^{-1}$ at 690 nm)^{49,92} using ten averages for each of the measurements. Individual cuvettes were amended with varying concentration (0 – 50 mM) of the target fluorocarboxylate quencher and Stern-Volmer analysis of the change in e_{aq}^- lifetime (τ) was used to determine the k_2 value. Unless otherwise indicated, reaction solutions were buffered at pH 9.2 (borate) and ionic strength was fixed using NaCl. Quenching due to buffer and electrolyte are expected to be negligible, and 0 mM fluorocarboxylate control samples highlight this point by displaying constant e_{aq}^- lifetime across experiments (Figure A.1 in Appendix A). Additional details of solution conditions and preparation are described in Appendix A. All samples were prepared and run in triplicate and uncertainties provided represent triplicate-averaged standard deviations. Separate experiments were conducted for selected fluorocarboxylates at pH 12.0 to evaluate the potential influence of solution pH on k_2 . In addition, τ in the absence of fluorocarboxylate quenchers was measured over a range of pH (3.5 – 12.0) and ionic strength (0 – 650 mM) values to assess the effects of these variables on background quenching. Due to a change in LFP setup during the course of the study, certain compounds (indicated in Table 2.1) were measured after exciting the sensitizer with 254 nm laser pulse. This is not expected to affect the measured rate constant values because the absorption spectrum of the sensitizer, $\text{K}_4\text{Fe}(\text{CN})_6$, shows strong absorption at all wavelengths <300 nm,⁹³ and tests conducted with TFA using both excitation wavelengths yielded similar k_2 values (see Figure A.2).

Density Functional Theory Calculations. DFT was used to calculate molecular property descriptors for the thirteen target fluorocarboxylate structures that were subjected to LFP measurements. Stationary points were located using the density functional $\omega\text{B97-XD}$ with the aug-cc-pVDZ basis sets as implemented in Gaussian 09 software version C.01. This functional was previously shown to successfully calculate the redox potential of PFAAs, making it an appropriate selection for our reaction of interest.⁹⁴ In addition, $\omega\text{B97-XD}$ includes dispersion corrections which are important for modeling the behavior of PFASs. The SMD implicit solvent model was used to simulate an aqueous environment. All fluorocarboxylates were assumed to be in the deprotonated state, the species that predominates at pH

conditions used in experiments and e_{aq}^- -based treatment applications. The calculated stationary points were characterized as minimum energy structures by computing the second gradients. Several global descriptors along with local properties such as bond dissociation energy (BDE; kcal/mol) and standard reduction potential (E_S° ; V) were calculated to use in reactivity and mechanistic analysis. Further description of the global and local molecular property descriptor variables along with equations are summarized in Appendix A and *vide infra*.

2.4 Results and Discussion

Kinetics Measurements. LFP kinetic traces collected for e_{aq}^- quenching by perfluorobutanoate (PFBA) are provided in Figure 2.1A (traces for all other compounds are provided in Appendix A). Following excitation, absorbance values at 690 nm, characteristic of e_{aq}^- ,^{49,92} decayed on a μ s timescale, and decay was accelerated by addition of increasing concentrations of the PFBA. Exponential fits of the individual traces were carried out to compute the lifetime (τ ; ns) of the transient e_{aq}^- species. The results of replicate transient spectra were found to be highly reproducible, with triplicate-averaged standard deviation values for τ varying by <10% of the average lifetime values. The resulting τ values were analyzed using a Stern-Volmer type relationship (i.e., $1/\tau$ vs. [PFBA]) to derive the value of the apparent bimolecular rate constant (k_2 ; $M^{-1} s^{-1}$) for e_{aq}^- reaction with PFBA (Figure 2.1B). Table 2.1 summarizes bimolecular rate constants measured here and elsewhere for thirteen C2-C4 fluorocarboxylates and their non-fluorinated analogues.

The influences of pH (3.0-12.0) and ionic strength (0-630 mM) on e_{aq}^- lifetimes in the absence of fluorocarboxylate quenchers are shown in Figure A.4 in the Appendix. It was found that the e_{aq}^- lifetime remained relatively constant from pH 9.0 to 12.0 but decreased appreciably at pH < 9.0 (Figure A.4). The decreased lifetime at lower pH conditions can be attributed to increasing concentration H^+ , which reacts with e_{aq}^- at diffusion-limited rates ($k_2 = 2.3 \times 10^{10} M^{-1}s^{-1}$).⁶² At higher pH conditions, this pathway becomes negligible compared to quenching by the solvent H_2O ($k_{obs} = 1.9 \times 10^1 s^{-1}$) and the $Fe(CN)_6^{3-}$ ($k_2 = 3.1 \times 10^9 M^{-1}s^{-1}$)⁶² added to the solution. This is supported by observation of nearly identical Stern-Volmer plots for experiments conducted at pH 9.2 and 12.0 (Figure A.4). This finding of pH invariance is also noteworthy because it contradicts reports that PFAS degradation by UV-sulfite constant irradiation is significantly faster at pH 12.0 (e.g., $t_{1/2} < 1$ h) than at pH 9.5 ($t_{1/2}$ 8-12 h).⁹⁵ The likely reason for this lies in how the rates are measured in LFP when compared to constant irradiation experiments. LFP measures the instantaneous reaction of e_{aq}^- with the PFAS whereas constant irradiation experiments measure the net effects of all reactions in the solution on PFAS degradation, which may be impacted by matrix constituents that react with e_{aq}^- in parallel with the target contaminant.

In the absence of the target contaminant (fluorocarboxylate quencher), e_{aq}^- may decay by three mechanisms: (1) reaction with $K_3Fe(CN)_6$,⁵⁰ (2) self-recombination,⁹⁶ and (3) reaction with solvent, i.e., water.⁹⁷ To ensure changes in e_{aq}^- lifetime could not be attributed to $K_3Fe(CN)_6$ an excess amount of this species was added to regard this reaction as pseudo first order (10 μ M $K_3Fe(CN)_6$ for photolysis of 40 μ M $K_4Fe(CN)_6$ with 266 nm light).⁵⁰ Radical recombination of e_{aq}^- in our kinetics measurements is encumbered by diffusion limitations imparted by the elevated ionic atmosphere (ionic strength; $\mu = 0.63$).⁹⁶ Measurements in the absence of fluorocarboxylate at varying ionic strength show that e_{aq}^- lifetime decreases only when μ increases from dilute conditions to 0.1 then remains relatively constant with further increases (Figure A.4). In the case where two ions are of the same charge and μ increases, formation of the encounter pair becomes more facile, resulting in increased quenching of the e_{aq}^- and hence a shorter lifetime due to increased electrostatic shielding that occurs.⁹⁸ Either way, all experiments with fluorocarboxylates were performed with a fixed μ to ensure that this variable is controlled for. Moreover, rate constants measured for selected fluorocarboxylates in the present study are comparable to those reported previously for the same compounds measured at lower μ and match well when correcting for these difference (*vide infra*).^{50,86} To further ensure that elevated μ did not affect reported kinetic values, Stern-Volmer analysis of PFBA at $\mu = 0.2$ (lowest attainable value with 50 mM fluorocarboxylate and 40 mM borate buffer) was conducted. Indeed, this value is comparable to that measured at $\mu = 0.63$ (Figure A.4). Lastly, the rate constant of e_{aq}^- and H_2O has previously been reported to be 19 s^{-1} , which is slow enough to be neglected.⁹⁹

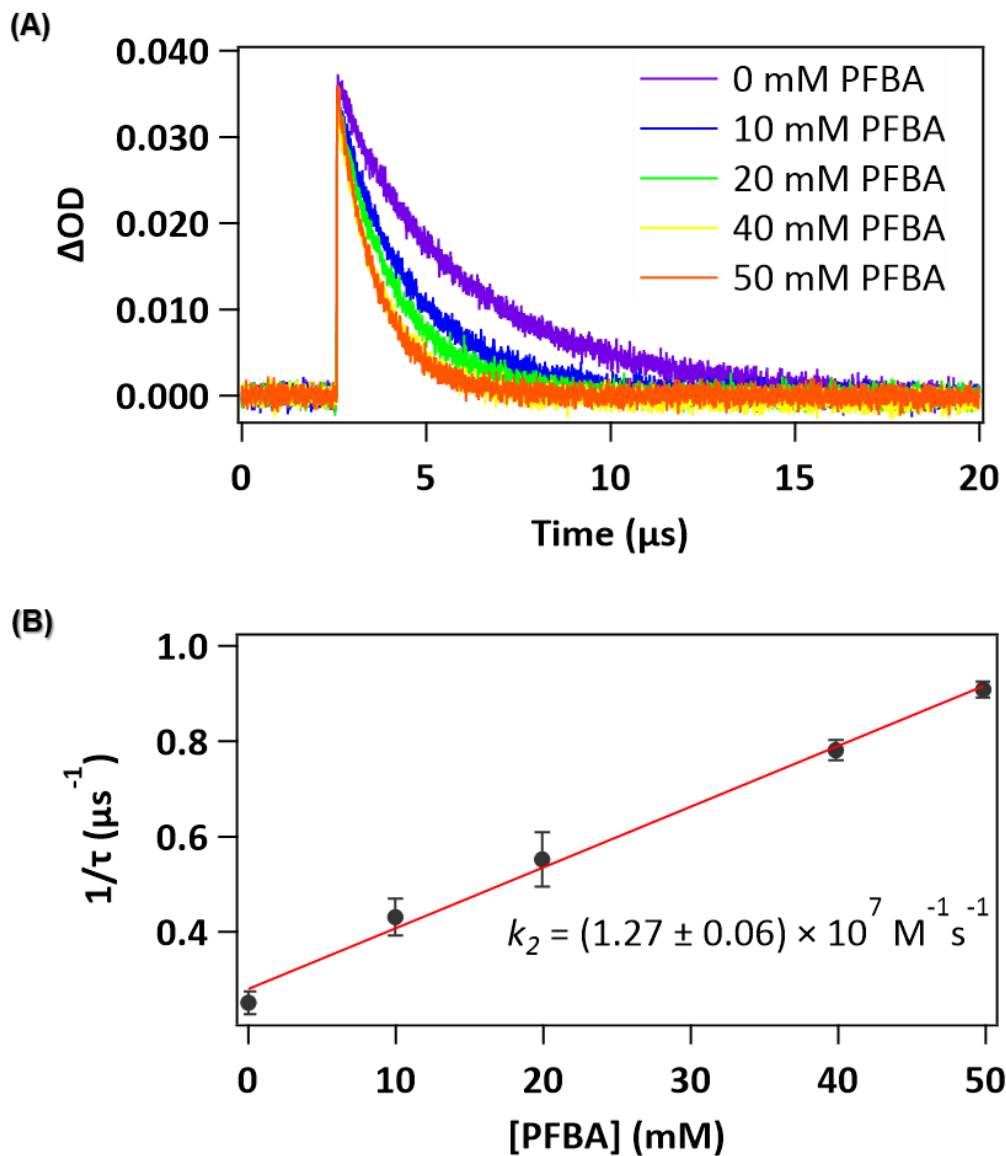


Figure 2.1 (A) Kinetic transient absorption traces for e_{aq}^- decay (measured at 690 nm) at pH 9.2 (40 mM borate buffer) in solutions containing 0 – 50 mM PFBA. Solution conditions: 40 μM $\text{K}_4\text{Fe}(\text{CN})_6$, 10 μM $\text{K}_3\text{Fe}(\text{CN})_6$, ionic strength = 630 mM (balanced using NaCl). (B) Resulting Stern-Volmer plot generated from model fits of the traces to determine e_{aq}^- lifetimes (τ ; μs) in each solution. Individual kinetic traces in panel (A) represent one of the triplicate measurements, and error bars in panel (B) represent one standard deviation based upon triplicate measurements. Traces and Stern-Volmer plots for all other compounds available in Appendix A.

Table 2.1 Summary of abbreviations, structures, solutions conditions, and k_2 values of ultra-short chain fluorocarboxylates determined in the current work along with previously reported values. Solution preparation details and kinetics data values can be found Appendix A.

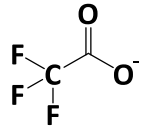
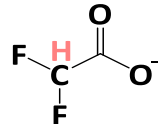
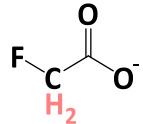
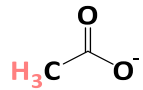
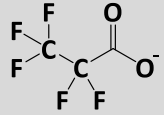
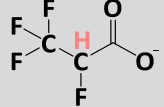
Name and Abbreviation	Length	Structure	pH	μ (mol L ⁻¹)	This Study k_2 (M ⁻¹ s ⁻¹)	Literature k_2 (M ⁻¹ s ⁻¹)
Trifluoroacetate (TFA)	C2		9.2	0.63	$(5.26 \pm 0.29) \times 10^6$ ^d	
			12.0	0.63	$(4.16 \pm 0.14) \times 10^6$ ^d	
			10.0	0.010		$(2.3 \pm 0.2) \times 10^6$ ^a
			10.0	0.065		$(3.0 \pm 0.2) \times 10^6$ ^a
			10.0	0.10		$(3.4 \pm 0.3) \times 10^6$ ^a
			10.0	N/A		$(2.6 \pm 0.6) \times 10^6$ ^b
Difluoroacetate (DFA)	C2		9.2	0.63	$(1.97 \pm 0.04) \times 10^7$ ^d	
			12.0	0.63	$(1.81 \pm 0.03) \times 10^7$ ^d	
Monofluoroacetate (MFA)	C2		9.2	0.63	$(1.32 \pm 0.05) \times 10^7$ ^d	
Acetate	C2		9.2	0.63	$(8.52 \pm 7.19) \times 10^4$	
			9.5-10.5	N/A		$(2.0 \pm 0.5) \times 10^6$ ^b
Pentafluoropropanoate (PFPrA)	C3		9.2	0.63	$(1.64 \pm 0.08) \times 10^7$ ^d	
			12.0	0.63	$(1.38 \pm 0.09) \times 10^7$ ^d	
			10.0	N/A		$(5.8 \pm 1.2) \times 10^8$ ^c
2,3,3,3-tetrafluoropropanoate (2H-PFPrA)	C3		9.2	0.63	$(5.58 \pm 0.56) \times 10^6$	

Table 2.1 Continued.

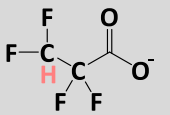
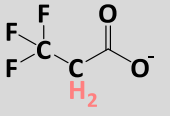
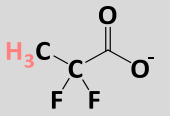
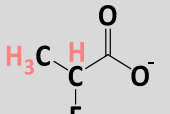
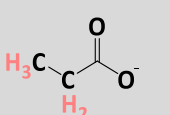
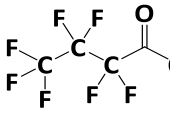
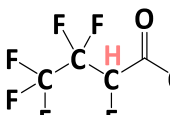
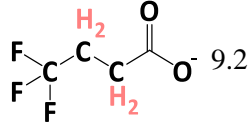
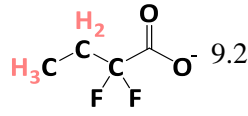
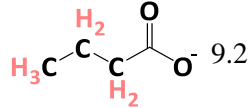
2,2,3,3-tetrafluoropropanoate (3H-PFPrA)	C3		9.2	0.63	$(6.17 \pm 0.16) \times 10^6$	
3,3,3-trifluoropropanoate (TriFPrA)	C3		9.2	0.63	$(1.28 \pm 0.08) \times 10^7$	
2,2-difluoropropanoate (DiFPrA)	C3		9.2	0.63	$(1.65 \pm 0.06) \times 10^7$	
2-fluoropropanoate (MFPrA)	C3		9.2	0.63	$(6.43 \pm 0.53) \times 10^6$	
Propanoate	C3		9.2	0.63	$(7.77 \pm 0.44) \times 10^5$	
Perfluorobutanoate (PFBA)	C4		9.2	0.63	$(1.27 \pm 0.06) \times 10^7$ ^d	
			12.0	0.63	$(1.29 \pm 0.06) \times 10^7$ ^d	$(1.3 \pm 0.1) \times 10^7$ ^a
			10.0	0.10		$(5.4 \pm 1.2) \times 10^8$ ^c
			10.0	N/A		
2H-perfluorobutanoate (2H-PFBA)	C4		9.2	0.63	$(1.32 \pm 0.004) \times 10^8$	

Table 2.1 Continued.

4,4,4-trifluorobutyrate (TriFBA)	C4		9.2	0.63	$(7.35 \pm 0.07) \times 10^7$
2,2-difluorobutanoate (DiFBA)	C4		9.2	0.63	$(8.81 \pm 0.13) \times 10^7$
Butanoate	C4		9.2	0.63	$(9.13 \pm 4.09) \times 10^5$

^aFrom ref ⁵⁰ (LFP at pH 10.0, μ varies, T = 25°C). ^bFrom ref ⁸⁶ (Pulse radiolysis in pH 9.5-10.5, μ and T not provided, 0.001 M methanol). ^cFrom ref ⁸⁷ (LFP at pH 10.0, μ not provided). ^dThe LFP experiments involving these compounds were performed using 254 nm light, while all others used 266 nm.

C2 Fluorocarboxylates. Measured k_2 values for ultra-short chain fluorocarboxylates varied widely from 5×10^6 to $1.3 \times 10^8 \text{ M}^{-1}\text{s}^{-1}$, a large range considering the structural similarity of target compounds. This highlights the sensitivity of e_{aq}^- reactions to small changes in molecular structure of the quenching substrates. Stern-Volmer plots for the three C2 fluoroacetates (TFA, DFA, MFA) are shown in Figure 2.2A. The relative reactivity from fastest to slowest [DFA ($1.97 \times 10^7 \text{ M}^{-1} \text{ s}^{-1}$) > MFA ($1.32 \times 10^7 \text{ M}^{-1} \text{ s}^{-1}$) > TFA ($5.26 \times 10^6 \text{ M}^{-1} \text{ s}^{-1}$)] varied ~4-fold. In comparison, non-fluorinated acetate exhibits much lower reactivity ($<10^6 \text{ M}^{-1} \text{ s}^{-1}$) with an uncertainty nearly as large as the value of k_2 measured. Among the C2 – C4 fluorocarboxylates measured in this study, previous reports are only available for TFA and PFBA.^{50,86,87} The k_2 values measured for these 2 compounds in the present study are similar to values reported by Huang et al. ($2.3\text{-}3.4 \times 10^6 \text{ M}^{-1} \text{ s}^{-1}$) and Anbar et al. ($2.6 \times 10^6 \text{ M}^{-1} \text{ s}^{-1}$) for TFA and ($1.3 \times 10^7 \text{ M}^{-1} \text{ s}^{-1}$) for PFBA.^{50,86} Huang et al. measured k_2 values for TFA at lower μ (0.01 – 0.1) than conditions used in the present study, but Figure 2.2B shows that linear extrapolation of their values to conditions used in the present study ($\mu = 0.63$) shows an almost perfect match (similar linear extrapolation of data for PFBA shown in Figure A.5).

In comparison, the k_2 value for TFA recently reported by Maza and coworkers ($5.0 \times 10^8 \text{ M}^{-1} \text{ s}^{-1}$) is nearly 2 orders-of-magnitude larger than the value measured here as well as values reported in the previous two studies.⁸⁷ While these authors recently posited that the lower k_2 values reported previously may result from aggregation processes occurring at elevated PFAS concentration we were unable to measure any appreciable reduction in the lifetime of e_{aq}^- when we added fluorocarboxylate concentrations matching their experiments (i.e., 0.1 mM, see Figure A.6).¹⁰⁰ Furthermore, aggregation of ultra-short chain fluorocarboxylates is much less likely than longer chain fluoroalkyl surfactants. It is hard to rationalize Maza et al.'s k_2 values from a practical standpoint as these values (on the order of $10^8 - 10^9 \text{ M}^{-1}\text{s}^{-1}$) would result in much faster degradation kinetics in bulk photolysis UV-ARP experiments. What's more is that both experimental and theoretical studies have found PFASs to be intrinsically more recalcitrant towards e_{aq}^- reactions than PFCAs,^{101,102} while Maza et al. report sulfonates to be faster reacting than carboxylates.

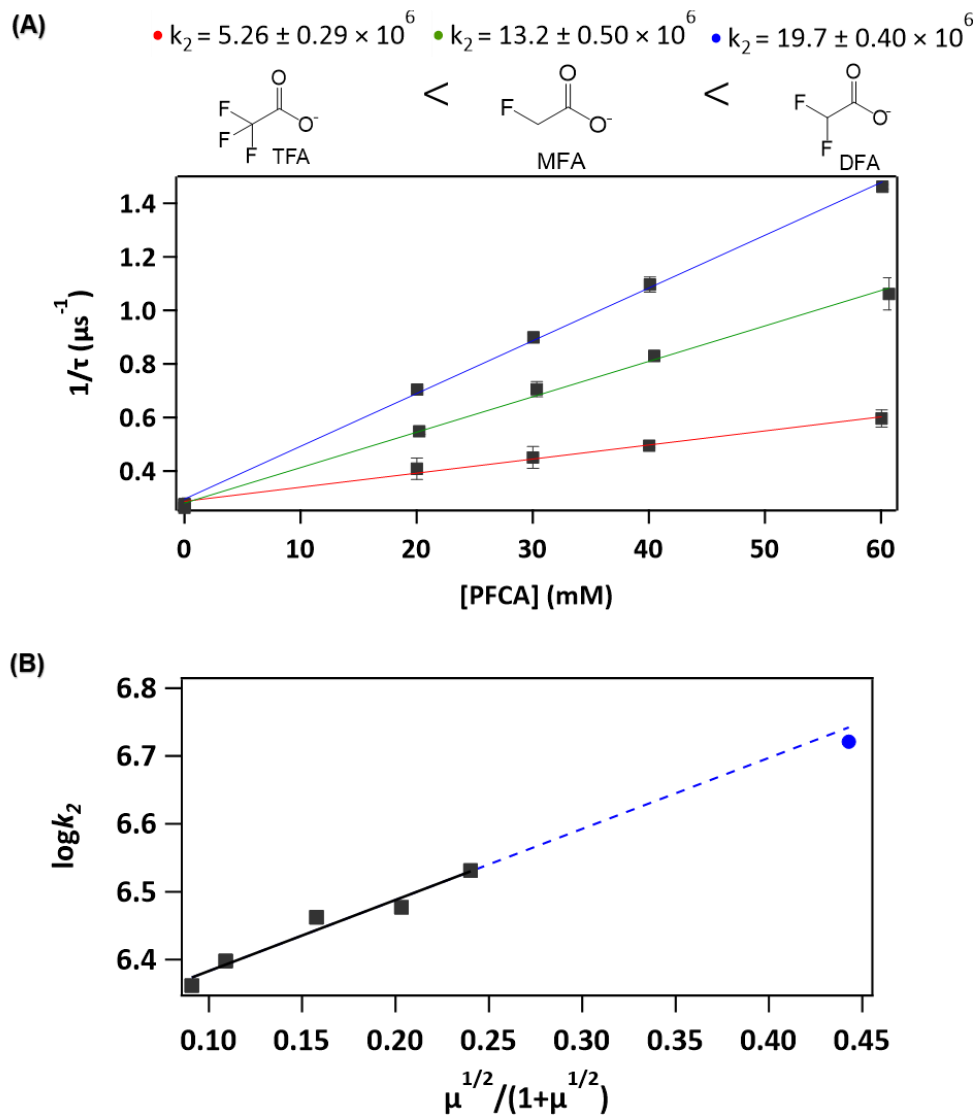


Figure 2.2 (A) Stern-Volmer plots for mono-, di-, and trifluoroacetate. Solution conditions are the same as Figure 2.1. Units for the k_2 values shown are $M^{-1}s^{-1}$. (B) Influence of solution ionic strength (μ) on k_2 for e_{aq}^- reaction with TFA, including data from the present study (\bullet) and from Huang et al. (\blacksquare)⁵⁰ Dashed line shows linear extrapolation between the data sets.

While our fluorinated compound data matches the previous work of Huang et al. and Anbar et al., to further validate our measurement protocol, we measured the k_2 values for chloroacetates which revealed much higher reactivity with e_{aq}^- : 1.2×10^9 to $10.3 \times 10^9 M^{-1} s^{-1}$ (see Figure A.7). This finding is consistent with previous values measured by pulse radiolysis studies (1.2×10^9 and $8.5 \times 10^9 M^{-1}s^{-1}$ for mono- and trichloroacetate, respectively),⁸⁶ as well as expectations due to the much weaker C-Cl bonds (e.g., 65-85 kcal mol⁻¹)¹⁰³ compared to C-F bonds (e.g., 110-130 kcal mol⁻¹).^{104,105} Thus, while chloroacetate species (and presumably bromo- and iodo- analogues) react with e_{aq}^- at nearly diffusion-

limited rates, comparable fluoroacetate species are much less reactive and will require extended treatment times or higher steady state concentrations of e_{aq}^- in practice.

C3-C4 Fluorocarboxylates. Similar to the C2 structures, the fluorinated C3 and C4 carboxylates were much more reactive with e_{aq}^- than the non-fluorinated analogues. No consistent trends were observed with respect to the effect of complete fluorination on reactivity trends in each group. Although the fully fluorinated TFA (C2) was less reactive than the partially fluorinated analogues, the fully fluorinated propanoate species, perfluoropropanoate (PFPrA), was among the most reactive of the C3 fluorocarboxylates, whereas the fully fluorinated PFBA species was among the least reactive of the C4 fluorocarboxylates. Comparison of the fully fluorinated species shows a reactivity trend of TFA < PFBA < PFPrA, but the overall difference in k_2 values was only a factor of ~3. In contrast, much larger variations were observed when one or more F atoms in PFBA are replaced by H atoms. For example, replacement of one F with H at the α -carbon position led to more than a 10-fold increase in k_2 . Interestingly, the same structural change to PFPrA resulted in a 3-fold decrease in k_2 , whereas replacement of both F on the α -carbon with H had no discernable effect. In general, partial replacement of F with H in the C4 PFBA structure led to large increases in k_2 , whereas similar changes in C3 PFPrA structure had much more limited, and generally negative, effects on k_2 .

Calculation of Molecular Properties. Molecular property descriptors for the thirteen fluorocarboxylate target compounds were calculated by DFT (Table A.3) to provide insights into the observed trends in measured k_2 values. Important properties calculated include ionization potential (IP; eV), chemical potential ($-\chi$; eV), electron affinity (EA; eV), dipole moment (δ ; debye), and electrophilicity index (ω ; eV). Collectively, the large positive IP values and small negative EA values are consistent with molecules in which adding an electron (i.e., reduction) is energetically more favorable than removing an electron (i.e., oxidation). This finding supports a growing body of literature that indicates that PFASs are more amenable towards reduction than oxidation.¹⁰⁶ The EA values for the perfluorinated structures (TFA, PFPrA, and PFBA) are also more negative than the others in their chain group (C2 vs. C3 vs. C4, respectively), which is to be expected from compounds containing more electron-withdrawing constituents. Additionally, across the whole series of compounds, the C4 molecules have the largest dipole moment (δ), followed by C3 then C2. This trend follows from the fact that larger molecules can accommodate a larger separation of charge. Further chemical interpretations of select DFT parameters are provided in Appendix A.

Bond dissociation energy (BDE; kcal/mol) values for individual C-C and C-F bond as well as reduction potential (E_s° ; V) for each C-F bond were also calculated (Figure A.8 and A.9, respectively). As expected, C-F bonds were found to be up to 40 kcal/mol stronger than C-C bonds within the fluorocarboxylate structures. It was also found that BDEs of C-F bonds at the α -carbon were about 110

kcal/mol, while C-F bonds in the middle of the chain were only slightly higher (112 kcal/mol), and C-F bonds at the terminus were significantly higher at about 122 kcal/mol. In addition, C-C bonds at the terminus were approximately 10 kcal/mol higher than C-C bonds involving the carboxylate headgroup. Reports which calculate molecular properties for ultra-short chain fluorocarboxylates are scarce, however some exist and can be used for comparison. BDE values calculated for the C-F bonds of TriFBA (122.7 kcal/mol) and TFA (116.8 kcal/mol) do agree reasonably well with a recent report by Bentel et al. (124.7 and 119.3 kcal/mol, respectively).¹⁰⁷ The small differences in values likely result from the use of different basis sets and level of theory. E_s° values of C-F bonds show a similar pattern as BDE: C-F bonds attached to the α -carbon are more easily reduced than those at the terminus.

Relation between Bimolecular Rate Constants and Calculated Chemical Properties. Molecular properties were analyzed against LFP-derived rate constant to assess the correlation between theoretical parameters and experimental values. Figure 2.3 shows correlation scatter plots between the $\log k_2$ values and each molecular property descriptor. When considering the full list of 13 compounds, there are no obvious single descriptor correlations (Figure 2.3A). One interpretation of this lack of correlation between computed global properties and experimentally determined rate constants is that the fluorocarboxylates considered in this study follow diverging reaction pathways despite limited differences.

For example, correlation may be more obvious when viewing subgroups of the target analytes that are more likely to react with e_{aq}^- by a common mechanism, e.g., just the fully perfluorinated species (i.e., TFA, PFPrA, PFBA; Figure 2.3B). There is both experimental and theoretical basis for the notion that e_{aq}^- reduction of perfluorocarboxylates (PFCAs) occurs at the α -carbon resulting in dissociation of an α -fluorine.^{94,102,108} Focusing on the C2 compounds, a similar rationale of e_{aq}^- attachment and F⁻ dissociation at the α -position can be made as there are no other C-F positions available (i.e., no β - or γ -positions). Therefore, it is possible that PFCAs and the C2 compounds react via a common mechanism and therefore would correlate more strongly with one or more molecular descriptor (Figure 2.3C). While Figure 2.3C does show potential correlations with a number of descriptors, particularly for chemical potential ($-\chi$), the small number of analytes in the subgroup prevent more definitive conclusions. The remainder of the dataset includes C3-C4 polyfluorinated carboxylates (Figure 2.3D) for which literature on site of e_{aq}^- attachment is not currently available. Inspection of this subgroup exhibits substantial scatter, however, semiquantitative correlation with dipole moment (δ) can be observed. In-depth mechanistic insights of both per- and polyfluorinated carboxylates are provided in the next section.

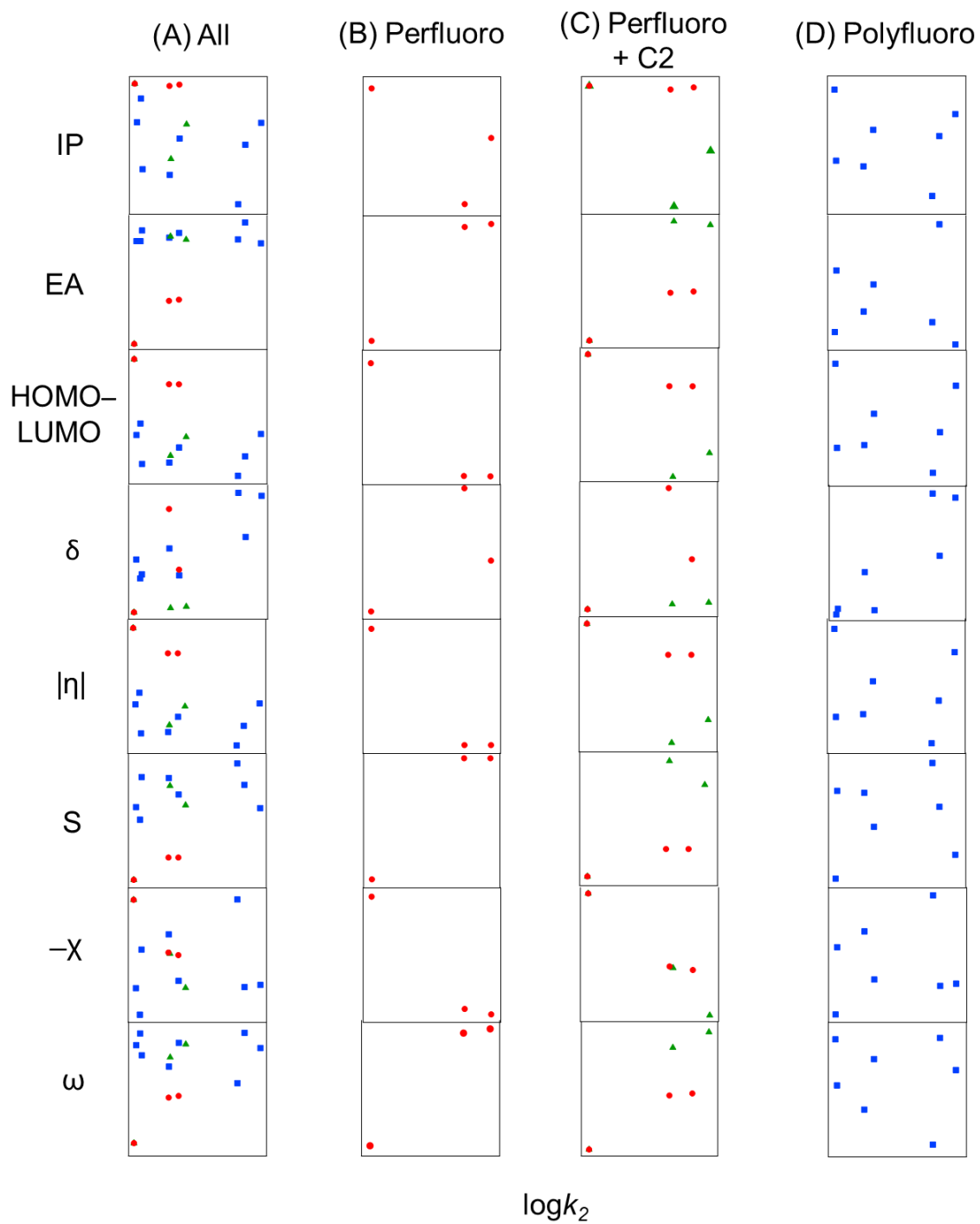
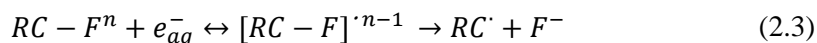
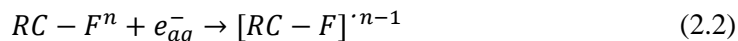
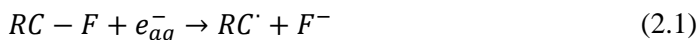


Figure 2.3 Scatter correlation plots between measured $\log k_2$ values and DFT-calculated molecular descriptors for (A) all compounds, (B) perfluorinated carboxylates only (●), (C) perfluorinated and C2 carboxylates (▲), and (D) polyfluorinated carboxylates only (■).

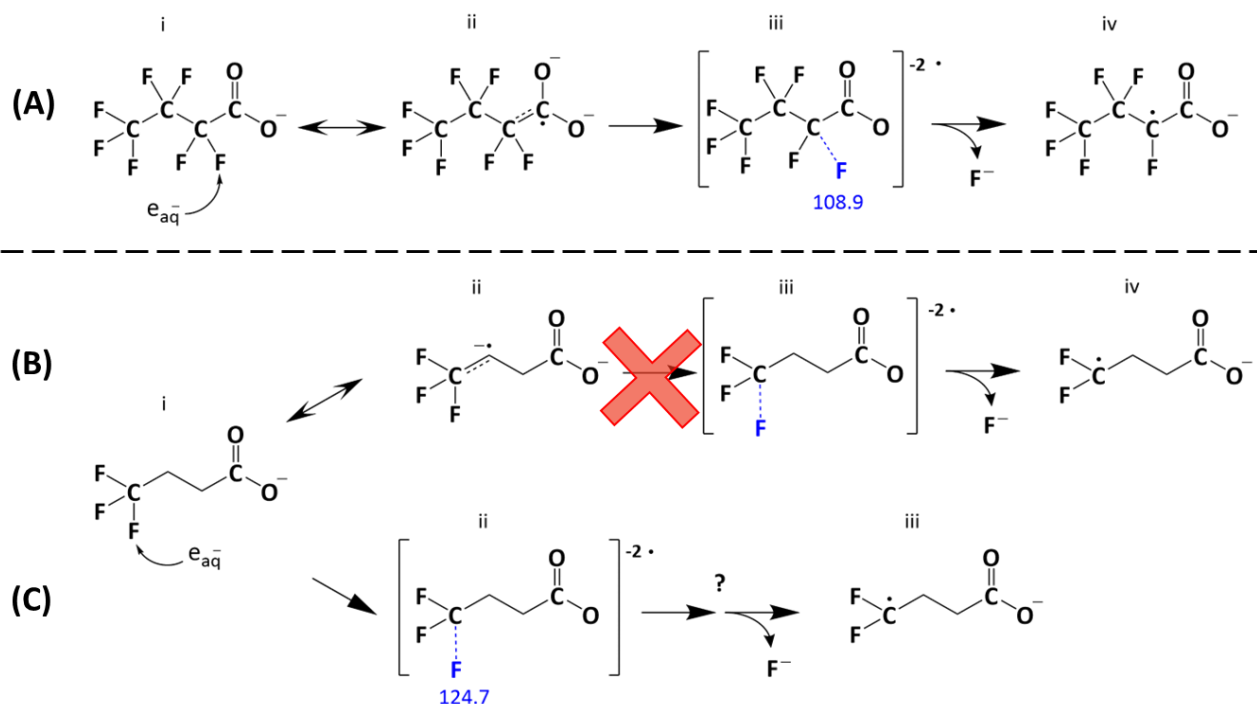
Mechanistic Insights. As previously mentioned, there is growing consensus that reduction of fully fluorinated PFCAs is initiated by e_{aq}^- insertion at the α -carbon,^{94,102,108} but less is established about reduction of partially fluorinated polyfluorinated carboxylates. Three elementary reaction mechanisms which could describe the initiation of fluorocarboxylate reduction by e_{aq}^- are concerted, associative, and stepwise cleavage mechanisms, which are described by equations (Eq 2.1), (Eq 2.2), and (Eq 2.3), respectively.¹⁰⁹



Of particular interest are the associative and stepwise reaction mechanisms since concerted pathways are more common in compounds containing weak C-X bonds which are unable to hold the e_{aq}^- (e.g., X = Br and I, depicted in Eq. 2.1). Associative mechanisms occur when e_{aq}^- irreversibly reacts with a bond that is strong enough to hold an extra electron (Eq. 2.2). This forms an anionic radical species which does not necessarily result in bond cleavage. The stepwise mechanism is initiated by a barrierless, single-electron transfer (SET) step which ensues the formation of an intermediate radical anion (Eq. 2.3). This species is resonance stabilized by the π -system of the carboxylate functional group allowing the spin density to eventually accumulate at the site of defluorination and bond cleavage follows.¹⁰²

Recently, Daily et al. did an in-depth, thermodynamic study that suggests which mechanism various compounds will undergo upon reaction with e_{aq}^- .¹⁰⁹ For MFA, TFA, and PFBA, the authors confirm reduction via a stepwise mechanism (PFBA shown below in Scheme 2.1A for example). While this study did not include C3-C4 polyfluorinated carboxylates, we posit that most of the compounds in our dataset have the functionality to undergo either associative or stepwise mechanisms due to the presence of both strong bonds able to hold an extra electron (associative) and a carboxylate functional group able to stabilize the radical anion species pre-bond cleavage (stepwise). To determine which mechanism each compound is most likely to undergo requires either an exhaustive computational study to obtain E_s° on all possible reaction sites for each mechanism or the use of methods such as ab initio molecular dynamics (AIMD) simulations which are outside the scope of this study. Rather, this study serves to provide accurate rate constants of fluorocarboxylate compounds and highlight potential mechanisms which could prove consequential in implementing e_{aq}^- ARPs in practice.

Scheme 2.1 Proposed mechanism for the initial reduction events involving (A) stepwise C-F bond cleavage for PFBA, (B) stepwise C-F bond cleavage for TriFBA, and (C) associative deactivation of e_{aq}^- for TriFBA. BDEs of bonds of interest are provided in blue in units of kcal/mol.



Two compounds which stand out as not containing functionality to support both mechanisms include the fluorotelomer carboxylic acids (FTCAs) TriFBA and TriFPrA. In FTCAs, the carbon adjacent to the carboxylate headgroup is not fluorinated, and so e_{aq}^- insertion cannot occur at the α -carbon (recall that e_{aq}^- is unreactive towards acetate, propanoate, and butanoate). Further, a recent study utilizing AIMD simulations reported that upon insertion, e_{aq}^- localizes in specific vicinities in PFAS compounds rather than delocalizing over the entire molecule.¹⁰² Therefore, e_{aq}^- insertion and localization in FTCAs occurs at positions other than the α -carbon, so these compounds are unable to impart the same π stabilization as those containing fluorine on the α -carbon. Scheme 2.1B depicts a hypothetical case in which a FTCA (TriFBA used for example) degrades via the stepwise mechanism. The radical anion formed is unstable (structure ii in Scheme 2.1B), so this pathway is unlikely to occur. Scheme 2.1C depicts the alternative case in which a FTCA (TriFBA used again for example) reacts via the associative mechanism. Here, the strong C-F bond of FTCAs holds on to the extra electron without necessarily resulting in cleavage. As a result, fast quenching of the e_{aq}^- as measured by LFP (structure ii represented in Scheme 2.1C) may not reflect the much lower rate at which degradation of the FTCA parent structure occurs,¹⁰⁷ i.e., through slower C-F or C-C bond cleavages (potential structure iii in Scheme 2.1C). We note that the mechanistic

insights provided here are focused on elucidating steps involving e_{aq}^- attachment to fluorocarboxylate and those immediately after, not necessarily pathways which could occur downstream of the initial reduction event (i.e., organic radical recombination of, for example, structure iv in Scheme 2.1A).

As previously mentioned, replacement of F atoms with H atoms in C4 fluorocarboxylates resulted in a stark increase in k_2 value for all substituted compounds. For example, TriFBA was almost 7x more reactive than PFBA. This is counter to trends found in UV-sulfite constant irradiation studies where Bentel et al. reported a half-life for PFBA of approximately 2 h (10 mM sulfite solution buffered at pH 9.5 and irradiated with an 18 W LP Hg light source), whereas TriFBA is only degraded ~10% within 48 h under the same conditions.¹⁰⁷ The reason for this inconsistency is attributed to differences in the underlying mechanisms by which each compound reacts with e_{aq}^- . TriFBA is proposed to react via an associative mechanism (rapid uptake of e_{aq}^- , but slow C-F cleavage), whereas PFBA reacts by stepwise mechanism (uptake of e_{aq}^- and subsequent C-F cleavage occur on similar timescales). LFP measures e_{aq}^- quenching explicitly, so it only reflects the initial uptake of e_{aq}^- by the fluorocarboxylate substrate. For compounds reacting by stepwise mechanism, this also reflects the rate of fluorocarboxylate degradation, but this may not be the case for compounds reacting by associative mechanism. Constant UV irradiation experiments, on the other hand, measure parent compound decay and therefore reflect compound degradation steps (e.g., C-F cleavage) that may be delayed compared to reaction with e_{aq}^- for compounds reacting by associative mechanisms. These findings are critical in that they highlight the plausibility of non-degradative mechanisms in polyfluorinated carboxylates.

2.5 Conclusions

Hydrated electron (e_{aq}^-) based ARPs are promising for treating recalcitrant pollutants such as PFAS, however, most studies are conducted in constant irradiation systems where only apparent rates of degradation and defluorination are able to be observed. More fundamental parameters, such as bimolecular rate constants (k_2) of e_{aq}^- with target compounds, are critical for evaluating and modeling efficacy of UV-ARPs across various environments. To our knowledge, only three reports in literature have provided k_2 values for the reaction between e_{aq}^- and PFAS, and none exist for polyfluorinated compounds. Here, we report k_2 values for thirteen ultra-short chain fluorocarboxylates which will serve as critical inputs in a comprehensive photochemical model for important treatment applications such as UV-sulfite and provide mechanistic insights into the reductive degradation of per- vs. polyfluorinated compounds. Results from this study highlight that subtle structural changes in fluorocarboxylates can yield vast differences in both reduction kinetics and controlling degradation pathways. Calculated molecular descriptors do not show a clear overall trend with observed k_2 values, suggesting the need for

more exhaustive dynamic simulation studies to probe the differences in reaction mechanisms. In light of recently proposed possible reaction mechanisms and observed rate constants, it is also recognized that many ubiquitous polyfluorinated structures likely undergo non-degradative mechanisms, posing an additional challenge for treating sites contaminated by diverse PFAS mixtures.

CHAPTER 3
INFLUENCE OF CARBONATE SPECIATION ON HYDRATED
ELECTRON TREATMENT PROCESSES

Based on a paper submitted to *Environmental Science & Technology*.

Camille K. Amador^{1,2}, Haden Cavalli², Raul Tenorio¹, Christopher P. Higgins¹, Shubham Vyas², and
Timothy J. Strathmann¹

3.1 Abstract

Advanced reduction processes (ARPs) that generate hydrated electron (e_{aq}^- ; e.g., UV-sulfite) have emerged as a promising remediation technology for recalcitrant water contaminants, including per- and polyfluoroalkyl substances (PFASs). The effectiveness of ARPs in different natural water matrices is determined, in large part, by the presence of non-target water constituents that act to quench e_{aq}^- or shield incoming UV photons from the applied photosensitizer. This study examined the pH-dependent quenching of e_{aq}^- by ubiquitous dissolved carbonate species (H_2CO_3^* , HCO_3^- , CO_3^{2-}), and quantified the relative importance of carbonate species to other abundant quenching agents (e.g., H_2O , H^+ , HSO_3^- , $\text{O}_{2(aq)}$) during ARP applications. Analysis of laser flash photolysis (LFP) kinetics data in relation to pH-dependent carbonate acid-base speciation yields species-specific bimolecular rate constants for e_{aq}^- quenching by H_2CO_3^* , HCO_3^- , and CO_3^{2-} ($k_{\text{H}_2\text{CO}_3^*} = 2.23 \pm 0.42 \times 10^9 \text{ M}^{-1} \text{ s}^{-1}$, $k_{\text{HCO}_3^-} = 2.18 \pm 0.73 \times 10^6 \text{ M}^{-1} \text{ s}^{-1}$, $k_{\text{CO}_3^{2-}} = 1.05 \pm 0.61 \times 10^5 \text{ M}^{-1} \text{ s}^{-1}$), with quenching dominated by H_2CO_3^* (which includes both $\text{CO}_{2(aq)}$ and H_2CO_3) at moderately alkaline pH conditions despite it being the minor species. Attempts to apply previously reported rate constants for e_{aq}^- quenching by $\text{CO}_{2(aq)}$, measured in acidic solutions equilibrated with $\text{CO}_{2(g)}$, overpredict quenching observed in this study at higher pH conditions typical of ARP applications. Moreover, kinetics simulations reveal that pH-dependent trends reported for UV-sulfite ARPs that have often been attributed to e_{aq}^- quenching by varying $[\text{H}^+]$ can instead be ascribed to variable acid-base speciation of dissolved carbonate and the sulfite sensitizer.

¹Department of Civil and Environmental Engineering, Colorado School of Mines, Golden, CO

²Department of Chemistry, Colorado School of Mines, Golden, CO

³Haley and Aldrich, Phoenix, AZ (Current Affiliation)

3.2 Introduction

Advanced reduction processes (ARPs) are a class of water treatment technologies that integrate activation methods (e.g., UV light, ultrasound) with reduced species (e.g., sulfite, dithionite) to generate reductive radicals that are highly reactive with many aquatic contaminants.¹¹⁰ Remediation strategies employing ARPs are emerging as promising options for chemicals that are resistant to oxidation, including per- and polyfluoroalkyl substances (PFASs), chlorinated solvents (e.g., trichloroethylene), and toxic oxyanions (e.g., ClO_4^- , BrO_3^- , CrO_4^{2-}).^{42-44,111-114} Among ARPs, UV photochemical processes that generate hydrated electrons (e_{aq}^-) have received growing attention due to their potential for degrading highly recalcitrant PFASs.¹¹⁵ Absorption of UV photons of sufficient energy by an appropriate photosensitizer species (e.g., sulfite, iodide, ferrocyanide) leads to electron ejection into the bulk solvent forming e_{aq}^- , a powerful reductant ($E_H^0 = -2.9 \text{ V}$).^{45,46} Practical remediation applications have focused on UV activation with sulfite (SO_3^{2-}) salts due to their low cost as well as the non-toxicity and ubiquity of the byproduct sulfate in natural water systems. Moreover, sulfite has the added benefit of scavenging dissolved oxygen,⁶³ a known quencher of e_{aq}^- ($k_2 = 1.9 \times 10^{10} \text{ M}^{-1}\text{s}^{-1}$),⁶² and has an extensive history of use at wastewater treatment facilities for dechlorination of treated wastewater before discharging.⁶¹

While e_{aq}^- is a strong reductant that is able to react with many contaminants of concern, it is also a transient species (lifetime $\sim 10^{-6} \text{ s}$)^{116,117} that is rapidly quenched by water and other non-target constituents commonly measured in groundwater, including $\text{O}_{2(aq)}$, H^+ , and NO_3^- .¹¹⁸⁻¹²⁰ As a result, the effectiveness of UV-sulfite and other ARPs in treating target contaminants is highly dependent on sourcewater composition and difficult to predict *a priori*. Applications involving e_{aq}^- for contaminant remediation typically require adjustment of pH to alkaline conditions (e.g., $\text{pH} \geq 9$),¹²¹ often assumed to be a requirement to limit e_{aq}^- quenching by H^+ ($2.3 \times 10^{10} \text{ M}^{-1}\text{s}^{-1}$).^{51,62,66} In fact, Bentel and co-workers recently reported that UV-sulfite treatment of PFASs is dramatically accelerated by increasing pH to 12.⁹⁵ Whereas $\sim 85\%$ defluorination of trifluoroacetate (TFA) was observed after 24 h of reaction at pH 9.5, complete defluorination was observed within 4 h at pH 12.⁹⁵

Although pH-dependent trends have often been attributed solely to changes in e_{aq}^- quenching by H^+ ,^{66,95,121} quantitative analysis of reactivity trends does not support this conclusion. For example, our recent work using laser flash photolysis (LFP) demonstrated invariance of e_{aq}^- lifetime from $9 < \text{pH} < 12$, suggesting that H^+ itself is not a significant e_{aq}^- quencher at these pH conditions.¹²² Additional work has highlighted the potential importance of weak acids as alternative quenchers of e_{aq}^- in both laboratory-prepared solutions and real-world water matrices.^{68,123} Weak acids exhibit pH-dependent changes in speciation that could influence rates of contaminant degradation observed in different solution matrices.

For example, Maza and coworkers recently showed that HSO_3^- , the conjugate acid species of the sulfite photosensitizer ($\text{p}K_a$ 7.2),^{63,124} is a significant quencher of e_{aq}^- ($1.2 \times 10^8 \text{ M}^{-1}\text{s}^{-1}$)⁶⁸ that will inhibit contaminant reactions to varying degrees during UV-sulfite treatment applications, depending on pH conditions.

Perhaps the most ubiquitous weak acids in natural water systems are carbonate species that are in equilibrium with atmospheric $\text{CO}_{2(g)}$ (e.g., H_2CO_3^* and HCO_3^-) and are a dominant pH buffer of natural water systems. Moreover, carbonate has been widely used in laboratory ARP studies to buffer pH conditions,^{85,95,107,125} and the results of a recent study show that increasing carbonate concentrations inhibit defluorination of perfluorooctanoic acid (PFOA) by e_{aq}^- .⁶⁴ While past reports of e_{aq}^- quenching by HCO_3^- ($<10^6 \text{ M}^{-1}\text{s}^{-1}$)¹²⁶ and CO_3^{2-} ($3.9 \times 10^5 \text{ M}^{-1}\text{s}^{-1}$)⁴⁷ suggest such species are unlikely to inhibit contaminant reactions with e_{aq}^- when present at environmentally relevant concentrations, dissolved CO_2 has been reported to react with e_{aq}^- at near diffusion-limited rates ($7.7 \times 10^9 \text{ M}^{-1}\text{s}^{-1}$)¹²⁷. However, it remains unclear whether $\text{CO}_{2(aq)}$ (the major contributor to H_2CO_3^*), a minor contributor to dissolved carbonate speciation at pH conditions typical of ARP applications, contributes significantly to e_{aq}^- scavenging treatment processes. Past reports of e_{aq}^- reactions with carbonate assumed quenching by single species, ignoring potential for simultaneous reactions with different (and otherwise minor) acid-base carbonate species that are in equilibrium with the species that predominates at a given pH condition. Thus, given the ubiquity of dissolved carbonate in natural water matrices, a more comprehensive study of e_{aq}^- quenching over a range of pH conditions typical of ARP applications that carefully quantifies the effects of changing acid-base driven carbonate speciation is warranted. Accurate rate constants for e_{aq}^- reactions with individual carbonate species will be critical inputs for comprehensive kinetic models for ARP remediation applications that require a full accounting of sources and sinks of e_{aq}^- in different water matrices.

In this study, we report on the effects of dissolved carbonate concentration and speciation on e_{aq}^- reactions. The inhibitory effect of dissolved carbonate on UV-sulfite treatment of perfluorooctane sulfonate (PFOS), a highly recalcitrant PFAS, was first confirmed and compared with recent reports for PFOA. LFP experiments were then conducted to quantify e_{aq}^- quenching by dissolved carbonate over a range of pH conditions (pH 5 – 12), and the resulting data were quantitatively analyzed in terms of changing acid-base carbonate speciation. Finally, species-specific bimolecular rate constants derived from this effort were then applied to quantify the potential contribution of dissolved carbonate species relative to other documented quencher species present during treatment applications, including H^+ and HSO_3^- .

3.3 Materials and Methods

Chemicals. A full list of chemicals used are provided in Appendix B. All stock solutions were prepared inside an anaerobic chamber (Coy Lab Products; 97% N₂, 3% H₂) using deoxygenated deionized water prepared as described in Appendix B.

Constant irradiation experiments. UV-sulfite reaction of PFOS was measured in solutions amended with varying concentrations of dissolved carbonate. Experiments were conducted using a light source and reactor described previously.⁸⁵ A solution containing 70 µg/L PFOS and sulfite (3 mM Na₂SO₃) was buffered at pH 10.0 (5 mM sodium tetraborate) and amended with 0 – 25 mM NaHCO₃. To eliminate e_{aq}^- scavenging by dissolved oxygen, solutions were deoxygenated by sparging with N_{2(g)} for 1 h before introducing PFOS and sulfite to initiate UV reactions. Sample aliquots were collected at pre-determined time intervals to measure changing PFOS concentrations which were measured by liquid chromatography with tandem mass spectrometry (LC-MS/MS) using procedures and instrumentation described elsewhere.¹²⁸ Solution pH was re-measured after the reaction was completed to evaluate any pH drift during experiments. Additional details on reaction solution preparation and analysis are described in Appendix B.

LFP experiments. Transient absorption spectra at 690 nm were collected (LP980 spectrophotometer equipped with an ICCD camera and photomultiplier tube, Edinburgh Instruments) to quantify the kinetics of e_{aq}^- quenching in solutions amended with varying sodium bicarbonate concentrations (0 – 500 mM) and adjusted to varying pH conditions (5.0 – 12.0). Generation of e_{aq}^- was achieved by irradiating a solution of K₄Fe(CN)₆ (40 µM) and K₃Fe(CN)₆ (10 µM) with an 8-10 mJ laser pulse (Surelite EX Nd:YAG laser, Continuum; details described elsewhere).¹²² Ten transient spectra were measured and averaged for each of solution. Unless otherwise noted, individual solutions containing K₄Fe(CN)₆, K₃Fe(CN)₆, the desired bicarbonate concentration, and NaCl (added to fix ionic strength near 0.5 M) were prepared in 50 mL polypropylene centrifuge tubes and adjusted to the desired pH condition using either 1 M HCl or NaOH. Three replicate 2.75 mL aliquots of each solution were then transferred to individual quartz cuvettes (Innovative Lab Supply) and sealed before they were removed from the anaerobic chamber and subjected to LFP measurement. Stern-Volmer analysis of the change in e_{aq}^- lifetime (τ) for all 15 measurements was used to determine the pH-dependent k_{app} value. Further details on solution preparation can be found in Appendix B.

A separate LFP experiment was conducted to measure e_{aq}^- quenching by dissolved H₂CO₃* (which includes both CO_{2(aq)} and H₂CO₃) under acidic pH conditions. A stock solution of 31.8 mM H₂CO₃* was prepared inside the anaerobic chamber by sparging deionized water with 1 atm CO_{2(g)} overnight; H₂CO₃* concentration was estimated using the Henry's Law constant for CO_{2(g)} (3.4×10^{-2}

mol/kg.bar at 20°C).¹²⁹ Aliquots of varying volume from this stock solution were mixed in a cuvette with solution containing $\text{K}_4\text{Fe}(\text{CN})_6$, $\text{K}_3\text{Fe}(\text{CN})_6$, and electrolyte and then immediately sealed with minimal headspace (3.5 mL total) before removing from the glovebox for LFP analysis of e_{aq}^- lifetimes. Replicate solutions were prepared in larger centrifuge tubes to measure pH of the solution before the reaction, and the 3.5 mL samples were pooled post reaction to measure the pH after LFP analysis.

Analysis and modeling. PFOS degradation kinetics observed in constant irradiation experiments followed a pseudo-first-order rate law, and corresponding rate constants (k_{obs} , h^{-1}) were determined by least-squares fit of the model to measurements. Apparent bimolecular rate constants for e_{aq}^- quenching by dissolved carbonate species at each pH condition (k_{app} , $\text{M}^{-1} \text{s}^{-1}$) were derived from LFP data using Stern-Volmer analyses of the changes in e_{aq}^- lifetimes (τ) as a function of total dissolved carbonate concentration (C_{T,CO_3}). Equilibrium acid-base speciation of dissolved carbonate and sulfite were calculated using Visual MINTEQ (Ver 3.1). MINTEQ calculations assumed an ionic strength of 0.5 M for LFP experiments, 0.05 M for the constant irradiation experiments, and a temperature of 20 °C for both. Species-specific carbonate- e_{aq}^- bimolecular rate constants were then determined by least-squares fits of the trends in measured k_{app} values in relation to carbonate speciation (Scientist Ver 3.0, Micromath Research). Scientist was also used to rule out the potential kinetic limitations of carbonate species interconversion reactions to the observed kinetics of e_{aq}^- quenching.

3.4 Results and Discussion

Effect of dissolved carbonate on PFAS degradation. Here, we first re-visited the effects of dissolved carbonate on the kinetics of e_{aq}^- ARP PFAS degradation by examining treatment of PFOS during UV-sulfite treatment, a commonly applied ARP. In the absence of carbonate, UV-sulfite treatment of PFOS with 3 mM sulfite (pH 10.0) yielded a k_{obs} value of $0.237 \pm 0.031 \text{ h}^{-1}$. This value dropped by >25% ($0.154 \pm 0.035 \text{ h}^{-1}$) and >50% ($0.105 \pm 0.027 \text{ h}^{-1}$) when 1 and 5 mM total dissolved carbonate, respectively, were added to the solution and pH was kept constant (Figure 3.1). These decreases in k_{obs} are particularly noteworthy since mM concentrations have often been applied to buffer pH in previous studies examining UV-sulfite treatment of PFASs.^{85,95,107,125} Moreover, this highlights that environmentally relevant concentrations of dissolved carbonate can inhibit PFAS degradation. Additionally, the pseudo first-order reaction rate constant (k_{obs} ; h^{-1}) obtained here for 5 mM added carbonate is not far off from previous reports by Tenorio and coworkers at similar conditions ($0.080 \pm 0.005 \text{ h}^{-1}$).⁸⁵ Further increases in carbonate concentration led to greater inhibition, where $k_{obs} = 0.066 \pm 0.024 \text{ h}^{-1}$ when 25 mM carbonate was added.

These findings are also consistent with earlier reports noting inhibited rates of PFAS treatment by e_{aq}^- ARPs. Ren et al. investigated the effect of carbonate, as well as other common, co-existing anions, on degradation and defluorination of PFOA, a commonly studied long-chain perfluoroalkyl carboxylic acid.⁶⁴ In the absence of carbonate, nearly 100% degradation of PFOA was observed within 1 h, while only about 55% of PFOA was degraded during the same time in the presence of 5 mM added carbonate, the lowest concentration studied. Not only was carbonate found to inhibit parent compound degradation, but it also decreased the extent of PFOA defluorination from nearly 90% (0 mM) to ~60% (5 mM) after 24 h. Further increases in carbonate concentration, up to 25 mM, led to further inhibition.

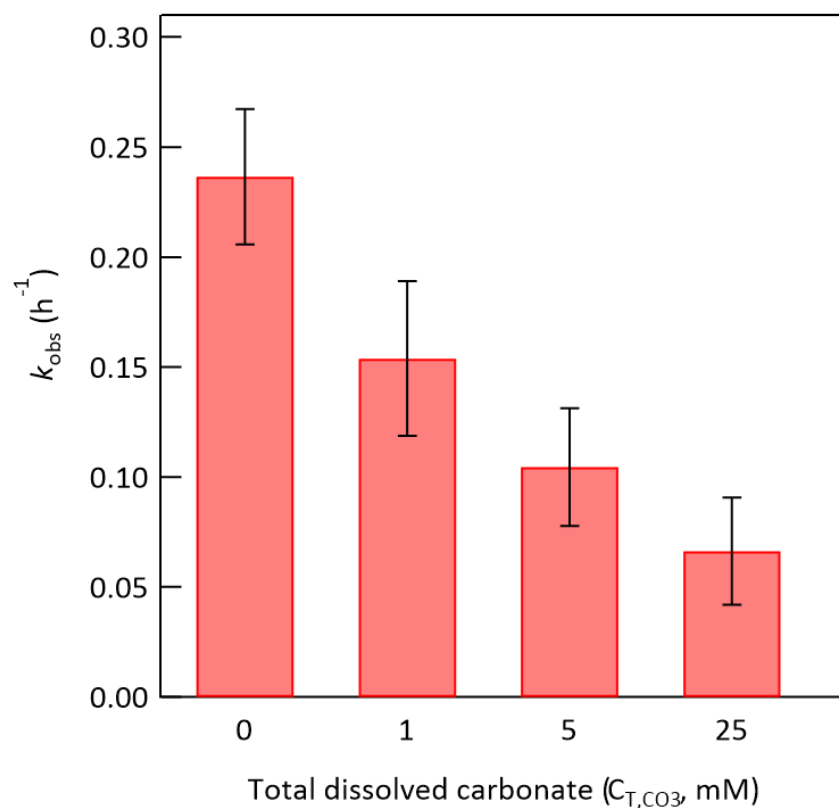


Figure 3.1 Effect of dissolved carbonate on the observed rate constant for PFOS degradation during UV-sulfite treatment. Reaction conditions: $[PFOS]_{initial} = 70 \mu g/L$, 3 mM Na_2SO_3 , irradiation with LP-Hg light source, pH 10.0 (5 mM borate buffer), 20°C. Error bars represent duplicate measurement-derived standard deviations.

Laser Flash Photolysis Measurements. The progressive inhibition of PFOS degradation observed with increasing total dissolved carbonate is consistent with competitive scavenging of the reactive e_{aq}^- by this solution component. Given the ubiquity of carbonate species in natural water matrices, this warrants further investigation to better predict its influence on treatment efficacy. LFP kinetic traces collected for e_{aq}^- quenching in solutions buffered at pH 9.3 and varying concentrations of carbonate are provided in Figure 3.2A (traces for all other pH conditions provided in Appendix B). Following excitation, absorbance values at 690 nm (characteristic of e_{aq}^- ⁴⁹) increase to an initial optical density (ΔOD) value of ~ 0.05 . Applying Beer's law and reported molar absorptivity for e_{aq}^- at 690 nm ($20560 \text{ M}^{-1} \text{ cm}^{-1}$),^{50,55} each laser pulse generated an initial e_{aq}^- concentration of $\sim 2.4 \text{ }\mu\text{M}$. Absorbance then decays on a μs timescale and was accelerated by addition of increasing concentrations of total dissolved carbonate. Rate constants were determined in a similar fashion as our previous study,¹²² and results of the replicate measurements were found to be highly reproducible. Briefly, lifetime of the transient e_{aq}^- species (τ ; ns) were analyzed using a Stern-Volmer type relationship (i.e., $1/\tau$ vs. C_{T,CO_3} ; Figures 3.2B-C) to derive apparent bimolecular rate constants (k_{app} ; $\text{M}^{-1}\text{s}^{-1}$) for e_{aq}^- reactions with dissolved carbonate at each pH condition. Table 3.1 summarizes k_{app} measured at various pH conditions from pH 5.0 – 12.

The results of these experiments show that values of k_{app} increase dramatically with decreasing pH conditions, with values increasing from $< 2 \times 10^5 \text{ M}^{-1} \text{ s}^{-1}$ at pH 12.0 to $4.63 (\pm 0.13) \times 10^9 \text{ M}^{-1} \text{ s}^{-1}$ for pH 5-5.5 prepared by equilibrating solutions with $\text{CO}_{2(g)}$ (Figure 3.2C). This trend is attributed to changes in the acid-base speciation of the dissolved carbonate species. The predominance of e_{aq}^- quenching by carbonate species is further supported by the fact that the measured lifetimes for e_{aq}^- (τ ; μs) in the absence of added carbonate show little change in value between pH 5.8 and 12.0 (Figure B.1), highlighting that H^+ , which varies 10-fold in concentration for each integer change in pH, is not a major quencher species compared to the solvent and the photosensitizer species. It follows that dissolved carbonate and its speciation may be determinative factors in the reported pH dependencies of e_{aq}^- -based ARPs,^{64,81,95} rather than variable $[\text{H}^+]$.

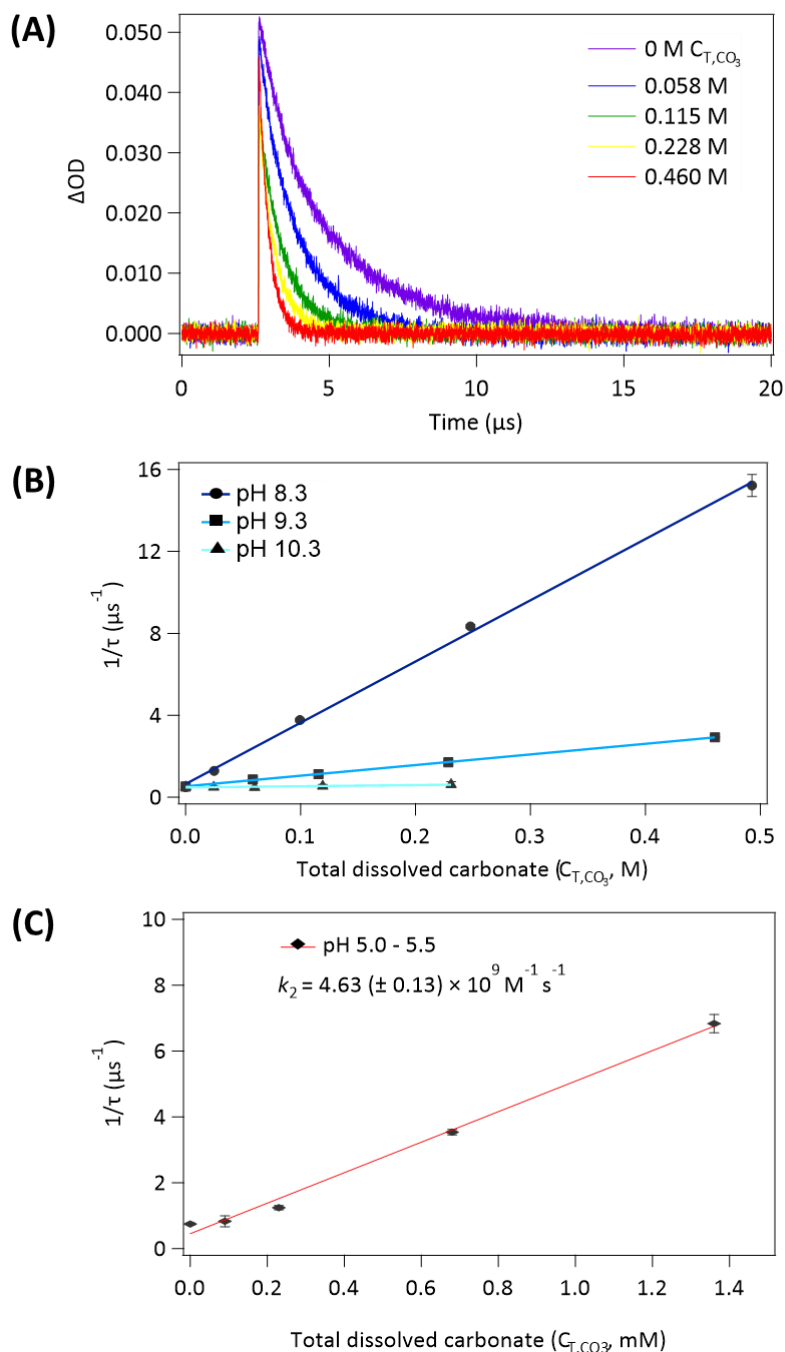


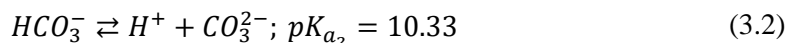
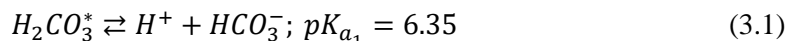
Figure 3.2 (A) Kinetic transient absorption traces for e_{aq}^- decay (measured at 690 nm) at pH 9.3 in solutions amended with varying concentrations of dissolved carbonate prepared from NaHCO_3 . Solution conditions: 40 μM $\text{K}_4\text{Fe}(\text{CN})_6$, 10 μM $\text{K}_3\text{Fe}(\text{CN})_6$, ionic strength = 0.47 M (balanced using NaCl). (B) Stern-Volmer plots for selected pH conditions generated from model fits of the traces to determine e_{aq}^- lifetimes in each solution (results for all pH conditions provided in SI). (C) Stern-Volmer plot for acidic solutions (pH 5.0 – 5.5) prepared by equilibrating $\text{CO}_{2(g)}$ with aqueous solutions then adding $\text{K}_4\text{Fe}(\text{CN})_6$, $\text{K}_3\text{Fe}(\text{CN})_6$ and NaCl . Individual kinetic traces in panel (A) represent the average of the triplicate measurements, and error bars in panels (B) and (C) represent one standard deviation based upon triplicate measurements. Apparent rate constants derived from Stern-Volmer analyses provided in Table 3.1.

Table 3.1 Summary of k_{app} values determined at various pH conditions using LFP along with corresponding α values at each condition determined using Visual MINTEQ at ionic strength (μ) of 0.5 M and temperature fixed at 20 °C.

pH	μ (M)	C_{T,CO_3}^{max} (M)	α_0	α_1	α_2	k_{app} ($M^{-1}s^{-1}$)
12.0	0.54	0.33	1.47×10^{-8}	0.009	0.991	$1.54 (\pm 1.13) \times 10^5$
11.0	0.52	0.33	1.36×10^{-6}	0.086	0.914	$1.81 (\pm 1.08) \times 10^5$
10.3	0.50	0.23	2.54×10^{-5}	0.321	0.679	$5.91 (\pm 2.30) \times 10^5$
9.8	0.45	0.44	1.50×10^{-4}	0.599	0.401	$1.37 (\pm 0.11) \times 10^6$
9.5	0.46	0.47	3.73×10^{-4}	0.748	0.251	$3.62 (\pm 0.13) \times 10^6$
9.3	0.47	0.46	6.52×10^{-4}	0.825	0.175	$5.18 (\pm 0.12) \times 10^6$
8.8	0.49	0.49	2.34×10^{-3}	0.935	0.063	$1.34 (\pm 0.04) \times 10^7$
8.3	0.50	0.49	7.69×10^{-3}	0.972	0.021	$2.99 (\pm 0.04) \times 10^7$
7.8	0.50	0.50	0.024	0.969	6.49×10^{-3}	$5.54 (\pm 0.15) \times 10^7$
7.3	0.47	0.45	0.073	0.925	1.96×10^{-3}	$1.02 (\pm 0.03) \times 10^8$
6.8	0.55	0.05	0.200	0.800	5.35×10^{-4}	$2.45 (\pm 0.15) \times 10^8$
6.3	0.56	0.05	0.442	0.558	1.18×10^{-4}	$6.65 (\pm 0.32) \times 10^8$
5.8	0.50	0.01	0.714	0.286	1.91×10^{-5}	$1.13 (\pm 0.09) \times 10^9$
5.0-5.5 ^a	0.47	0.0014	0.94-0.83	0.06- 0.17	$<6 \times 10^{-6}$	$4.63 (\pm 0.13) \times 10^9$

^aSolution pH varied from 5.0 to 5.5 as concentration of $H_2CO_3^*$ stock solution, prepared by equilibrating water with 1 atm $CO_2(g)$, added to unbuffered solution increased.

Quantitative analysis of kinetics in terms of carbonate speciation. Figure 2.3 shows the measured values of k_{app} as a function of pH along with fits of a model that assumes parallel reactions of e_{aq}^- with different species of dissolved carbonate. As a diprotic acid, dissolved carbonate speciation can be described by acid dissociation constants:



Therefore, speciation shifts from predominantly $H_2CO_3^*$ (which includes both $CO_{2(aq)}$ and H_2CO_3 , with the former accounting for >99% of the total) at the lowest pH conditions examined, to predominantly HCO_3^- at pH conditions between the two pK_a values, and finally to predominantly CO_3^{2-} at the highest pH conditions examined (Figure B.2 in Appendix B). It is in line with the observed pH-dependence of kinetics trends, that e_{aq}^- reactivity follows $H_2CO_3^* > HCO_3^- > CO_3^{2-}$. If we consider that e_{aq}^- reacts in parallel with individual carbonate species, we can formulate a relationship between k_{app} and the species-specific bimolecular rate constants ($k_{H_2CO_3^*}$, $k_{HCO_3^-}$, and $k_{CO_3^{2-}}$, $M^{-1} s^{-1}$):

$$k_{app} = k_{H_2CO_3^*}\alpha_0 + k_{HCO_3^-}\alpha_1 + k_{CO_3^{2-}}\alpha_2 \quad (3.3)$$

where the α values represent the fractional contribution of the corresponding species to total dissolved carbonate. Attempts to apply the model described in Eq. 3.3 using literature values of $k_{H_2CO_3^*}$ (7.7×10^9

$M^{-1}s^{-1}$),¹³⁰ $k_{HCO_3^-}$ ($6 \times 10^5 M^{-1}s^{-1}$),¹²⁶ and $k_{CO_3^{2-}}$ ($3.9 \times 10^5 M^{-1}s^{-1}$)^{47,130,131} reported by separate investigators was unsuccessful. Although the general trend of increasing reactivity with decreasing pH is predicted, the modeled k_{app} values over-predict measurements by up to a factor ~ 2 over the entire pH range examined (Figure 3.3, dashed line). The overprediction may result from the fact that past studies measuring carbonate reactivity with e_{aq}^- only considered contributions from a single species in each study. Most importantly, model predictions are dominated by extrapolation of the reported $k_{H_2CO_3^*}$ value measured under acidic pH conditions to much higher pH conditions that are representative of conditions used for ARPs in practice (e.g., pH > 9).

Re-fitting of Eq. 3.3 to the measured k_{app} values in this study yields updated values for $k_{H_2CO_3^*} = 2.23 (\pm 0.42) \times 10^9 M^{-1} s^{-1}$, $k_{HCO_3^-} = 2.18 (\pm 0.73) \times 10^6 M^{-1}s^{-1}$, and $k_{CO_3^{2-}} = 1.05 (\pm 0.61) \times 10^5 M^{-1}s^{-1}$ that more closely match the observed e_{aq}^- quenching over the full range of pH conditions (Figure 3.3, bold line).

Comparing these species-specific values reveals that $k_{H_2CO_3^*}$ derived from fitting the pH-dependent data is >3 -fold lower than that measured at acidic conditions alone ($7.7 \times 10^9 M^{-1}s^{-1}$),¹³⁰ whereas $k_{HCO_3^-}$ and $k_{CO_3^{2-}}$ are >3 -fold higher and lower, respectively, than the values reported previously ($6 \times 10^5 M^{-1}s^{-1}$ and $3.90 \times 10^5 M^{-1}s^{-1}$)^{47,131}. We hypothesize that the differences result largely from the assumption in earlier studies that the carbonate species in question was the sole quencher of e_{aq}^- . For example, the value for $k_{CO_3^{2-}}$ was measured at pH 11.4 where CO_3^{2-} accounts for 93% of C_{T,CO_3} , but contribution of HCO_3^- to the rate constant was not considered despite this species accounting for 7% of C_{T,CO_3} and being 20-fold more reactive than CO_3^{2-} .^{47,62} In addition, no mention is made of the pH at which the value for $k_{HCO_3^-}$ was measured.¹³¹ Additional factors responsible may include differences in ionic strength or temperature. We employed a high ionic strength (0.5 M) to ensure that this parameter was constant when varying added $NaHCO_3$ (up to 0.50 M) during LFP experiments. That is, electrolyte (NaCl) was added as an offset when low $NaHCO_3$ was employed and omitted when $NaHCO_3$ was high. Failure to specifically account for this variable in earlier studies may also have affected the resulting rate constant values.

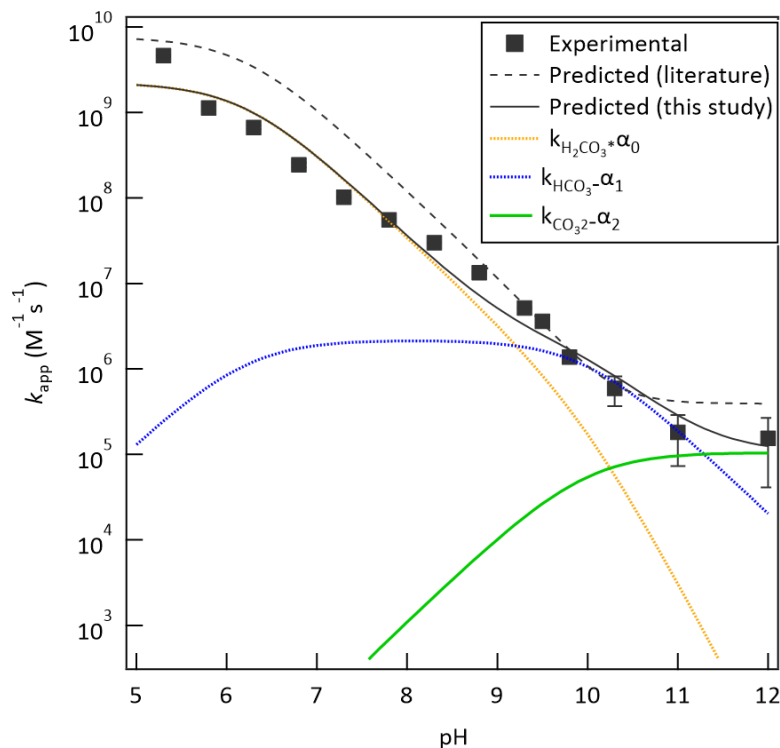
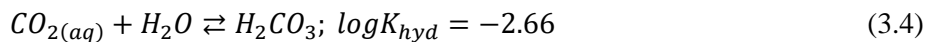


Figure 3.3 Effect of pH on measured and model-predicted apparent rate constants for e_{aq}^- reaction with dissolved carbonate species. Simulated contributions of $H_2CO_3^*$ ($2.23 \times 10^9 M^{-1} s^{-1}$; beveled orange line), HCO_3^- ($2.18 \times 10^6 M^{-1} s^{-1}$; beveled blue line), and CO_3^{2-} ($1.05 \times 10^5 M^{-1} s^{-1}$; beveled green line) to the overall quenching (solid black line) are also shown. Dashed black line shows model predictions using rate constants previously reported in literature.^{47,130,131}

Figure 3.3 also illustrates the relative contributions of individual carbonate species to net quenching of e_{aq}^- at different pH conditions. This shows that $H_2CO_3^*$ is the dominant quencher species at $pH < 9$ despite the fact that it is a minor contributor to carbonate speciation at $pH > 6.35$. The dominance of quenching by $H_2CO_3^*$ at $pH < 9$ is further highlighted by the fact that all the individual measured e_{aq}^- measurements at these pH conditions (40 different data points at varying concentration and pH conditions) fall onto a single Stern-Volmer type plot when the x-axis is re-defined by the calculated concentration of $H_2CO_3^*$ (Figure B.3) rather than total dissolved carbonate (C_{T,CO_3}). It is also notable that the resulting k_{app} value derived from this data set ($1.42 (\pm 0.04) \times 10^9 M^{-1} s^{-1}$) is similar to the value of $k_{H_2CO_3^*}$ obtained from fitting the pH-dependent k_{app} data set with Eq. 3.3. Nevertheless, ARP applications are most often being conducted at $pH \geq 9$, where HCO_3^- is a major contributor to e_{aq}^- quenching and cannot be ignored. For example, this analysis indicates that HCO_3^- is responsible for 85% of the carbonate inhibition of PFOS degradation rates observed in Figure 3.1.

Reaction mechanisms. Model fits are consistent with e_{aq}^- quenching by $H_2CO_3^*$, HCO_3^- , and CO_3^{2-} species. $H_2CO_3^*$ is defined to include both $CO_{2(aq)}$ and H_2CO_3 , which are related by hydration/dehydration equilibrium:



Hence, this equilibrium is strongly shifted to the left and $H_2CO_3^*$ is dominated by $CO_{2(aq)}$ (i.e., $[CO_{2(aq)}] \approx C_{T,CO_3}$ at $pH < pK_{a1}$). Earlier reports document that the reaction of $CO_{2(aq)}$ with e_{aq}^- yields CO_2 radical anion ($CO_2^{\cdot-}$), confirmed by transient absorption spectroscopy¹³²:



While most studies to date show that increasing dissolved carbonate acts to inhibit rates of e_{aq}^- ARPs,^{64,133} a recent report suggests that $CO_2^{\cdot-}$, itself, may react with more recalcitrant PFASs (e.g., perfluorobutane sulfonate).¹³⁴ However, the importance of PFAS reactions compared to other processes that rapidly consume $CO_2^{\cdot-}$, including near diffusion-limited radical recombination reactions, remains to be established.^{51,84,132} Still, further studies of the fate and reactivity of $CO_2^{\cdot-}$ is warranted given the likelihood for generation of this transient species during e_{aq}^- ARPs in carbonate-containing natural water matrices.

The minor contributor to $H_2CO_3^*$, H_2CO_3 , and its conjugate base HCO_3^- are Brønsted acids, where the acidic proton can react with e_{aq}^- to yield atomic hydrogen in the same manner as H_3O^+ ions:¹³⁵



Because of its minor contribution to $H_2CO_3^*$, we are unable to directly quantify the reactivity of H_2CO_3 with e_{aq}^- , separate from $CO_{2(aq)}$, but previous work has shown that the reactivity of different Brønsted acids vary with acid strength according to the following relationship:⁶⁸

$$\frac{k_2}{p} = G_A \left(\frac{qK_A}{p} \right)^\beta \quad (3.9)$$

where k_2 , K_a , p , and q respectively represent the bimolecular rate constant for Brønsted acid reactivity with e_{aq}^- , the acid dissociation constant, the number of dissociable protons available in the acid, and the number of equivalent sites at which a proton can be attached to in the conjugate base. G_A and β are constants distinct to similar types of acids.¹³⁵ Using data presented by Maza and coworkers⁶⁸ for a series of Brønsted acids together with the pK_{a1} of H_2CO_3 (3.45),¹³⁶ we estimate k_2 for H_2CO_3 of $4.8 \times 10^8 \text{ M}^{-1}\text{s}^{-1}$ (Figure B.4). It is worth noting that the estimated $k_{H_2CO_3}$ is more than 4 times lower than the value determined for $H_2CO_3^*$ from fitting experimental data ($2.23 \times 10^9 \text{ M}^{-1} \text{ s}^{-1}$), further supporting the conclusion that $CO_{2(aq)}$ is the dominant species contributing to e_{aq}^- scavenging. It is also worth noting that

lower reactivity of HCO_3^- determined from model fitting ($2.18 \times 10^6 \text{ M}^{-1} \text{ s}^{-1}$) is consistent with the Brønsted relationship described by Eq 3.9, and similar in magnitude to the value reported for e_{aq}^- quenching by NH_4^+ ($1.30 \times 10^6 \text{ M}^{-1} \text{ s}^{-1}$),¹³⁷ a Brønsted acid of similar strength to HCO_3^- . The fully deprotonated (CO_3^{2-}) species still reacts with e_{aq}^- , albeit very slowly. To the best of our knowledge, there are no literature reports on the product of the reaction between e_{aq}^- and CO_3^{2-} or similar polyatomic ions such as SO_3^{2-} despite rate constants being available for both.^{47,62,138,139}

Relative importance of carbonate species to other quenchers. Data presented in Figure 3.1 shows the importance of carbonate species as e_{aq}^- quenchers that inhibit ARP treatment of PFOS. We can more generally evaluate the importance of dissolved carbonate species relative to other quencher species expected to be abundant in natural water matrices during ARP treatment applications. The net contribution of individual quenchers can be quantified by the product of their concentration and bimolecular rate constant for reaction with e_{aq}^- , $k_i[i]$. For carbonate species, this can be formulated according to the following expression:

$$k_{\text{H}_2\text{CO}_3^*}[\text{H}_2\text{CO}_3^*] + k_{\text{HCO}_3^-}[\text{HCO}_3^-] + k_{\text{CO}_3^{2-}}[\text{CO}_3^{2-}] \quad (3.10)$$

Other e_{aq}^- quenchers expected to be common in groundwater matrices during ARP treatments include the conjugate acid of the sulfite photosensitizer, HSO_3^- ($1.2 \times 10^8 \text{ M}^{-1} \text{ s}^{-1}$),⁶⁸ H^+ ($2.3 \times 10^{10} \text{ M}^{-1} \text{ s}^{-1}$),^{62,140} dissolved O_2 ($1.9 \times 10^{10} \text{ M}^{-1} \text{ s}^{-1}$),¹¹⁸ and nitrate ($9.7 \times 10^9 \text{ M}^{-1} \text{ s}^{-1}$)^{62,141}. It follows that total quenching of e_{aq}^- can be formulated as:

$$\begin{aligned} \sum k_i[i] = & k_{\text{H}_2\text{CO}_3^*}[\text{H}_2\text{CO}_3^*] + k_{\text{HCO}_3^-}[\text{HCO}_3^-] + k_{\text{CO}_3^{2-}}[\text{CO}_3^{2-}] + k_{\text{HSO}_3^-}[\text{HSO}_3^-] \\ & + k_{\text{H}^+}[\text{H}^+] + k_{\text{O}_2}[\text{O}_2] + k_{\text{NO}_3^-}[\text{NO}_3^-] \end{aligned} \quad (3.11)$$

Figure 3.4 illustrates the predicted contribution of individual quencher species and overall quenching in solutions at varying pH conditions (Figure 3.4A) and varying total dissolved carbonate concentrations (Figure 3.4B). If we first consider matrices free of O_2 and NO_3^- , we observe strong pH dependence for the rates of quenching by different species resulting from shifts toward conjugate acid species with elevated reactivity. This trend is consistent with experimental observations that UV-sulfite treatment efficacy decreases with decreasing pH.^{64,107,121} Comparing the contributions of different quencher species, it appears that carbonate and bisulfite species are the major quenchers anticipated at most conditions, with the relative contributions being dependent on their respective concentrations in the matrix of interest. For example, if the trends for 1 mM total dissolved carbonate and 10 mM sulfite are compared, simulations in Figure 3.4A show that carbonate quenching dominates at $\text{pH} < 6.5$ and > 9.6 , but sulfite dominates at pH conditions in between. When a lower sulfite concentration (3 mM) is used for treatment, such as in the PFOS experiments shown in Figure 3.1, carbonate species become the dominant quencher over the entire pH range. Investigations into UV-ARPs have often used 10 mM sulfite as a sensitizer along with 5 mM carbonate as

a buffer.^{85,95,101} This system is represented by the dashed line in Figure 3.4A, which shows that the curve representing total background quenching nearly overlaps the line for 5 mM carbonate suggesting that carbonate alone is responsible for any pH dependent processes involving e_{aq}^- processes. It is also noteworthy that H^+ contributes negligibly to e_{aq}^- quenching across the full range of pH conditions. As shown in Figure 3.4B, carbonate quenching becomes important relative to anticipated sulfite quenching as total dissolved carbonate approaches millimolar levels, typical of many natural water matrices. Inclusion of quenching by carbonate species is expected to be important within models for ARP treatment of PFAS and other recalcitrant contaminants.

Figure 3.4B also shows that quenching from dissolved O_2 and NO_3^- will be dominant when present in the matrix at elevated levels, highlighting the need to characterize these species in sourcewaters being subjected to treatment. Although dissolved O_2 has a very high reactivity with e_{aq}^- , it is expected to be very low in concentration during UV-sulfite treatment applications because sulfite is an effective scavenger of O_2 and suppresses its concentration.⁶³ In fact, recent studies show that there is little benefit to actively deoxygenating solutions prior to UV-sulfite treatment since the sensitizer effectively suppresses dissolved oxygen concentrations and eliminates scavenging of e_{aq}^- generated upon UV irradiation.⁵⁹ Still, this is an issue to be aware of when applying other ARPs. Nitrate is also known to be a strong scavenger of e_{aq}^- , so nitrate-contaminated water matrices will require denitrification before applying ARPs to treat less reactive contaminants like PFASs. The ARPs themselves can remove the nitrate, but the additional e_{aq}^- demand of the matrix needs to be accounted for in treatment system design. These findings provide critical insights into the operative mechanisms responsible for poor performance of ARPs often observed at lower pH conditions. They also provide mechanistic support for the recent design recommendations to adjust pH conditions prior to UV-sulfite treatment.⁹⁵ Ultimately, quantitative information on background scavenging of sourcewater matrices, such as those provided here, provides critical information needed to improve predictions and design of ARP technologies for treatment of recalcitrant micropollutants such as PFASs.

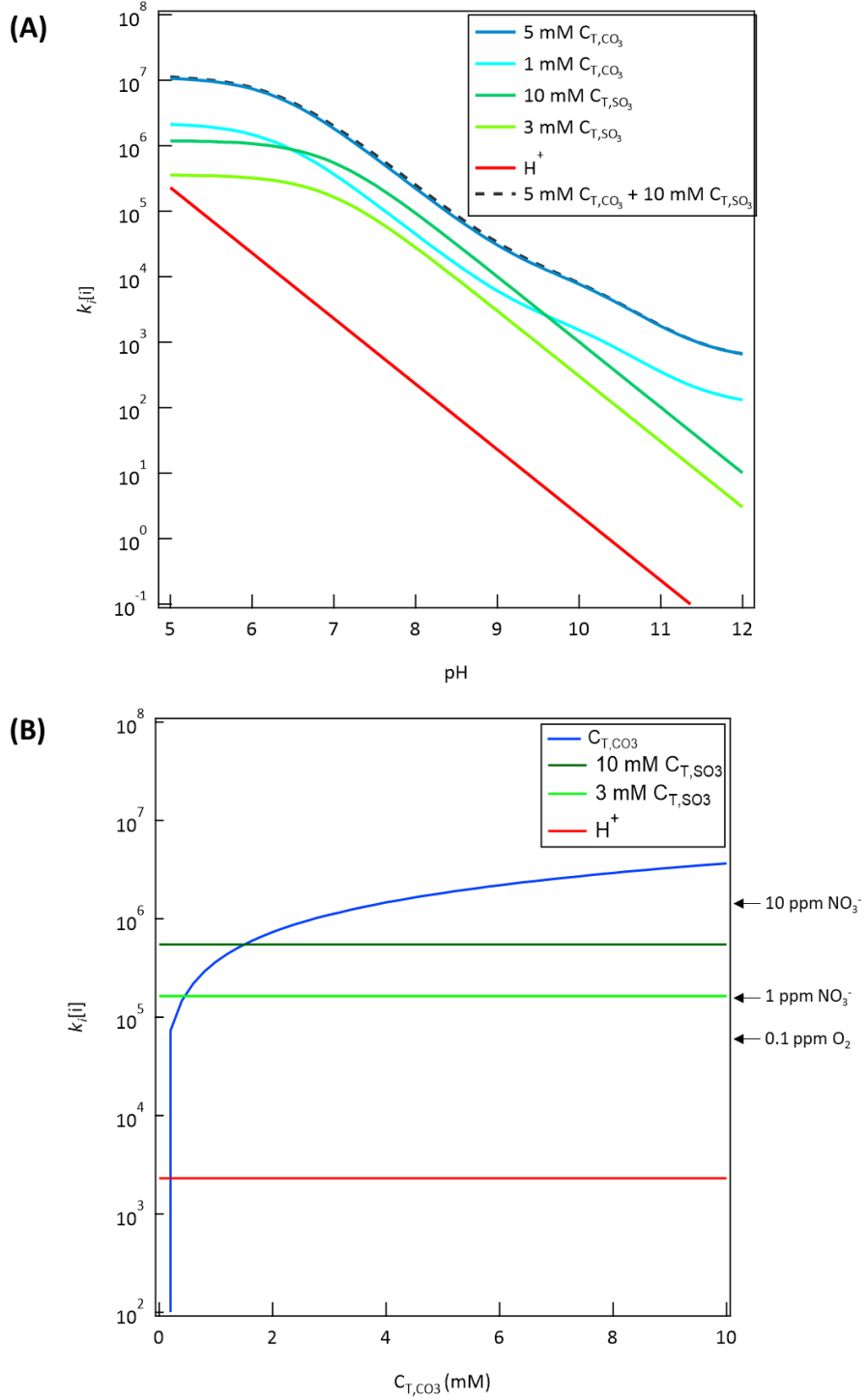


Figure 3.4 Simulation of the rates e_{aq}^- scavenging by dissolved carbonate species in comparison with other common scavengers expected during groundwater treatment with UV-sulfite. (A) influence of pH, and (B) influence of variable carbonate concentration at pH 7.0.

CHAPTER 4
KINETIC MODEL FOR PREDICTING PFAS DEGRADATION
DURING UV-SULFITE TREATMENT

Based on a paper in preparation.

Camille K. Amador^{1,2}, Michael Dooley², Raul Tenorio³, Christopher P. Higgins¹, Shubham Vyas², and Timothy J. Strathmann¹

4.1 Abstract

Hydrated electron processes such as UV-sulfite show great potential in remediating recalcitrant water contaminants including per- and polyfluoroalkyl substances (PFAS), however treatment efficacy is contingent upon many factors relating to sourcewater composition and characteristics of the UV light source. Here we provide critical insights into the complex roles of important solution parameters (e.g., pH and non-target water constituents) on contaminant abatement through a newly developed UV-sulfite kinetic model. The model sufficiently predicts parent compound decay profiles of ubiquitous perfluoroalkyl acids (PFAAs) in different environments and facilitates the quantitative interpretation of system and solution parameters on treatment results. Changes in solution pH and dissolved carbonate concentration were well characterized by the model and results confirm that enhanced degradation of PFAS at highly alkaline pH conditions is due to speciation of e_{aq}^- quenchers such as sulfite and carbonate rather than H^+ . TriFBA, a polyfluorinated alkyl acid, was not well-predicted using the previously reported k_2 value which corroborates but does not confirm that per- and polyfluorinated carboxylates undergo diverging reaction mechanisms as postulated in previous work. To model longer-chain PFAS with more reaction sites, a rate constant for PFHxA was determined using LFP ($k_2 = 3.84 \pm 0.30 \times 10^7 \text{ M}^{-1} \text{ s}^{-1}$) while rate constants for insoluble or nonreactive structures were estimated using k_{obs} and e_{aq}^- availability; both methods simulate experimental data well. The proposed model successfully links the disparate means of investigating e_{aq}^- processes, namely, UV photolysis and LFP/pulse radiolysis and provides the framework needed to estimate UV-sulfite treatment efficacy of perfluoroalkyl acids ahead of treatment.

¹Department of Civil and Environmental Engineering, Colorado School of Mines, Golden, CO

²Department of Chemistry, Colorado School of Mines, Golden, CO

³Haley and Aldrich, Phoenix, AZ (Current Affiliation)

4.2 Introduction

Advanced reduction processes (ARPs) have gained a lot of traction in environmental remediation due to their ability to transform highly oxidized chemicals such as chlorinated solvents and toxic oxyanions at ambient temperatures and pressures.^{43,44,112,113} UV-ARPs based on the photochemical generation of hydrated electrons (e_{aq}^-) are especially useful for the transformation of highly recalcitrant per- and polyfluoroalkyl substances (PFAS).¹¹¹ Development of UV-ARPs in practice has focused on the UV-sulfite system because of the low cost and ubiquity of sulfite in existing water treatment plants (e.g., for dichlorination)⁶¹, as well as the fact that the byproduct sulfate is naturally occurring and not harmful to human health. The UV-sulfite system also has the added benefit of rapidly depleting dissolved oxygen from solution creating highly desirable conditions for hydrated electron processes.^{63,84}

Studies investigating the use of e_{aq}^- based UV-ARPs for remediation are performed either by constant UV irradiation or, more rarely, by laser flash photolysis (LFP) and pulse radiolysis techniques. While these methodologies aim to study the same reaction (e_{aq}^- with PFAS or other target contaminants), there are key inconsistencies in the results obtained when comparing the two approaches. The effect of solution pH on the kinetics of the reaction is one key area of misalignment. Bentel et al. report significantly enhanced degradation of perfluorocarboxylates (PFCAs) in UV-sulfite systems when pH is increased from 9.5 to 12.0, however our recent work shows pH invariance for both bimolecular rate constant (k_2 ; $M^{-1} s^{-1}$) of PFCAs with e_{aq}^- as well as e_{aq}^- lifetime.^{95,122} Another important inconsistency involves the effect of functional headgroup and chain length on the kinetics of the reaction, as well as their absolute values. For example, both Park et al. and Bentel et al. report increasing transformation of PFASs by e_{aq}^- in the UV-iodide and sulfite system, respectively, with increasing chain length.^{107,142} Meanwhile, chain length was found to have negligible effect on PFCA degradation, and overall kinetics of PFCA transformation were found to be faster than PFASs. These experimental results were corroborated by theoretical insights provided by Van Hoomissen and Vyas, who found aqueous vertical attachment energy (VAE) from instantaneous electron addition to vary with chain length for PFASs but not for PFCAs.⁹⁴ Maza et al., however, report k_2 values for PFASs to be up to 5x higher than PFCAs and did not observe chain length dependence for the PFASs.⁸⁷ Moreover, the PFCA values reported by Maza et al. are up to 2 orders of magnitude greater than those previously reported using ferrocyanide LFP and pulse radiolysis.^{50,86,122,143}

Recently, Jiang et al. used pulse radiolysis to determine the k_2 values for PFOS and PFBS with e_{aq}^- . In this study, PFBS was found to be unreactive with an estimated k_2 value $< 10^6 M^{-1} s^{-1}$ which contradicts the value reported by Maza et al. ($1.8 \times 10^9 M^{-1} s^{-1}$), however is in alignment with many

constant UV irradiation experiments that report little to no degradation of PFBS.^{85,107,134} Interestingly, the k_2 value for PFOS was determined to be around $4.5 \times 10^9 \text{ M}^{-1} \text{ s}^{-1}$, which is not far off from that of Maza et al. ($2.4 \times 10^9 \text{ M}^{-1} \text{ s}^{-1}$). The study by Jiang et al. seems to confirm the low reactivity of PFBS as well as qualitatively support the chain length dependence of PFSA transformation. The reactivity of PFOS reported by Maza et al. also seems to be confirmed by Jiang et al., however it is hard to reconcile this when, to the best of our knowledge, all constant UV irradiation studies have found PFOS to be less reactive than PFOA, whose k_2 value was previously found to be $1.7 \times 10^7 \text{ M}^{-1} \text{ s}^{-1}$.⁵⁰

Development of a photochemical model to quantitatively predict PFAS degradation kinetics across diverse environments is an alternative approach to studying e_{aq}^- processes.⁹² Methods such as this are common in advanced oxidation processes (AOPs),^{102,108} however models involving ARPs are limited.^{66,109} Kinetic models will be useful in simulating parent compound decay profiles during UV-ARP treatment in different environments, minimizing the need to run multiple batch experiments to ascertain the effect of single parameters and optimize reaction conditions. These models will also be useful to quantitatively interpret system and solution parameters on treatment efficacy. As a result, this photochemical model will reconcile the discrepancies between the two methodologies by using the fundamental kinetic values measured by LFP and pulse radiolysis to predict degradation in constant UV irradiation systems ahead of treatment.

UV-sulfite processes have already been shown to successfully transform both PFCAs and PFASs,^{59,85,111} however achieving full mineralization is highly dependent on solution conditions.⁶⁴ A photochemical model describing the kinetics and efficiency of UV-sulfite processes has previously been formulated by Li et al. using monochloroacetic acid (MCAA) as a model compound.⁸⁴ The authors successfully predict the degradation profiles of MCAA in various environments, but the model has yet to be applied to e_{aq}^- processes for PFAS degradation. Fennell et al. recently developed a model based on e_{aq}^- exposure per fluence rate (or $R_{e,UV}$) that successfully predicted MCAA transformation in the UV-sulfite system.¹³³ Because the k_2 values for PFOS vary over two orders of magnitude^{87,134,143} the authors performed least squares fit to estimate a k_{PFOS} that would match their experiments ($5.7 \times 10^6 \text{ M}^{-1} \text{ s}^{-1}$). While these works undoubtedly contribute to the development of a quantitative model to understand UV-ARP systems, the model still lacks the ability to quantitatively interpret the effects of individual parameters on treatment efficacy such as pH, UV intensity, sensitizer concentration, and more. Moreover, this study has not been able to reconcile the discrepancy between constant UV irradiation systems and LFP/pulse radiolysis as the current values for PFOS significantly overpredict their experimental results.

The ideal photochemical model will include inputs regarding important constituents present in water (e.g., e_{aq}^- scavengers), inputs regarding system parameters (e.g., photon flux, UV lamp intensity), and solution conditions (pH). In this study, we adapt the model developed by Li et al. to predict

degradation profiles of PFAS during UV-sulfite treatment in diverse environments which, for the first time, links results from constant UV irradiation experiments to k_2 values for e_{aq}^- reactions with individual PFAS and non-target scavengers. Bimolecular rate constants for the target contaminant with e_{aq}^- from our previous study,¹²² as well as others,^{50,86} were used to predict results and the simulations were compared. Important scavengers were selected due to their reported rate constants ($> 10^6 \text{ M}^{-1} \text{ s}^{-1}$) or their abundance in solution (e.g., solvent, H_2O). UV photoreactions were conducted at different pH values and total dissolved carbonate concentration ($C_{\text{T,CO}_3}$) using PFCAs, PFSAs, as well as a fluorotelomer carboxylate, and the model was used to simulate their degradation profiles.

4.3 Materials and Methods

Chemicals. All chemicals and solvents were used as received without further purification. A full list can be found in Appendix C.

UV photoreactions. Constant UV-sulfite irradiation of all PFAS was performed using a light source and reactor previously described.⁸⁵ Photoreactions were performed in a solution containing 100 $\mu\text{g/L}$ of each select PFAS with 10 mM Na_2SO_3 and specified concentrations of NaHCO_3 . Solution pH was adjusted using 1 M HCl or 1 M NaOH and buffered using either carbonate or borate. Detailed reaction conditions are specified for each experiment throughout the text. To eliminate e_{aq}^- scavenging by dissolved oxygen, solutions were deoxygenated by sparging with $\text{N}_{2(\text{g})}$ for 1 h before introducing PFAS and sulfite to initiate UV reactions. Sample aliquots were collected at pre-determined time intervals to measure changing PFAS concentrations which were measured by liquid chromatography with tandem mass spectrometry (LC-MS/MS) using procedures described in Appendix C and instrumentation described elsewhere.¹²⁸ Solution pH was re-measured after the reaction was completed to evaluate any pH drift during experiments. Additional details on preparation, reaction conditions, and analysis are described in Appendix C.

Laser flash photolysis. A Nd:YAG laser was used with a 4th harmonic generator to produce 266 nm light (details described elsewhere).¹²² Generation of e_{aq}^- was achieved by irradiating an anoxic solution of 40 μM $\text{K}_4\text{Fe}(\text{CN})_6$ and 10 μM $\text{K}_3\text{Fe}(\text{CN})_6$ with an 8-10 mJ laser pulse. Decay of e_{aq}^- was monitored by tracking the change in absorbance of its characteristic peak at 690 nm ($\epsilon = 20560 \text{ M}^{-1} \text{ cm}^{-1}$) using ten averages for each of the measurements.^{49,92} All LFP experiments were performed under anoxic conditions. Solutions were buffered at pH 9.2 using sodium tetraborate and ionic strength as fixed across samples using NaCl. All samples were prepared and run in triplicate and uncertainties provided represent standard deviations. Individual cuvettes were amended with varying concentration of the target PFAS

quencher and Stern-Volmer analysis of the change in e_{aq}^- lifetime (τ) was used to determine the k_2 value. Additional details on reaction solution preparation and are described Appendix C.

4.4 Results and Discussion

Effect of solution conditions on PFBA degradation kinetics. Efficacy of UV-ARPs is contingent upon e_{aq}^- availability throughout the reaction and higher concentrations are strongly favored for optimal contaminant transformation. PFAS contaminated water typically contains concentrations in the ppt – ppb range which would be inefficient to directly treat with UV processes due to the large volume of media needing treatment.³⁰ Many studies have emphasized the importance of prior steps to concentrate the PFAS before being subjected to destruction methods such as UV-sulfite for increased efficiency.⁵⁹ This concentration step, which typically involves resins or membranes,^{59,128} can inadvertently concentrate common ions present and impact degradation performance. Chloride and phosphate were not found to appreciably inhibit PFOA degradation by UV-sulfite up to 150 and 25 mM, respectively.⁶⁴ Nitrate and carbonate, however, exhibited significant inhibitory effects at concentrations of 2 and 5 mM, respectively. Despite earlier reports that carbonate did not have an observable impact on degradation of monochloroacetate (MCAA) in the UV-sulfite system,⁸⁴ our recent report shows that PFOS degradation kinetics are inhibited by the presence of even 1 mM carbonate, while a previous report by Ren et al. exhibits similar effect on PFOA defluorination.⁶⁴ From this, it is clear that carbonate and alkalinity are important factors to consider if ARPs are to be utilized for contaminant remediation.

Here we perform UV-sulfite photolysis reactions to confirm the effect of dissolved carbonate on the kinetics of e_{aq}^- ARPs for PFAS degradation using PFBA as a representative compound. In the absence of carbonate, typical UV-sulfite conditions (pH 9.5, 10 mM SO_3^{2-} , 20°C) yield an observed rate constant (k_{obs}) for PFBA of $1.31 \pm 0.09 \text{ h}^{-1}$ (Figure 4.1A). This value dropped by almost 50% ($0.665 \pm 0.039 \text{ h}^{-1}$) and >70% ($0.373 \pm 0.025 \text{ h}^{-1}$) in the presence of 5 and 10 mM total dissolved carbonate ($\text{C}_{\text{T,CO}_3}$), respectively, and this decrease continue up to 25 mM $\text{C}_{\text{T,CO}_3}$ ($0.109 \pm 0.005 \text{ h}^{-1}$), the highest concentration investigated. Similar effects were observed for PFPrA and TFA as well (Figure C.2).

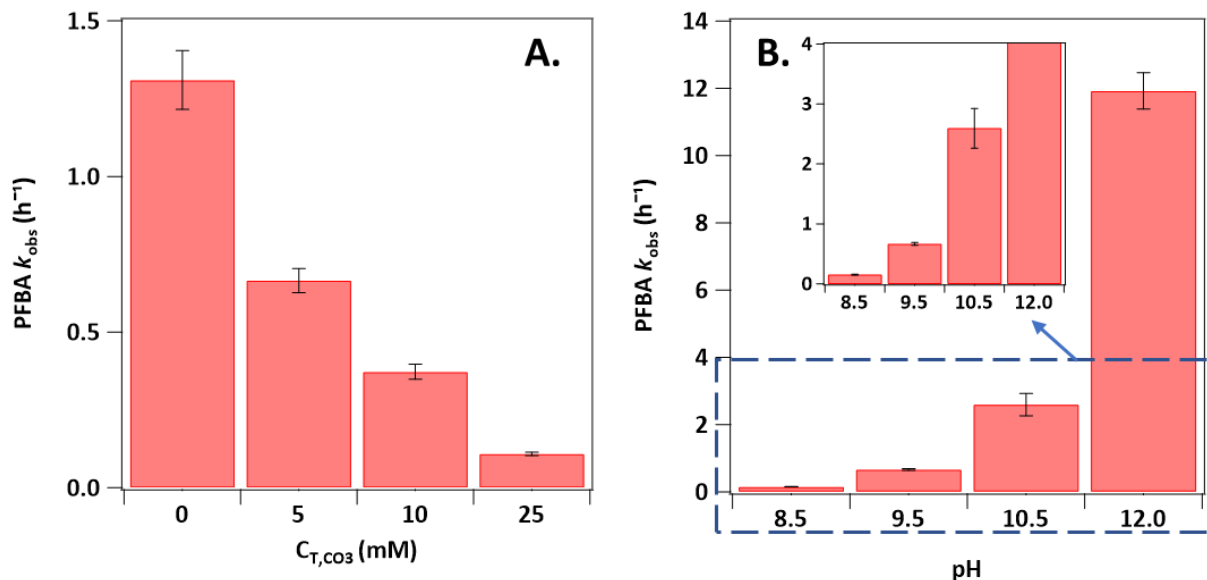


Figure 4.1 Effect of (A) dissolved carbonate and (B) pH on the observed rate constant of PFBA degradation during UV-sulfite treatment. Reaction conditions for $[PFBA]_{initial} = 100 \mu\text{g/L}$, 10 mM Na_2SO_3 , irradiation with LP-Hg light source, 20°C. For (A) pH was adjusted to 9.5^a for each condition, and for (B) 5 mM carbonate buffer was used. Error bars represent duplicate measurement-derived standard deviations. ^aThe 0 mM C_{T,CO_3} experiment was buffered at pH 9.5 using 5 mM borate buffer, known to be unreactive towards e_{aq}^- .¹⁴⁴

There is consensus in the literature that higher pH favors contaminant degradation in the UV-sulfite system. For example, Bentel et al. report significantly enhanced degradation of PFCAs at pH 9.5 vs pH 12. In their study, degradation of all target PFCAs was accomplished in 1 h at pH 12, however at pH 9.5, target PFCAs were still present after 24 h of photolysis.⁹⁵ In addition, Ren et al. report about 85% PFOA defluorination after 4 h of UV-sulfite treatment at pH 12, while at pH 9 only about 65% defluorination was achieved. This seems to contrast our recent work using LFP which shows pH invariance for both bimolecular rate constant (k_2 ; $\text{M}^{-1} \text{s}^{-1}$) of PFCAs with e_{aq}^- as well as e_{aq}^- lifetime (τ).¹²² If the rate at which e_{aq}^- reacts with PFAS as well as its lifetime does not change when increasing pH, one would expect the observed degradation to be unchanged as well. Because of this perceived discrepancy, we revisit the effect of pH on the kinetics of e_{aq}^- ARPs for PFAS degradation again using PFBA as a representative compound. At pH 8.5, UV-sulfite treatment of PFBA with 10 mM sulfite (5 mM carbonate buffer) exhibited very slow degradation with a k_{obs} of $0.151 \pm 0.011 \text{ h}^{-1}$. The kinetics of the reaction can be slightly increased when solution pH is raised to 9.5 and 10.5: $0.665 \pm 0.039 \text{ h}^{-1}$ and $2.59 \pm 0.32 \text{ h}^{-1}$, respectively (Figure 4.1B). However, the most marked increase occurs between pH 10.5 and 12.0 where k_{obs} increases by nearly a factor of 5 to $11.92 \pm 2.31 \text{ h}^{-1}$. Similar effects are observed for PFPrA and TFA as well (Figure C.3). The drastic enhancement in reaction kinetics at pH 12.0 likely occurs because

of two important factors. First, at 12.0 sulfite is present almost entirely as SO_3^{2-} (>99.999%), the species responsible for e_{aq}^- ejection into solvent, whereas at pH 10.5 the conjugate acid HSO_3^- accounts for at least 0.03% of total dissolved sulfite (C_{T,CO_3}). While this may seem minimal, HSO_3^- directly contributes to its deactivation ($k_2 = 1.2 \times 10^8 \text{ M}^{-1} \text{ s}^{-1}$).⁶⁸ Second and perhaps more importantly, carbonate speciation above pH 10.5 quickly shifts away from H_2CO_3^* and HCO_3^- (fast e_{aq}^- quenchers) and towards CO_3^{2-} . At pH 10.5, the former two species account for 29% of C_{T,CO_3} , whereas at pH 12 they only account for 1%.

The marked decrease in PFOS degradation kinetics in the presence of dissolved carbonate as well as the dramatic shifts in PFOS degradation kinetics when varying solution pH highlight the importance of sourcewater composition in dictating UV-sulfite treatment efficacy. From this, we propose that with information on geochemical solution conditions and UV light source, it is possible to ascertain the availability of e_{aq}^- during treatment which is expected to be directly related to contaminant degradation.

Kinetic model. UV-ARP treatment results can be described by a pseudo-first order kinetic equation in which there is a steady-state concentration of the reactive species (e_{aq}^-) throughout the duration of the reaction:

$$\ln\left(\frac{C}{C_0}\right) = -k_{obs}t = -k_2[e_{aq}^-]_{ss}t \quad (4.1)$$

where C represents the concentration of the target contaminant, k_{obs} represents the observed rate constant in UV photolysis experiments (h^{-1}), t represents time (h), k_2 represents the bimolecular rate constant of the target contaminant with e_{aq}^- ($\text{M}^{-1} \text{ s}^{-1}$), and $[e_{aq}^-]_{ss}$ represents the steady-state concentration of hydrated electron in the system, or e_{aq}^- availability (M).

Hydrated electron availability. $[e_{aq}^-]_{ss}$ is a function of processes that produce e_{aq}^- and reactions that quench it from solution:

$$[e_{aq}^-]_{ss} = \frac{r_e}{\sum k_i[Q]_i + k_2[C]} \quad (4.2)$$

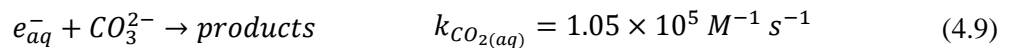
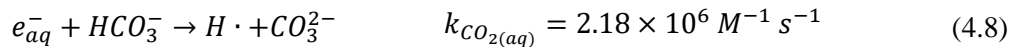
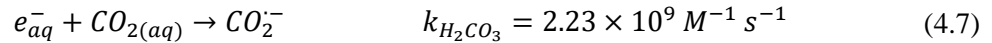
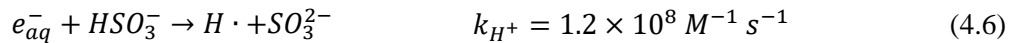
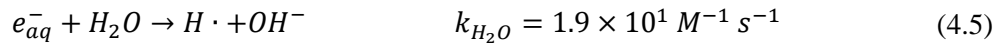
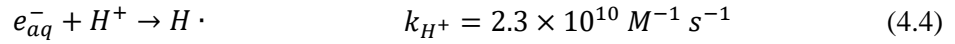
where r_e ($\text{M}\cdot\text{s}^{-1}$) represents the rate of hydrated electron production and the term $\sum k_i[Q]_i$ (s^{-1}) represents the summation of the bimolecular rate constants of all important quenchers present multiplied by their respective concentration in solution. This can be taken as an estimate of background scavenging capacity of a system or a measure of the constituents which compete with target contaminants for e_{aq}^- reactions.

Rate of hydrated electron production has previously been described by Li et al.⁸⁴:

$$r_e = \frac{\rho_0 \times \varphi \times (1 - e^{-aL\ln(10)})}{V} \times \frac{\varepsilon S}{a} \quad (4.3)$$

where ρ_0 is the photon flow ($E \cdot s^{-1}$), φ is the effective quantum yield ($mol \cdot E^{-1}$), a is the decadic absorbance by solution (cm^{-1}), L is the effective path length (cm), V is solution volume (L), ϵ is the decadic molar extinction coefficient ($M^{-1} \cdot cm^{-1}$), and S is the sensitizer concentration (M).

While the summation $\sum k_i[Q]_i$ technically represents e_{aq}^- quenching by all scavengers present, it is only necessary to include scavengers whose product of $k_i[Q]_i$ will be larger or comparable to that of $k_2[C]$ (the k_2 value of a target PFAS reacting with e_{aq}^- multiplied by its concentration). Acidic proton (H^+) has long been recognized as the putative e_{aq}^- quencher in UV-ARPs at circumneutral pH conditions.^{53,81,145} It quenches e_{aq}^- at diffusion limited rates (Eq. 4.4) and so will be accounted for when determining e_{aq}^- quenching. Solvent (H_2O) will also be included in the model because, although the reaction between H_2O and e_{aq}^- is slow (Eq. 4.5), its concentration is high enough (55.5 M) to warrant its inclusion. Maza et al. previously reported that bisulfite (HSO_3^-), the conjugate acid species of the sulfite photosensitizer (pK_a 7.2),¹²⁴ is a significant quencher of e_{aq}^- at certain pH conditions and so is also important to consider (Eq. 4.6).⁶⁸ Our previous work suggests that dissolved carbonate is an important scavenger when present at environmentally relevant concentrations and therefore elicits inclusion to quantify background scavenging (Eq. 4.7-4.9). Concentrations of quenchers ($[Q]_i$) at various pH conditions can be determined using Visual MINTEQ. Values for our system regarding rate of e_{aq}^- production (r_e), background scavenging capacity $\sum k_i[Q]_i$, and ultimately e_{aq}^- availability ($[e_{aq}^-]_{ss}$) can be found in the Table C.3.



Predicting ultra-short chain PFCA degradation kinetics. Eq. 4.1 indicates that PFAS degradation follows second-order kinetics and is dependent on the concentration of the target contaminant as well as the reactive species (e_{aq}^-). The latter of these is described by Eq. 4.2, which highlights that if a co-existing constituent exists in high enough concentration or possesses a high enough reactivity with e_{aq}^- , then its presence will appreciably decrease $[e_{aq}^-]_{ss}$, thereby inhibiting contaminant transformation.

The solid circles in Figure 4.2 depict the PFBA curves from which the k_{obs} in Figure 4.1 were derived. Similar profiles for PFPrA and TFA can be found in Figure C.4. By accounting for the quenchers discussed above as well as parameters of the UV light source (Eq. 4.3), Eq. 4.1 can simulate the decay profiles of PFBA (solid lines in Figure 4.2A) in the presence of varying amounts of the added C_{T,CO_3} quencher. The model does an excellent job at predicting degradation of the target contaminant when C_{T,CO_3} is varied suggesting that (1) k_2 values measured previously for PFBA, PFPrA, and TFA are accurate and relevant to UV-sulfite ARPs,¹²² (2) the quenchers included sufficiently account for background scavenging in our system, and (3) the species-specific k_2 values derived for ubiquitous carbonate species are reliable. Results for the 0 mM C_{T,CO_3} condition and simulation is interesting in that, for each compound, degradation is relatively overpredicted which we attribute to the presence of unaccounted for quenchers (e.g., carbonate) that are likely present in the lab-grade water. In fact, our previous work showed that environmentally relevant concentrations of dissolved carbonate can significantly inhibit PFAS degradation in the UV-sulfite system. An important finding which arises from this analysis is the true nature of the pH dependence of UV-ARPs which has commonly been attributed to variable H^+ quenching.^{53,53,81} Bentel et al. recently postulated that the dramatic enhancement of PFCA degradation kinetics was due to higher e_{aq}^- availability (due to less quenching by H^+) and lowered redox potential at pH 12.⁹⁵ The former of these hypotheses is partially correct, however it is due to carbonate speciation, not H^+ , that e_{aq}^- availability is greater and hence results in enhanced degradation. Table C.3 shows that scavenging due to H^+ is more than three orders of magnitude lower than that due to carbonate.

Data points in Figure 4.2B display the decay profiles of PFBA at various pH conditions which were used to determine the k_{obs} in Figure 4.1B. By performing a similar analysis as above, we can simulate PFBA decay profiles at the different pH conditions (solid lines). Data for PFPrA and TFA are provided in Figure C.5. The model again does an excellent job at predicting degradation of the target contaminant when pH is varied. What's more is that the simulations capture the drastic enhancement in PFCA degradation from pH 9.5 to 10.5 and 10.5 to 12.0. It is important to note that these simulations are highly accurate, yet not exact. This is to be expected when considering that these are not model fits of the experimental data; they are true predictions of contaminant decay in photolysis experiments composed of fundamental values obtained using LFP and actinometry. Exact simulations of decay profiles are not expected nor are they the goal. Rather this study aims to provide accurate estimates of parent compound

decay profiles in different environments and to allow for the quantitative interpretation of the effects that each system and solution parameter has on overall treatment efficacy. Taken together this model can help to optimize reaction conditions ahead of treatment which will greatly save time and resources.

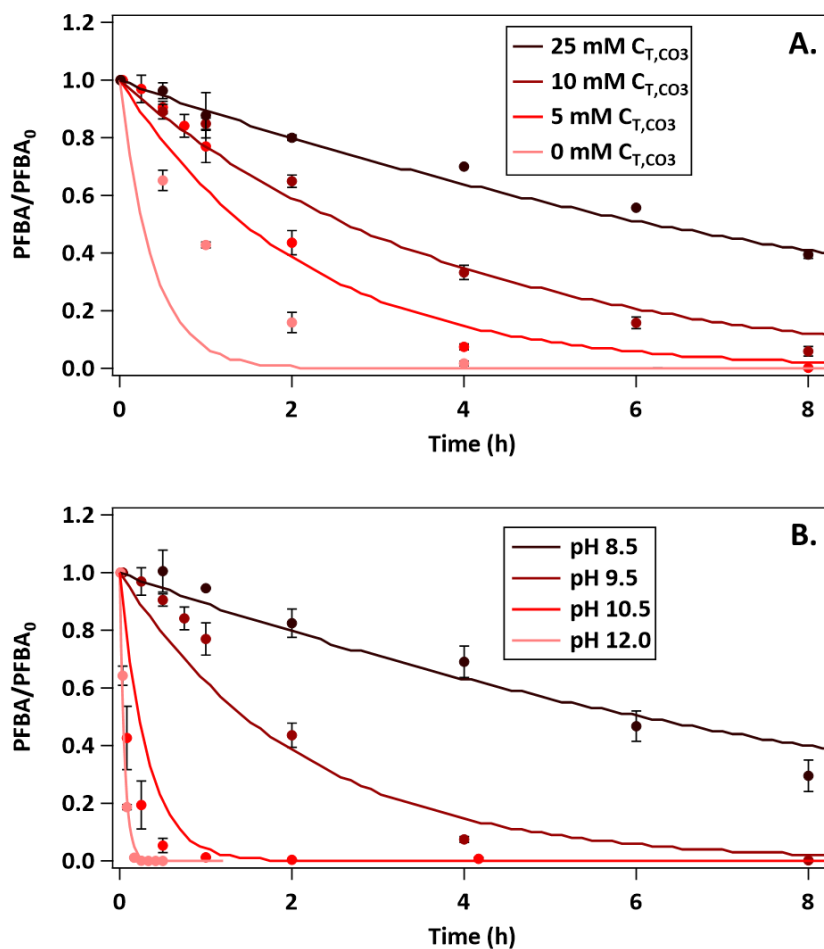


Figure 4.2 Degradation profiles of PFBA during UV-sulfite photolysis at (A) various C_{T,CO_3} conditions and (B) pH conditions. Symbols represent experimental data while solid lines represent model predictions. Reaction conditions are described in Figure 4.1.

Degradation kinetics of more complicated fluorocarboxylate systems. PFBA was chosen as a representative PFAS compound because we have previously determined its k_2 value with e_{aq}^- making it a convenient choice to test the model.¹²² Attempts were made to expand the suite of compounds to longer-chain PFCAs and polyfluorinated carboxylates in order to investigate how the model performs for more complicated systems containing a greater number of reaction sites such as PFHxA or PFOA. This requires accurate k_2 values which can be determined using laser flash photolysis (LFP) through Stern-Volmer analysis. LFP experiments require high concentration of added PFAS to appreciably alter the lifetime of

e_{aq}^- between samples and so is limited by the critical micelle concentration (CMC). Short and ultra-short chain PFCAs such as PFBA, PFPrA, and TFA are not expected to agglomerate in the way that longer-chain PFCAs do, therefore determining short-chain k_2 values is more straightforward. The CMCs of the C6 and C8 PFCAs, PFHxA and PFOA, are reported to be 82 mM and 9 mM at 20 °C, respectively, significantly limiting their dissolution, especially for PFOA.^{146,147} Nevertheless, a Stern-Volmer relationship for PFHxA was able to be constructed, and the corresponding k_2 value was found to be $3.84 \pm 0.30 \times 10^7 \text{ M}^{-1} \text{ s}^{-1}$ (Figure 4.3A and 4.3B).

In addition to LFP experiments, PFHxA was subjected to UV-sulfite photolysis experiments at pH 9.5 and 12 (10 mM sulfite, 5 mM carbonate buffer) and, as expected, exhibited a drastic increase in degradation kinetics at the higher pH value (data markers in Figure 4.3C). When using the LFP-derived k_2 value in the proposed model, simulations well predict the drastic increase in PFHxA kinetics at the two different pH conditions. So far, LFP-derived k_2 values for PFCAs has been successful in modeling degradation of all compounds attempted (i.e., PFBA, PFPrA, TFA, PFHxA). Another fluorocarboxylate structure we can test the model against is trifluorobutanoate (TriFBA), a fluorotelomer carboxylate (FTCA) characterized by hydrogenated carbons between the fluorocarbon tail and the acidic headgroup. In our previous study, we measured a high k_2 value for TriFBA of $7.35 \times 10^7 \text{ M}^{-1} \text{ s}^{-1}$ which was surprising considering TriFBA was found to be unreactive by Bentel et al. during UV-sulfite treatment.^{107,122}

We postulated that this discrepancy was due to diverging mechanisms of perfluorinated vs polyfluorinated compounds. Perfluorinated structures are proposed to undergo a stepwise elementary reaction mechanism which involves the formation of an intermediate radical anion that is resonance stabilized by the π -system of the carboxylate headgroup. This resonance stabilization allows the spin density to accumulate about the C-F bond and bond cleavage follows. Polyfluorinated structures, however, cannot impart the same pi-stabilization because electron attachment occurs at the γ -carbon, nonadjacent to the carboxylate moiety. These compounds likely undergo an associative mechanism, in which the strong C-F bond of FTCAs holds on to the extra electron without necessarily resulting in bond cleavage.¹²² As a result, fast e_{aq}^- quenching is measured by LFP, although degradation, which is measured in UV photolysis experiments, may not have occurred. UV-sulfite photolysis experiments using TriFBA were performed to confirm its recalcitrance during treatment. Indeed, we observed no degradation at pH 9.5, similar to Bentel et al.¹⁰⁷ (data markers in Figure C.6). Minimal degradation was observed at pH 12 during the first hour of treatment; however, concentration remained constant through the end of the reaction. Upon attempts to simulate the data using our previously determined k_2 value,¹²² we found the model to severely overpredict degradation which corroborates but does not confirm the idea that FTCAs could undergo a nondegradative associative mechanism with e_{aq}^- .

Like the other perfluorinated carboxylates, experimental data of UV-sulfite photolysis reactions using PFOA shows a stark increase in degradation kinetics when increasing pH from 9.5 to 12 (data markers in Figure 4.4A). LFP experiments to determine a k_2 value for e_{aq}^- reactions with PFOA were performed in order to model the data, however, we were unable to construct a Stern-Volmer plot despite using conditions similar to Maza et al. (Figure C.7) who report a k_2 value for PFOA of $7.1 \times 10^8 \text{ M}^{-1} \text{ s}^{-1}$.⁸⁷ For PFAS whose k_2 values were difficult to determine experimentally due to insolubility and/or low reactivity, estimates were back-calculated using observed rate constant (k_{obs}) and $[e_{aq}^-]_{ss}$, discussed in the following section.

Back calculating rate constants. Measuring kinetics values using LFP for certain PFAS structures is difficult if a compound has a low CMC or is particularly unreactive. Therefore, we devised an alternative means of determining rate constant which involves estimation using the following equation:

$$k_{est} = \frac{\overline{k_{obs}}}{\overline{[e_{aq}^-]_{ss}}} \quad (10)$$

In which $\overline{k_{obs}}$ (h^{-1}) represents the average observed rate constant at pH 9.5 and 12.0 for a particular compound and $\overline{[e_{aq}^-]_{ss}}$ (M) represents the average e_{aq}^- availability. Using this analysis, we calculate a k_{est} value for PFOA to be $1.59 \times 10^7 \text{ M}^{-1} \text{ s}^{-1}$, which is almost two orders of magnitude lower than that reported by Maza et al.⁸⁷ The model using k_{est} for PFOA exhibits a nearly perfect prediction of its degradation which is perhaps expected since it is more of a data fit rather than a true model prediction (solid lines in Figure 4.4A). This method provides a widely applicable approach to estimate rate constants for e_{aq}^- reactions with PFAS, values which are critical in assessing their efficacy.¹⁰⁹ Using this method, rate constants can be estimated for the full suite of PFAS during UV-ARP treatment based on e_{aq}^- availability (from the mathematical model) and observed rate constant (from prior experiments). This facilitates the prediction of decay profiles for structurally diverse PFAS ahead of UV-sulfite treatment in diverse environments.

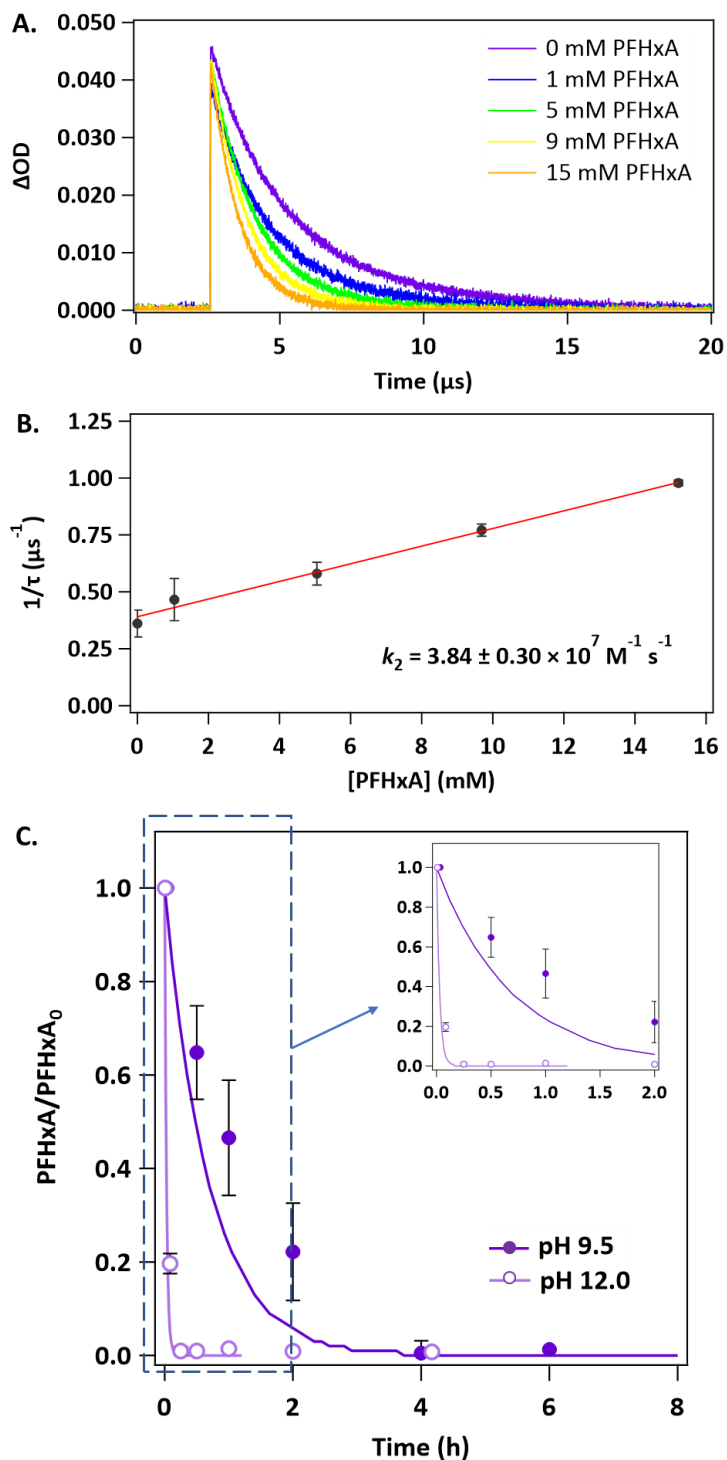


Figure 4.3 (A) Kinetic transient absorption traces for e_{aq}^- decay (measured at 690 nm) at pH 9.5 in solutions amended with varying concentrations of PFHxA and (B) its corresponding Stern-Volmer plot. Solution conditions 40 μM $K_4Fe(FN)_6$, 10 μM $K_3Fe(FN)_6$, ionic strength = 0.137 M (balanced using NaCl), T = 20 °C, and 40 mM borate buffer. (C) Degradation profile of PFHxA at pH 9.5 and 12 along with model predictions shown as solid lines. Reaction conditions: 10 mM sulfite, 5 mM carbonate, T = 20°C.

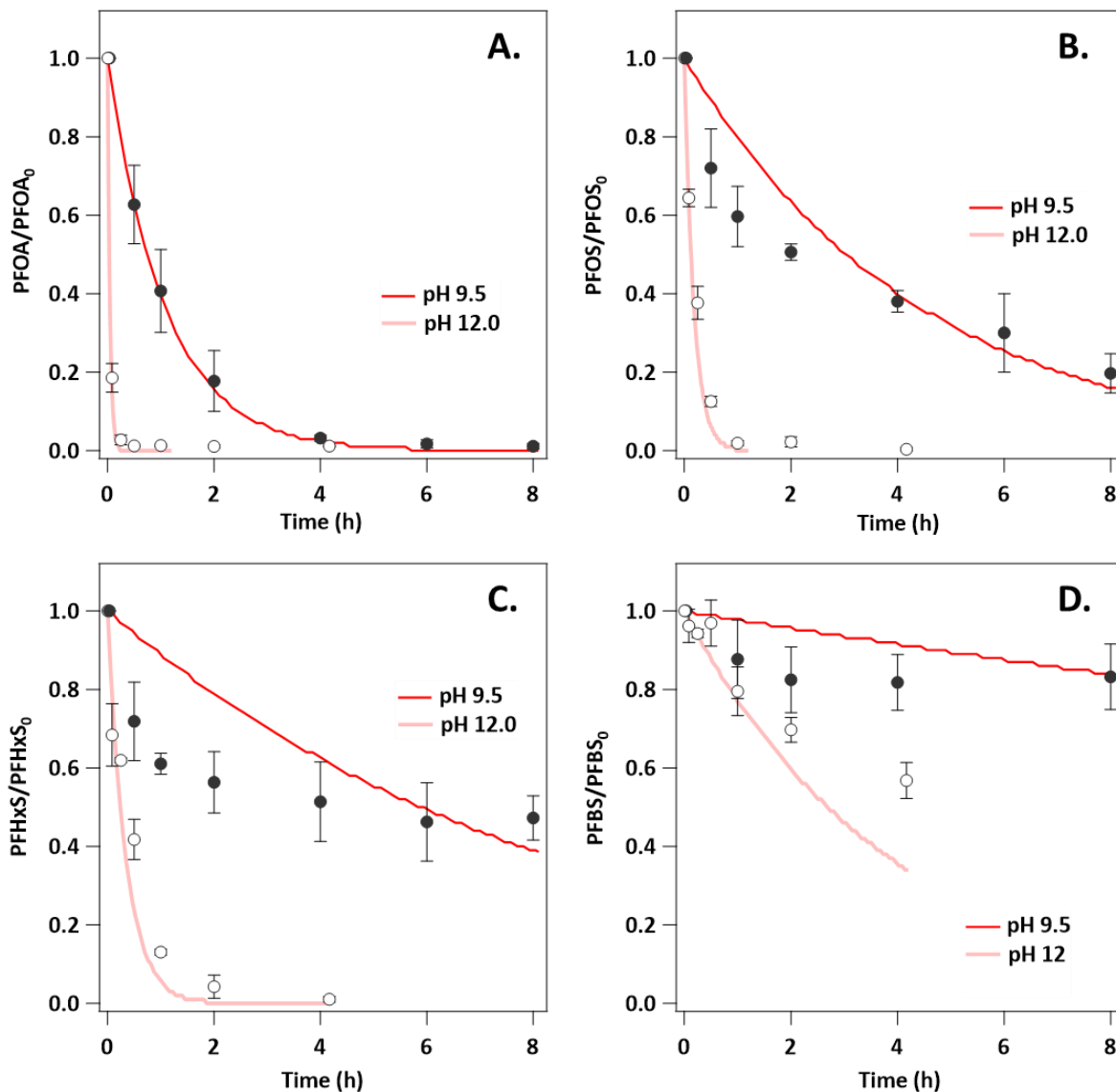


Figure 4.4 Degradation profile for (A) PFOA, (B) PFOS, (C) PFHxS, and (D) PFBS during UV-sulfite photolysis. Reaction conditions: 10 mM sulfite, 5 mM carbonate, $T = 20\text{ }^{\circ}\text{C}$. Experimental data are shown as circles while model simulations using k_{est} values are shown as solid lines.

Sulfonate photoreactions. Another class of environmentally relevant PFAS compounds are perfluorosulfonates (PFSAs). These structures have been found to be more recalcitrant than their carboxylate analogues in many destructive techniques^{80,107} and therefore, it is important to test the model's ability to predict their degradation during UV-ARP treatment. As expected, degradation of the C4, C6, and C8 perfluorosulfonates was far more sluggish than their carboxylate analogues for each chain length (data markers in Figure 4.4B-4.4D). Interestingly, all three perfluorosulfonates investigated, including highly recalcitrant PFBS,⁸⁵ also displayed some level of pH dependent degradation suggesting

that UV-ARPs are capable of remediating even the most intractable perfluorinated compounds given that e_{aq}^- availability is maximized.

To model the decay profiles in Figure 4.4 k_2 values are required, however, rate constants for PFASs are rare. In addition, because the sulfonate headgroup is sterically bulkier than that of carboxylate, the CMCs of PFASs are lower too.¹⁴⁶ Attempts were made to measure k_2 values for the C4 and C6 sulfonates (PFBS and PFHxS) using LFP, however their poor solubilities and low reactivity hindered us from doing so (Figure C.8 and C.9). Instead, we invoked the method described above for back calculating the rate constants from their k_{obs} and e_{aq}^- availability. By this method, PFOS, PFHxS, PFBS, and TFMS yielded k_{est} values of $3.91 \times 10^6 \text{ M}^{-1} \text{ s}^{-1}$, $2.02 \times 10^6 \text{ M}^{-1} \text{ s}^{-1}$, $3.38 \times 10^5 \text{ M}^{-1} \text{ s}^{-1}$, and $2.73 \times 10^4 \text{ M}^{-1} \text{ s}^{-1}$ respectively. The model fits for PFOS or PFHxS underpredict degradation at pH 9.5 during the first few hours of the reaction then improves thereafter (solid lines Figure 4.4B and 4.4C). This underprediction could be due to errors in k_{est} , deviation from pseudo-first order behavior, or occurrence of side reactions. Enhanced degradation with elevated pH is successfully predicted for both compounds, and simulations at the higher pH value are highly accurate. For PFBS and TFMS, two highly recalcitrant PFAAs, the model fits indeed exhibits minimal degradation even at the high pH value (Figure 4.4D and C6, respectively), however results are much less accurate when compared to the others considered in this study. Nevertheless, slightly enhanced degradation is observed in experiments as well as predicted in the models for all four sulfonates.

The proposed model in Eq. 4.1 successfully models UV-sulfite degradation profiles in different conditions of all perfluorinated compounds for which accurate k_2 values exist. For compounds that accurate k_2 values are not available, Eq. 4.10 provides a means of estimating a rate constant which yields decent model fits of experimental data. Taken together, modeling degradation profiles allows for the accurate estimation of UV-ARP treatment efficacy in new environments if information on geochemical solution conditions and UV light source are known. In addition, rate constant estimates provide a means of roughly estimating degradation profiles for compounds which k_2 are difficult to determine. Overall, the model presented here facilitates the quantitative interpretation of the complex effects that solution parameters (pH, sensitizer dose, co-constituents, etc.) have on treatment results.

Reconciling LFP and UV photolysis methods. Bimolecular rate constant for e_{aq}^- reactions with PFAS are sparsely available in the literature, however they exhibit wide variability when comparing results from different studies. Early reports by Anbar et al. and Huang et al. report a k_2 value for TFA of $2.6 \times 10^6 \text{ M}^{-1} \text{ s}^{-1}$ and $3.4 \times 10^6 \text{ M}^{-1} \text{ s}^{-1}$.^{50,86} More than a decade later, Maza et al. reported surprising findings that TFA yielded a k_2 value of $5.0 \times 10^8 \text{ M}^{-1} \text{ s}^{-1}$, more than two orders of magnitude higher than the previous two studies.⁸⁷ The other PFCAs studied by Maza et al. also exhibited extremely fast reactivity with e_{aq}^- , and the PFASs were even more reactive with rate constants $\sim 10^9 \text{ M}^{-1} \text{ s}^{-1}$. This is

surprising because, as mentioned previously, PFASs have been reported on multiple occasions to be more recalcitrant than PFCAs.^{85,107} The most recent report of k_2 values for e_{aq}^- reactions with PFAS measured $< 10^6 \text{ M}^{-1} \text{ s}^{-1}$ and $4.5 \times 10^9 \text{ M}^{-1} \text{ s}^{-1}$ for PFBS and PFOS, respectively. It is hard to rationalize why such variability exists in the literature. It has been postulated that micellar aggregation of PFAS could decrease their rate constants, however variability exists for ultra-short chain structures such as TFA (C2) which do not aggregate the way that long chain structures do.

Importantly, rate constants in the 10^8 - $10^9 \text{ M}^{-1} \text{ s}^{-1}$ range are difficult to justify based on UV photolysis experiments as well. For example, when using the value reported by Maza et al. ($5.0 \times 10^8 \text{ M}^{-1} \text{ s}^{-1}$)⁸⁷ to simulate TFA degradation during UV-sulfite treatment (data markets in Figure C.10), the model predicts destruction of 100% of the target contaminant within minutes (beveled line in Figure C.10). In contrast, when using the values reported in our previous work ($5.26 \times 10^6 \text{ M}^{-1} \text{ s}^{-1}$)¹²² and by Huang et al. ($3.4 \times 10^6 \text{ M}^{-1} \text{ s}^{-1}$)⁵⁰, the model prediction significantly improves (solid line and dashed line in Figure C.10, respectively). For simplicity, only the pH 9.5 experimental data is shown. Although we were not able to measure a k_2 value for PFOA (Figure C.7), Huang et al. report a value of $1.7 \times 10^7 \text{ M}^{-1} \text{ s}^{-1}$ which reflects experimental results well (dashed line in Figure C.10).⁵⁰ The value reported by Maza et al. again predicts complete degradation of the target contaminant within minutes (beveled line in Figure C.10).

As far as we know, the fundamental kinetics of e_{aq}^- reactions with PFAS measured using LFP and pulse radiolysis has never been discussed in terms of its practical implication on UV-ARP treatment results. Similarly, results from UV photolysis experiments are not discussed in the context of fundamental reactivity. That is to say that these two methodologies, although investigating the same reaction, are currently taken separately with no link to each other. The model proposed in this work provides a means of bridging this gap and reconciling their inconsistencies. An important misalignment between LFP and UV photolysis studies involves the effect of pH on reaction kinetics. While observed PFAS degradation kinetics in UV-sulfite photolysis experiments are highly dependent on pH, kinetics measured using LFP show pH independence above pH 9.0.^{95,122} Results of the present study conclusively suggest that it is variable speciation of nontarget constituents that are responsible for enhanced PFAS degradation at highly alkaline conditions, and not decreased H^+ scavenging or elevated e_{aq}^- reactivity as previously postulated.⁹⁵ This finding highlights the importance of characterizing solution conditions prior to treatment to achieve maximum contaminant transformation, and the model developed in this study facilitates the estimation and optimization of these conditions for practical application.

The effect of acidic headgroup and chain length on kinetics is another important inconsistency between LFP and UV photolysis studies. UV-sulfite and UV-iodide data has suggested that PFSA degradation by e_{aq}^- increases with increasing chain length while PFCAs show no dependence.^{107,142} A computational study supported these results by reporting that the energy associated with electron

attachment increases from the C4-C8 PFSA, while the C3-C8 PFCAs showed little variation.⁹⁴ In contrast, the values recently measured by Maza et al. using LFP show no trend in chain-length for either group of structures.⁸⁷ What's more is that many PFAS destruction studies (not limited to UV-ARPs) have found PFASs to be more recalcitrant than their PFCA analogues,^{80,101,125} however Maza et al. report k_2 values for PFSA to be consistently higher than that of PFCAs.⁸⁷

In the current study, the four PFSA studied show a clear increase in reactivity as chain length increases while the five PFCAs studied do not (Figure 4.5). Although the k_2 for PFOA was estimated using Eq. 4.10, ($1.60 \times 10^7 \text{ M}^{-1} \text{ s}^{-1}$), it is very close to the value experimentally measured by Huang et al. ($1.70 \times 10^7 \text{ M}^{-1} \text{ s}^{-1}$)⁵⁰ and therefore still provides useful information regarding the dependence of PFCA kinetics on chain-length in LFP studies. Meanwhile, the k_2 values for the PFSA were all estimated using Eq. 4.10, preventing claims involving LFP studies and fundamental rate constants, however the increasing trend still corroborates UV photolysis findings. Similar plots for k_{obs} can be found in Figure C.11. A table of bimolecular rate constants as well as observed rate constants can be found in Table 4.1.

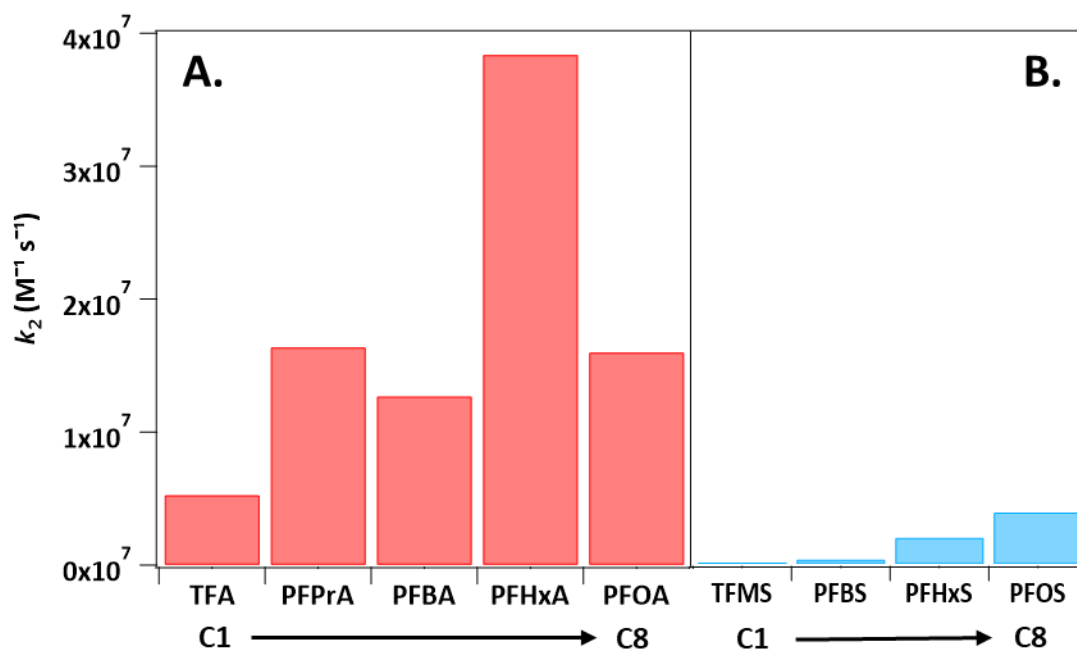


Figure 4.5 Influence of chain length on rate constant for PFCAs vs. PFSA.

Table 4.1 Summary of rate constants of per- and polyfluoroalkyl substances. Reaction conditions: 10 mM sodium sulfite, 5 mM sodium bicarbonate. ^aUnless otherwise noted, rate constants are from Amador et al.¹²² ^bEstimated bimolecular rate constants. ^cRate constant determined using LFP in this study. ^dTenorio et al.⁸⁵ Reaction conditions: 10 mM sodium sulfite, 5 mM sodium bicarbonate, pH 9.5, T = 20 °C.

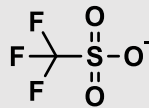
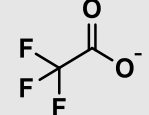
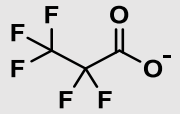
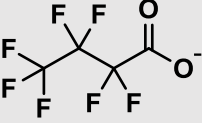
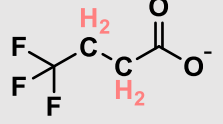
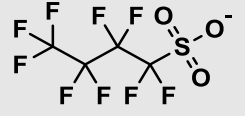
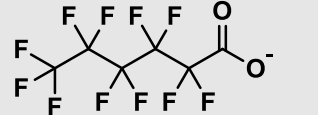
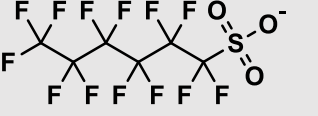
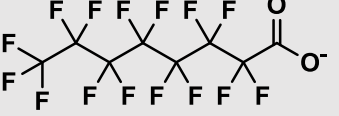

Name and Abbreviation	Chain Length	Structure	k_2 (M ⁻¹ s ⁻¹) ^a	k_{obs} at pH 9.5		k_{obs} at pH 12	Factor increase
				This study (h ⁻¹)	Literature (h ⁻¹)	This study (h ⁻¹)	
Trifluoromethane sulfonate (TFMS)	C1		2.76×10^4 ^b	No deg.	N/A	0.039 ± 0.021	N/A
Trifluoroacetate (TFA)	C2		5.26×10^6	0.259 ± 0.024	N/A	6.21 ± 0.54	~24
Perfluoropropionate (PFPrA)	C3		1.64×10^7	0.839 ± 0.099	N/A	6.47 ± 1.67	~8
Perfluorobutanoate (PFBA)	C4		1.27×10^7	0.665 ± 0.039	0.306 ± 0.042 ^d	11.92 ± 2.31	~18
4,4,4-Trifluorobutyrate (TriFBA)	C4		7.35×10^7 2.68×10^4 ^b	No deg.	N/A	0.038 ± 0.0176	N/A
Perfluorobutane sulfonate (PFBS)	C4		3.81×10^5 ^b	0.0165 ± 0.012	No deg. ^d	0.138 ± 0.012	~8

Table 4.1 Continued.

Perfluorohexanoate (PFHxA)	C6		3.84×10^{7c}	0.967 ± 0.062	0.462 ± 0.003^d	20.25 ± 2.28	~21
Perfluorohexane sulfonate (PFHxS)	C6		2.02×10^{6b}	0.072 ± 0.022	0.018 ± 0.001^d	1.13 ± 0.10	~16
Perfluorooctanoate (PFOA)	C8		1.60×10^{7b}	0.583 ± 0.054	0.649 ± 0.114^d	8.46 ± 1.43	~15
Perfluorooctane sulfonate (PFOS)	C8		3.92×10^{6b}	0.168 ± 0.023	0.080 ± 0.005^d	1.47 ± 0.21	~9

4.5 Practical Implications

Photochemical models are an alternative approach to gaining quantitative information on the chemistry of UV-ARPs. The model developed in this work can simulate contaminant decay profiles in new environments providing a means for estimating and optimizing efficacy ahead of treatment. In addition, this model can quantitatively interpret the complex effects that various system and solution parameters have on overall transformation without needing to run multiple batch experiments to ascertain the effect of a single variable. This method provides critical insights into the complex roles of pH and carbonate quenching on e_{aq}^- processes and provides the tools needed to quantify quenching by other weak acids simultaneously present (e.g., HSO_3^-). The simulations successfully predicted contaminant decay profiles in different environments of PFCAs whose k_2 values are available. In addition, we measure an LFP-derived k_2 value for PFHxA which simulated the UV-sulfite data well. Rate constants were estimated for PFAS such as PFHxS and PFBS whose k_2 values are difficult to determine due to their low solubility and low reactivities which allows for many other PFAS structures to be simulated in different conditions using the model. Attempts to model the data using recently reported k_2 values in the 10^8 - 10^9 range severely overpredict degradation and hence are of little practical significance. Further, UV-sulfite experiments confirm chain-length dependent kinetics of PFASs and independence of PFCAs. For the first time, we link the methodologies of LFP and UV photolysis and reconcile points of contention especially relating to pH effects. Overall, this UV-sulfite photochemical model can predict PFAS decay in different environments, quantitatively interpret the effects of source water composition, and facilitate the optimization of reaction conditions for maximum contaminant degradation prior to treatment; all which will help streamline the development of this treatment method.

CHAPTER 5

CONCLUSIONS AND FUTURE WORK

Water is crucial to support every aspect of life, and although the world's available water supply is limited, it is used carelessly and managed poorly. Urbanization and industrialization produce massive amounts of new and diverse chemicals each year which inevitably proliferate in the environment and contaminate our already fragile water supply. Per- and polyfluoroalkyl substances are a prime representation of the issue of environmental ubiquity and structural diversity. PFAS alone encompass over 9,000 unique structures,¹⁴⁸ and conventional water treatment methods are largely ineffective at remediating their contamination. This highlights the importance of developing innovative treatment technologies to keep up with the PFAS production as well as other emerging contaminants of concern.

Advanced reduction processes (ARPs) based on generation of e_{aq}^- have shown promise in destroying recalcitrant contaminants at ambient temperatures and pressures using UV light and low-cost reducing agents such as sodium sulfite. Significant research efforts have been applied to investigate various aspects of e_{aq}^- processes for PFAS degradation including different means of e_{aq}^- generation (i.e., sensitizers), substrate scope, solution conditions, and more. That said, we still do not have a comprehensive kinetics model for predicting PFAS transformation by UV-based ARPs using process conditions, water quality parameters, and PFAS structure. This thesis tackled this important gap in the field, filling in critical data gaps and synthesizing findings from multiple techniques, including (i) transient absorption spectroscopy measurements of PFAS reactivity with e_{aq}^- , (ii) density functional theory calculations of PFAS molecular property descriptors, (iii) constant UV irradiation PFAS treatment data, (iv) scavenging analysis of non-target natural water constituents, and (v) process kinetics modeling.

5.1 Chapter Summaries

The photochemical model developed in this thesis provides an alternative approach to optimizing the UV-sulfite system and gaining quantitative information of the chemistry of e_{aq}^- processes. Each chapter contains critical insights necessary for the development of the model. Chapter 1 introduces the problem addressed by the thesis, addressing the need for new and innovative water treatment methods to deal with the PFAS contamination in water, highlights why UV-ARPs are a promising means for remediation, outlines discrepancies in the literature and areas for improvement, and finally, describes the ways in which a photochemical model can expedite the use of e_{aq}^- processes in practical treatment approaches.

Chapter 2 applies laser flash photolysis (LFP) methods to accurately measure the bimolecular rate constants of e_{aq}^- reactions with PFAS and density functional theory to propose a mechanism by which these reactions occur. Through these efforts, we report that ultra-short chain fluorocarboxylates exhibit wide ranging reactivity with e_{aq}^- despite structural similarities of the compounds in the dataset. In addition, we postulate that nondegradative mechanisms are prevalent for environmentally relevant structures posing serious issues for e_{aq}^- treatment processes in practice.

While Chapter 2 concerns the kinetics of the reactions between e_{aq}^- and target contaminants, Chapter 3 investigates the kinetics of e_{aq}^- reactions with common non-target water constituents. Specifically, Chapter 3 reports on the influence that dissolved carbonate speciation has on e_{aq}^- treatment processes by using LFP and nonlinear regression analysis to determine species-specific k_2 values for the carbonate system. These values allow for the quantitative comparison of the impact of carbonate to that of common water constituents such as H^+ , NO_3^- , and O_2 and the UV sensitizer SO_3^{2-} . In this chapter, we show that dissolved $CO_{2(aq)}$, the dominant carbonate species under acidic pH conditions is an efficient e_{aq}^- scavenger, and its presence at even trace levels can significantly inhibit UV-ARP treatment efficacy at higher pH conditions where UV-ARPs are typically applied.

Finally, in Chapter 4 we adapted a photochemical model introduced by Li et al.⁸⁴ to predict UV-sulfite treatment of individual PFASs in water with different characteristics (e.g., pH, dissolved carbonate concentration) using data collected in Chapters 2 and 3 as key model input. This model can be used to estimate the performance of UV-sulfite treatment for PFAS remediation in different environments by accounting for certain aspects regarding geochemical solution conditions and UV light source. For most PFASs studied, the model successfully predicts marked variations in PFAS degradation kinetics that were observed depending on PFAS structure, pH, and dissolved carbonate concentration. Thus, the resulting model will be a valuable tool for engineers designing and applying UV-sulfite and other UV-ARPs for remediation of PFAS-contaminated water with diverse site conditions. The fifth and concluding chapter then summarizes key findings and contributions from the thesis and provides strategic recommendations for future directions regarding the development of UV treatment methods for PFAS remediation.

5.2 Future Work

Integration of oxidation and reduction processes to enhance the performance of UV treatment

UV-ARPs are an attractive means for contaminant remediation because they operate at ambient temperatures and pressure, are low cost, produce innocuous byproducts, and their means of activation (i.e., UV light and sulfite) are already widely used in water treatment. Perhaps the biggest challenge facing the use of UV-ARPs for PFAS degradation is its inability to completely mineralize the target

contaminant in reasonable time. However, the success of UV-ARPs in transforming the most recalcitrant perfluorinated structures (e.g., PFOA, PFOS, PFBA, PFBS), which stems from the high reactivity of e_{aq}^- with highly oxidized functional groups, such as carbon-halogen bonds, has elicited significant attention in environmental remediation due to its ability to directly cleave C-F bonds. Because of this high reactivity with C-F, e_{aq}^- treatment tends to leave behind hydrogen-rich residues (e.g., fluorotelomers) which are far less reactive towards e_{aq}^- .

Oxidation processes exhibit reactivity towards contrasting PFAS moieties. While transformation of PFAS by reduction preferentially cleaves C-F bonds, transformation by oxidation preferentially cleaves C-H and C-C bonds. The products of these reactions are polyfluorinated and chain-shortened compounds, respectively. As these reactions proceed, the degradation products formed from each process become less and less reactive in that system. For example, the polyfluorinated compounds formed from ARPs are less reactive towards reductive species (e_{aq}^-) while the short-chain perfluorinated compounds formed from AOPs are unreactive towards oxidative species (e.g., $\cdot\text{OH}$). Interestingly, the degradation products of each process, while recalcitrant in the original system, is reactive in the other. Therefore, these two methods have opposite strengths and taken together could yield significant synergistic effects.

Integrated oxidative-reductive processes have recently been investigated, however the two processes were performed in separated batch reactors which complicates its operation.¹²⁵ The simultaneous production of highly reductive and oxidative radicals in the same reactor could reap the benefits of both systems and achieve deep defluorination of structurally diverse PFAS compounds. A significant challenge of creating an integrated oxidative-reductive system is that the radicals generated from the disparate sensitizers will quench each other. However, if one could separate the radicals, perhaps on different surfaces or catalyst layers, then the simultaneous generation of oxidative and reductive radicals can be achieved in the same system. Photocatalysts could help achieve this separation by concentrating the production of radicals on the catalyst surface. In addition, catalysts are advantageous because they are capable of continuously producing reactive species with high turnover numbers allowing for elevated concentrations of the reactive species over the course of the reaction. Various photocatalysts such as BN (boron nitride),¹⁴⁹ indium oxide (In_2O_3),¹⁵⁰ and $\beta\text{-Ga}_2\text{O}_3$ ¹⁵¹ have already been shown to successfully degrade PFOA through oxidation by reactive oxygen species (e.g., O_2^- , $\cdot\text{OH}$), although have had little success for sulfonates such as PFOS. Coupling UV-ARP processes that reduce perfluoroalkyl sulfonic acids to the corresponding fluorotelomer sulfonates (FTSs) followed by oxidation of the FTSs to shorter chain perfluorocarboxylic acids (PFCAs), with process repetition sequentially shortening the PFCA chain, could provide a means to mineralization of PFASs. In addition, a potentially interesting and practical source of oxidative radicals is dissolved organic matter (DOM). Upon absorption of light, DOM undergoes a series of photophysical and photochemical processes to generate various reactive

intermediates such as hydroxyl radical ($\cdot\text{OH}$), singlet oxygen ($^1\text{O}_2$), and triplet state DOM ($^3\text{DOM}^*$). If DOM, either naturally occurring or artificially added, could be sorbed onto a catalyst support (e.g., graphene, silica) by mixing, simple oxidative localities could be present in the system.

Photocatalysts producing e_{aq}^- are far less studied, however a water-soluble iridium catalyst has been reported to degrade chloroacetate by e_{aq}^- reduction.¹⁵² Iridium is not an ideal catalyst for water treatment because it is a rare, precious metal, however it is likely that other photocatalysts can produce e_{aq}^- as well. While it would be interesting to see if the iridium catalyst proposed by Kerzig et al.¹⁵² is capable of degrading PFAS, it is perhaps of more practical importance to investigate cheaper materials capable of generating e_{aq}^- upon irradiation. The incorporation of both photocatalysts into the same system could result in the deep defluorination of structurally diverse PFAS compounds. Moreover, BN and $\beta\text{-Ga}_2\text{O}_3$ are heterogenous catalysts and exist as a slurry whereas the iridium catalyst is water soluble. The separation of these materials into two different phases could inhibit the recombination of oxidative and reductive radicals increasing their availability for contaminant degradation. Regardless, there are countless photocatalysts, supports, and modifications to explore for UV treatment of water.

Impact of dissolved organic matter on hydrated electron processes

Reactivity of e_{aq}^- reactions with common water constituents is important in assessing the efficacy of ARPs in natural waters because e_{aq}^- are rapidly quenched by various nontarget constituents. Chapter 3 of this thesis identified ubiquitous carbonate species as efficient e_{aq}^- quenchers and provided species-specific k_2 values for each. This allows the effect of alkalinity, which is coupled with pH, to be quantitatively described. The kinetics of e_{aq}^- with many common ions such as PO_4^{3-} , NO_3^- , and Cl^- have also been previously reported, but data is currently lacking for another likely e_{aq}^- quencher, dissolved organic matter (DOM). Despite its ubiquity in natural waters, the reactivity between DOM and e_{aq}^- remains unexplored save for qualitative results reported in batch experiments.^{64,65,153} DOM is a complex, soluble organic compound with no definitive structure. This makes deriving accurate properties and kinetics values difficult because of its variability. Humic acid (HA) is composed of several carbonyl-containing functional groups such as aldehydes, ketones, and quinones and is often used as a surrogate for DOM. Using HA as a model compound, it could be possible to estimate a k_{app} value for e_{aq}^- with DOM which is of significant practical interest. Despite organic matter being ubiquitously present in many water matrices such as surface freshwater, municipal wastewater, groundwater, and landfill leachate,¹⁵⁴⁻¹⁵⁶ no studies exist solely focusing on the effect of DOM in various e_{aq}^- systems. Importantly, the impact of HA on e_{aq}^- processes is dependent on sensitizer system (e.g., iodide, sulfite, NTA, etc.) and both enhancement and inhibition have been reported due to its presence. There are many mechanisms by which HA can

affect UV-ARPs such as UV blocking as well as quenching and production of e_{aq}^- and other reactive species. Because of the importance of DOM in PFAS-contaminated matrices, a systematic study should be conducted investigating the competitive effects of each enhancement and inhibiting mechanisms for each sensitizer system.

Quantitative structure-activity relationships to predict bimolecular rate constants for hydrated electron reactions with PFAS

This thesis provides k_2 values for thirteen ultra-short chain fluorocarboxylates, ten of which have not been measured previously. Chapter 2 reports that PFAS reactivity with e_{aq}^- can vary drastically based on molecular structure, and Chapter 4 highlights the sensitivity of UV-ARP treatment efficacy to k_2 value of the target contaminant with e_{aq}^- . Together, these results suggest that accurate k_2 values are of utmost importance in assessing the ability of UV-ARPs to transform contaminants. Determining k_2 values for PFAS is achieved through LFP and pulse radiolysis methods using Stern-Volmer analysis. This technique requires high concentrations of the target contaminant to significantly alter e_{aq}^- lifetime. Because the critical micelle concentration (CMC) of many PFAS compounds is relatively low,¹⁵⁷ it is difficult to measure k_2 values of many structures in this manner. Furthermore, each year many new PFASs are introduced by industry, and experimental measurement of all possible structures is time-consuming. It follows that development of methodologies for predicting k_2 values for reactions of e_{aq}^- with PFAS structures *a priori* is a critical need for application of UV-ARPs in the future.

Establishing quantitative structure activity relationships (QSARs) is a computational means to correlate molecular structure with chemical reactivity. Once a sufficient QSAR model is established, it can yield reactivity estimates with minimal additional effort. Li et al. established a QSAR model for aliphatic compounds with e_{aq}^- that is based on various molecular descriptors with the energy of the lowest unoccupied molecular orbital (E_{LUMO}) being the most weighted. The R^2 values for their model was 0.751 which indeed shows correlation, however even a factor of 1.2 difference in k_2 can yield a significant impact on degradation.¹⁰⁹ It is possible that the model formulated by Li et al could be tailored for PFAS reactivity specifically, if more k_2 values were known. With the recently reported $R_{e-,UV}$ method,¹³³ it becomes possible to derive k_2 values for minimally soluble PFAS compounds from observed rate constants (k_{obs}) and hydrated electron concentration. Building a QSAR model specifically for e_{aq}^- reactions with structurally diverse PFAS could significantly improve the estimation of k_2 values allowing for the accurate prediction of degradation profiles of environmentally relevant structures. Computational tools like DFT can also be employed to calculate important molecular property descriptors for the growing number of PFAS structures.

Impact of additional reactive species on the results of UV-ARPs

An interesting finding in the literature involves pH condition and degradation products. Qu et al.¹²¹ and Bentel et al.⁹⁵ report the detection of disparate degradation products when photolysis was performed at different pH conditions. In both studies, the authors report the generation and accumulation of chain-shortened products at lower pH values whereas at high pH values chain-shortened products formed in minimal amounts then decayed away. This indicates that at lower pH conditions ($\text{pH} \leq 9$), C-C bond cleavage is an important pathway with further degradation of the chain-shortened products being inhibited, while C-F bond cleavage prevails at higher pH. Moreover, C-C bonds are not known to be amenable towards reactions with e_{aq}^- as evidenced by the negligible transformation of nonfluorinated carboxylic acids such as butanoic acid,¹²² suggesting that a different reactive species could be responsible for C-C bond cleavage at $\text{pH} \leq 9$. On that note, it is generally surprising that chain-shortened products are observed in reductive systems since these are the main transformation products of oxidative reactions which undergo an entirely different mechanism.

The presence of oxidative species could be responsible for generating chain-shortened products. For example, sulfite radical anion ($SO_3^{\cdot-}$) generated from sulfite photolysis was postulated to be responsible for the transformation of vinyl chloride which corroborates previous work suggesting that $SO_3^{\cdot-}$ is a mild oxidant.¹⁵⁸ Other reductive species such as the hydrogen atom (H^\cdot), generated from the quenching of e_{aq}^- by various acids (e.g., HSO_3^- and H^+), could also play a role in PFAS transformation through C-C bond rupture. Because HSO_3^- and H^+ are more abundant at lower pH conditions, it is feasible that e_{aq}^- is mostly consumed by these species making H^\cdot the dominant reactive radical.¹⁴⁴ Other reactive species present which could participate in contaminant transformation in UV-ARP systems are CO_2 radical anion ($CO_2^{\cdot-}$; generated from the reaction of $CO_{2(aq)}$ and e_{aq}^-), superoxide radical anion ($O_2^{\cdot-}$; generated from the reaction of DO with e_{aq}^-), and reactive nitrogen species (RNS) when nitrate is present.

REFERENCES

- (1) Carson, R. *Silent Spring*, 40th anniversary ed., 1st Mariner Books ed.; Houghton Mifflin: Boston, 2002.
- (2) Bernhardt, E. S.; Rosi, E. J.; Gessner, M. O. Synthetic Chemicals as Agents of Global Change. *Front Ecol Environ* **2017**, *15* (2), 84–90. <https://doi.org/10.1002/fee.1450>.
- (3) United Nations Environment Programme. Introduction: Chemicals and Waste in the Broader Sustainable Development Context - Global Chemicals Outlook II. **2019**.
- (4) Wang, Z.; Walker, G. W.; Muir, D. C. G.; Nagatani-Yoshida, K. Toward a Global Understanding of Chemical Pollution: A First Comprehensive Analysis of National and Regional Chemical Inventories. *Environ. Sci. Technol.* **2020**, *54* (5), 2575–2584. <https://doi.org/10.1021/acs.est.9b06379>.
- (5) Prüss-Ustün, A.; Bartram, J.; Clasen, T.; Colford, J. M.; Cumming, O.; Curtis, V.; Bonjour, S.; Dangour, A. D.; De France, J.; Fewtrell, L.; Freeman, M. C.; Gordon, B.; Hunter, P. R.; Johnston, R. B.; Mathers, C.; Mäusezahl, D.; Medlicott, K.; Neira, M.; Stocks, M.; Wolf, J.; Cairncross, S. Burden of Disease from Inadequate Water, Sanitation and Hygiene in Low- and Middle-income Settings: A Retrospective Analysis of Data from 145 Countries. *Trop Med Int Health* **2014**, *19* (8), 894–905. <https://doi.org/10.1111/tmi.12329>.
- (6) Fuller, R.; Landrigan, P. J.; Balakrishnan, K.; Bathan, G.; Bose-O'Reilly, S.; Brauer, M.; Caravanos, J.; Chiles, T.; Cohen, A.; Corra, L.; Cropper, M.; Ferraro, G.; Hanna, J.; Hanrahan, D.; Hu, H.; Hunter, D.; Janata, G.; Kupka, R.; Lanphear, B.; Lichtveld, M.; Martin, K.; Mustapha, A.; Sanchez-Triana, E.; Sandilya, K.; Schaeffli, L.; Shaw, J.; Seddon, J.; Suk, W.; Téllez-Rojo, M. M.; Yan, C. Pollution and Health: A Progress Update. *The Lancet Planetary Health* **2022**, *6* (6), e535–e547. [https://doi.org/10.1016/S2542-5196\(22\)00090-0](https://doi.org/10.1016/S2542-5196(22)00090-0).
- (7) Scheringer, M. LONG-RANGE TRANSPORT OF ORGANIC CHEMICALS IN THE ENVIRONMENT. *Environ Toxicol Chem* **2009**, *28* (4), 677. <https://doi.org/10.1897/08-324R.1>.
- (8) Alexander, Martin. Biodegradation of Organic Chemicals. *Environ. Sci. Technol.* **1985**, *19* (2), 106–111. <https://doi.org/10.1021/es00132a602>.
- (9) Buck, R. C.; Franklin, J.; Berger, U.; Conder, J. M.; Cousins, I. T.; de Voogt, P.; Jensen, A. A.; Kannan, K.; Mabury, S. A.; van Leeuwen, S. P. Perfluoroalkyl and Polyfluoroalkyl Substances in the Environment: Terminology, Classification, and Origins. *Integr Environ Assess Manag* **2011**, *7* (4), 513–541. <https://doi.org/10.1002/ieam.258>.
- (10) O'Hagan, D. Understanding Organofluorine Chemistry. An Introduction to the C–F Bond. *Chem. Soc. Rev.* **2008**, *37* (2), 308–319. <https://doi.org/10.1039/B711844A>.
- (11) Tsang, W.; Burgess, D. R.; Babushok, V. On the Incinerability of Highly Fluorinated Organic Compounds. *Combustion Science and Technology* **1998**, *139* (1), 385–402. <https://doi.org/10.1080/00102209808952095>.

- (12) Winchell, L. J.; Ross, J. J.; Wells, M. J. M.; Fonoll, X.; Norton, J. W.; Bell, K. Y. Per- and Polyfluoroalkyl Substances Thermal Destruction at Water Resource Recovery Facilities: A State of the Science Review. *Water Environment Research* **2021**, *93* (6), 826–843. <https://doi.org/10.1002/wer.1483>.
- (13) *Organofluorine Chemistry: Principles and Commercial Applications*; Banks, R. E., Smart, B. E., Tatlow, J. C., Eds.; Springer US : Imprint : Springer: Boston, MA, 1994.
- (14) Lemal, D. M. Perspective on Fluorocarbon Chemistry. *J. Org. Chem.* **2004**, *69* (1), 1–11. <https://doi.org/10.1021/jo0302556>.
- (15) Kirsch, P. *Modern Fluoroorganic Chemistry: Synthesis, Reactivity, Applications*, 1st ed.; Wiley, 2004. <https://doi.org/10.1002/352760393X>.
- (16) Glüge, J.; Scheringer, M.; Cousins, I. T.; DeWitt, J. C.; Goldenman, G.; Herzke, D.; Lohmann, R.; Ng, C. A.; Trier, X.; Wang, Z. An Overview of the Uses of Per- and Polyfluoroalkyl Substances (PFAS). *Environ. Sci.: Processes Impacts* **2020**, *22* (12), 2345–2373. <https://doi.org/10.1039/D0EM00291G>.
- (17) Berhanu, A.; Mutanda, I.; Taolin, J.; Qaria, M. A.; Yang, B.; Zhu, D. A Review of Microbial Degradation of Per- and Polyfluoroalkyl Substances (PFAS): Biotransformation Routes and Enzymes. *Science of The Total Environment* **2023**, *859*, 160010. <https://doi.org/10.1016/j.scitotenv.2022.160010>.
- (18) Garnett, J.; Halsall, C.; Vader, A.; Joerss, H.; Ebinghaus, R.; Leeson, A.; Wynn, P. M. High Concentrations of Perfluoroalkyl Acids in Arctic Seawater Driven by Early Thawing Sea Ice. *Environ. Sci. Technol.* **2021**, *55* (16), 11049–11059. <https://doi.org/10.1021/acs.est.1c01676>.
- (19) Yeung, L. W. Y.; Dassuncao, C.; Mabury, S.; Sunderland, E. M.; Zhang, X.; Lohmann, R. Vertical Profiles, Sources, and Transport of PFASs in the Arctic Ocean. *Environ. Sci. Technol.* **2017**, *51* (12), 6735–6744. <https://doi.org/10.1021/acs.est.7b00788>.
- (20) Barbo, N.; Stoiber, T.; Naidenko, O. V.; Andrews, D. Q. Locally Caught Freshwater Fish across the United States Are Likely a Significant Source of Exposure to PFOS and Other Perfluorinated Compounds. *Environmental Research* **2023**, *220*, 115165. <https://doi.org/10.1016/j.envres.2022.115165>.
- (21) Barry, V.; Winqvist, A.; Steenland, K. Perfluorooctanoic Acid (PFOA) Exposures and Incident Cancers among Adults Living Near a Chemical Plant. *Environmental Health Perspectives* **2013**, *121* (11–12), 1313–1318. <https://doi.org/10.1289/ehp.1306615>.
- (22) Braun, J. M.; Chen, A.; Romano, M. E.; Calafat, A. M.; Webster, G. M.; Yolton, K.; Lanphear, B. P. Prenatal Perfluoroalkyl Substance Exposure and Child Adiposity at 8 Years of Age: The HOME Study: Prenatal PFAS Exposure and Child Adiposity. *Obesity* **2016**, *24* (1), 231–237. <https://doi.org/10.1002/oby.21258>.
- (23) Grandjean, P.; Andersen, E. W.; Budtz-Jørgensen, E.; Nielsen, F.; Mølbak, K.; Weihe, P.; Heilmann, C. Serum Vaccine Antibody Concentrations in Children Exposed to Perfluorinated Compounds. *JAMA* **2012**, *307* (4). <https://doi.org/10.1001/jama.2011.2034>.

- (24) Borg, D.; Lund, B.-O.; Lindquist, N.-G.; Håkansson, H. Cumulative Health Risk Assessment of 17 Perfluoroalkylated and Polyfluoroalkylated Substances (PFASs) in the Swedish Population. *Environment International* **2013**, *59*, 112–123. <https://doi.org/10.1016/j.envint.2013.05.009>.
- (25) Wang, J.; Wang, X.; Sheng, N.; Zhou, X.; Cui, R.; Zhang, H.; Dai, J. RNA-Sequencing Analysis Reveals the Hepatotoxic Mechanism of Perfluoroalkyl Alternatives, HFPO2 and HFPO4, Following Exposure in Mice: Hepatotoxic Mechanism of HFPO2 and HFPO4 in Mice. *J. Appl. Toxicol.* **2017**, *37* (4), 436–444. <https://doi.org/10.1002/jat.3376>.
- (26) Caverly Rae, J. M.; Craig, L.; Slone, T. W.; Frame, S. R.; Buxton, L. W.; Kennedy, G. L. Evaluation of Chronic Toxicity and Carcinogenicity of Ammonium 2,3,3,3-Tetrafluoro-2-(Heptafluoropropoxy)-Propanoate in Sprague–Dawley Rats. *Toxicology Reports* **2015**, *2*, 939–949. <https://doi.org/10.1016/j.toxrep.2015.06.001>.
- (27) Blaine, A. C.; Rich, C. D.; Hundal, L. S.; Lau, C.; Mills, M. A.; Harris, K. M.; Higgins, C. P. Uptake of Perfluoroalkyl Acids into Edible Crops via Land Applied Biosolids: Field and Greenhouse Studies. *Environ. Sci. Technol.* **2013**, *47* (24), 14062–14069. <https://doi.org/10.1021/es403094q>.
- (28) Rich, C. D.; Blaine, A. C.; Hundal, L.; Higgins, C. P. Bioaccumulation of Perfluoroalkyl Acids by Earthworms (*Eisenia Fetida*) Exposed to Contaminated Soils. *Environ. Sci. Technol.* **2015**, *49* (2), 881–888. <https://doi.org/10.1021/es504152d>.
- (29) Moody, C. A.; Hebert, G. N.; Strauss, S. H.; Field, J. A. Occurrence and Persistence of Perfluorooctanesulfonate and Other Perfluorinated Surfactants in Groundwater at a Fire-Training Area at Wurtsmith Air Force Base, Michigan, USA Electronic Supplementary Information (ESI) Available: Map of Location of Wurtsmith Air Force Base, Oscoda, MI and Surrounding States. See <http://www.rsc.org/Suppdata/Em/B2/B212497a/>. *J. Environ. Monitor.* **2003**, *5* (2), 341–345. <https://doi.org/10.1039/b212497a>.
- (30) Hu, X. C.; Andrews, D. Q.; Lindstrom, A. B.; Bruton, T. A.; Schaidler, L. A.; Grandjean, P.; Lohmann, R.; Carignan, C. C.; Blum, A.; Balan, S. A.; Higgins, C. P.; Sunderland, E. M. Detection of Poly- and Perfluoroalkyl Substances (PFASs) in U.S. Drinking Water Linked to Industrial Sites, Military Fire Training Areas, and Wastewater Treatment Plants. *Environ. Sci. Technol. Lett.* **2016**, *3* (10), 344–350. <https://doi.org/10.1021/acs.estlett.6b00260>.
- (31) Wang, Z.; Cousins, I. T.; Scheringer, M.; Buck, R. C.; Hungerbühler, K. Global Emission Inventories for C4–C14 Perfluoroalkyl Carboxylic Acid (PFCA) Homologues from 1951 to 2030, Part I: Production and Emissions from Quantifiable Sources. *Environment International* **2014**, *70*, 62–75. <https://doi.org/10.1016/j.envint.2014.04.013>.
- (32) Murray, C. C.; Marshall, R. E.; Liu, C. J.; Vatankhah, H.; Bellona, C. L. PFAS Treatment with Granular Activated Carbon and Ion Exchange Resin: Comparing Chain Length, Empty Bed Contact Time, and Cost. *Journal of Water Process Engineering* **2021**, *44*, 102342. <https://doi.org/10.1016/j.jwpe.2021.102342>.
- (33) Meegoda, J. N.; Bezerra de Souza, B.; Casarini, M. M.; Kewalramani, J. A. A Review of PFAS Destruction Technologies. *IJERPH* **2022**, *19* (24), 16397. <https://doi.org/10.3390/ijerph192416397>.

- (34) Gomez-Ruiz, B.; Gómez-Lavín, S.; Diban, N.; Boiteux, V.; Colin, A.; Dauchy, X.; Urtiaga, A. Efficient Electrochemical Degradation of Poly- and Perfluoroalkyl Substances (PFASs) from the Effluents of an Industrial Wastewater Treatment Plant. *Chemical Engineering Journal* **2017**, *322*, 196–204. <https://doi.org/10.1016/j.cej.2017.04.040>.
- (35) Liang, S.; Mora, R.; Huang, Q.; Casson, R.; Wang, Y.; Woodard, S.; Anderson, H. Field Demonstration of Coupling Ion-Exchange Resin with Electrochemical Oxidation for Enhanced Treatment of per- and Polyfluoroalkyl Substances (PFAS) in Groundwater. *Chemical Engineering Journal Advances* **2022**, *9*, 100216. <https://doi.org/10.1016/j.cej.2021.100216>.
- (36) Schaefer, C. E.; Andaya, C.; Burant, A.; Condee, C. W.; Urtiaga, A.; Strathmann, T. J.; Higgins, C. P. Electrochemical Treatment of Perfluorooctanoic Acid and Perfluorooctane Sulfonate: Insights into Mechanisms and Application to Groundwater Treatment. *Chemical Engineering Journal* **2017**, *317*, 424–432. <https://doi.org/10.1016/j.cej.2017.02.107>.
- (37) Rodriguez-Freire, L.; Balachandran, R.; Sierra-Alvarez, R.; Keswani, M. Effect of Sound Frequency and Initial Concentration on the Sonochemical Degradation of Perfluorooctane Sulfonate (PFOS). *Journal of Hazardous Materials* **2015**, *300*, 662–669. <https://doi.org/10.1016/j.jhazmat.2015.07.077>.
- (38) Vecitis, C. D.; Park, H.; Cheng, J.; Mader, B. T.; Hoffmann, M. R. Kinetics and Mechanism of the Sonolytic Conversion of the Aqueous Perfluorinated Surfactants, Perfluorooctanoate (PFOA), and Perfluorooctane Sulfonate (PFOS) into Inorganic Products. *J. Phys. Chem. A* **2008**, *112* (18), 4261–4270. <https://doi.org/10.1021/jp801081y>.
- (39) Kulkarni, P. R.; Richardson, S. D.; Nzeribe, B. N.; Adamson, D. T.; Kalra, S. S.; Mahendra, S.; Blotevogel, J.; Hanson, A.; Dooley, G.; Maraviov, S.; Popovic, J. Field Demonstration of a Sonolysis Reactor for Treatment of PFAS-Contaminated Groundwater. *J. Environ. Eng.* **2022**, *148* (11), 06022005. [https://doi.org/10.1061/\(ASCE\)EE.1943-7870.0002064](https://doi.org/10.1061/(ASCE)EE.1943-7870.0002064).
- (40) Wang, J.; Lin, Z.; He, X.; Song, M.; Westerhoff, P.; Doudrick, K.; Hanigan, D. Critical Review of Thermal Decomposition of Per- and Polyfluoroalkyl Substances: Mechanisms and Implications for Thermal Treatment Processes. *Environ. Sci. Technol.* **2022**, *56* (9), 5355–5370. <https://doi.org/10.1021/acs.est.2c02251>.
- (41) Gu, Y.; Liu, T.; Zhang, Q.; Dong, W. Efficient Decomposition of Perfluorooctanoic Acid by a High Photon Flux UV/Sulfite Process: Kinetics and Associated Toxicity. *Chemical Engineering Journal* **2017**, *326*, 1125–1133. <https://doi.org/10.1016/j.cej.2017.05.156>.
- (42) Bao, Y.; Huang, J.; Cagnetta, G.; Yu, G. Removal of F-53B as PFOS Alternative in Chrome Plating Wastewater by UV/Sulfite Reduction. *Water Research* **2019**, *163*, 114907. <https://doi.org/10.1016/j.watres.2019.114907>.
- (43) Liu, X.; Vellanki, B. P.; Batchelor, B.; Abdel-Wahab, A. Degradation of 1,2-Dichloroethane with Advanced Reduction Processes (ARPs): Effects of Process Variables and Mechanisms. *Chemical Engineering Journal* **2014**, *237*, 300–307. <https://doi.org/10.1016/j.cej.2013.10.037>.
- (44) Liu, X.; Zhang, T.; Shao, Y. Aqueous Bromate Reduction by UV Activation of Sulfite: Aqueous Bromate Reduction by UV Activation of Sulfite. *Clean Soil Air Water* **2014**, *42* (10), 1370–1375. <https://doi.org/10.1002/clen.201300646>.

- (45) Marcus, R. A. Theory of Electron-Transfer Reaction Rates of Solvated Electrons. *The Journal of Chemical Physics* **1965**, *43* (10), 3477–3489. <https://doi.org/10.1063/1.1696504>.
- (46) Baxendale, J. H. Addendum: Redox Potential and Hydration Energy of the Hydrated Electron. *Radiation Research Supplement* **1964**, *4*, 139. <https://doi.org/10.2307/3583573>.
- (47) Nash, K.; Mulac, W.; Noon, M.; Fried, S.; Sullivan, J. C. Pulse Radiolysis Studies of U(VI) Complexes in Aqueous Media. *Journal of Inorganic and Nuclear Chemistry* **1981**, *43* (5), 897–899. [https://doi.org/10.1016/0022-1902\(81\)80146-7](https://doi.org/10.1016/0022-1902(81)80146-7).
- (48) Hart, E. J.; Boag, J. W. **Absorption Spectrum of the Hydrated Electron in Water and in Aqueous Solutions.** *J. Am. Chem. Soc.* **1962**, *84* (21), 4090–4095. <https://doi.org/10.1021/ja00880a025>.
- (49) Abramczyk, H.; Werner, B.; Kroh, J. Absorption Spectra of the Solvated Electron in Hydrocarbons. *J. Phys. Chem.* **1992**, *96* (24), 9674–9677. <https://doi.org/10.1021/j100203a021>.
- (50) Huang, L.; Dong, W.; Hou, H. Investigation of the Reactivity of Hydrated Electron toward Perfluorinated Carboxylates by Laser Flash Photolysis. *Chemical Physics Letters* **2007**, *436* (1–3), 124–128. <https://doi.org/10.1016/j.cplett.2007.01.037>.
- (51) Cui, J.; Gao, P.; Deng, Y. Destruction of Per- and Polyfluoroalkyl Substances (PFAS) with Advanced Reduction Processes (ARPs): A Critical Review. *Environ. Sci. Technol.* **2020**, *54* (7), 3752–3766. <https://doi.org/10.1021/acs.est.9b05565>.
- (52) Awtrey, A. D.; Connick, R. E. The Absorption Spectra of I_2 , I_3^- , I^- , IO_3^- , $S_4O_6^{=}$ and $S_2O_3^{=}$. Heat of the Reaction $I_3^- = I_2 + I^-$. *J. Am. Chem. Soc.* **1951**, *73* (4), 1842–1843. <https://doi.org/10.1021/ja01148a504>.
- (53) Yu, K.; Li, X.; Chen, L.; Fang, J.; Chen, H.; Li, Q.; Chi, N.; Ma, J. Mechanism and Efficiency of Contaminant Reduction by Hydrated Electron in the Sulfite/Iodide/UV Process. *Water Research* **2018**, *129*, 357–364. <https://doi.org/10.1016/j.watres.2017.11.030>.
- (54) Qu, Y.; Zhang, C.; Li, F.; Chen, J.; Zhou, Q. Photo-Reductive Defluorination of Perfluorooctanoic Acid in Water. *Water Research* **2010**, *44* (9), 2939–2947. <https://doi.org/10.1016/j.watres.2010.02.019>.
- (55) Sauer, M. C.; Crowell, R. A.; Shkrob, I. A. Electron Photodetachment from Aqueous Anions. 1. Quantum Yields for Generation of Hydrated Electron by 193 and 248 Nm Laser Photoexcitation of Miscellaneous Inorganic Anions. *J. Phys. Chem. A* **2004**, *108* (25), 5490–5502. <https://doi.org/10.1021/jp049722t>.
- (56) Kaper, J. M.; Gebhard, O.; van den Berg, C. J.; Veldstra, H. Studies on Indolepyruvic Acid. *Archives of Biochemistry and Biophysics* **1963**, *103* (3), 475–487. [https://doi.org/10.1016/0003-9861\(63\)90441-7](https://doi.org/10.1016/0003-9861(63)90441-7).
- (57) Tian, H.; Gao, J.; Li, H.; Boyd, S. A.; Gu, C. Complete Defluorination of Perfluorinated Compounds by Hydrated Electrons Generated from 3-Indole-Acetic-Acid in Organomodified Montmorillonite. *Sci Rep* **2016**, *6* (1), 32949. <https://doi.org/10.1038/srep32949>.

- (58) Sun, Z.; Zhang, C.; Xing, L.; Zhou, Q.; Dong, W.; Hoffmann, M. R. UV/Nitriilotriacetic Acid Process as a Novel Strategy for Efficient Photoreductive Degradation of Perfluorooctanesulfonate. *Environ. Sci. Technol.* **2018**, *52* (5), 2953–2962. <https://doi.org/10.1021/acs.est.7b05912>.
- (59) Liu, C. J.; McKay, G.; Jiang, D.; Tenorio, R.; Cath, J. T.; Amador, C.; Murray, C. C.; Brown, J. B.; Wright, H. B.; Schaefer, C.; Higgins, C. P.; Bellona, C.; Strathmann, T. J. Pilot-Scale Field Demonstration of a Hybrid Nanofiltration and UV-Sulfite Treatment Train for Groundwater Contaminated by Per- and Polyfluoroalkyl Substances (PFASs). *Water Research* **2021**, 117677. <https://doi.org/10.1016/j.watres.2021.117677>.
- (60) Li, X.; Ma, J.; Liu, G.; Fang, J.; Yue, S.; Guan, Y.; Chen, L.; Liu, X. Efficient Reductive Dechlorination of Monochloroacetic Acid by Sulfite/UV Process. *Environ. Sci. Technol.* **2012**, *46* (13), 7342–7349. <https://doi.org/10.1021/es3008535>.
- (61) Sathasivan, A.; Herath, B. S.; Senevirathna, S. T. M. L. D.; Kastl, G. Dechlorination in Wastewater Treatment Processes. In *Current Developments in Biotechnology and Bioengineering*; Elsevier, 2017; pp 359–380. <https://doi.org/10.1016/B978-0-444-63665-2.00014-X>.
- (62) Buxton, G. V.; Greenstock, C. L.; Helman, W. P.; Ross, A. B. Critical Review of Rate Constants for Reactions of Hydrated Electrons, Hydrogen Atoms and Hydroxyl Radicals ($\cdot\text{OH}/\cdot\text{O}^-$ in Aqueous Solution. *Journal of Physical and Chemical Reference Data* **1988**, *17* (2), 513–886. <https://doi.org/10.1063/1.555805>.
- (63) Hayon, E.; Treinin, A.; Wilf, J. Electronic Spectra, Photochemistry, and Autoxidation Mechanism of the Sulfite-Bisulfite-Pyrosulfite Systems. SO_2^- , SO_3^- , SO_4^- , and SO_5^- Radicals. *J. Am. Chem. Soc.* **1972**, *94* (1), 47–57. <https://doi.org/10.1021/ja00756a009>.
- (64) Ren, Z.; Bergmann, U.; Leiviskä, T. Reductive Degradation of Perfluorooctanoic Acid in Complex Water Matrices by Using the UV/Sulfite Process. *Water Research* **2021**, *205*, 117676. <https://doi.org/10.1016/j.watres.2021.117676>.
- (65) Sun, Z.; Zhang, C.; Chen, P.; Zhou, Q.; Hoffmann, M. R. Impact of Humic Acid on the Photoreductive Degradation of Perfluorooctane Sulfonate (PFOS) by UV/Iodide Process. *Water Research* **2017**, *127*, 50–58. <https://doi.org/10.1016/j.watres.2017.10.010>.
- (66) Fennell, B. D.; Mezyk, S. P.; McKay, G. Critical Review of UV-Advanced Reduction Processes for the Treatment of Chemical Contaminants in Water. *ACS Environ. Au* **2022**, *2* (3), 178–205. <https://doi.org/10.1021/acsenvironau.1c00042>.
- (67) Fischer, M.; Warneck, P. Photodecomposition and Photooxidation of Hydrogen Sulfite in Aqueous Solution. *J. Phys. Chem.* **1996**, *100* (37), 15111–15117. <https://doi.org/10.1021/jp953236b>.
- (68) Maza, W. A.; Breslin, V. M.; Plymale, N. T.; DeSario, P. A.; Epshteyn, A.; Owrutsky, J. C.; Pate, B. B. Nanosecond Transient Absorption Studies of the PH-Dependent Hydrated Electron Quenching by HSO_3^- . *Photochem. Photobiol. Sci.* **2019**, *18* (6), 1526–1532. <https://doi.org/10.1039/C9PP00063A>.
- (69) Park, H.; Vecitis, C. D.; Cheng, J.; Dalleska, N. F.; Mader, B. T.; Hoffmann, M. R. Reductive Degradation of Perfluoroalkyl Compounds with Aqueated Electrons Generated from Iodide Photolysis at 254 Nm. *Photochem. Photobiol. Sci.* **2011**, *10* (12), 1945. <https://doi.org/10.1039/c1pp05270e>.

- (70) Brennan, N. M.; Evans, A. T.; Fritz, M. K.; Peak, S. A.; von Holst, H. E. Trends in the Regulation of Per- and Polyfluoroalkyl Substances (PFAS): A Scoping Review. *IJERPH* **2021**, *18* (20), 10900. <https://doi.org/10.3390/ijerph182010900>.
- (71) Xiao, X.; Ulrich, B. A.; Chen, B.; Higgins, C. P. Sorption of Poly- and Perfluoroalkyl Substances (PFASs) Relevant to Aqueous Film-Forming Foam (AFFF)-Impacted Groundwater by Biochars and Activated Carbon. *Environ. Sci. Technol.* **2017**, *51* (11), 6342–6351. <https://doi.org/10.1021/acs.est.7b00970>.
- (72) Franke, V.; McCleaf, P.; Lindegren, K.; Ahrens, L. Efficient Removal of Per- and Polyfluoroalkyl Substances (PFASs) in Drinking Water Treatment: Nanofiltration Combined with Active Carbon or Anion Exchange. *Environ. Sci.: Water Res. Technol.* **2019**, *5* (11), 1836–1843. <https://doi.org/10.1039/C9EW00286C>.
- (73) Appleman, T. D.; Higgins, C. P.; Quiñones, O.; Vanderford, B. J.; Kolstad, C.; Zeigler-Holady, J. C.; Dickenson, E. R. V. Treatment of Poly- and Perfluoroalkyl Substances in U.S. Full-Scale Water Treatment Systems. *Water Research* **2014**, *51*, 246–255. <https://doi.org/10.1016/j.watres.2013.10.067>.
- (74) Fabregat-Palau, J.; Vidal, M.; Rigol, A. Examining Sorption of Perfluoroalkyl Substances (PFAS) in Biochars and Other Carbon-Rich Materials. *Chemosphere* **2022**, *302*, 134733. <https://doi.org/10.1016/j.chemosphere.2022.134733>.
- (75) Lee, T.; Speth, T. F.; Nadagouda, M. N. High-Pressure Membrane Filtration Processes for Separation of Per- and Polyfluoroalkyl Substances (PFAS). *Chemical Engineering Journal* **2022**, *431*, 134023. <https://doi.org/10.1016/j.cej.2021.134023>.
- (76) Zhuo, Q.; Deng, S.; Yang, B.; Huang, J.; Yu, G. Efficient Electrochemical Oxidation of Perfluorooctanoate Using a Ti/SnO₂-Sb-Bi Anode. *Environ. Sci. Technol.* **2011**, *45* (7), 2973–2979. <https://doi.org/10.1021/es1024542>.
- (77) Moriwaki, H.; Takagi, Y.; Tanaka, M.; Tsuruho, K.; Okitsu, K.; Maeda, Y. Sonochemical Decomposition of Perfluorooctane Sulfonate and Perfluorooctanoic Acid. *Environ. Sci. Technol.* **2005**, *39* (9), 3388–3392. <https://doi.org/10.1021/es040342v>.
- (78) Sahu, S. P.; Qanbarzadeh, M.; Ateia, M.; Torkzadeh, H.; Maroli, A. S.; Cates, E. L. Rapid Degradation and Mineralization of Perfluorooctanoic Acid by a New Petitjeanite Bi₃O(OH)(PO₄)₂ Microparticle Ultraviolet Photocatalyst. *Environ. Sci. Technol. Lett.* **2018**, *5* (8), 533–538. <https://doi.org/10.1021/acs.estlett.8b00395>.
- (79) Zhang, Z.; Chen, J.-J.; Lyu, X.-J.; Yin, H.; Sheng, G.-P. Complete Mineralization of Perfluorooctanoic Acid (PFOA) by γ -Irradiation in Aqueous Solution. *Sci Rep* **2015**, *4* (1), 7418. <https://doi.org/10.1038/srep07418>.
- (80) Hao, S.; Choi, Y.-J.; Wu, B.; Higgins, C. P.; Deeb, R.; Strathmann, T. J. Hydrothermal Alkaline Treatment for Destruction of Per- and Polyfluoroalkyl Substances in Aqueous Film-Forming Foam. *Environ. Sci. Technol.* **2021**, *55* (5), 3283–3295. <https://doi.org/10.1021/acs.est.0c06906>.
- (81) Song, Z.; Tang, H.; Wang, N.; Zhu, L. Reductive Defluorination of Perfluorooctanoic Acid by Hydrated Electrons in a Sulfite-Mediated UV Photochemical System. *Journal of Hazardous Materials* **2013**, *262*, 332–338. <https://doi.org/10.1016/j.jhazmat.2013.08.059>.

- (82) DiMento, B. P.; Tusei, C. L.; Aeppli, C. Photochemical Degradation of Short-Chain Chlorinated Paraffins in Aqueous Solution by Hydrated Electrons and Hydroxyl Radicals. *Chemosphere* **2022**, *303*, 134732. <https://doi.org/10.1016/j.chemosphere.2022.134732>.
- (83) Jiao, H.; Zhang, C.; Yang, M.; Wu, Y.; Zhou, Q.; Hoffmann, M. R. Photoreductive Defluorination of Trifluoroacetic Acid (TFA) in the Aqueous Phase by Hydrated Electrons. *Chemical Engineering Journal* **2022**, *430*, 132724. <https://doi.org/10.1016/j.cej.2021.132724>.
- (84) Li, X.; Fang, J.; Liu, G.; Zhang, S.; Pan, B.; Ma, J. Kinetics and Efficiency of the Hydrated Electron-Induced Dehalogenation by the Sulfite/UV Process. *Water Research* **2014**, *62*, 220–228. <https://doi.org/10.1016/j.watres.2014.05.051>.
- (85) Tenorio, R.; Liu, J.; Xiao, X.; Maizel, A.; Higgins, C. P.; Schaefer, C. E.; Strathmann, T. J. Destruction of Per- and Polyfluoroalkyl Substances (PFASs) in Aqueous Film-Forming Foam (AFFF) with UV-Sulfite Photoreductive Treatment. *Environ. Sci. Technol.* **2020**, *54* (11), 6957–6967. <https://doi.org/10.1021/acs.est.0c00961>.
- (86) Anbar, M.; Hart, E. J. The Reaction of Haloaliphatic Compounds with Hydrated Electrons ¹. *J. Phys. Chem.* **1965**, *69* (1), 271–274. <https://doi.org/10.1021/j100885a041>.
- (87) Maza, W. A.; Breslin, V. M.; Owrutsky, J. C.; Pate, B. B.; Epshteyn, A. Nanosecond Transient Absorption of Hydrated Electrons and Reduction of Linear Perfluoroalkyl Acids and Sulfonates. *Environ. Sci. Technol. Lett.* **2021**, *8* (7), 525–530. <https://doi.org/10.1021/acs.estlett.1c00383>.
- (88) Ruyle, B. J.; Pickard, H. M.; LeBlanc, D. R.; Tokranov, A. K.; Thackray, C. P.; Hu, X. C.; Vecitis, C. D.; Sunderland, E. M. Isolating the AFFF Signature in Coastal Watersheds Using Oxidizable PFAS Precursors and Unexplained Organofluorine. *Environ. Sci. Technol.* **2021**, *55* (6), 3686–3695. <https://doi.org/10.1021/acs.est.0c07296>.
- (89) Ghisi, R.; Vamerali, T.; Manzetti, S. Accumulation of Perfluorinated Alkyl Substances (PFAS) in Agricultural Plants: A Review. *Environmental Research* **2019**, *169*, 326–341. <https://doi.org/10.1016/j.envres.2018.10.023>.
- (90) Gordon, S. C. Toxicological Evaluation of Ammonium 4,8-Dioxa-3H-Perfluorononanoate, a New Emulsifier to Replace Ammonium Perfluorooctanoate in Fluoropolymer Manufacturing. *Regulatory Toxicology and Pharmacology* **2011**, *59* (1), 64–80. <https://doi.org/10.1016/j.yrtph.2010.09.008>.
- (91) Sun, M.; Arevalo, E.; Strynar, M.; Lindstrom, A.; Richardson, M.; Kearns, B.; Pickett, A.; Smith, C.; Knappe, D. R. U. Legacy and Emerging Perfluoroalkyl Substances Are Important Drinking Water Contaminants in the Cape Fear River Watershed of North Carolina. *Environ. Sci. Technol. Lett.* **2016**, *3* (12), 415–419. <https://doi.org/10.1021/acs.estlett.6b00398>.
- (92) Hart, E. J. The Hydrated Electron: Properties and Reactions of This Most Reactive and Elementary of Aqueous Negative Ions Are Discussed. *Science* **1964**, *146* (3640), 19–25. <https://doi.org/10.1126/science.146.3640.19>.
- (93) Harish, S.; Joseph, J.; Phani, K. L. N. Interaction between Gold (III) Chloride and Potassium Hexacyanoferrate (II/III)—Does It Lead to Gold Analogue of Prussian Blue? *Electrochimica Acta* **2011**, *56* (16), 5717–5721. <https://doi.org/10.1016/j.electacta.2011.04.044>.

- (94) Van Hoomissen, D. J.; Vyas, S. Early Events in the Reductive Dehalogenation of Linear Perfluoroalkyl Substances. *Environ. Sci. Technol. Lett.* **2019**, *6* (6), 365–371. <https://doi.org/10.1021/acs.estlett.9b00116>.
- (95) Bentel, M. J.; Liu, Z.; Yu, Y.; Gao, J.; Men, Y.; Liu, J. Enhanced Degradation of Perfluorocarboxylic Acids (PFCAs) by UV/Sulfite Treatment: Reaction Mechanisms and System Efficiencies at pH 12. *Environ. Sci. Technol. Lett.* **2020**, *7* (5), 351–357. <https://doi.org/10.1021/acs.estlett.0c00236>.
- (96) Schmidt, K. H.; Bartels, D. M. Lack of Ionic Strength Effect in the Recombination of Hydrated Electrons: $(E^-)_{Aq} + (E^-)_{Aq} \rightarrow 2(OH^-) + H_2$. *Chemical Physics* **1995**, *190* (1), 145–152. [https://doi.org/10.1016/0301-0104\(94\)00332-5](https://doi.org/10.1016/0301-0104(94)00332-5).
- (97) Schwarz, H. A. Reaction of the Hydrated Electron with Water. *J. Phys. Chem.* **1992**, *96* (22), 8937–8941. <https://doi.org/10.1021/j100201a044>.
- (98) *Chemical Kinetics*; Elsevier, 2007. <https://doi.org/10.1016/B978-0-444-52186-6.X5000-7>.
- (99) Swallow, A. J. RECENT RESULTS FROM PULSE RADIOLYSIS. *Photochem Photobiol* **1968**, *7* (6), 683–694. <https://doi.org/10.1111/j.1751-1097.1968.tb08053.x>.
- (100) Maza, W. A.; Etz, B. D.; Schutt, T. C.; Chaloux, B. L.; Breslin, V. M.; Pate, B. B.; Shukla, M. K.; Owrutsky, J. C.; Epshteyn, A. Impact of Submicellar Aggregation on Reduction Kinetics of Perfluorooctanoate by the Hydrated Electron. *Environ. Sci. Technol. Lett.* **2022**, *9* (3), 226–232. <https://doi.org/10.1021/acs.estlett.1c01020>.
- (101) Liu, Z.; Chen, Z.; Gao, J.; Yu, Y.; Men, Y.; Gu, C.; Liu, J. Accelerated Degradation of Perfluorosulfonates and Perfluorocarboxylates by UV/Sulfite + Iodide: Reaction Mechanisms and System Efficiencies. *Environ. Sci. Technol.* **2022**, *56* (6), 3699–3709. <https://doi.org/10.1021/acs.est.1c07608>.
- (102) Biswas, S.; Yamijala, S. S. R. K. C.; Wong, B. M. Degradation of Per- and Polyfluoroalkyl Substances with Hydrated Electrons: A New Mechanism from First-Principles Calculations. *Environ. Sci. Technol.* **2022**, *56* (12), 8167–8175. <https://doi.org/10.1021/acs.est.2c01469>.
- (103) Szwarc, M.; Taylor, J. W. Determination of Some Carbon-Chlorine Bond Dissociation Energies. *The Journal of Chemical Physics* **1954**, *22* (2), 270–274. <https://doi.org/10.1063/1.1740050>.
- (104) Mazurek, U.; Schwarz, H. Carbon–Fluorine Bond Activation—Looking at and Learning from Unsolvated Systems. *Chem. Commun.* **2003**, No. 12, 1321–1326. <https://doi.org/10.1039/B211850E>.
- (105) Burdeniuc, J.; Jedicka, B.; Crabtree, R. H. Recent Advances in C–F Bond Activation. *Chem. Ber./Recl.* **1997**, *130* (2), 145–154. <https://doi.org/10.1002/cber.19971300203>.
- (106) Bao, Y.; Deng, S.; Jiang, X.; Qu, Y.; He, Y.; Liu, L.; Chai, Q.; Mumtaz, M.; Huang, J.; Cagnetta, G.; Yu, G. Degradation of PFOA Substitute: GenX (HFPO–DA Ammonium Salt): Oxidation with UV/Persulfate or Reduction with UV/Sulfite? *Environ. Sci. Technol.* **2018**, *acs.est.8b02172*. <https://doi.org/10.1021/acs.est.8b02172>.

- (107) Bentel, M. J.; Yu, Y.; Xu, L.; Li, Z.; Wong, B. M.; Men, Y.; Liu, J. Defluorination of Per- and Polyfluoroalkyl Substances (PFASs) with Hydrated Electrons: Structural Dependence and Implications to PFAS Remediation and Management. *Environ. Sci. Technol.* **2019**, *53* (7), 3718–3728. <https://doi.org/10.1021/acs.est.8b06648>.
- (108) Chen, Z.; Tian, H.; Li, H.; Li, J.; Hong, R.; Sheng, F.; Wang, C.; Gu, C. Application of Surfactant Modified Montmorillonite with Different Conformation for Photo-Treatment of Perfluorooctanoic Acid by Hydrated Electrons. *Chemosphere* **2019**, *235*, 1180–1188. <https://doi.org/10.1016/j.chemosphere.2019.07.032>.
- (109) Daily, R.; Minakata, D. Reactivities of Hydrated Electrons with Organic Compounds in Aqueous-Phase Advanced Reduction Processes. *Environ. Sci.: Water Res. Technol.* **2022**, *8* (3), 543–574. <https://doi.org/10.1039/D1EW00897H>.
- (110) Vellanki, B. P.; Batchelor, B.; Abdel-Wahab, A. Advanced Reduction Processes: A New Class of Treatment Processes. *Environmental Engineering Science* **2013**, *30* (5), 264–271. <https://doi.org/10.1089/ees.2012.0273>.
- (111) Gu, Y.; Dong, W.; Luo, C.; Liu, T. Efficient Reductive Decomposition of Perfluorooctanesulfonate in a High Photon Flux UV/Sulfite System. *Environ. Sci. Technol.* **2016**, *50* (19), 10554–10561. <https://doi.org/10.1021/acs.est.6b03261>.
- (112) Vellanki, B. P.; Batchelor, B. Perchlorate Reduction by the Sulfite/Ultraviolet Light Advanced Reduction Process. *Journal of Hazardous Materials* **2013**, *262*, 348–356. <https://doi.org/10.1016/j.jhazmat.2013.08.061>.
- (113) Jung, B.; Nicola, R.; Batchelor, B.; Abdel-Wahab, A. Effect of Low- and Medium-Pressure Hg UV Irradiation on Bromate Removal in Advanced Reduction Process. *Chemosphere* **2014**, *117*, 663–672. <https://doi.org/10.1016/j.chemosphere.2014.09.086>.
- (114) Botlaguduru, V. S. V.; Batchelor, B.; Abdel-Wahab, A. Application of UV–Sulfite Advanced Reduction Process to Bromate Removal. *Journal of Water Process Engineering* **2015**, *5*, 76–82. <https://doi.org/10.1016/j.jwpe.2015.01.001>.
- (115) Gu, Y.; Liu, T.; Wang, H.; Han, H.; Dong, W. Hydrated Electron Based Decomposition of Perfluorooctane Sulfonate (PFOS) in the VUV/Sulfite System. *Science of The Total Environment* **2017**, *607–608*, 541–548. <https://doi.org/10.1016/j.scitotenv.2017.06.197>.
- (116) Lapointe, F.; Wolf, M.; Campen, R. K.; Tong, Y. Probing the Birth and Ultrafast Dynamics of Hydrated Electrons at the Gold/Liquid Water Interface via an Optoelectronic Approach. *J. Am. Chem. Soc.* **2020**, *142* (43), 18619–18627. <https://doi.org/10.1021/jacs.0c08289>.
- (117) Abel, B.; Buck, U.; Sobolewski, A. L.; Domcke, W. On the Nature and Signatures of the Solvated Electron in Water. *Phys. Chem. Chem. Phys.* **2012**, *14* (1), 22–34. <https://doi.org/10.1039/C1CP21803D>.
- (118) Milosavljevic, B. H.; Micic, O. I. Solvated Electron Reactions in Water-Alcohol Solutions. *J. Phys. Chem.* **1978**, *82* (12), 1359–1362. <https://doi.org/10.1021/j100501a007>.

- (119) Gonzalez, M.; Oliveros, E.; Worner, M.; Braun, A. Vacuum-Ultraviolet Photolysis of Aqueous Reaction Systems. *Journal of Photochemistry and Photobiology C: Photochemistry Reviews* **2004**, *5* (3), 225–246. <https://doi.org/10.1016/j.jphotochemrev.2004.10.002>.
- (120) Barat, F.; Gilles, L.; Hickel, B.; Lesigne, B. Effect of the Dielectric Constant on the Reactivity of the Solvated Electron. *J. Phys. Chem.* **1973**, *77* (13), 1711–1715. <https://doi.org/10.1021/j100632a024>.
- (121) Qu, Y.; Zhang, C.-J.; Chen, P.; Zhou, Q.; Zhang, W.-X. Effect of Initial Solution PH on Photo-Induced Reductive Decomposition of Perfluorooctanoic Acid. *Chemosphere* **2014**, *107*, 218–223. <https://doi.org/10.1016/j.chemosphere.2013.12.046>.
- (122) Amador, C. K.; Van Hoomissen, D. J.; Liu, J.; Strathmann, T. J.; Vyas, S. Ultra-Short Chain Fluorocarboxylates Exhibit Wide Ranging Reactivity with Hydrated Electrons. *Chemosphere* **2023**, *311*, 136918. <https://doi.org/10.1016/j.chemosphere.2022.136918>.
- (123) Levin, P. P.; Brzhevskaya, O. N.; Nedelina, O. S. Kinetics of Hydrated Electron Reactions with Phosphate Anions: A Laser Photolysis Study. *Russ Chem Bull* **2007**, *56* (7), 1325–1328. <https://doi.org/10.1007/s11172-007-0202-1>.
- (124) Dogliotti, L.; Hayon, E. Flash Photolysis Study of Sulfite, Thiocyanate, and Thiosulfate Ions in Solution. *J. Phys. Chem.* **1968**, *72* (5), 1800–1807. <https://doi.org/10.1021/j100851a073>.
- (125) Liu, Z.; Bentel, M. J.; Yu, Y.; Ren, C.; Gao, J.; Pulikkal, V. F.; Sun, M.; Men, Y.; Liu, J. Near-Quantitative Defluorination of Perfluorinated and Fluorotelomer Carboxylates and Sulfonates with Integrated Oxidation and Reduction. *Environ. Sci. Technol.* **2021**, *55* (10), 7052–7062. <https://doi.org/10.1021/acs.est.1c00353>.
- (126) Thomas, J. K.; Gordon, S.; Hart, E. J. The Rates of Reaction of the Hydrated Electron in Aqueous Inorganic Solutions ¹. *J. Phys. Chem.* **1964**, *68* (6), 1524–1527. <https://doi.org/10.1021/j100788a043>.
- (127) Gordon, S.; Hart, E. J.; Matheson, M. S.; Rabani, J.; Thomas, J. K. Reactions of the Hydrated Electron. *Discuss. Faraday Soc.* **1963**, *36*, 193. <https://doi.org/10.1039/df9633600193>.
- (128) Ellis, A. C.; Liu, C. J.; Fang, Y.; Boyer, T. H.; Schaefer, C. E.; Higgins, C. P.; Strathmann, T. J. Pilot Study Comparison of Regenerable and Emerging Single-Use Anion Exchange Resins for Treatment of Groundwater Contaminated by per- and Polyfluoroalkyl Substances (PFASs). *Water Research* **2022**, *223*, 119019. <https://doi.org/10.1016/j.watres.2022.119019>.
- (129) Lisovskaya, A.; Bartels, D. M. Reduction of CO₂ by Hydrated Electrons in High Temperature Water. *Radiation Physics and Chemistry* **2019**, *158*, 61–63. <https://doi.org/10.1016/j.radphyschem.2019.01.017>.
- (130) Getoff, N. Possibilities on the Radiation-Induced Incorporation of CO₂ and CO into Organic Compounds☆. *International Journal of Hydrogen Energy* **1994**, *19* (8), 667–672. [https://doi.org/10.1016/0360-3199\(94\)90151-1](https://doi.org/10.1016/0360-3199(94)90151-1).
- (131) Hentz, R. R.; Farhataziz; Milner, D. J.; Burton, M. γ Radiolysis of Liquids at High Pressures. III. Aqueous Solutions of Sodium Bicarbonate. *The Journal of Chemical Physics* **1967**, *47* (2), 374–377. <https://doi.org/10.1063/1.1711902>.

- (132) Neta, P.; Simic, M.; Hayon, E. Pulse Radiolysis of Aliphatic Acids in Aqueous Solutions. I. Simple Monocarboxylic Acids. *J. Phys. Chem.* **1969**, *73* (12), 4207–4213. <https://doi.org/10.1021/j100846a029>.
- (133) Fennell, B. D.; Odorisio, A.; McKay, G. Quantifying Hydrated Electron Transformation Kinetics in UV-Advanced Reduction Processes Using the $R_{e-,UV}$ Method. *Environ. Sci. Technol.* **2022**, *56* (14), 10329–10338. <https://doi.org/10.1021/acs.est.2c02003>.
- (134) Jiang, Z.; Adjei, D.; Denisov, S. A.; Mostafavi, M.; Ma, J. Transient Kinetics of Short-Chain Perfluoroalkyl Sulfonate with Radiolytic Reducing Species. *Environ. Sci. Technol. Lett.* **2022**, *acs.estlett.2c00837*. <https://doi.org/10.1021/acs.estlett.2c00837>.
- (135) Jortner, J.; Ottolenghi, M.; Rabani, J.; Stein, G. Conversion of Solvated Electrons into Hydrogen Atoms in the Photo- and Radiation Chemistry of Aqueous Solutions. *The Journal of Chemical Physics* **1962**, *37* (10), 2488–2495. <https://doi.org/10.1063/1.1733033>.
- (136) Adamczyk, K.; Prémont-Schwarz, M.; Pines, D.; Pines, E.; Nibbering, E. T. J. Real-Time Observation of Carbonic Acid Formation in Aqueous Solution. *Science* **2009**, *326* (5960), 1690–1694. <https://doi.org/10.1126/science.1180060>.
- (137) Hart, E. J.; Gordon, S.; Thomas, J. K. Rate Constants of Hydrated Electron Reactions with Organic Compounds ¹. *J. Phys. Chem.* **1964**, *68* (6), 1271–1274. <https://doi.org/10.1021/j100788a001>.
- (138) Zagorski, Z. P.; Sehested, K.; Nielsen, S. O. Pulse Radiolysis of Aqueous Alkaline Sulfite Solutions. *J. Phys. Chem.* **1971**, *75* (23), 3510–3517. <https://doi.org/10.1021/j100692a004>.
- (139) Anbar, M. The Reactions of Hydrated Electrons with Organic Compounds. In *Advances in Physical Organic Chemistry*; Elsevier, 1969; Vol. 7, pp 115–151. [https://doi.org/10.1016/S0065-3160\(08\)60264-6](https://doi.org/10.1016/S0065-3160(08)60264-6).
- (140) *Solvated Electron*; Hart, E. J., Ed.; Advances in Chemistry; AMERICAN CHEMICAL SOCIETY: WASHINGTON, D.C., 1965; Vol. 50. <https://doi.org/10.1021/ba-1965-0050>.
- (141) Wallace, S. C.; Thomas, J. K. Reactions in Micellar Systems. *Radiation Research* **1973**, *54* (1), 49. <https://doi.org/10.2307/3573865>.
- (142) Park, H.; Vecitis, C. D.; Cheng, J.; Choi, W.; Mader, B. T.; Hoffmann, M. R. Reductive Defluorination of Aqueous Perfluorinated Alkyl Surfactants: Effects of Ionic Headgroup and Chain Length. *J. Phys. Chem. A* **2009**, *113* (4), 690–696. <https://doi.org/10.1021/jp807116q>.
- (143) Szajdzinska-Pietek, E.; Gebicki, J. L. Pulse Radiolytic Investigation of Perfluorinated Surfactants in Aqueous Solutions. *Res. Chem. Intermed.* **2000**, *26* (9), 897–912. <https://doi.org/10.1163/156856700X00381>.
- (144) Hart, E. J. The Hydrated Electron. In *Survey of Progress in Chemistry*; Elsevier, 1969; Vol. 5, pp 129–184. <https://doi.org/10.1016/B978-0-12-395706-1.50010-8>.
- (145) Gu, J.; Ma, J.; Jiang, J.; Yang, L.; Yang, J.; Zhang, J.; Chi, H.; Song, Y.; Sun, S.; Tian, W. Q. Hydrated Electron (E_{aq}⁻) Generation from Phenol/UV: Efficiency, Influencing Factors, and Mechanism. *Applied Catalysis B: Environmental* **2017**, *200*, 585–593. <https://doi.org/10.1016/j.apcatb.2016.07.034>.

- (146) Kancharla, S.; Jahan, R.; Bedrov, D.; Tsianou, M.; Alexandridis, P. Role of Chain Length and Electrolyte on the Micellization of Anionic Fluorinated Surfactants in Water. *Colloids and Surfaces A: Physicochemical and Engineering Aspects* **2021**, *628*, 127313. <https://doi.org/10.1016/j.colsurfa.2021.127313>.
- (147) Nakayama, H. Krafft Temperatures of Perfluoro-Octanoic Acid and of Its Salts. *BCSJ* **1967**, *40* (7), 1592–1595. <https://doi.org/10.1246/bcsj.40.1592>.
- (148) Foster, M.; Rainey, M.; Watson, C.; Dodds, J. N.; Kirkwood, K. I.; Fernández, F. M.; Baker, E. S. Uncovering PFAS and Other Xenobiotics in the Dark Metabolome Using Ion Mobility Spectrometry, Mass Defect Analysis, and Machine Learning. *Environ. Sci. Technol.* **2022**, *56* (12), 9133–9143. <https://doi.org/10.1021/acs.est.2c00201>.
- (149) Duan, L.; Wang, B.; Heck, K.; Guo, S.; Clark, C. A.; Arredondo, J.; Wang, M.; Senftle, T. P.; Westerhoff, P.; Wen, X.; Song, Y.; Wong, M. S. Efficient Photocatalytic PFOA Degradation over Boron Nitride. *Environ. Sci. Technol. Lett.* **2020**, *7* (8), 613–619. <https://doi.org/10.1021/acs.estlett.0c00434>.
- (150) Li, X.; Zhang, P.; Jin, L.; Shao, T.; Li, Z.; Cao, J. Efficient Photocatalytic Decomposition of Perfluorooctanoic Acid by Indium Oxide and Its Mechanism. *Environ. Sci. Technol.* **2012**, *46* (10), 5528–5534. <https://doi.org/10.1021/es204279u>.
- (151) Zhao, B.; Zhang, P. Photocatalytic Decomposition of Perfluorooctanoic Acid with β -Ga₂O₃ Wide Bandgap Photocatalyst. *Catalysis Communications* **2009**, *10* (8), 1184–1187. <https://doi.org/10.1016/j.catcom.2009.01.017>.
- (152) Kerzig, C.; Guo, X.; Wenger, O. S. Unexpected Hydrated Electron Source for Preparative Visible-Light Driven Photoredox Catalysis. *J. Am. Chem. Soc.* **2019**, *141* (5), 2122–2127. <https://doi.org/10.1021/jacs.8b12223>.
- (153) Guo, C.; Zhang, C.; Sun, Z.; Zhao, X.; Zhou, Q.; Hoffmann, M. R. Synergistic Impact of Humic Acid on the Photo-Reductive Decomposition of Perfluorooctanoic Acid. *Chemical Engineering Journal* **2019**, *360*, 1101–1110. <https://doi.org/10.1016/j.cej.2018.10.204>.
- (154) Ma, H. Characterization of Isolated Fractions of Dissolved Organic Matter from Natural Waters and a Wastewater Effluent. *Water Research* **2001**, *35* (4), 985–996. [https://doi.org/10.1016/S0043-1354\(00\)00350-X](https://doi.org/10.1016/S0043-1354(00)00350-X).
- (155) Shon, H. K.; Vigneswaran, S.; Snyder, S. A. Effluent Organic Matter (EfOM) in Wastewater: Constituents, Effects, and Treatment. *Critical Reviews in Environmental Science and Technology* **2006**, *36* (4), 327–374. <https://doi.org/10.1080/10643380600580011>.
- (156) Huo, S.; Xi, B.; Yu, H.; He, L.; Fan, S.; Liu, H. Characteristics of Dissolved Organic Matter (DOM) in Leachate with Different Landfill Ages. *Journal of Environmental Sciences* **2008**, *20* (4), 492–498. [https://doi.org/10.1016/S1001-0742\(08\)62085-9](https://doi.org/10.1016/S1001-0742(08)62085-9).
- (157) Kancharla, S.; Choudhary, A.; Davis, R. T.; Dong, D.; Bedrov, D.; Tsianou, M.; Alexandridis, P. GenX in Water: Interactions and Self-Assembly. *Journal of Hazardous Materials* **2022**, *428*, 128137. <https://doi.org/10.1016/j.jhazmat.2021.128137>.

- (158) Neta, P.; Huie, R. E.; Ross, A. B. Rate Constants for Reactions of Inorganic Radicals in Aqueous Solution. *Journal of Physical and Chemical Reference Data* **1988**, *17* (3), 1027–1284. <https://doi.org/10.1063/1.555808>.
- (159) Cárdenas-Jirón, G. I.; Gutiérrez-Oliva, S.; Melin, J.; Toro-Labbé, A. Relations between Potential Energy, Electronic Chemical Potential, and Hardness Profiles. *J. Phys. Chem. A* **1997**, *101* (25), 4621–4627. <https://doi.org/10.1021/jp9638705>.
- (160) Chen, L.-Q. Chemical Potential and Gibbs Free Energy. *MRS Bull.* **2019**, *44* (7), 520–523. <https://doi.org/10.1557/mrs.2019.162>.
- (161) Pearson, R. G. Acids and Bases. *Science* **1966**, *151* (3707), 172–177. <https://doi.org/10.1126/science.151.3707.172>.
- (162) Parr, R. G.; Szentpály, L. v.; Liu, S. Electrophilicity Index. *J. Am. Chem. Soc.* **1999**, *121* (9), 1922–1924. <https://doi.org/10.1021/ja983494x>.
- (163) Dorfman, L. M.; Taub, I. A. **Pulse Radiolysis Studies. III. Elementary Reactions in Aqueous Ethanol Solution.** *J. Am. Chem. Soc.* **1963**, *85* (16), 2370–2374. <https://doi.org/10.1021/ja00899a006>.
- (164) Phillips, G. O.; Power, D. M.; Sewart, M. C. G. Effects of γ -Irradiation on Sulphonamides. *Radiation Research* **1973**, *53* (2), 204. <https://doi.org/10.2307/3573525>.

APPENDIX A
SUPPLEMENTARY INFORMATION FOR CHAPTER 2

A.1 Methods

Reagents. All chemicals were used as received without further purification. Sodium heptafluorobutyrate (98%); sodium pentafluoropropionate (98%); 4,4,4-trifluorobutyric acid (98%); and 3,3,3-trifluoropropanoic acid (98%) were purchased from Oakwood Chemical. Sodium trifluoroacetate (97%); difluoroacetic acid, sodium salt (97%); sodium monofluoroacetate (99%); and 2H-perfluorobutyric acid (97%) were purchased from abcr. 2,2,3,3-tetrafluoropropanoic acid (95%); 2,2-difluoropropanoic acid (95%); and 2,3,3,3-tetrafluoropropanoic acid (95%) were purchased from Enamine. 2,2-difluorobutanoic acid (97%) was purchased from Aaron Chemicals. 2-fluoropropanoic acid (97%) was purchased from Manchester Organics. Butanoic ($\geq 99\%$) and propanoic ($\geq 99.5\%$) acid were purchased from Sigma-Aldrich. Glacial acetic acid (99–100%) was purchased from Macron Fine Chemicals. Potassium ferricyanide (100.2%), sodium chloride (100.5%), and sodium hydroxide (97.5%) were purchased from Fisher Chemical. Sodium borate, tetra (99.5–101.5%) was purchased from Baker & Adamson. Potassium ferrocyanide (101.3%) was purchased from J.T. Baker.

Solution Preparation. Deoxygenated water was used to prepare all solutions inside an anaerobic glovebox to eliminate scavenging of e_{aq}^- by oxygen. Briefly, this was prepared by boiling nanopure water for 3 h while stirring and sparging with $N_{2(g)}$. Stock solution concentrations are summarized in Table A.1. All reactions were performed in the following conditions unless otherwise stated: fifteen separate cuvettes were prepared containing triplicates of 0, 10, 20, 40, and 50 mM quencher along with 40 μM $\text{K}_4\text{Fe}(\text{CN})_6$, 10 μM $\text{K}_3\text{Fe}(\text{CN})_6$ in 40 mM borate buffer at pH 9.2 (25 ml total for each sample). The pH value 9.2 was selected because it is commonly used in hydrated electron treatment studies^{41,53,84}. Borate buffer was chosen because it is known to be unreactive towards the hydrated electron and absorbs negligibly at 254 nm^{60,144}. Ionic strength of all solutions was fixed at 0.63 by adding NaCl to balance ionic strength contributions from the quencher and pH buffer. The elevated ionic strength was used to ensure that this variable could be fixed while adding relatively high concentrations of the target quenchers (up to 60 mM for fluorocarboxylates; up to 500 mM for unfluorinated carboxylates). While use of up to 60 mM fluorocarboxylate is beneficial in LFP experiments for determining k_2 values, these elevated concentrations are not required for UV-ARPs in practice. In fact, constant irradiation experiments are often conducted in systems containing ppt – ppb levels of PFAS which are typical of PFAS-contaminated waters^{81,85,107}. We also note that any e_{aq}^- quenching due to added buffer or electrolyte will be accounted for in the fluorocarboxylate blank sample since these concentrations were kept constant in each

measurement. This point is highlighted by the data provided in Figure A.1, which shows that e_{aq}^- lifetime in the absence of added fluorocarboxylate quencher was found to be similar for all measurements done at the same excitation wavelengths, i.e., 254 nm and 266 nm (Figure A.1). e_{aq}^- lifetime data for PFBA at pH 9.5 and 12 (Figure A.1) also shows that background quenching at the two different pH conditions are within error of each other.

The 25 ml samples were prepared in 50 ml centrifuge tubes before transferring triplicate 2.75 ml aliquots to quartz cuvettes, capping, and covering with parafilm. Cuvettes were then removed from the glovebox and immediately used in laser flash photolysis experiments. The remaining solution was used to check the pH of the sample before flash photolysis. To ensure pH was constant during reactions, pH was also measured after flash photolysis by pooling solutions from the three replicate cuvettes. For experiments conducted at pH 12, borate buffer was excluded and 1 M NaOH was used to set the pH value.

Table A.1 Chemical concentrations of stock solutions used in experiments. ^aFluorocarboxylate stock solutions were prepared in deoxygenated water from chemicals containing no organic cosolvent to avoid artifacts such as e_{aq}^- reacting with non-target constituents.

Solution	Component	Concentration (mM)
Salt offset	NaCl	500
Potassium ferricyanide	$K_3Fe(CN)_6$	10
Potassium ferrocyanide	$K_4Fe(CN)_6 \cdot 3H_2O$	10
Buffer and electrolyte	$Na_2B_4O_7 \cdot 10H_2O$	50
	NaCl	500
Fluorocarboxylates, sodium salt ^a	Various	500
Fluorocarboxylates, acid form ^a	Various	500
	NaOH	500

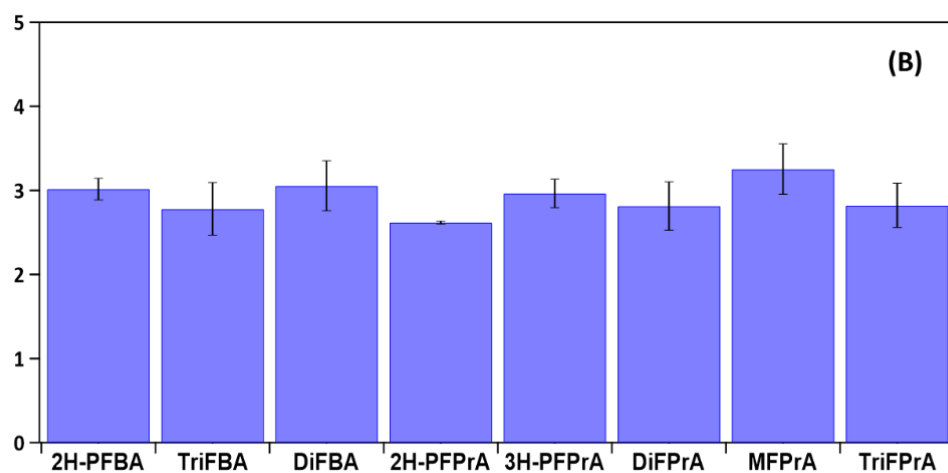
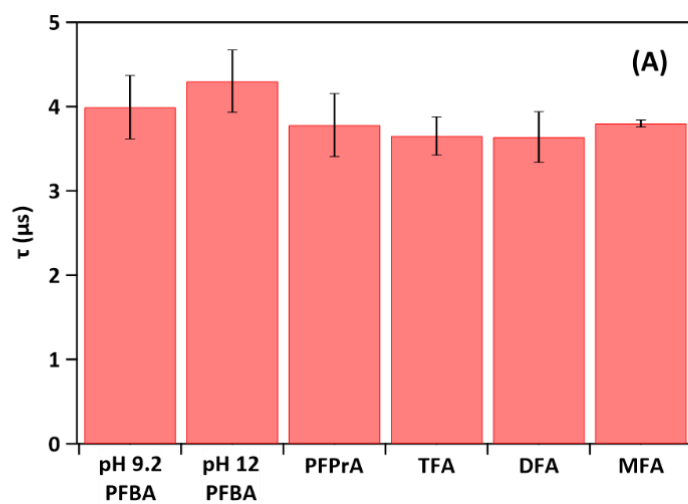


Figure A.1 Lifetime of e_{aq}^- in the absence of added fluorocarboxylate quencher (i.e., the 0 mM control samples) using excitation wavelengths: (A) 254 nm and (B) 266 nm.

TFA Kinetic Data Obtained Using 254 and 266 nm Light Sources.

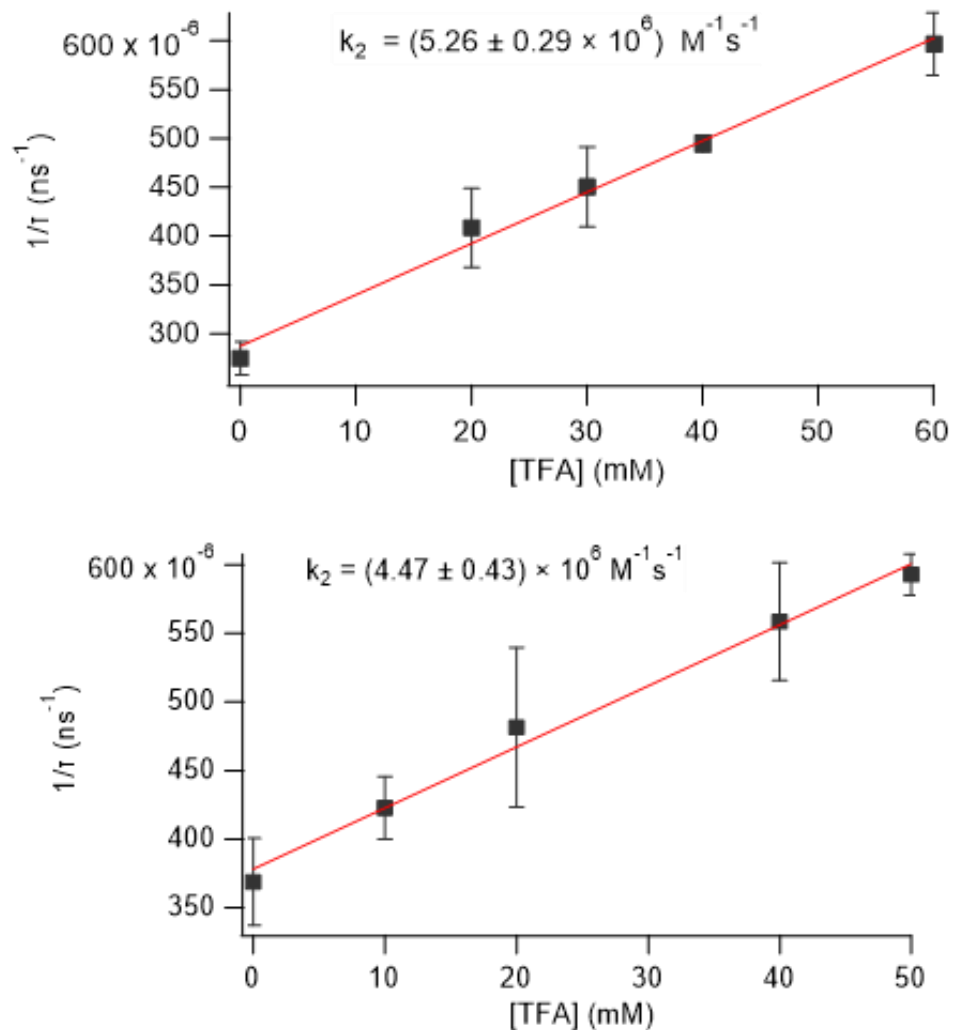


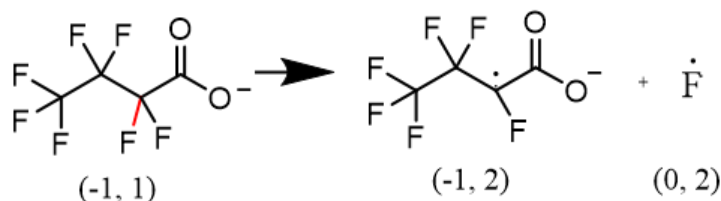
Figure A.2 TFA Stern-Volmer plots determined following $\text{Fe}(\text{CN})_6^{4-}$ photolysis by 254 nm (left) and 266 nm (right) light. Detailed solution conditions can be found in Figure 2.1.

Density functional theory parameter equations for global properties.

Table A.2 Equations used to calculate global properties of fluorocarboxylates using DFT-calculated properties.

DFT parameter	Shorthand	Equation	
Ionization Potential	IP	$-E_{HOMO}$	Eq. S.1
Electron Affinity	EA	$-E_{LUMO}$	Eq. S.2
HOMO-LUMO Gap	$E_{HOMO}-E_{LUMO}$	$E_{HOMO} - E_{LUMO}$	Eq. S.3
Dipole	δ	<i>As is</i>	Eq. S.4
Hardness	η	$\frac{IP - EA}{2}$	Eq. S.5
Softness	S	$\frac{1}{\eta}$	Eq. S.6
Chemical Potential	χ	$\frac{IP + EA}{2}$	Eq. S.7
Electrophilicity Index	ω	$\frac{\chi^2}{2\eta}$	Eq. S.8

Density functional theory equations for global properties. Bond dissociation energies (BDEs) were calculated by taking the difference in enthalpies of the optimized geometries of the products and reactants after breaking each unique C-C and C-F bond, as depicted in Figure A.3. E_s° was calculated using similar geometries with the calculated Gibbs free energy used in the Nernst equation.



$$\begin{aligned} \blacksquare BDE &= \sum H_{prod} - \sum H_{react} \\ &= \left(H_{PFCA^{-1}, minus F} + H_F \right) - H_{PFCA^{-1}} \end{aligned}$$

$$\begin{aligned} \blacksquare E_s^\circ &= \frac{\Delta G}{nF} - SHE \\ &= \frac{G_{PFCA^{-1}} - (G_{PFCA^{-1}, minus F} + G_F)}{nF} - SHE \end{aligned}$$

Figure A.3 Example calculation of BDE and E_s° of PFBA determined using the ω B97-XD/aug-cc-pVDZ basis set and level of theory. The SMD implicit solvent model to mimic an aqueous solution environment and all PFCAs were taken to be in the anionic state. “H” denotes enthalpy, while G, n, F, and SHE represent Gibbs free energy, number of electrons transferred, Faraday’s constant, and the standard hydrogen electrode, respectively.

A.2 Chemical Interpretations of Select DFT Parameters

Chemical interpretations of select DFT parameters are discussed. Only those which are not commonly encountered are considered. Hardness (η) and chemical potential ($-\chi$) both describe chemical changes within a system. While η describes a molecule's resistance to charge transfer,¹⁵⁹ $-\chi$ characterizes a molecule's general tendency to form new substances.¹⁶⁰ Compounds with small η values can be said to be less resistant towards charge transfer, while those with large $-\chi$ can be said to have a greater tendency to react and form a new substance. In both cases, this would conceptually describe a compound amenable to change. The inverse of η is softness (S); a soft molecule could describe one with low (or zero) positive charge, or one that is easily polarizable;¹⁶¹ consequently, softness describes a molecule's tendency to undergo charge transfer. The last molecular property of interest is electrophilicity index (ω), which measures the electrophilic power of a compound. This could be seen as a molecule ability to "soak up" electrons.¹⁶² Negative values of ω correspond to a positive change in energy of the system ($\Delta E > 0$) when it "soaks up" electrons. Therefore, less negative values correspond to more favorable charge transfer process.

A.3 Additional data

Effects of Solution Conditions on hydrated electron lifetime.

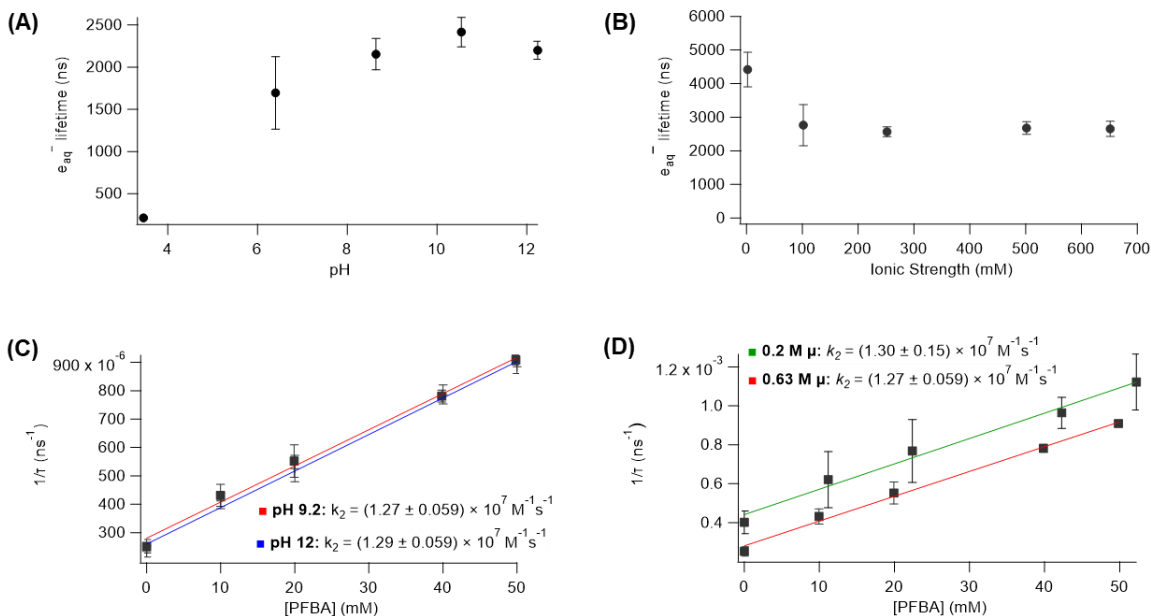


Figure A.4 Effects of (A) pH and (B) ionic strength on lifetimes of e_{aq}^- in the absence of fluorocarboxylate quenchers, along with comparison of the kinetics of e_{aq}^- reaction with PFBA measured at (C) pH 9.2 and pH 12, and (D) $\mu = 0.2$ and 0.63. Solution conditions are the same as those in Figure 1. Ionic strength in (A) kept constant at 0.63 using NaCl. Solution pH in (B) titrated to pH 12 using 1 M NaOH (no buffer). Ionic strength in (C) is 0.63. Solution pH in (D) is 9.2.

Rate constant ionic strength extrapolation.

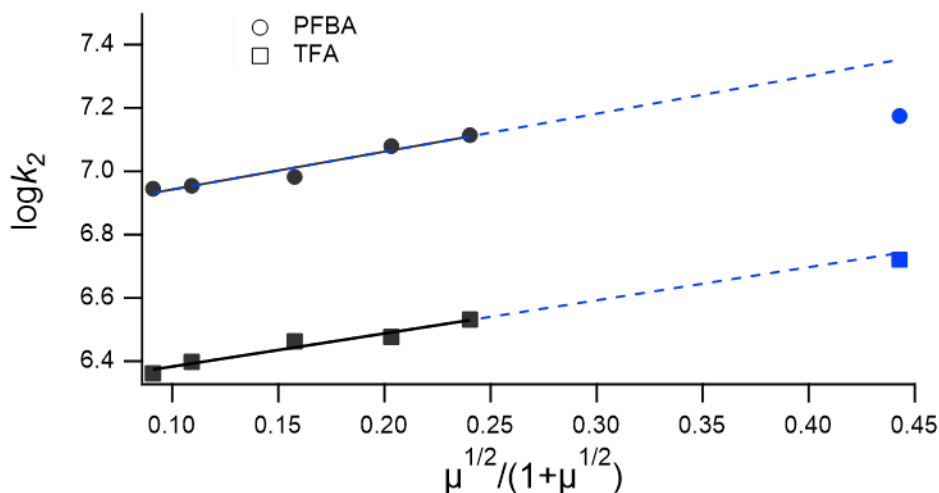


Figure A.5 Plots showing influence of ionic strength on measured $\log k_2$ values for PFBA and TFA, including data from the present study (blue symbols) and data previously reported by Huang *et al.*⁵⁰ (black symbols). Dashed blue lines show extrapolation of the trend reported by Huang and co-workers to conditions used in the present study.

Hydrated electron lifetime in the presence of sub-millimolar concentrations of various fluorocarboxylates.

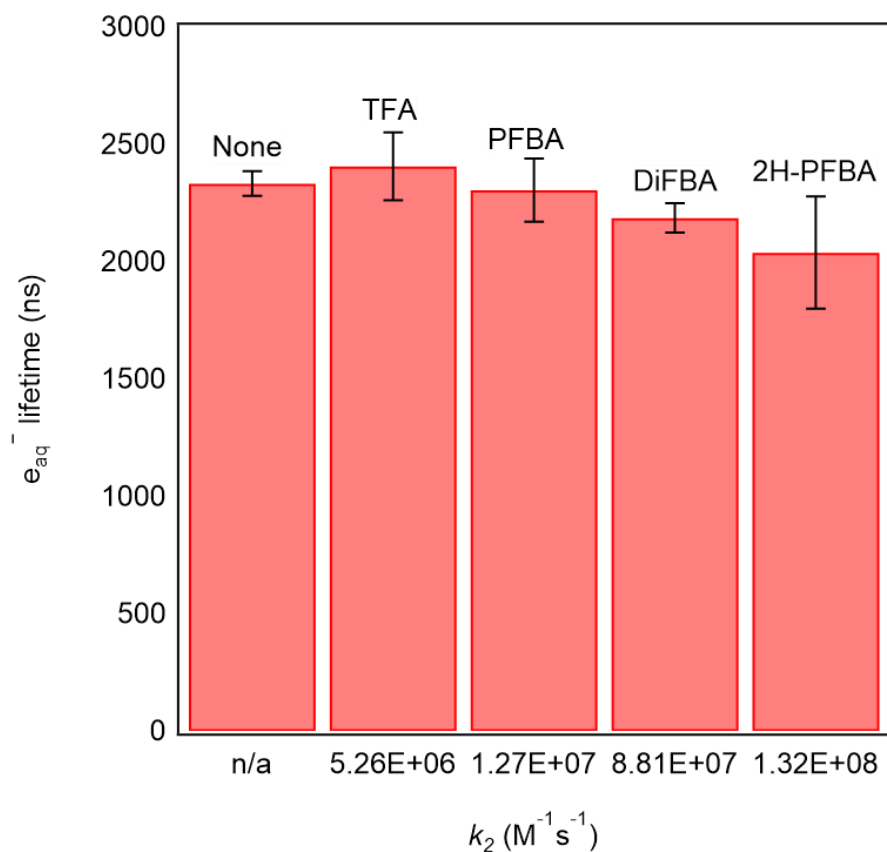


Figure A.6 Hydrated electron lifetime measurements in the absence and presence of various fluorocarboxylates added at a concentration of 0.1 mM. Other solution conditions: 40 μM $K_4Fe(CN)_6$, 10 μM $K_3Fe(CN)_6$, 40 mM borate buffer, pH 9.2, ionic strength kept constant at 630 mM using NaCl.

Stern-Volmer plots for mono-, di-, and trichloroacetate.

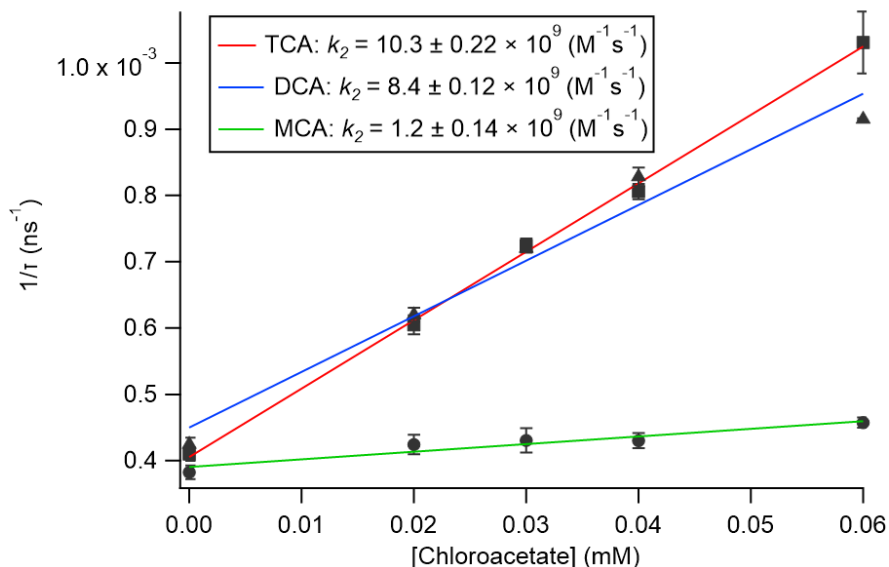


Figure A.7 Stern-Volmer plots for mono-, di-, and trichloroacetate reduction by e_{aq}^- produced at similar conditions as those described in Figure 2.1.

Global molecular property descriptors.

Table A.3 Global molecular properties of fluorocarboxylates in the anionic singlet state calculated by density functional theory.

No. carbons	Substrate ^a	IP (eV)	EA (eV)	HOMO–LUMO Gap (eV)	δ (Debye)	η (eV)	S (meV ⁻¹)	$-\chi$ (eV)	ω (eV)
2	TFA	9.73	-2.10	11.8	6.19	5.92	-84.5	-3.812	1.23
	DFA	9.48	-1.37	10.9	6.50	5.43	-92.2	-4.054	1.51
	MFA	9.27	-1.35	10.6	6.42	5.31	-94.2	-3.960	1.48
3	PFPrA	9.72	-1.79	11.5	8.47	5.76	-86.9	-3.964	1.36
	2H-PFPrA	9.49	-1.38	10.9	9.01	5.44	-92.0	-4.055	1.51
	3H-PFPrA	9.64	-1.38	11.0	8.00	5.51	-90.7	-4.128	1.55
	TriFPrA	9.17	-1.36	10.5	9.60	5.26	-95.0	-3.907	1.45
	DiFPrA	9.39	-1.32	10.7	8.16	5.36	-93.3	-4.035	1.52
	MFPrA	9.20	-1.31	10.5	8.22	5.26	-95.1	-3.949	1.48
	4	PFBA	9.71	-1.80	11.5	11.7	5.76	-86.8	-3.957
2H-PFBA		9.49	-1.40	10.9	12.4	5.44	-91.9	-4.046	1.50
TriFBA		8.99	-1.37	10.4	12.6	5.18	-96.5	-3.811	1.40
DiFBA		9.36	-1.25	10.6	10.2	5.30	-94.3	-4.052	1.55

^aFull names and structures of individual fluorocarboxylates provided in Table 1.

Bond Dissociation Energy and Reduction Potential Values.

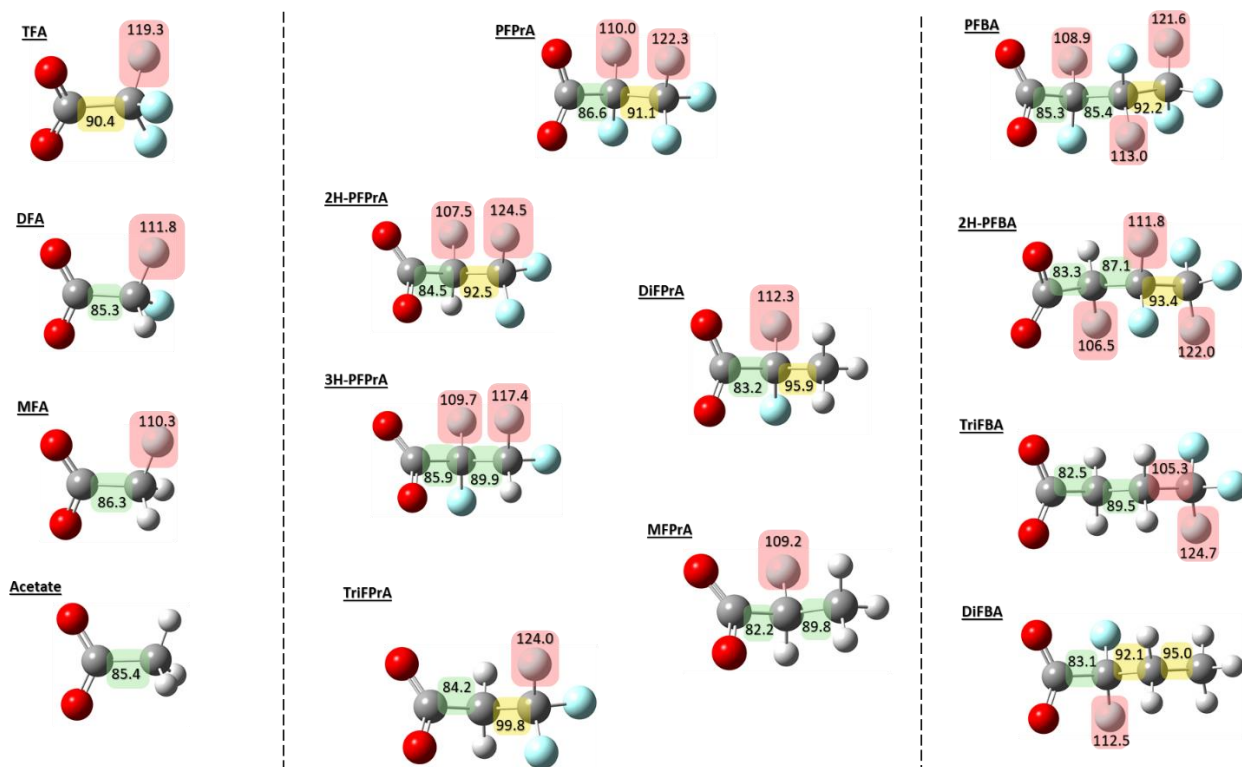


Figure A.8 Bond dissociation energies for each unique C-C and C-F bond in the fluorocarboxylate structures. Values provided in kcal/mol and are separated by two carbon (left), three carbon (middle), and four carbon (right) compounds. Bonds highlighted in red depict strong bonds that are relatively hard to break (≥ 100 kcal/mol), while yellow and green depict moderate (90–100 kcal/mol) and weak (< 90 kcal/mol) bonds, respectively. Red atoms = oxygen; blue = fluorine; grey = hydrogen.

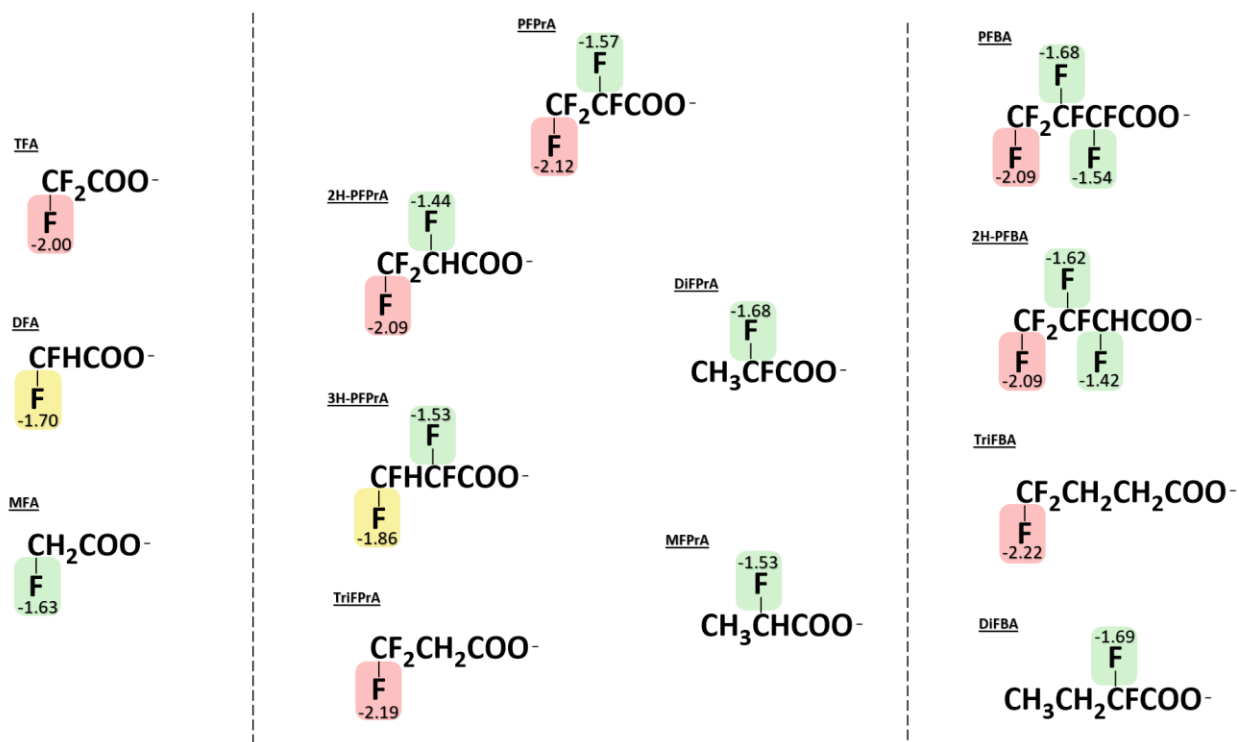


Figure A.9 Reduction potentials in volts for each unique C-F bond. As before, these are separated by four, three, and two carbon compounds. Values in red represent bonds that are relatively hard to reduce (≥ 2 V), while yellow and green depict moderately (1.7–1.9 V) and easily (< 1.7 V) reducible bonds, respectively.

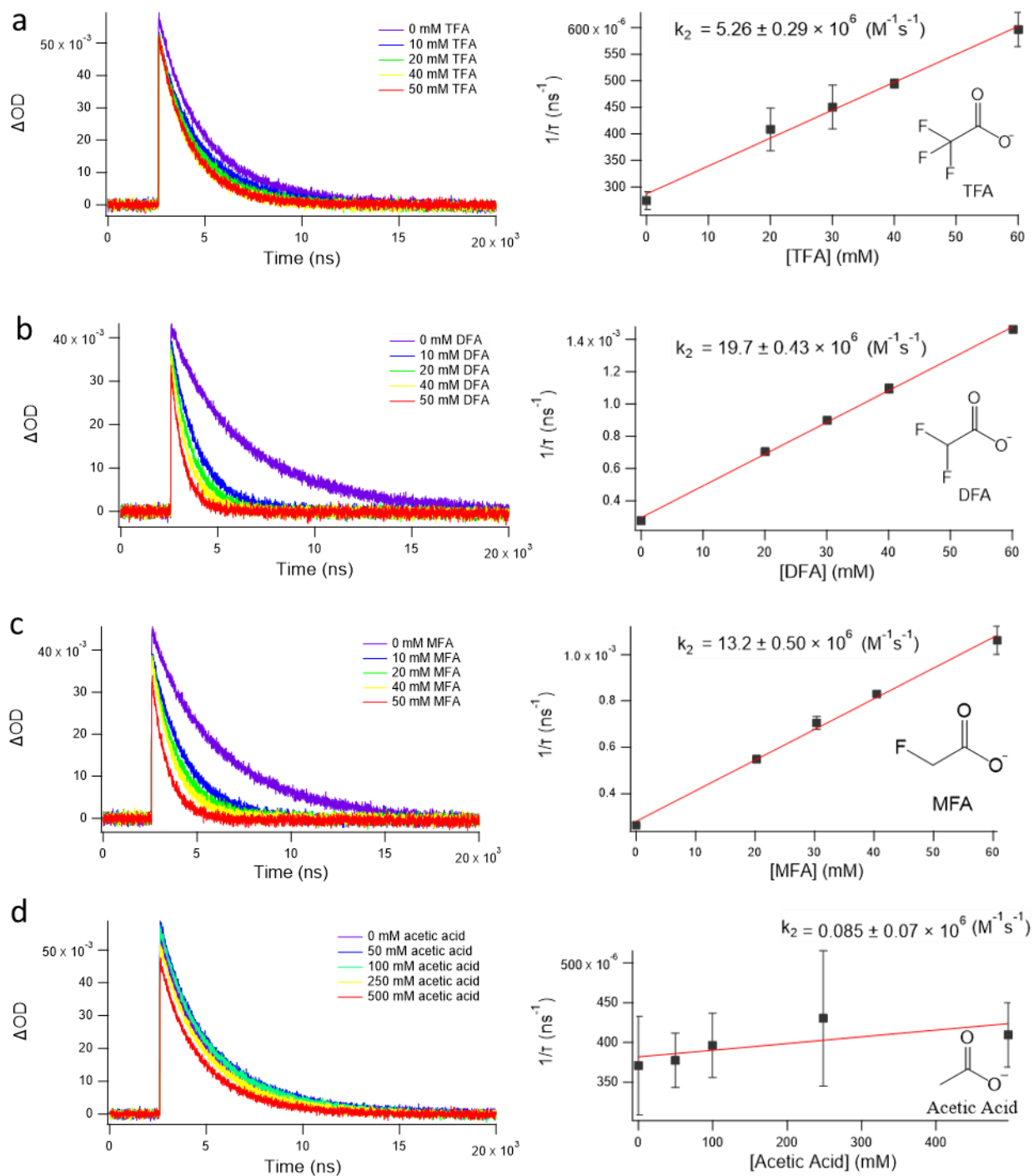


Figure A.10 (Left) Transient absorbance traces depicting the decay of the characteristic 690 nm e_{aq}^- peak after photolyzing $K_4Fe(CN)_6$ with 254 or 266 nm light (specified in Table 2.1). (Right) Corresponding Stern-Volmer plots. Error bars represent one standard deviation, and uncertainties of the k_2 values represent standard errors of the regression-derived slope values using the *linest* function in Excel. Solution conditions the same as Figure 2.1.

Figure A.10 Continued.

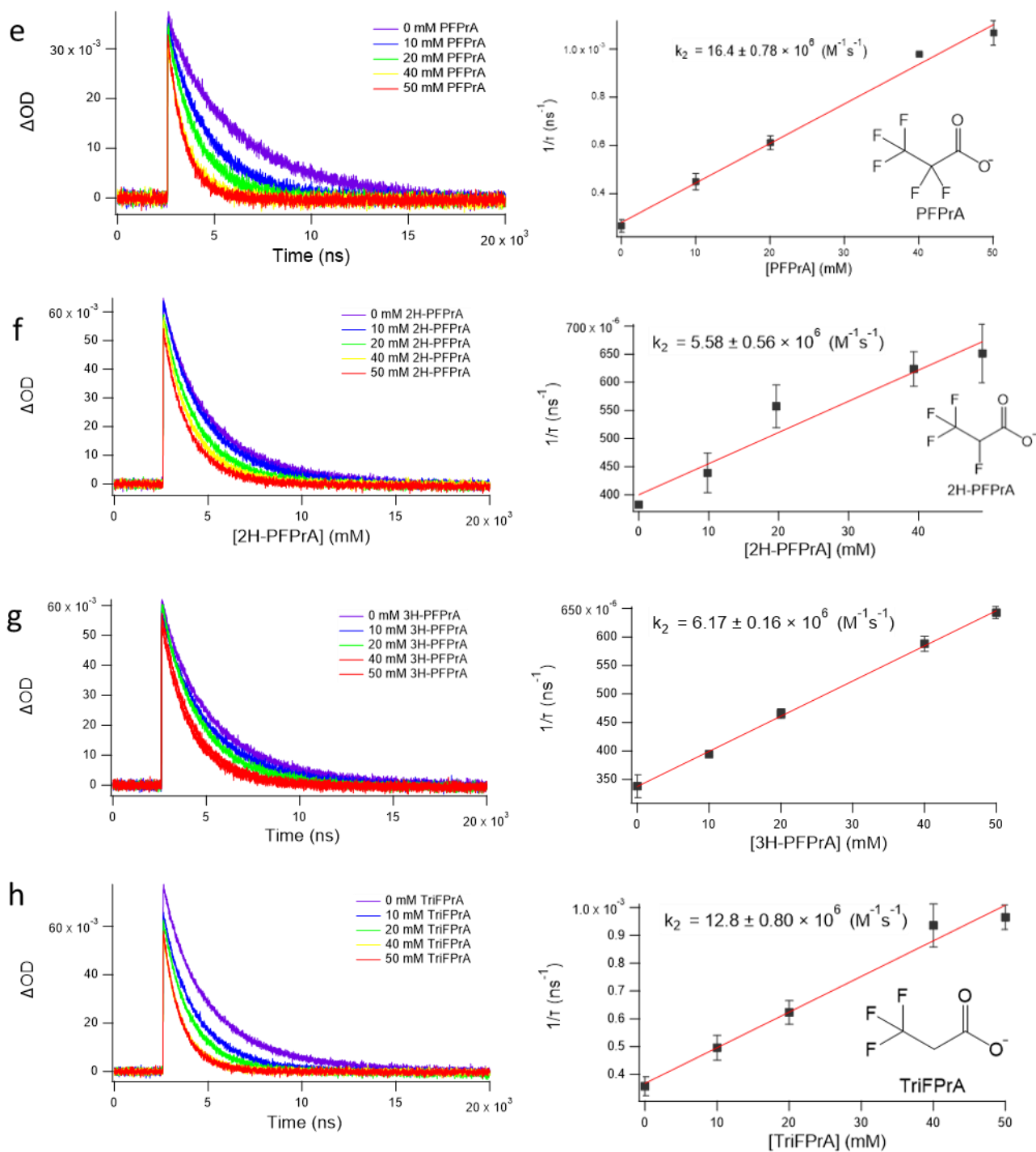


Figure A.10 Continued.

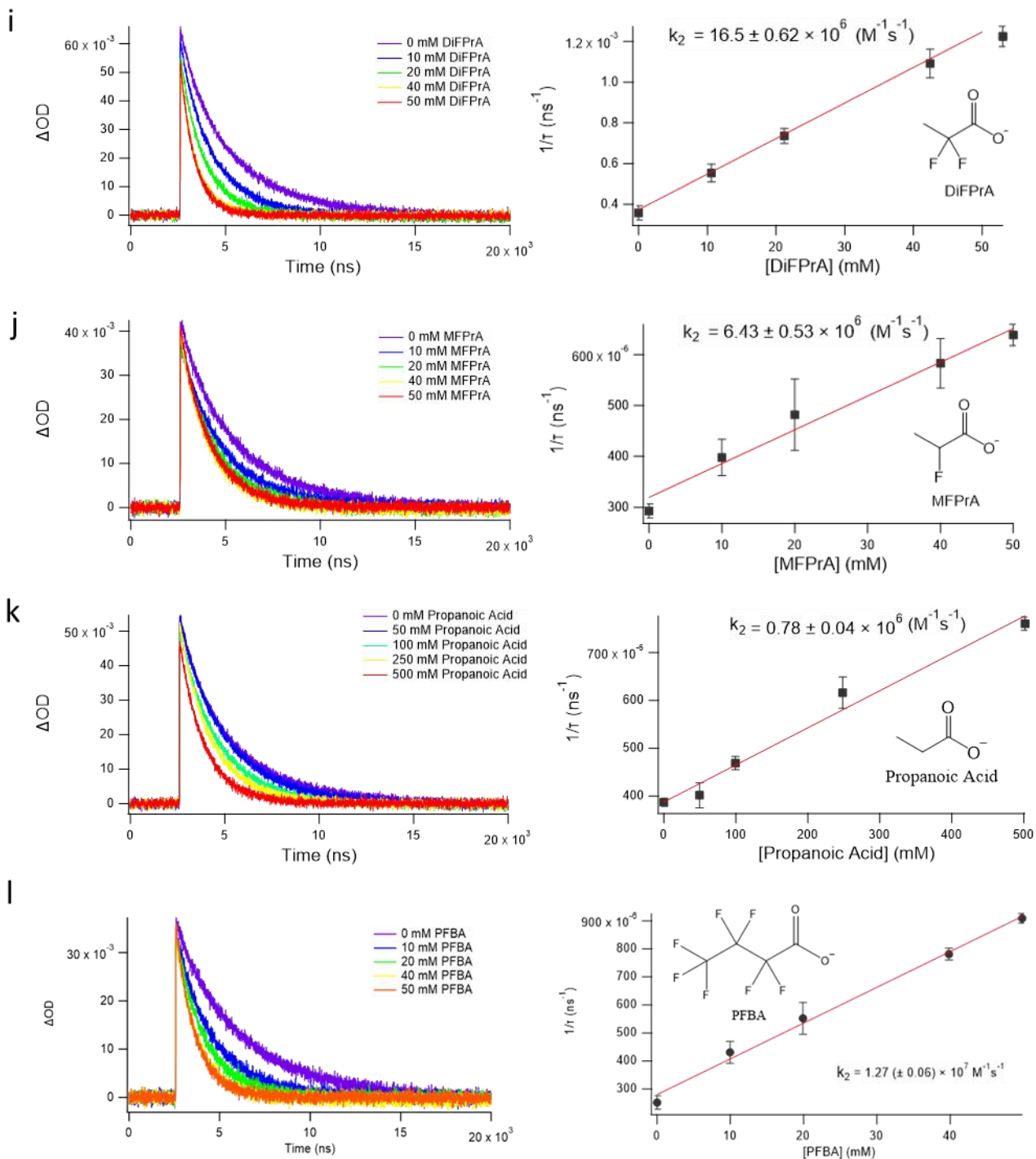
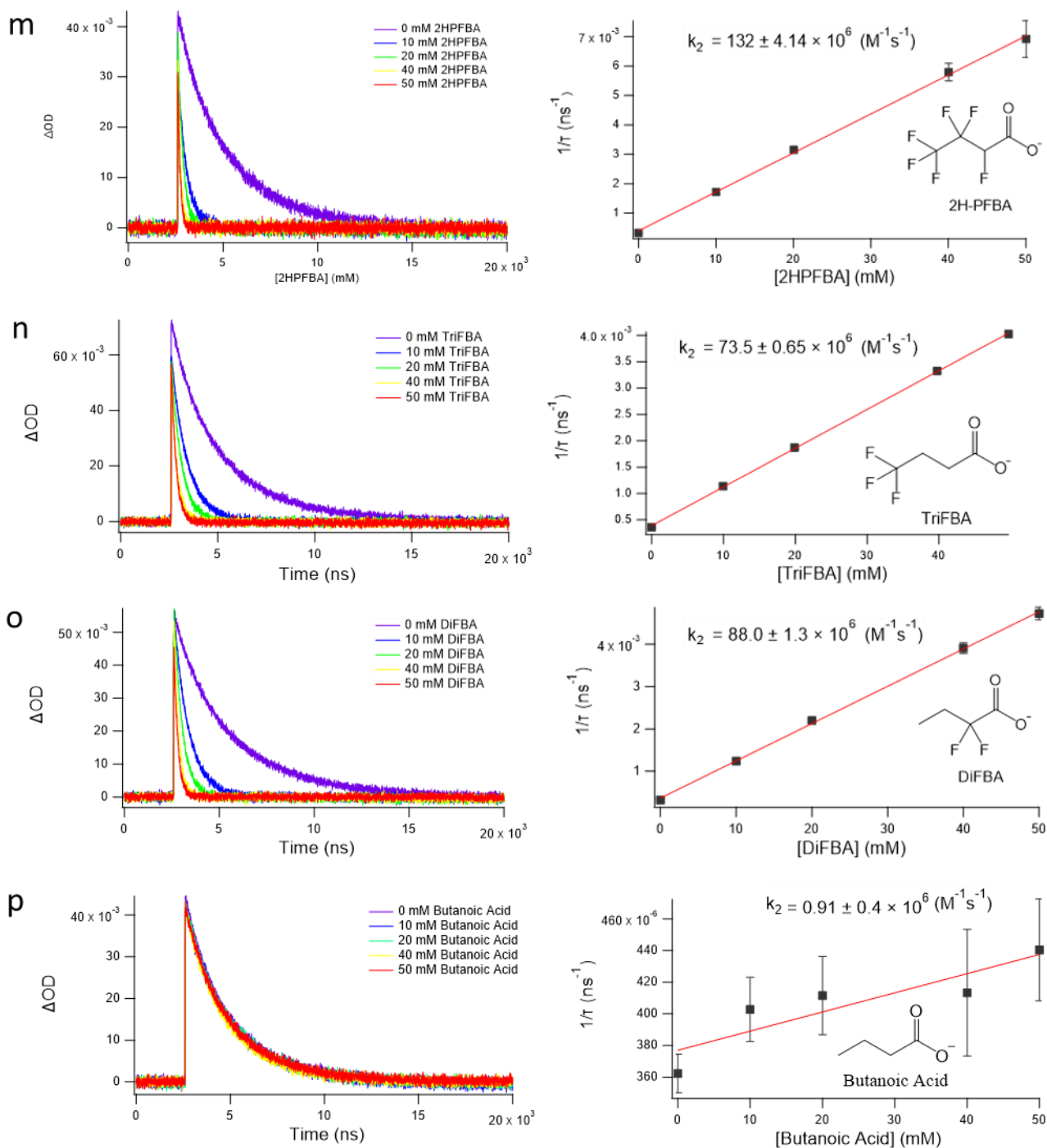


Figure A.10 Continued.



Optimized ω B97-XD/aug-cc-pVDZ geometries in SMD.

Table A.4 Optimized ω B97-XD/aug-cc-pVDZ geometries in SMD.

Trifluoroacetate (TFA) - Charge = -1 Multiplicity = 1

C	0	1.234438	-0.93491	0.222272
C	0	-0.24679	-0.46595	0.082474
O	0	-0.88065	-0.91519	-0.89149
O	0	-0.61467	0.316403	0.984358
F	0	1.435651	-1.57203	1.398435
F	0	1.62863	-1.77643	-0.74985
F	0	2.083883	0.117728	0.198474

Difluoroacetate (DFA) - Charge = -1 Multiplicity = 1

C	0	-0.52891	0.005426	-0.02025
C	0	1.015214	0.020126	0.006813
O	0	1.595948	1.127418	0.024751
O	0	1.528925	-1.12561	-0.00612
F	0	-0.99266	-0.62892	1.115282
F	0	-1.0632	1.267218	0.006056
H	0	-0.93386	-0.52063	-0.89278

Monofluoroacetate (MFA) - Charge = -1 Multiplicity = 1

C	0	-0.52619	0.024879	0.019179
C	0	0.99792	-0.01317	0.008869
O	0	1.52959	0.909914	-0.66922
O	0	1.597179	-0.91456	0.643613
F	0	-1.08484	-1.0149	0.782532
H	0	-0.90714	-0.07734	-1.00478
H	0	-0.87131	0.971909	0.452596

Perfluoropropionate (PFPrA) - Charge = -1 Multiplicity = 1

C	0	1.205033	-0.74987	0.211816
C	0	-0.33842	-0.48718	0.172599
O	0	-0.85006	-0.52215	-0.96411
O	0	-0.86515	-0.25411	1.278502
C	0	2.04887	0.532603	0.034226
F	0	1.783267	1.411424	1.009862
F	0	1.784928	1.115	-1.14228
F	0	3.35936	0.251931	0.073845
F	0	1.583924	-1.30826	1.393455
F	0	1.584257	-1.6082	-0.77442

Table A.4 Continued.

2,3,3,3-tetrafluoropropanoate (2H-PFPrA) - Charge = -1 Multiplicity = 1

C	0	-0.05633	0.467708	0.05026
C	0	-1.44819	-0.19609	-0.09598
O	0	-2.06421	-0.46826	0.956367
O	0	-1.81863	-0.38188	-1.28036
C	0	1.079501	-0.43635	-0.42477
F	0	1.022994	-1.66011	0.141651
F	0	2.280098	0.086597	-0.10239
F	0	0.224642	0.768414	1.377217
H	0	-0.0172	1.397823	-0.52926
F	0	1.065946	-0.60619	-1.75607

2,2,3,3-tetrafluoropropanoate (3H-PFPrA) - Charge = -1 Multiplicity = 1

C	0	0.203281	0.546623	-0.15832
C	0	1.537581	-0.24277	0.002137
O	0	2.254501	-0.36125	-1.0105
O	0	1.720941	-0.68157	1.160303
C	0	-1.02983	-0.31419	0.13477
F	0	-1.06834	-1.33259	-0.77536
F	0	-2.15814	0.431908	-0.04524
F	0	0.184361	1.598112	0.723359
F	0	0.073317	1.083998	-1.40341
H	0	-1.02612	-0.72673	1.148414

3,3,3-trifluoropropanoate (TriFPrA) - Charge = -1 Multiplicity = 1

C	0	0.226878	-0.36047	-0.8538
C	0	1.553048	-0.00847	-0.15147
O	0	2.29129	-0.97205	0.183684
O	0	1.805186	1.212509	0.024769
C	0	-0.97888	-0.03567	-0.01586
H	0	0.181812	-1.43225	-1.07161
H	0	0.135106	0.203774	-1.78951
F	0	-1.17465	1.288457	0.1749
F	0	-0.9164	-0.59124	1.220751
F	0	-2.11958	-0.50464	-0.58244

Table A.4 Continued.

2,2-difluoropropanoate (DiFPrA) - Charge = -1 Multiplicity = 1

C	0	-0.02609	0.450715	0.032736
C	0	-1.4397	-0.16798	-0.14484
O	0	-1.91251	-0.76956	0.84741
O	0	-1.9475	-0.0484	-1.28493
C	0	1.091137	-0.46187	-0.39441
F	0	0.045886	1.639486	-0.67492
F	0	0.157178	0.824016	1.352303
H	0	0.966907	-0.71993	-1.45219
H	0	1.060115	-1.37936	0.205044
H	0	2.053666	0.042044	-0.24611

2-fluoropropanoate (MFPrA) - Charge = -1 Multiplicity = 1

C	0	-0.51873	0.031088	0.050003
C	0	1.013141	0.024002	-0.0342
O	0	1.643463	1.088706	0.182755
O	0	1.518282	-1.09382	-0.3334
C	0	-1.17574	-0.15105	-1.30255
F	0	-0.97282	1.253834	0.60252
H	0	-0.89073	-1.12383	-1.72106
H	0	-0.85828	0.638867	-1.99639
H	0	-2.26739	-0.1234	-1.19842
H	0	-0.83548	-0.74899	0.754314

Perfluorobutanoate (PFBA) - Charge = -1 Multiplicity = 1

C	0	1.208096054	-0.781809703	0.196053419
F	0	1.517274933	-1.35556174	1.391878265
F	0	1.590582932	-1.656099098	-0.773648585
C	0	-0.3286993	-0.476047966	0.11737567
O	0	-0.880643606	-0.746938315	-0.965607384
O	0	-0.80821861	0.017299202	1.15848437
C	0	2.072904029	0.498828401	0.048079972
F	0	1.614303295	1.217868162	-1.004596443
F	0	1.94482022	1.250485138	1.162505324
C	0	3.593958346	0.27380965	-0.185375298
F	0	3.824018655	-0.245596332	-1.392681737
F	0	4.23038546	1.448515177	-0.108490102
F	0	4.103916593	-0.542946576	0.74099653

Table A.4 Continued.

2H-perfluorobutanoate (2H-PFBA) - Charge = -1 Multiplicity = 1

C	0	-0.84234	-0.47549	0.210621
F	0	-0.59213	-0.68351	1.563073
C	0	-2.23203	0.174022	-0.01269
O	0	-2.60264	0.211498	-1.21022
O	0	-2.8425	0.582178	0.99809
C	0	0.286784	0.41215	-0.32106
F	0	0.254118	0.440662	-1.67669
F	0	0.147693	1.694075	0.118715
C	0	1.720951	-0.03859	0.076291
F	0	1.8921	-1.34107	-0.18611
F	0	2.625623	0.651501	-0.63153
F	0	1.965253	0.171985	1.371803
H	0	-0.79732	-1.44543	-0.29756

4,4,4-trifluorobutanoate (TriFBA) - Charge = -1 Multiplicity = 1

C	0	-2.29251	0.028336	-0.02491
C	0	-0.88024	-0.54787	0.097631
H	0	-0.48773	-0.33903	1.099356
H	0	-0.91773	-1.63288	-0.05583
C	0	0.023663	0.094019	-0.95867
H	0	-0.352	-0.10426	-1.97008
H	0	0.082455	1.180739	-0.81858
C	0	1.433531	-0.42433	-0.91275
O	0	-3.07791	-0.51978	-0.85048
O	0	-2.58045	1.031662	0.688286
F	0	2.217913	0.15904	-1.85259
F	0	1.51417	-1.76032	-1.13088
F	0	2.042212	-0.20115	0.278124

2,2-difluorobutanoate (DiFBA) - Charge = -1 Multiplicity = 1

C	0	-1.25807	0.035195	0.036068
C	0	0.16275	-0.56529	0.211972
C	0	1.264904	0.388302	-0.1942
H	0	1.07358	0.67041	-1.23814
H	0	1.143395	1.29362	0.414889
C	0	2.667955	-0.18745	-0.03549
H	0	2.809669	-1.07673	-0.66243
H	0	3.407066	0.563093	-0.34174
H	0	2.874094	-0.45967	1.007365
O	0	-1.81701	-0.17167	-1.06664
O	0	-1.69018	0.712012	0.999479
F	0	0.261153	-1.74118	-0.51052
F	0	0.333858	-0.95751	1.529062

APPENDIX B
SUPPLEMENTARY INFORMATION FOR CHAPTER 3

B.1 Methods

Reagents.

Constant irradiation and LFP experiments. All chemicals were used as received without further purification. Potassium ferricyanide (100.2%), sodium chloride (100.5%), sodium hydroxide (97.5%), and sodium bicarbonate (99.7%-100.3%) were purchased from Fisher Chemical. Sodium borate, tetra (99.5–101.5%) was purchased from Baker & Adamson. Potassium ferrocyanide (101.3%) was purchased from J.T. Baker. Hydrochloric acid (36.5%-38% was purchased from Macron Fine Chemicals. Sodium sulfite ($\geq 98\%$), and perfluorooctane sulfonate (98%) were purchased from Sigma-Aldrich.

Deoxygenated water was used to prepare all solutions inside an anaerobic glovebox (Coy Labs) to eliminate scavenging of e_{aq}^- by dissolved oxygen, unless otherwise noted. Briefly, this was prepared by boiling nanopure water for 3 h while stirring and sparging with $N_{2(g)}$. After sparging, the deoxygenated water was transferred into the glovebox and allowed to equilibrate with the atmosphere (97% $N_{2(g)}$, 3% $H_{2(g)}$) overnight while stirring.

LC-QqQ-MS analysis. Optima® HPLC-grade ammonium hydroxide solution (AmOH), Optima® HPLC-grade ammonium acetate (AmAc). Optima® HPLC-grade water, and Optima® HPLC-grade methanol were purchased from Fischer Scientific.

Method for constant UV-sulfite irradiation experiments and analysis.

Photoreactions. Stock solutions for constant irradiation experiments are summarized in Table B.1. Final reaction volume was 575 ml for all constant irradiation experiments, and pH was adjusted to pH 10 using 1 M NaOH and buffered using 5 mM borate. Sodium tetraborate was used as a buffer because it is not an e_{aq}^- quencher.⁹² Borate and carbonate solutions (570 ml total in nanopure water) were added to the reactors and deoxygenated by sparging $N_{2(g)}$ into the systems while stirring for 1 h prior to the reaction. In addition, UV lamps were warmed up for 15 min prior to initiating photoreactions. Solutions of sulfite and PFOS were prepared in vials within the glovebox (~5 ml total), then removed from the chamber and immediately spiked into the photoreactor using stainless-steel syringes to initiate the photoreaction. 5 ml aliquots were then collected from the reactors at predetermined timepoints using the stainless-steel syringes and were stored at 4 °C until analysis. Syringes were rinsed with 25 ml nanopure water in between samples. Solution pH was re-measured after the reaction was completed to evaluate any pH drift during experiments.

LC-QqQ-MS sample preparation and analysis. Reaction samples were diluted to fall within the range of the calibration curve (0.1 – 7.5 ug/L) PFOS using 80:20 MeOH:H₂O and diluted AmOH. Double

blanks (80:20 MeOH and diluted AmOH) were injected throughout the analysis to verify no contamination. Calibration standards were matrix-matched to the diluted reaction samples to ensure background levels were consistent between the standards and samples (67 μM sulfite and 33 μM borate after dilution). Lab blanks were injected at the beginning of analysis to ensure matrix components did not contain target compound (PFOS). 100 μL of each sample and calibration standard was injected using a CTC PAL autosampler onto an Agilent 1200 Series LC high-pressure liquid chromatography (HPLC) system set up with a guard column (SecurityGuard, Phenomenex), two guard cartridges (ZORBAX Diol, Agilent, 6 μm , 4.6 \times 12.5 mm), and a Gemini C18 analytical column (3 mm \times 100 mm, 5 μm ; Phenomenex). Column oven temperature was fixed at 40 $^{\circ}\text{C}$. The mobile phases consisted of 20 mM AmAc (mobile phase A) and methanol (mobile phase B). A gradient method was used, as described in Table B.2.

LFP solution preparation. All stock solutions (Table B.1) and reaction samples were prepared in the glovebox using deoxygenated water (prepared as described above). Unless otherwise noted, reaction samples were first prepared in 5 \times 50 ml centrifuge tubes with an increasing amount of bicarbonate quencher along with 40 μM $\text{K}_4\text{Fe}(\text{CN})_6$, 10 μM $\text{K}_3\text{Fe}(\text{CN})_6$, and NaCl as an electrolyte to balance ionic strength at ~ 0.5 M. 1 M NaOH and 1 M HCl were used to adjust pH to the desired condition. Final volume of each reaction sample was 20 ml, and 3 \times 2.75 ml aliquots of the solutions were transferred to 15 separate cuvettes for triplicate measurement. Cuvettes were then covered with parafilm and immediately run in LFP experiments after removing from the glovebox. Additions of bicarbonate quencher were 0-0.5 M for pH conditions 12.0 to 7.3, 0.0-0.05 M for pH 6.8 to 6.3, and finally 0-0.01 M for pH 5.8. Various amounts of carbonate were added based on pH condition because at the highly alkaline conditions, the quenching reaction was slow and required high quencher concentrations to observe e_{aq}^- lifetime changes, while the opposite is true at moderate and low pH values. To ensure pH was constant during reactions, pH was measured after flash photolysis by pooling solutions from the three replicate cuvettes for a total volume of 8.5 ml.

CO_2 saturated solution was prepared from the deoxygenated water in the glovebox by bubbling $\text{CO}_{2(\text{g})}$ at 1 atm for 14 h into a 250 ml sidearm flask affixed with a holed stopper to ensure that CO_2 did not saturate the glovebox atmosphere. Gas was allowed to exit the flask through a tube secured to the sidearm that led outside the glovebox. This solution was used to measure the bimolecular rate constant of H_2CO_3^* (which consists of mostly $\text{CO}_{2(\text{aq})}$ and some H_2CO_3) in acidic conditions. For this experiment, to ensure $\text{CO}_{2(\text{aq})}$ did not partition into the gas phase, samples were made directly in the quartz cuvettes at a total volume of 3.5 ml to minimize headspace. Addition of $\text{CO}_{2(\text{aq})}$ quencher for this experiment was 0-1.36 mM, while other conditions were identical to those above (40 μM $\text{K}_4\text{Fe}(\text{CN})_6$, 10 μM $\text{K}_3\text{Fe}(\text{CN})_6$,

and NaCl for ionic strength balance at 0.5 M). pH was measured after flash photolysis by pooling solutions from the three replicate cuvettes for a total volume of 10.5 ml.

Table B.1 Chemical concentrations of stock solutions used in constant irradiation (C.I.) and laser flash photolysis (LFP) experiments.

Stock solution	Component	Experiment type	Deoxygenated?	Concentration
Borate buffer	Na ₂ B ₄ O ₇ • 10 H ₂ O	C.I.	No	0.05 M
Sodium sulfite	Na ₂ SO ₃	C.I.	Yes	1.64 M
NaOH	NaOH	C.I.	No	1 M
HCl	HCl	C.I.	No	1 M
PFOS	PFOS	C.I.	Yes	172.5 mg/L
Sodium bicarbonate	NaHCO ₃	C.I.	No	0.96 M
Salt offset	NaCl	LFP	Yes	1 M
Potassium ferricyanide	K ₃ Fe(CN) ₆	LFP	Yes	5 mM
Potassium ferrocyanide	K ₄ Fe(CN) ₆ •3H ₂ O	LFP	Yes	10 mM
NaOH	NaOH	LFP	Yes	1 M
HCl	HCl	LFP	Yes	1 M
Sodium bicarbonate	NaHCO ₃	LFP	Yes	0.5 M
CO _{2(aq)} saturated solution	CO _{2(aq)}	LFP	Yes	31.8 mM ^a

^aSolution was saturated with CO₂ at room temperature giving a CO₂ concentration of 0.0318 (Henry's law constant K_H = 0.034 mol/kgBar).¹²⁹

Table B.2 Gradient pump method used for PFOS analysis on LC-QqQ-MS.

Total time (min)	Flow rate (µl/min)	A (%)	B (%)
0	600	90	10
0.5	600	90	10
1	600	50	50
8.5	600	1	99
10	600	1	99

B.2 Additional Data

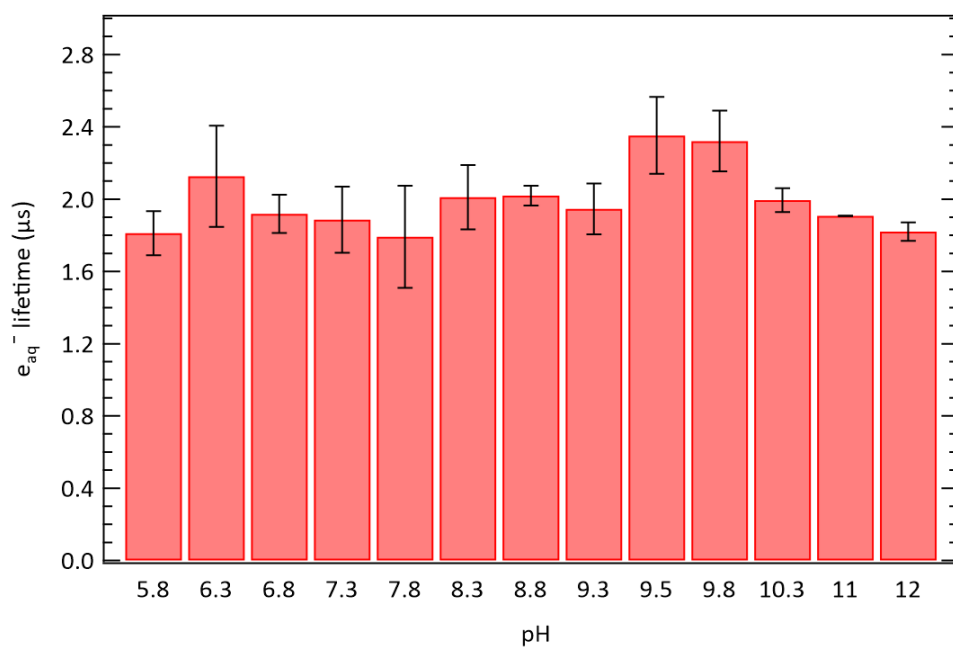


Figure B.1 Hydrated electron lifetimes measured at various pH conditions in the absence of added carbonate. Reaction conditions are listed in Table 3.1.

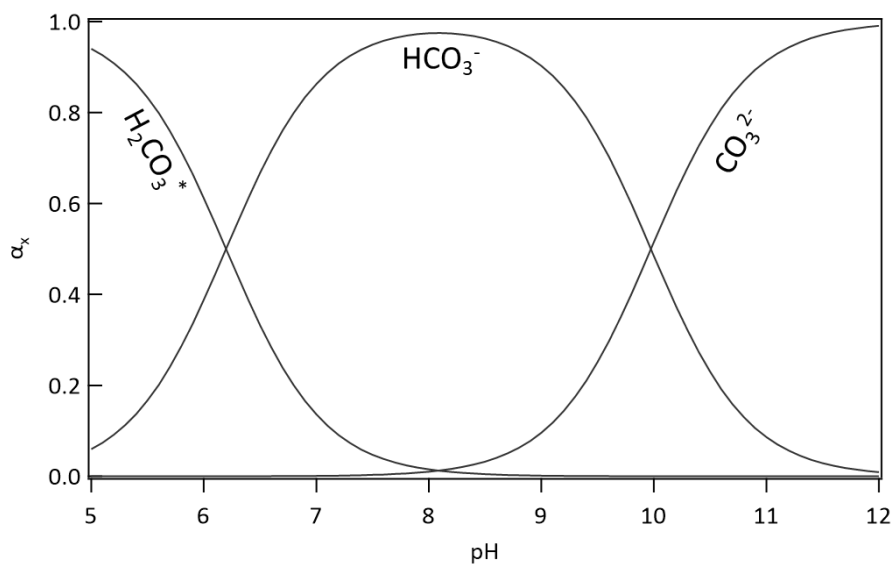


Figure B.2 Speciation diagram of dissolved carbonate at I.S. = 0.5 M and 20 °C calculated using Visual MINTEQ.

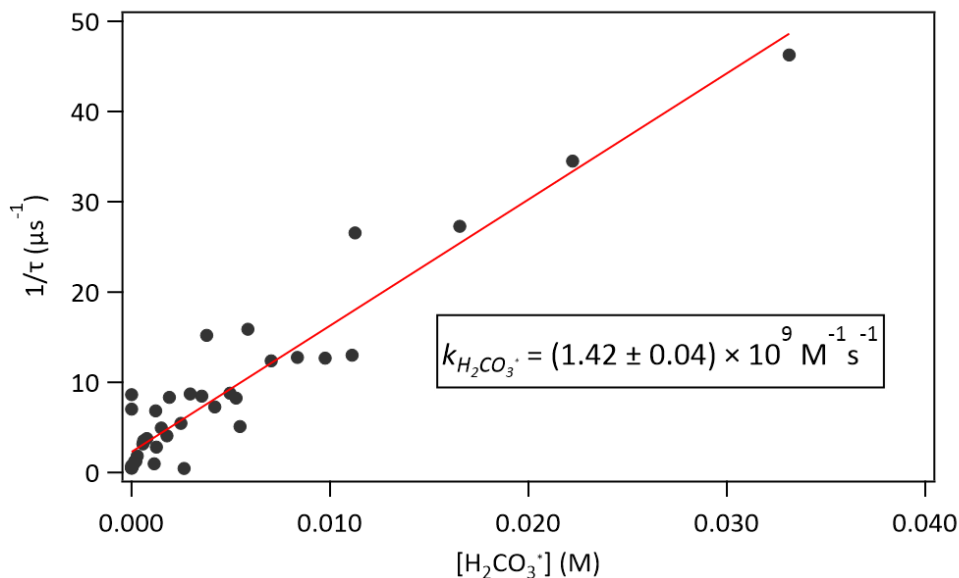


Figure B.3 Stern-Volmer plot for all LFP measurements at pH conditions < 9 where e_{aq}^- lifetimes are plotted as a function of H_2CO_3^* . Species concentrations were calculated using Visual MINTEQ.

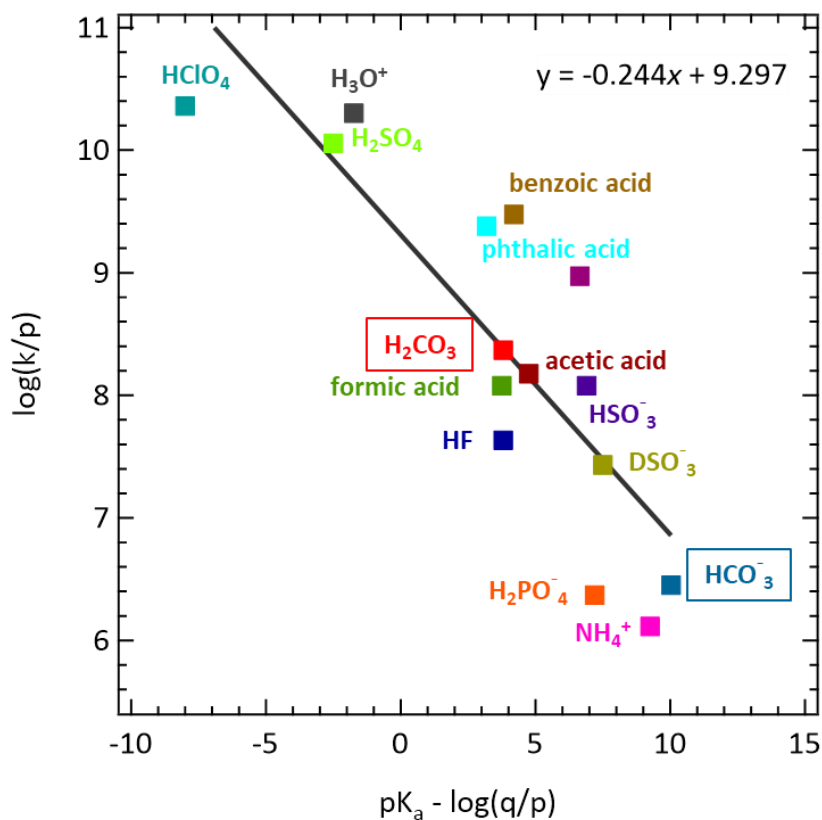


Figure B.4 Bronsted law for the conversion of e_{aq}^- to H^\bullet by HCO_3^- (from this study), as well as values for other protonated acids. Solid black line represents the line of best fit determined from linear regression used to predict $k_{\text{H}_2\text{CO}_3}$ ($\text{p}K_a = 3.5$, red symbol). Refs^{68,135,163,164}.

B.3 LFP Transient Traces and Stern-Volmer Plots

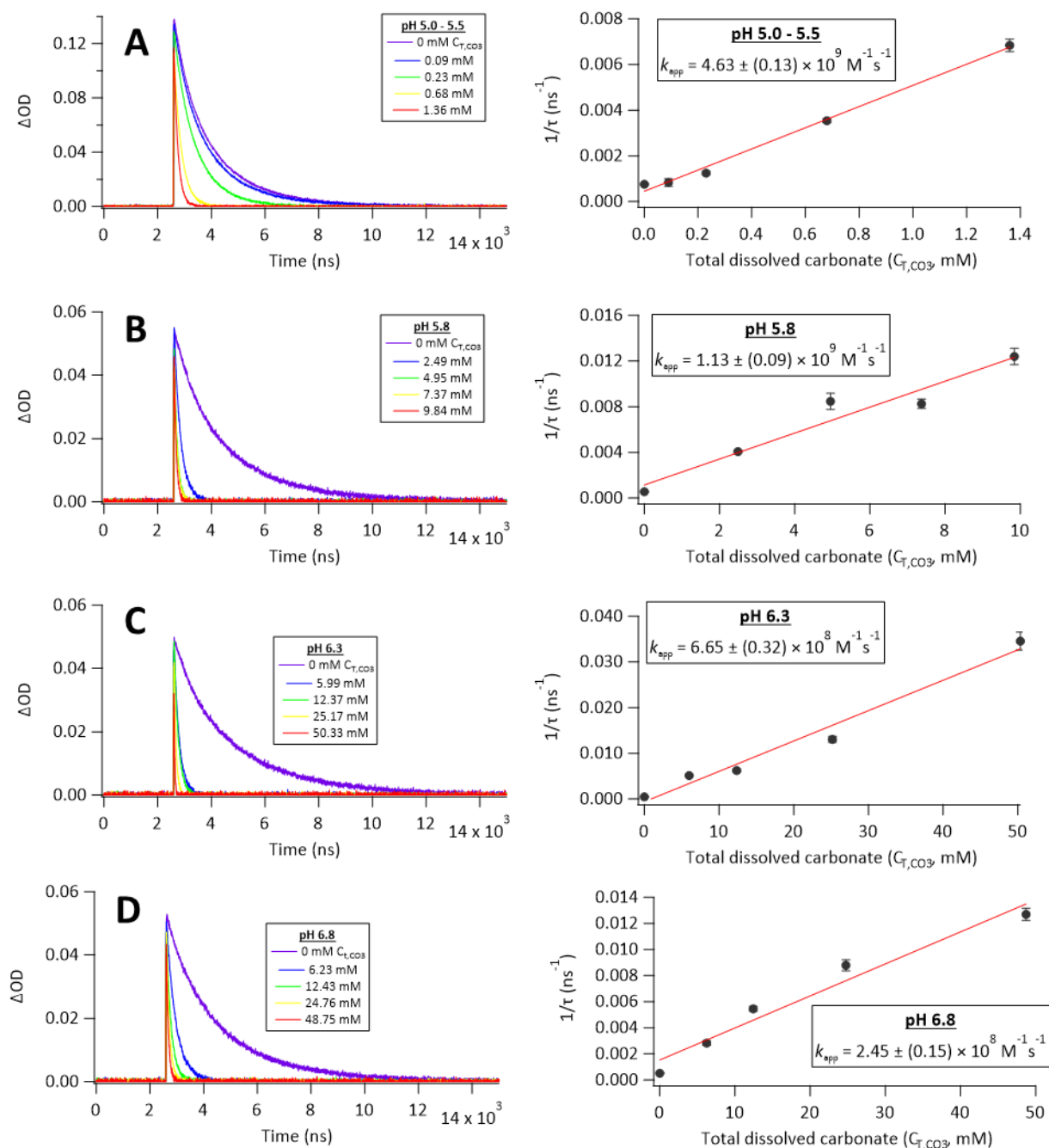


Figure B.5 (Left) Transient absorbance traces depicting the decay of the characteristic 690 nm e_{aq}^- peak after photolyzing $K_4Fe(CN)_6$ with 266 nm light. (Right) Corresponding Stern-Volmer plots. Error bars represent one standard deviation. Uncertainties of the k_{app} values represent standard errors of the regression-derived slope values using the *linest* function in Excel. Solution conditions are outlined in Table 3.1.

Figure B.5 Continued.

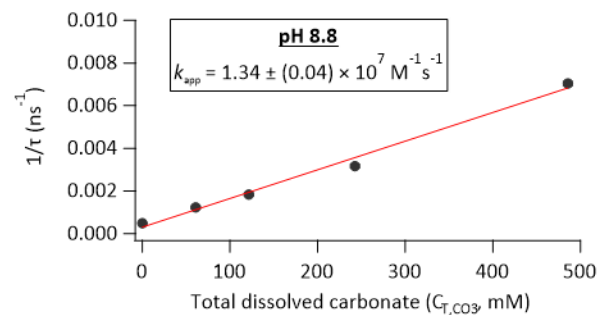
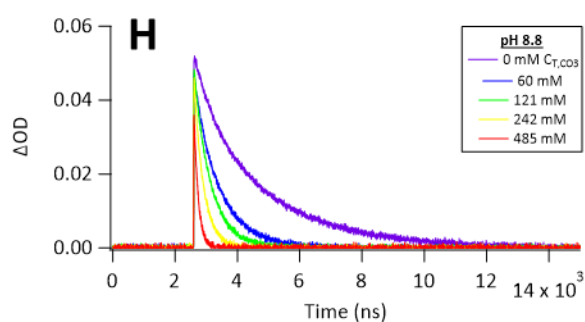
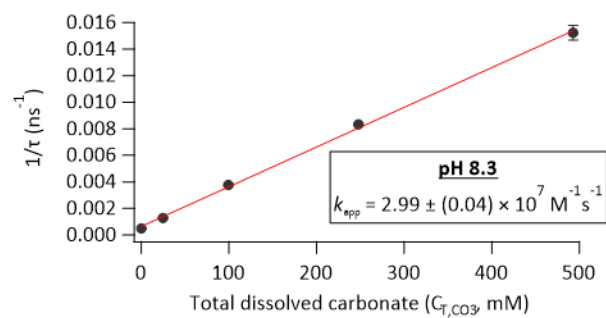
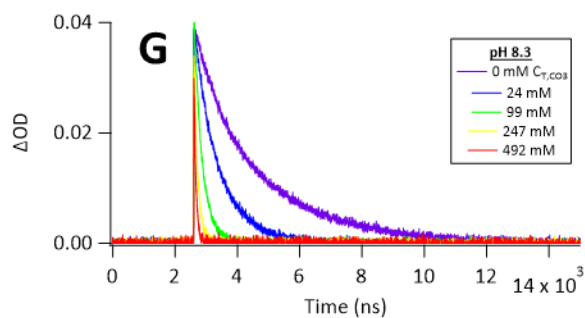
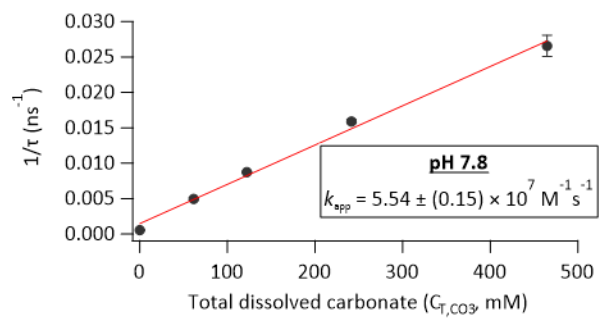
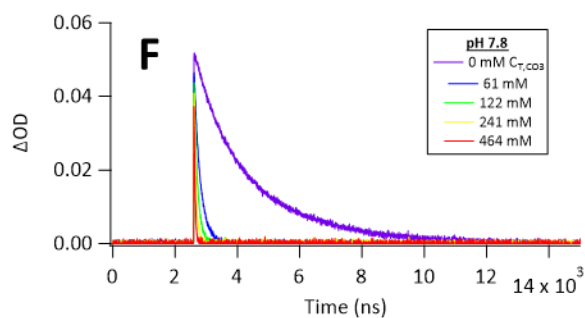
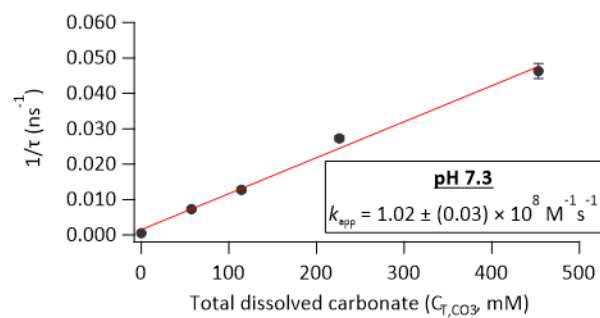
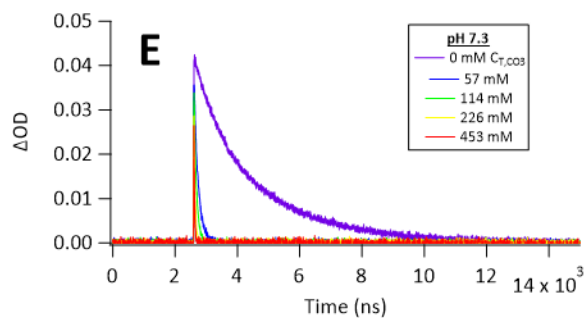


Figure B.5 Continued.

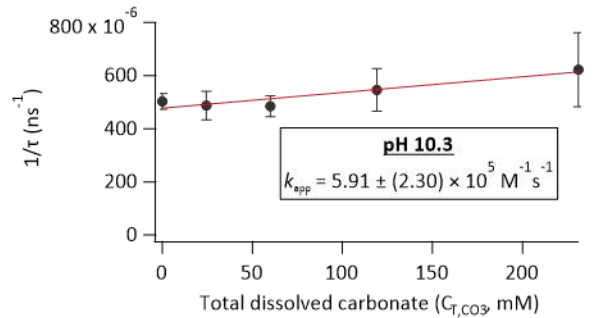
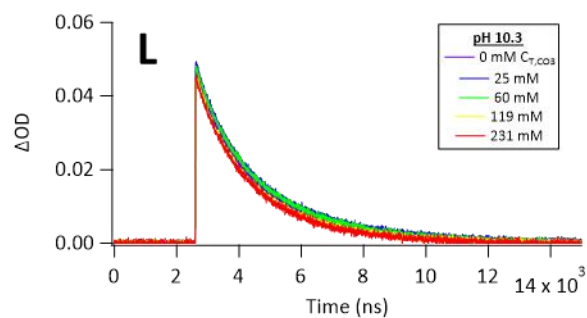
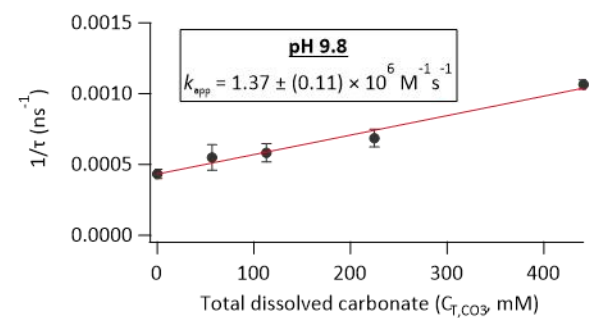
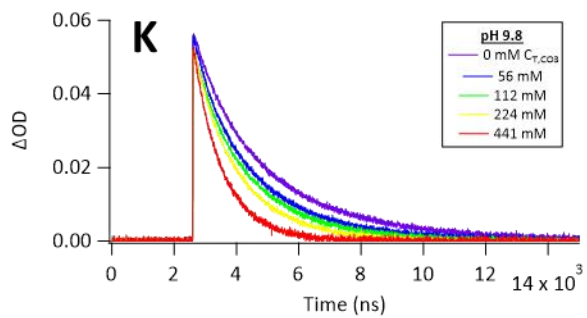
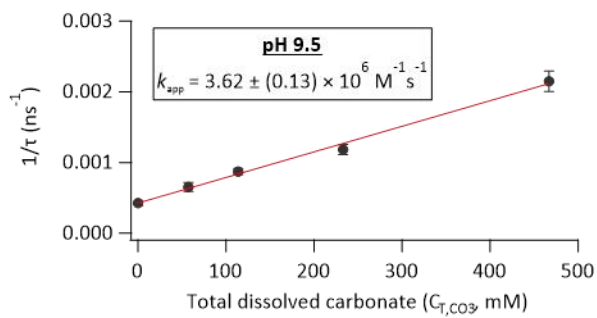
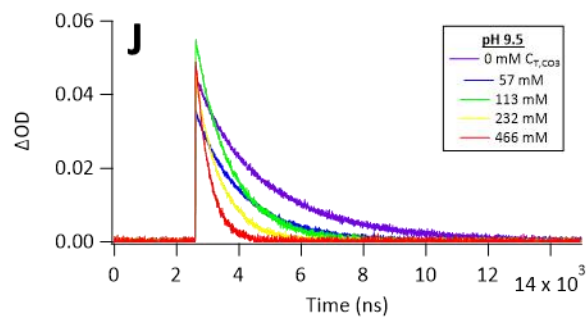
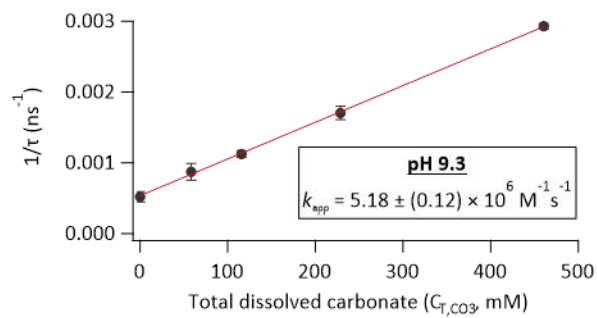
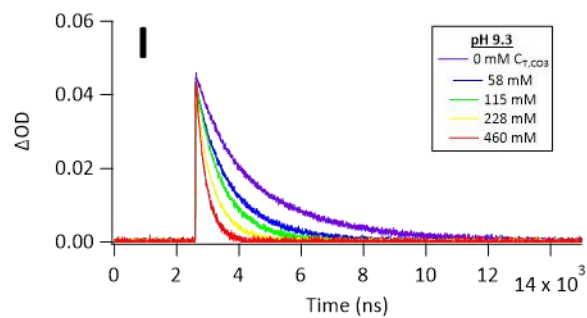
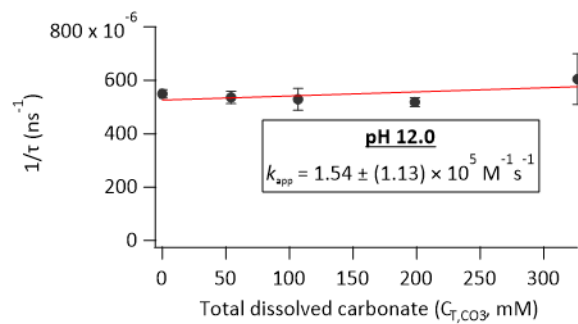
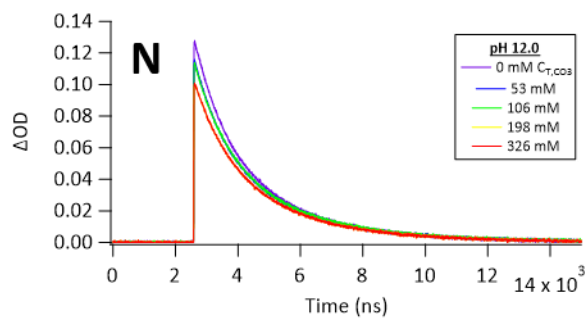
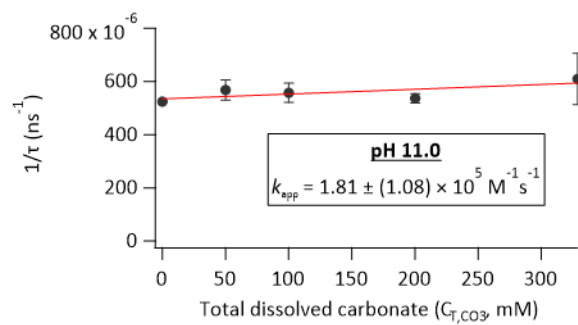
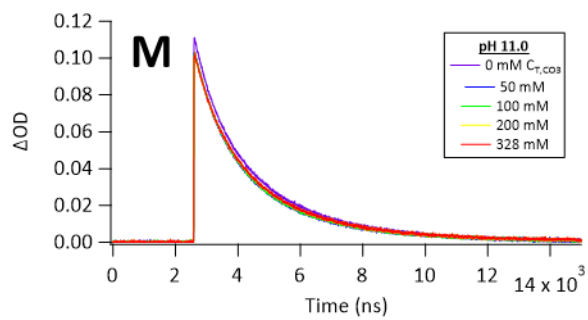


Figure B.5 Continued.



APPENDIX C
SUPPLEMENTARY INFORMATION FOR CHAPTER 4

C.1 Methods

Reagents.

UV photoreactions and LFP experiments. All chemicals were used as received without further purification. Potassium ferricyanide (100.2%), sodium chloride (100.5%), sodium hydroxide (97.5%), and sodium bicarbonate (99.7%-100.3%) were purchased from Fisher Chemical. Sodium borate, tetra (99.5–101.5%) was purchased from Baker & Adamson. Potassium ferrocyanide (101.3%) was purchased from J.T. Baker. Hydrochloric acid (36.5%-38% was purchased from Macron Fine Chemicals. Sodium sulfite ($\geq 98\%$), and perfluorooctane sulfonate (98%) were purchased from Sigma-Aldrich. Sodium heptafluorobutyrate (98%), sodium pentafluoropropionate (98%), and sodium trifluoroacetate (97%) were purchased from Oakwood Chemical.

Deoxygenated water was used to prepare solutions inside an anaerobic glovebox (Coy Labs) to eliminate scavenging of e_{aq}^- by dissolved oxygen. Briefly, this was prepared by boiling nanopure water for 3 h while stirring and sparging with $N_2(g)$. After sparging, the deoxygenated water was transferred into the glovebox and allowed to equilibrate with the atmosphere (97% $N_2(g)$, 3% $H_2(g)$) overnight while stirring.

LC-QqQ-MS analysis. Optima® HPLC-grade ammonium hydroxide solution (AmOH), Optima® HPLCgrade ammonium acetate (AmAc). Optima® HPLC-grade water, and Optima® HPLC-grade methanol were purchased from Fischer Scientific.

UV photoreactions and analysis.

Photoreactions. Stock solutions for constant irradiation experiments are summarized in Table C.1. Final reaction volume was 575 ml for all constant irradiation experiments, and pH was adjusted using 1 M NaOH or 1 M HCl and buffered using 5 mM borate or carbonate. Sodium tetraborate was used as a buffer because it is not a e_{aq}^- quencher.⁹² Sodium carbonate was used to simulate natural waters and emulate typical UV-sulfite reaction conditions.^{85,95} Borate and carbonate solutions (570 ml total in nanopure water) were added to the reactors and deoxygenated by sparging $N_{2(g)}$ into the systems while stirring for 1 h prior to the reaction. In addition, UV lamps were warmed up for 15 min prior to initiating photoreactions. Solutions of sulfite and PFAS were prepared in vials within the glovebox (~5 ml total), then removed from the chamber and immediately spiked into the photoreactor using stainless-steel syringes to initiate the photoreaction. 5 ml aliquots were then collected from the reactors at predetermined timepoints using the stainless-steel syringes and were stored at 4 °C until analysis. Syringes were rinsed

with 25 ml nanopure water in between samples. Solution pH was re-measured after the reaction was completed to evaluate any pH drift during experiments.

LC-QqQ-MS sample preparation and analysis. Reaction samples were diluted to fall within the range of the calibration curve (0.1 – 15 ug/L) PFAS using 80:20 MeOH:H₂O and diluted AmOH. Double blanks (80:20 MeOH and diluted AmOH) were injected throughout the analysis to verify no contamination. Calibration standards were matrix-matched to the diluted reaction samples to ensure background levels were consistent between the standards and samples (~67 μM sulfite and ~33 μM carbonate/borate after dilution). Lab blanks were injected at the beginning of analysis to ensure matrix components did not contain target compound (PFAS). 1 ml of each sample and calibration standard was injected using a CTC PAL autosampler onto an Agilent 1200 Series LC high-pressure liquid chromatography (HPLC) system set up with a guard column (SecurityGuard, Phenomenex), two guard cartridges (ZORBAX Diol, Agilent, 6 μm, 4.6 × 12.5 mm), and an RSpak JJ-50 2D (2.0mm i.d. × 150mm length, 5m; Shodex, Showa Denko). Column oven temperature was fixed at 40 °C. The mobile phases consisted of 50 mM AmAc adjusted to pH 9.0 (mobile phase A) and acetonitrile (mobile phase B). A simple gradient method was used, as described in Table C.2.

LFP solution preparation.

All stock solutions (Table C.1) and reaction samples were prepared in the glovebox using deoxygenated water (prepared as described above). Unless otherwise noted, reaction samples were first prepared in 5 × 50 ml centrifuge tubes with an increasing amount of the target PFAS along with 40 μM K₄Fe(CN)₆, 10 μM K₃Fe(CN)₆, 40 mM borate buffer, and NaCl as an electrolyte to balance ionic strength. Final volume of each reaction sample was 25 ml, and 3 × 2.75 ml aliquots of the solutions were transferred to 15 separate cuvettes for triplicate measurement. Cuvettes were then covered with parafilm and immediately run in LFP experiments after removing from the glovebox. Various amounts of the target PFAS were added (as specified in their Stern-Volmer plots, *vide infra*) based on their critical micelle concentrations. To ensure pH was constant during reactions, pH was measured after flash photolysis by pooling solutions from the three replicate cuvettes for a total volume of 8.5 ml.

Table C.1 Chemical concentrations of stock solutions used in constant irradiation (C.I.) and laser flash photolysis (LFP) experiments.

Stock solution	Component	Experiment type	Deoxygenated?	Concentration
Borate buffer	Na ₂ B ₄ O ₇ • 10 H ₂ O	C.I.	No	0.05 M
Sodium sulfite	Na ₂ SO ₃	C.I.	Yes	1.64 M
NaOH	NaOH	C.I.	No	1 M
HCl	HCl	C.I.	No	1 M
Various PFAS	Multiple	C.I.	Yes	100,000 µg/L
Sodium bicarbonate	NaHCO ₃	C.I.	No	0.575 M
Salt offset	NaCl	LFP	Yes	0.05 M
Potassium ferricyanide	K ₃ Fe(CN) ₆	LFP	Yes	8 mM
Potassium ferrocyanide	K ₄ Fe(CN) ₆ •3H ₂ O	LFP	Yes	10 mM
Various PFAS	Multiple	LFP	Yes	Variable

Table C.2 Gradient pump method used for PFOS analysis on LC-QqQ-MS.

Total time (min)	Flow rate (µl/min)	A (%)	B (%)
0	250	100	0
30	250	0	100

Ionic strength corrections for k₂ values.

Because many of the reactions investigated in this work involve two anionic species (e.g., e_{aq}^- with CF₃COO⁻, HCO₃⁻, etc.) ionic strength (μ) will influence their kinetics. Therefore, rate constants were adjusted in the following manner. Huang et al. previously reported bimolecular rate constants of TFA, PFBA, and PFOA at various ionic strength conditions (reproduced in Figure C.1 as solid squares or circles).⁵⁰ Our previous work reported rate constants for TFA and PFBA which follow the ionic strength trend well (shown as a hollow square or circle in Figure C.1).¹²² By fitting this data to a line, $\log k_2$ value can be estimated at different ionic strength conditions. The experimentally measured k_2 values used in this study are tabulated in Table C.3 along with estimated values of structures whose rate constants are difficult to determine due to insolubility or poor reactivity (e.g., PFBS), discussed in the main text. Using the correction factors for TFA and PFBA, other anions were extrapolated to the appropriate ionic strength value based on experimental conditions of the UV photolysis reaction (typically 0.045 M). While sulfite and carbonate species might not adhere to the same ionic strength factors as PFAS, the main quenchers (H₂CO₃^{*} and CO_{2(aq)}) are neutral species whose reactions are not affected by μ . In addition, the correction for HSO₃⁻, the next most important quencher, results in a miniscule change in k_2 .

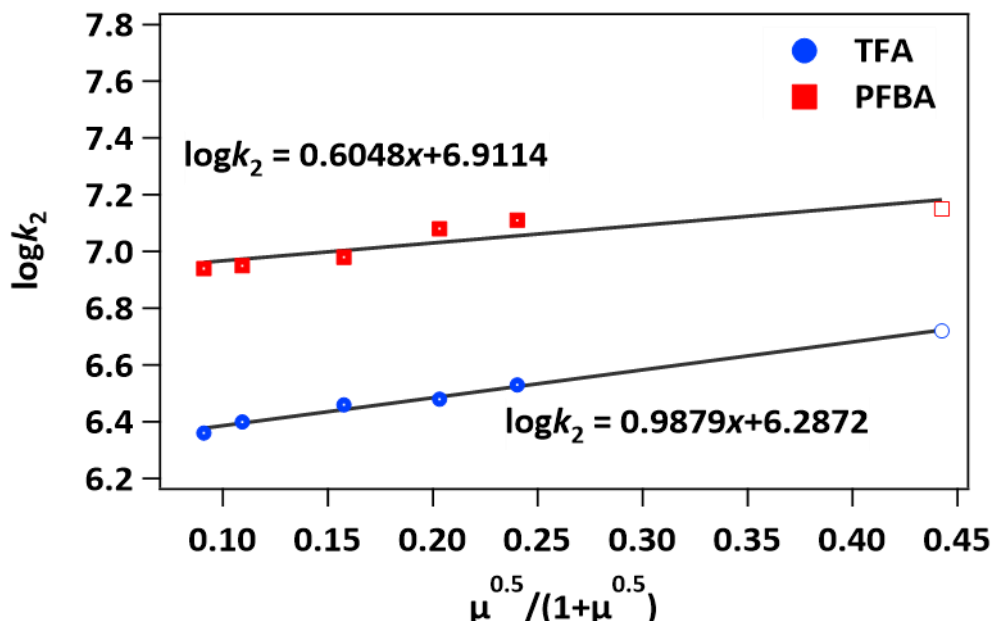


Figure C.1 k_2 dependence on μ for TFA and PFBA obtained from Huang et al. (solid markers) and this study (hollow markers) used for ionic strength corrections.

Table C.3 Comparison of measured, estimated, and corrected rate constants for reactions of e_{aq}^- with target contaminants and other quenchers at specified ionic strengths.

Substrate	k_2 ($M^{-1} s^{-1}$)			
	Measured $\mu = 0.5$ M	Measured $\mu = 0.63^b$	Estimated N/A	Corrected $\mu = 0.045^c$
HSO_3^-	1.20×10^{8c}			1.26×10^8
$H_2CO_3^*$	2.23×10^{9a}			N/A ^f
HCO_3^-	2.18×10^{6a}			1.41×10^6
CO_3^{2-}	1.05×10^{5a}			6.81×10^4
TFA		5.26×10^6		3.40×10^6
PFPrA		1.67×10^7		1.08×10^7
PFBA		1.27×10^7		8.20×10^6
TriFBA		7.37×10^7		4.76×10^7
PFHxA		3.84×10^{7d}		2.48×10^7
PFOA			1.60×10^7	1.03×10^7
TFMS			2.76×10^4	1.78×10^4
PFBS			3.81×10^5	2.46×10^5
PFHxS			2.03×10^6	1.31×10^6
PFOS			3.92×10^6	2.53×10^6

^aFrom our previous work involving carbonate speciation. ^bFrom our previous work involving fluorocarboxylate reactions with e_{aq}^- .¹²² ^cFrom Maza et al. at $\mu \sim 0.03$ M which does not require correction.⁶⁸

^dMeasured in this study at $\mu = 0.14$ M. ^eCorrected using the ionic strength correction equations obtained from Huang et al. and our previous LFP study (see Figure C.1). ^f $H_2CO_3^*$ and $CO_{2(aq)}$ are neutral species whose reactions are unaffected by μ .

C.2 Additional Data

Table C.4 Values to determined rate of hydrated electron production , background scavenging capacity, and hydrated electron availability at pH 9.5 and 12.

	9.5	12
Volume (V; L)	0.575	0.575
Photon flow (ρ_0; $\mu\text{E/s}$)	2.2×10^{-6}	2.2×10^{-6}
Decadic molar absorption coefficient (a; cm^{-1})	0.1796	0.1715
Path length (L; cm)	2.85	2.85
Quantum yield (ϕ; mol/E)	0.108	0.108
Molar extinction coefficient (ϵ; $\text{M}^{-1} \text{cm}^{-1}$)	18.00	17.15
Sensitizer concentration (S; M)	9.97351×10^{-3}	9.99992×10^{-3}
Rate of e_{aq}^- production (r_e; $\text{M}^{-1} \cdot \text{h}^{-1}$)	1.030×10^{-3}	1.005×10^{-3}
Scavenging from H^+ (h^{-1})	2.62×10^4	8.28×10^1
Scavenging from $\text{C}_{\text{T},\text{CO}_3}$ (h^{-1})	5.21×10^7	2.38×10^6
Scavenging from $\text{C}_{\text{T},\text{SO}_3}$ (h^{-1})	1.14×10^7	3.64×10^4
Background scavenging capacity ($\Sigma k_i[\text{Q}_i]$; h^{-1})	6.37×10^7	2.55×10^6
e_{aq}^- availability ($[e_{\text{aq}}^-]_{\text{SS}}$; μM)	1.62×10^{-5}	3.94×10^{-4}

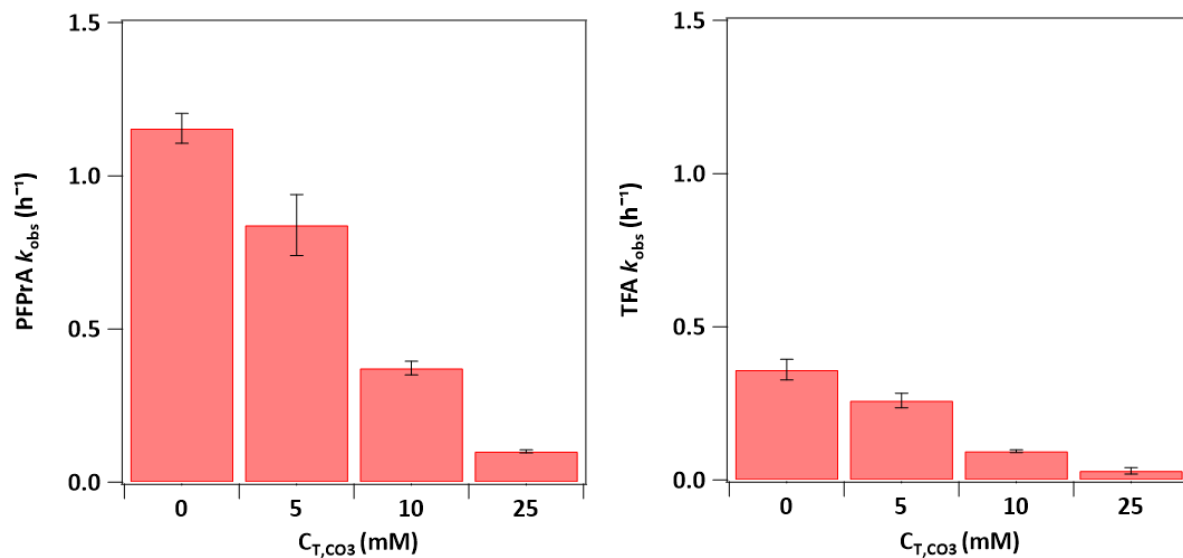


Figure C.2 Effect of dissolved carbonate on observed rate constants of (left) PFPrA and (right) TFA. Reaction conditions are described in Figure 4.1.

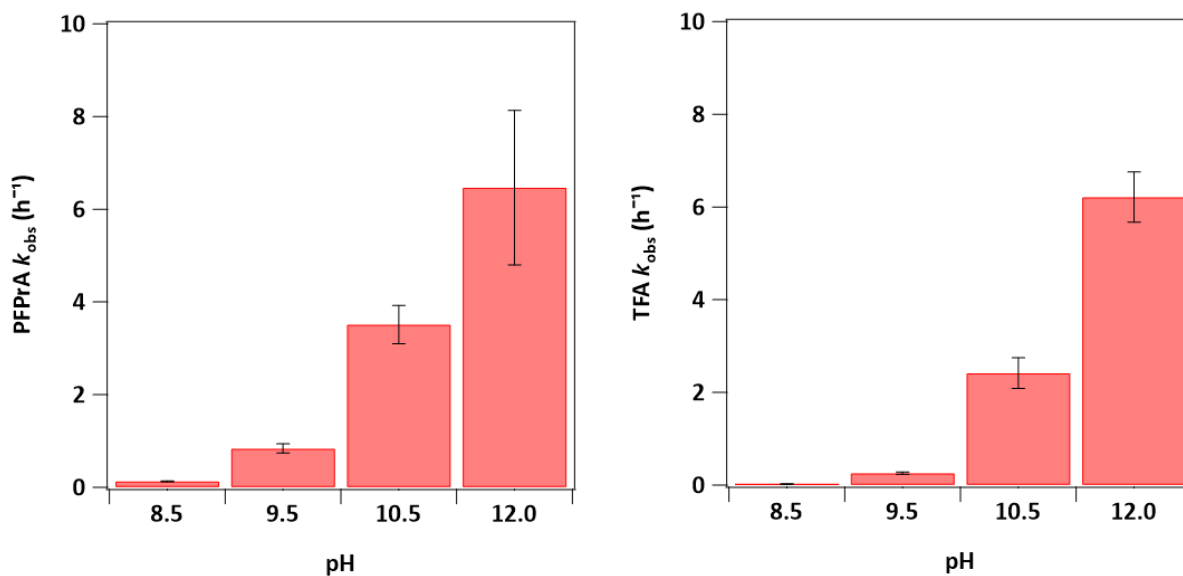


Figure C.3 Effect of pH on observed rate constants of (left) PFPrA and (right) TFA. Reaction conditions are described in Figure 4.1.

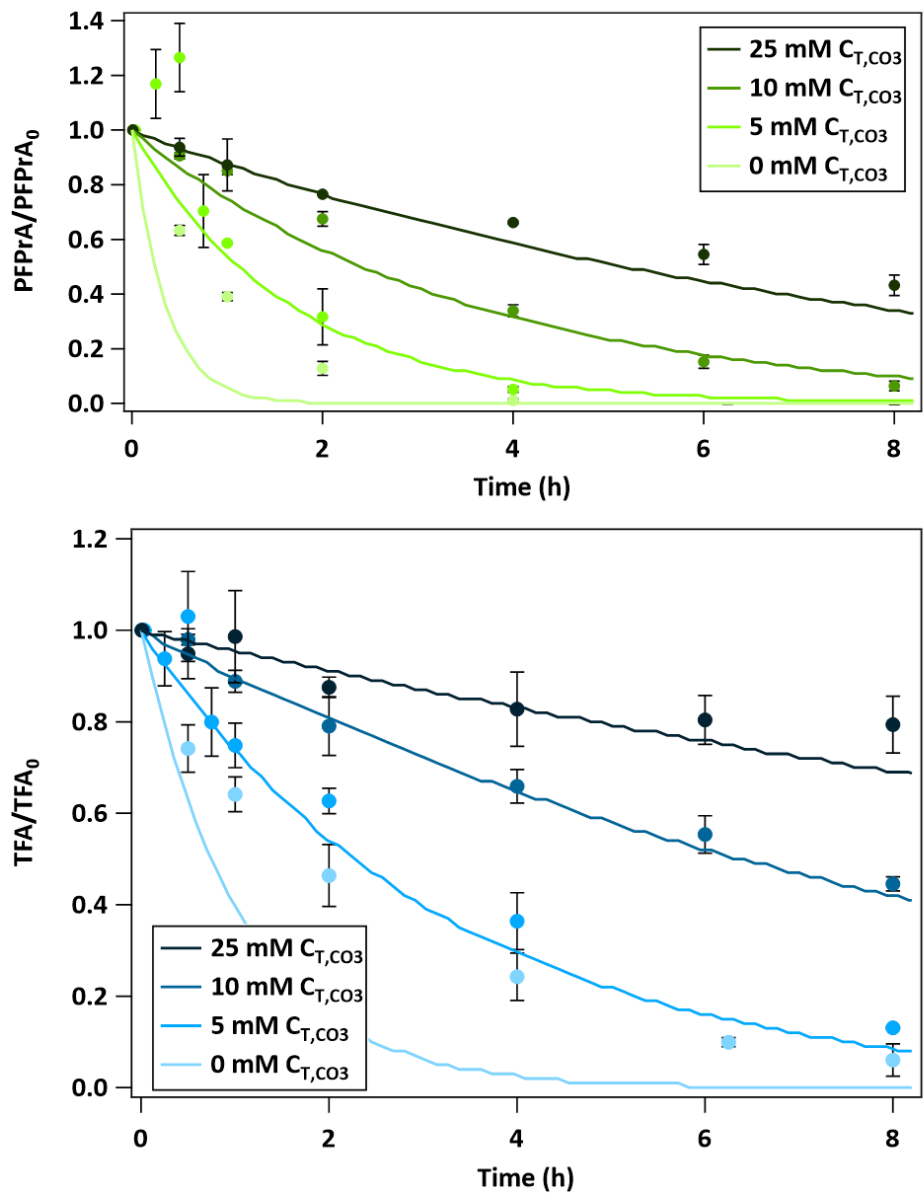


Figure C.4 Degradation profiles of (top) PFPrA and (bottom) TFA during UV-sulfite photolysis at various C_{T,CO3} conditions. Symbols represent experimental data while solid lines represent model predictions. Reaction conditions are described in Figure 4.1.

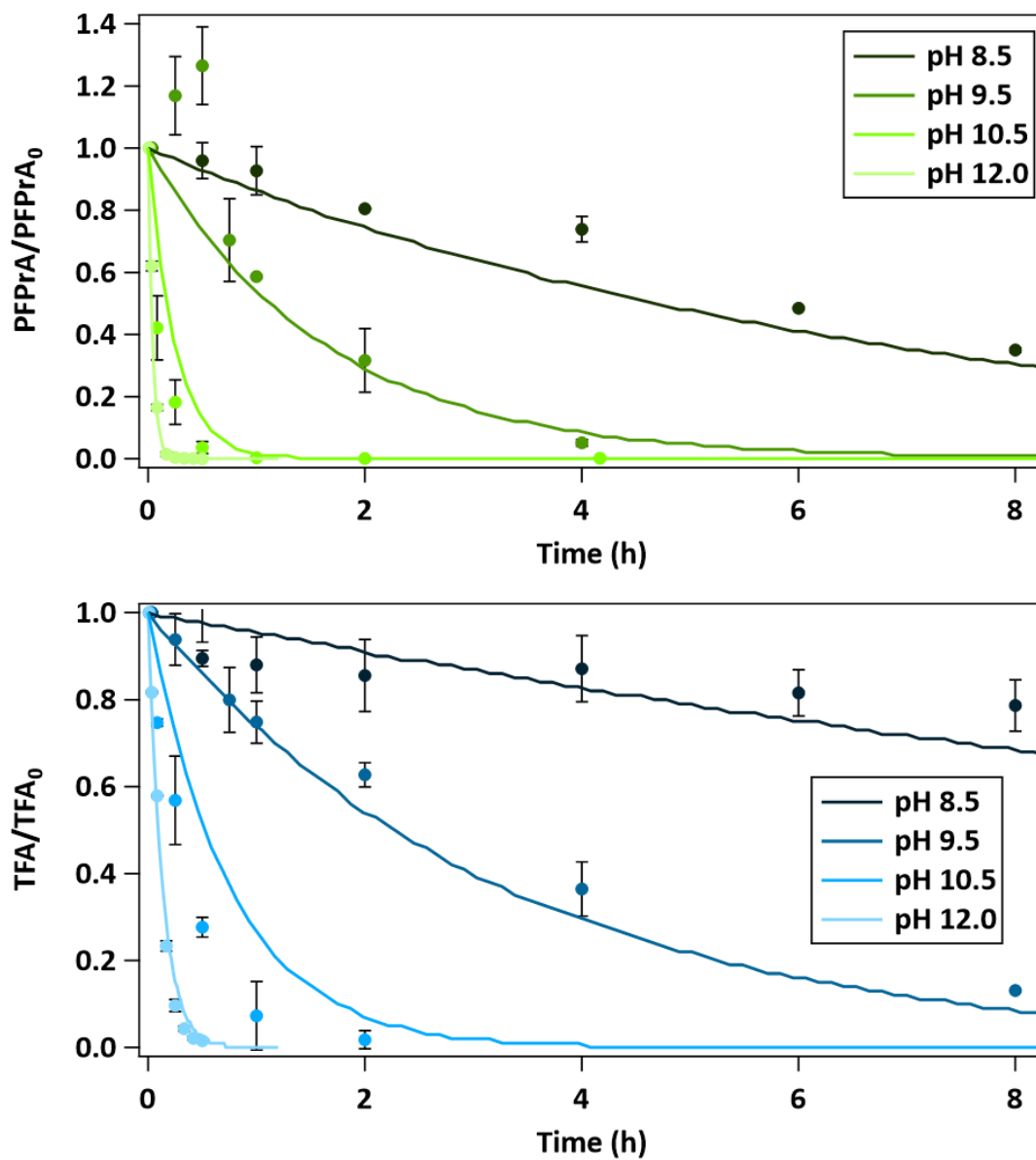


Figure C.5 Degradation profiles of (top) PFPrA and (bottom) TFA during UV-sulfite photolysis at various pH conditions. Symbols represent experimental data while solid lines represent model predictions. Reaction conditions are described in Figure 4.1.

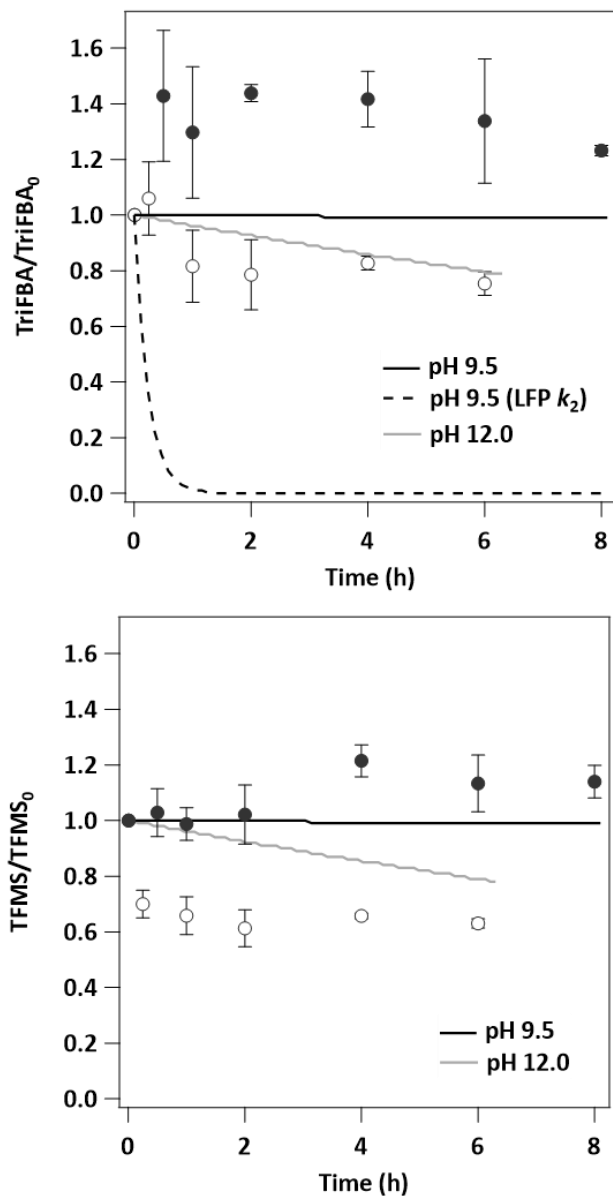


Figure C.6 Degradation profiles of (top) TriFBA and (bottom) TFMS during UV-sulfite photolysis at pH 9.5 and 12. Experimental data is represented by symbols while model simulations are shown as solid lines. Bimolecular rate constant for TriFBA modeling was measured in our previous work, while that for TFMS was estimated using a method described in Chapter 4.

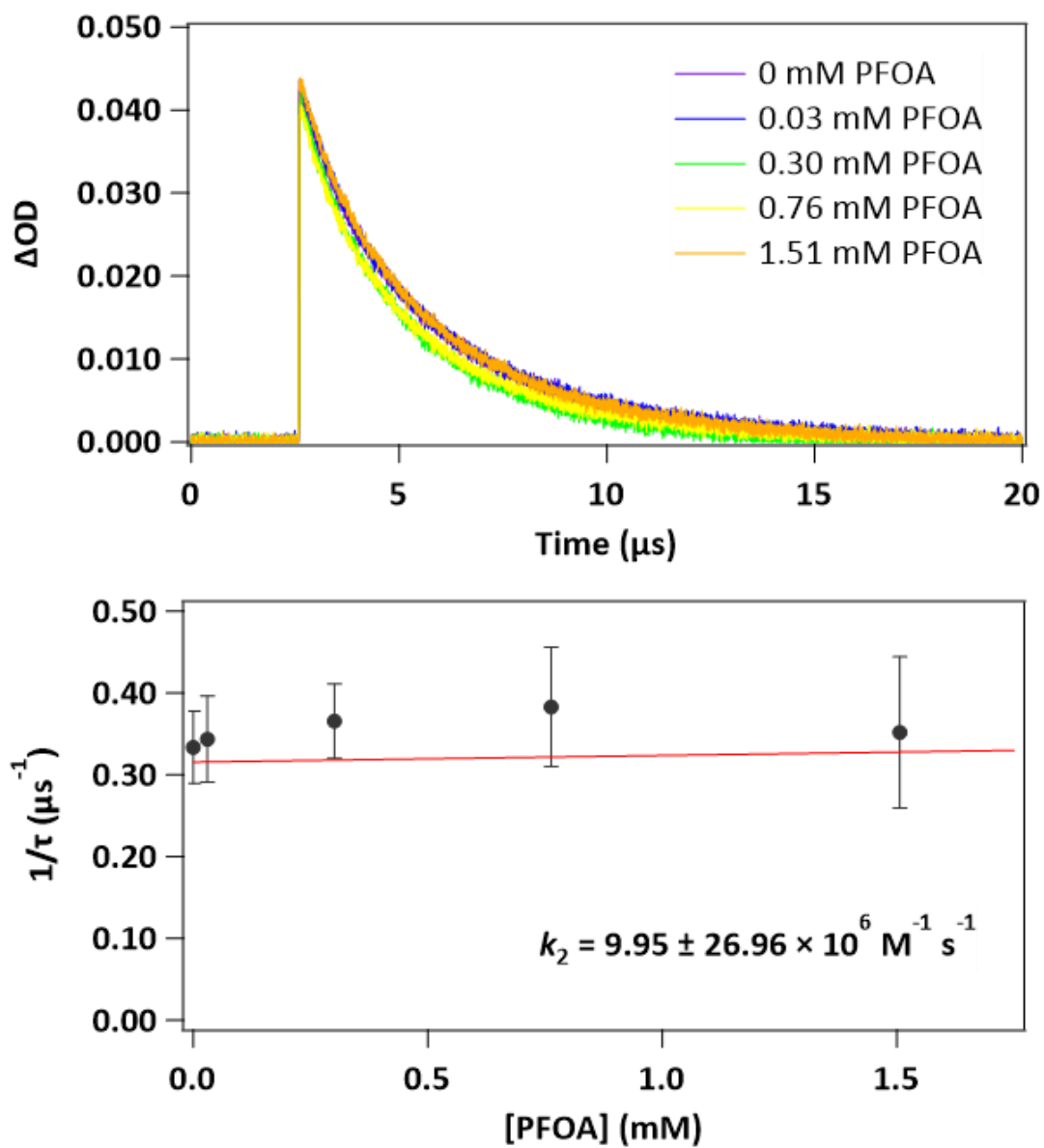


Figure C.7 (Top) Kinetic transient absorption traces for e_{aq}^- decay (measured at 690 nm) at pH 9.5 in solutions amended with varying concentrations of PFOA and (bottom) its corresponding Stern-Volmer plot. Solution conditions are described in Figure 4.3.

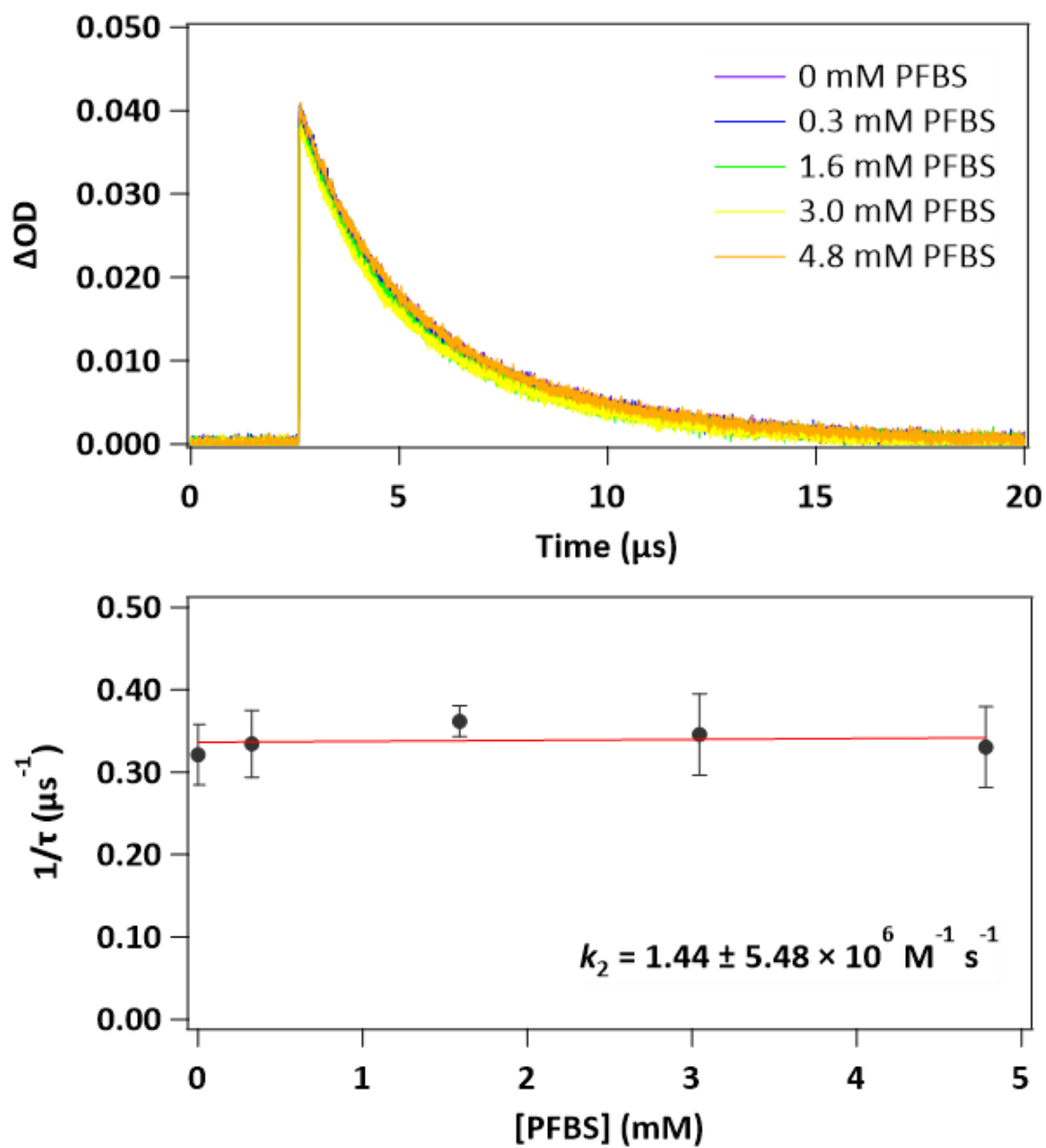


Figure C.8 (Top) Kinetic transient absorption traces for e_{aq}^- decay (measured at 690 nm) at pH 9.5 in solutions amended with varying concentrations of PFBS and (bottom) its corresponding Stern-Volmer plot. Solution conditions are described in Figure 4.3.

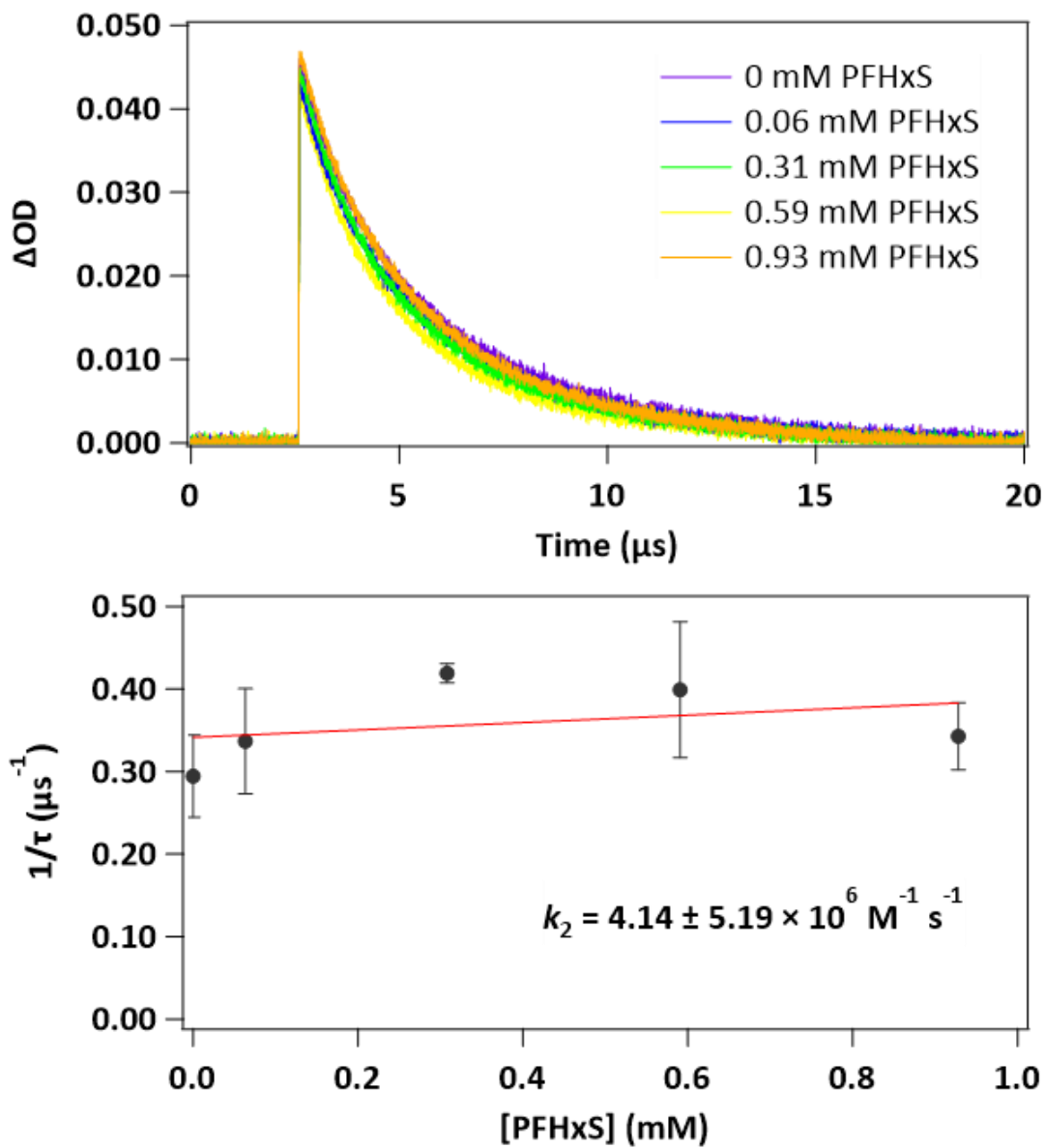


Figure C.9 (Top) Kinetic transient absorption traces for e_{aq}^- decay (measured at 690 nm) at pH 9.5 in solutions amended with varying concentrations of PFHxS and (bottom) its corresponding Stern-Volmer plot. Solution conditions are described in the main text in Figure 4.3.

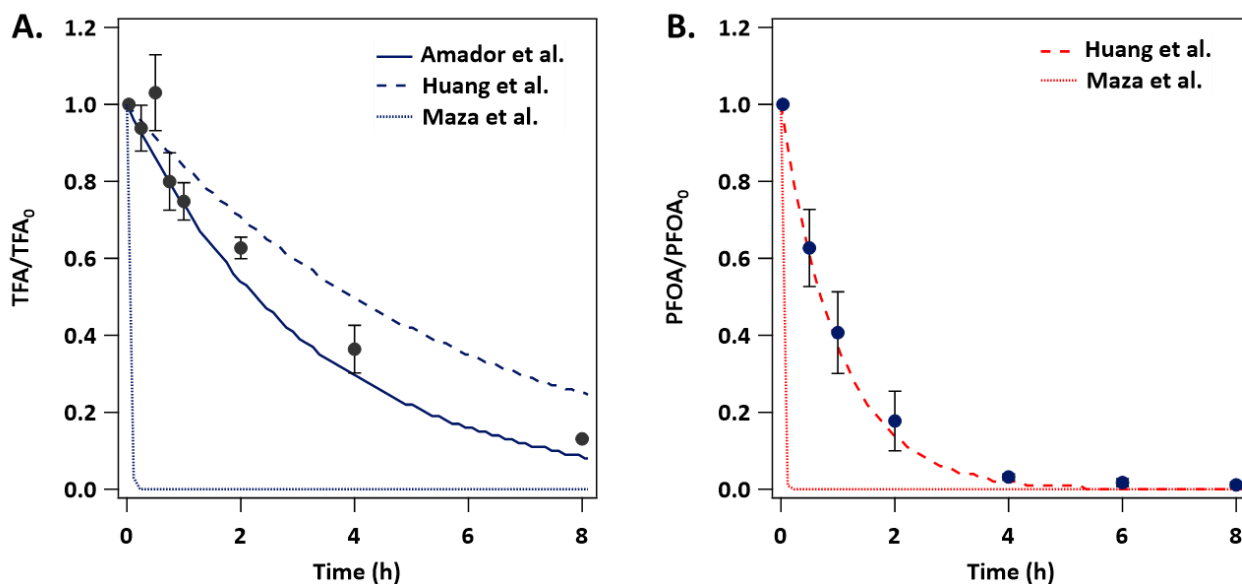


Figure C.10 Degradation profile for (A) TFA and (B) PFOA during UV-sulfite photolysis. Reaction conditions: 10 mM sulfite, 5 mM carbonate, T = 20 °C. Experimental data are shown as circles while model simulations are shown as lines. Rate constants are from Amador et al.,¹²² Huang et al.,⁵⁰ and Maza et al.⁸⁷

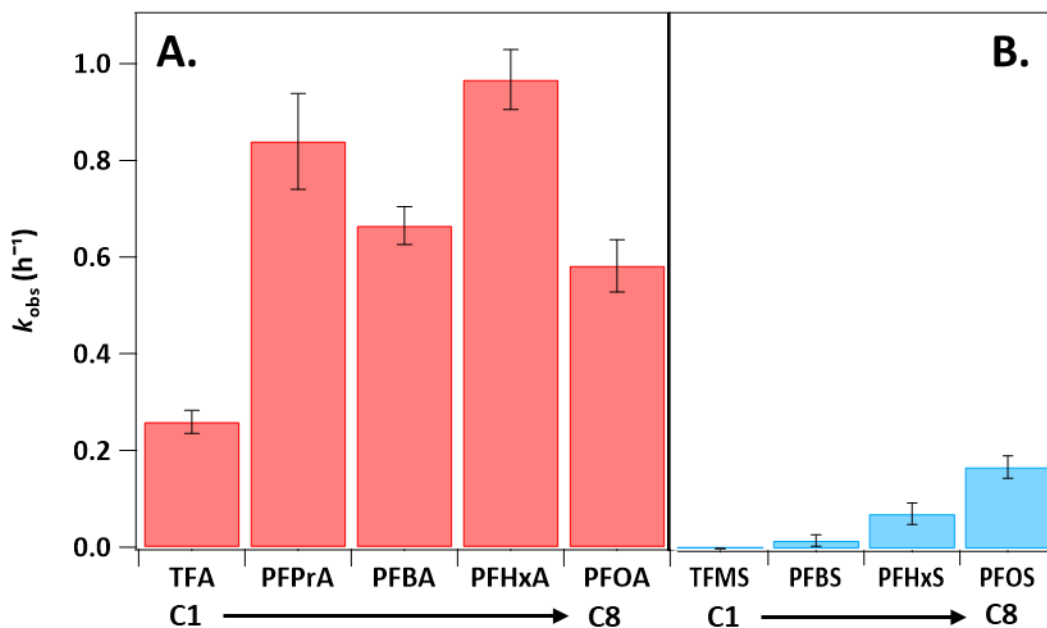


Figure C.11 Observed rate constants of (A) PFCAs vs. (B) PFSAs. Reaction conditions are described in Figure 4.4.

APPENDIX D
COPYRIGHT PERMISSIONS


Permissions to include previously published (and submitted) material in this thesis is below.

Permissions for Chapter 2

1. Permission from Chemosphere regarding the reproduction of the full article in this thesis is not required as the author of this work provided it is not commercially published (see below).

CCC | RightsLink

Home | Help | Live Chat | Sign in | Create Account

 **Ultra-short chain fluorocarboxylates exhibit wide ranging reactivity with hydrated electrons**

Author:
Camille K. Amador, Daniel J. Van Hoomissen, Jiaojin Liu, Timothy J. Strathmann, Shubham Vyas

Publication: Chemosphere

Publisher: Elsevier

Date: January 2023

© 2022 Elsevier Ltd. All rights reserved.



Journal Author Rights

Please note that, as the author of this Elsevier article, you retain the right to include it in a thesis or dissertation, provided it is not published commercially. Permission is not required, but please ensure that you reference the journal as the original source. For more information on this and on your other retained rights, please visit: <https://www.elsevier.com/about/our-business/policies/copyright#Author-rights>

BACK | CLOSE WINDOW

© 2023 Copyright - All Rights Reserved | Copyright Clearance Center, Inc. | Privacy statement | Data Security and Privacy | For California Residents | Terms and Conditions Comments? We would like to hear from you. E-mail us at customer-care@copyright.com

2. Permission from Daniel J. Van Hoomissen

D Daniel Van Hoomissen - NOAA Affiliate <daniel.van-hoomissen@noaa.gov>  
To: Camille Amador Tue 3/21/2023 1:56 PM






CAUTION: This email originated from outside of the Colorado School of Mines organization. Do not click on links or open attachments unless you recognize the sender and know the content is safe.

I, Daniel Van Hoomissen, give you permission to our published work in your upcoming doctoral dissertation which is tentatively titled "KINETICS AND MECHANISMS OF HYDRATED ELECTRON REACTIONS DURING UV-ADVANCED REDUCTION PROCESSES."

Daniel Van Hoomissen (he/him/his)
Research Scientist 1
Cooperative Institute for Research In Environmental Sciences (CIRES)
National Oceanic and Atmospheric Administration (NOAA)
ESRL R/CSL5

Email: daniel.van-hoomissen@noaa.gov
Mobile: 907-315-9233

3. Permission from Jiaoqin Liu

CA Camille Amador     
To: Daniel Van Hoomissen - NOAA Affiliate <daniel.van-hoomissen@noaa.gov>; Jiaoqin Liu <jiaoqin1017@163.com>; Timm Strathmann +1 other Tue 3/21/2023 1:22 PM

Dear Co-authors,

I hope this email finds you well. I am writing to request your permission to use our published work in my upcoming doctoral dissertation which is tentatively titled "KINETICS AND MECHANISMS OF HYDRATED ELECTRON REACTIONS DURING UV-ADVANCED REDUCTION PROCESSES." The DOI in question is provided here: [10.1016/j.chemosphere.2022.136918](https://doi.org/10.1016/j.chemosphere.2022.136918). This requested permission extends to any future versions of my dissertation, electronic publication by the Colorado School of Mines, and publication through ProQuest.







If you agree to these arrangements, please send me your approval by replying to this email with affirmation.

Thank you so much for your contribution to this work!

Best,
Chiqui

D Daniel Van Hoomissen - NOAA Affiliate
CAUTION: This email originated from outside of the Colorado School of Mines organization. Do not click on links or open attachments unless you recognize the sender an... Tue 3/21/2023 1:56 PM

TS Timm Strathmann
I affirm Tue 3/21/2023 2:32 PM

JL Jiaoqin Liu <jiaoqin1017@163.com>      
To: Camille Amador <amador@mines.edu> Thu 3/23/2023 8:55 PM

CAUTION: This email originated from outside of the Colorado School of Mines organization. Do not click on links or open attachments unless you recognize the sender and know the content is safe.

Dear Chiqui,

Congrats on your upcoming graduation! I agree that you should use our published work in your upcoming doctoral dissertation. Congratulations again!
Is everyone in our group going well? And say hello to timm and vyas. I miss you guys so much.

Best wishes

4. Permission from Timothy J. Strathmann

CA Camille Amador
To: Daniel Van Hoomissen - NOAA Affiliate <daniel.van-hoomissen@noaa.gov> +3 others
Tue 3/21/2023 1:22 PM

Dear Co-authors,

I hope this email finds you well. I am writing to request your permission to use our published work in my upcoming doctoral dissertation which is tentatively titled "KINETICS AND MECHANISMS OF HYDRATED ELECTRON REACTIONS DURING UV-ADVANCED REDUCTION PROCESSES." The DOI in question is provided here: [10.1016/j.chemosphere.2022.136918](https://doi.org/10.1016/j.chemosphere.2022.136918). This requested permission extends to any future versions of my dissertation, electronic publication by the Colorado School of Mines, and publication through ProQuest.

If you agree to these arrangements, please send me your approval by replying to this email with affirmation.

Thank you so much for your contribution to this work!

Best,
Chiqui


D Daniel Van Hoomissen - NOAA Affiliate
CAUTION: This email originated from outside of the Colorado School of Mines organization. Do not click on links or open atta...
Tue 3/21/2023 1:56 PM

TS Timm Strathmann [in](#)
To: Camille Amador <amador@mines.edu>
Tue 3/21/2023 2:32 PM

I affirm
...

5. Permission from Shubham Vyas

Request for permission to use material from a Chemosphere paper you are co-authored on 🔍 📄

 **Shubham Vyas** [in](#)
To: Camille Amador (STUDENT)
Thu 3/30/2023 6:15 AM

I, Shubham Vyas, approve that Camille Amador can use our published research paper ([10.1016/j.chemosphere.2022.136918](https://doi.org/10.1016/j.chemosphere.2022.136918)) in her doctoral dissertation.

Best
Shubham Vyas

Sent from Samsung Galaxy smartphone.
Get [Outlook for Android](#)

...

Okay, thank you! Thank you so much! Great, thanks!

← Reply → Forward